Dissertation

submitted to the

Combined Faculty of Natural Sciences and Mathematics

of the Ruperto Carola University Heidelberg, Germany

for the degree of

Doctor of Natural Sciences

Presented by

Sebastian Brabetz, M.Sc.

born in: Steinfurt

Oral examination: 7/23/2018

Molecular and preclinical evaluation of patient-derived orthotopic xenograft models of pediatric brain tumors

Referees: Prof. Dr. Michael Boutros

Prof. Dr. Stefan M. Pfister

Declaration

The work presented in the following dissertation was performed in the Division of Pediatric Neurooncology (Prof. Dr. Stefan M. Pfister) at the German Cancer Research Center (DKFZ) in Heidelberg, Germany, between January 2014 and May 2018.

Herewith I declare that I have written and submitted this dissertation myself and in this process have not used any other sources than those indicated. Parts of this dissertation were submitted to *Nature Medicine* in July 2017. These sections, written together with my co-shared first authors Dr. Susanne N. Gröbner (DKFZ, Heidelberg, Germany) and Dr. Sarah E. S. Leary (Seattle Children's and the University of Washington, Seattle, USA and Fred Hutchinson Cancer Research Center, Seattle, USA), are marked with footnotes. Contributions of authors other than myself are indicated in the Material and Methods section, within figure legends, and in footnotes.

I hereby declare that I have not applied to be examined at any other institution, nor have I used the dissertation in this or any other form at any other institution as an examination paper, nor submitted it to any other faculty as a dissertation.

_____

Sebastian Brabetz

To my mother

Zusammenfassung

Tumore des zentralen Nervensystems sind nach Leukämien die häufigsten pädiatrischen Krebserkrankungen. Obwohl immer mehr Patienten geheilt werden können, leiden Überlebende häufig an den schwerwiegenden Langzeitfolgen der intensiven Behandlungen. Deshalb sind neue Behandlungsstrategien zwingend erforderlich. Dies umfasst sowohl neuartige zielgerichtete Therapien, als auch die Verbesserung von bisherigen Behandlungsprotokollen in Abhängigkeit von neuen molekularen Hirntumor-Subtypen. Jedoch macht sowohl die Seltenheit von pädiatrischen Hirntumoren als auch die Vielzahl der Tumorsubtypen in der pädiatrischen Neuroonkologie die klinische Forschung sehr anspruchsvoll, da es bis zu einem Jahrzehnt dauern kann, in einer klinischen Studie zwei Behandlungsarme einer seltenen Tumorentität miteinander zu vergleichen. Präklinische Modellsysteme eröffnen die Möglichkeit, unterschiedliche Behandlungsstrategien für die klinische Forschung vorab zu priorisieren. Hierbei haben sich Patienten-basierte Xenotransplantate als ein nützliches Modellsystem für sowohl die akademische Forschung als auch für die pharmazeutische Industrie herausgestellt. Jedoch ist es bis heute, aufgrund der Seltenheit von pädiatrischen Hirntumoren, nicht gelungen, eine umfassende Sammlung dieser Modelle zu erstellen, die auch das weite Spektrum der unterschiedlichen Tumorsubtypen abdeckt.

Um eine systematische präklinische Evaluation von pädiatrischen Hirntumoren zu ermöglichen, wurden in dieser Arbeit 130 orthotope Patienten-basierte Xenotransplantatmodelle untersucht, welche entweder lokal generiert oder von fünf kollaborierenden Zentren gesammelt wurden. Die Anwachsrate für hochgradige pädiatrische Hirntumore in Mäusen betrug im Durschnitt 30%. Zusätzlich wuchsen die Modelle nach einer Kryopräservierung erneut an, was demonstriert, dass diese eine nachhaltige Ressource darstellen. Histopathologische Analysen bestätigten zudem, dass die Xenotransplantatmodelle morphologisch immer noch den Tumor reflektieren, der zu ihrer Generierung benutzt wurde. Um eine umfassende molekularen Charakterisierung zu ermöglichen, wurden die Xenotransplantatmodelle und, falls vorhanden, die dazugehörigen Patiententumore, sowohl mittels Methylierungs- und Transkriptomsanalysen, als auch mittels Exom- und Genomsequenzierungen analysiert.

Die molekulare Klassifikation der Xenotransplantatmodelle zeigte, dass die hier analysierte Kohorte 22 unterschiedliche molekulare Subtypen von pädiatrischen Hirntumoren umfasst, wobei für viele davon bisher noch keine Modellsysteme existierten. In der Kohorte bestand eine Anreicherung von aggressiven Tumorsubtypen, selbst innerhalb von WHO Grad IV Tumoren, wohingegen niedriggradigere Tumore gar nicht vertreten waren. Ein Vergleich der genetischen Alternationen in den molekularen Subtypen der Xenotransplantatkohorte im Vergleich zu Patiententumorkohorten aus früheren Studien zeigte eine Anreicherung von

genetischen Alterationen, welche bereits mit einer schlechten Prognose assoziiert worden sind. Zudem wurden auch Anreicherungen von *KBTBD4*-Insertionen in Gruppe 3 Medulloblastomen als auch von *GFI1B*-Aktivierungen in Gruppe 4 Medulloblastomen detektiert. Dies lässt schlussfolgern, dass diese Läsionen womöglich ebenfalls mit einer schlechten Prognose für Patienten einhergehen könnten.

Insgesamt repräsentieren die Xenotransplantatmodelle ihren zugrundeliegenden Patiententumor sehr gut auf Ebene der Mutationen, der Kopienzahlveränderungen, des Methyloms und des Transkriptoms. Die am Tumorwachstum beteiligten Alterationen wurden nahezu immer im Xenotransplantatmodell beibehalten, aber die Modelle entwickelten sich auch evolutionär weiter. Veränderungen von Patiententumor zu Xenotransplantatmodell im Rahmen des Transkriptoms und des Methyloms konnten größtenteils auf den Verlust des humanen Stromas zurückgeführt werden. Starke klonale Auswüchse waren selten und limitiert auf entitätsspezifische Läsionen, wie das Auswachsen von *MYC*-Amplifikationen in Gruppe 3 Medulloblastomen, und ereigneten sich häufig in der ersten Passage.

Die präklinische Evaluation der Xenotransplantatmodelle basierend auf molekularen „Targets“ konnte die vorhergesagte Sensitivität gegenüber zielgerichteten Inhibitoren bestätigen. Wie bereits in Patienten gesehen, konnte die Langzeittherapie mit dem SMO Inhibitor Erismodegib resistente Tumoren erzeugen.

Um die Modellsysteme und die zugehörigen molekularen Daten öffentlich zugänglich zu machen, wurde das Online-Tool „PDX Explorer“ (https://hgserver1.amc.nl/cgi-bin/r2/main.cgi?&dscope=PDX_OLSON&option=about_dscope) etabliert, welche es möglich macht, die hier beschriebene Sammlung von Patienten-basierten Xenotransplantatmodellen zu durchsuchen und geeignete Modelle für individuelle wissenschaftliche Fragenstellungen zu finden.

Zusammenfassend stellt diese Studie die bisher größte Sammlung von Patienten-basierten orthotopen Xenotransplantatmodellen von pädiatrischen Hirntumoren dar und bestätigt, dass diese zuverlässige Modellsysteme darstellen. Diese Arbeit stellt somit eine bislang einzigartige Ressource zur Untersuchung der Tumorbiologie dar und bietet Ansätze, um Behandlungsstrategien für Kinder mit malignen Hirntumoren zu verbessern.

Summary

Tumors of the nervous system are, after leukemias, the most common pediatric cancers. Although an increasing numbers of patients can be cured, survivors often suffer from severe sequelae of the intensive treatment regimens. Therefore, new treatment strategies are desperately needed. These include new targeted therapeutical approaches, but also the refinement of current treatment protocols based on the finding of new molecular subgroups of brain tumors. However, the rarity of pediatric brain tumors and the multitude of various tumor subgroups make clinical investigations highly challenging, as it can take up to a decade to compare two treatment arms from rare tumor entities within a clinical trial. Preclinical model systems can prioritize therapeutic strategies for clinical investigations. Patient-derived xenograft models have become a useful preclinical model system for both academia and the pharmaceutical industry. However, until now, the rarity of pediatric brain tumors has hindered the generation of a sufficiently large collection of patient-derived xenograft models representing the broad spectrum of various types of pediatric brain tumors.

In order to allow systematic preclinical evaluation in pediatric brain tumors, here, 130 patient-derived orthotopic xenograft models were both locally generated and collected from five different collaborating centers. Engraftment rates for high-grade pediatric brain tumors were on average 30%, and patient-derived orthotopic xenograft models could be re-grown after cryo preservation, demonstrating that these model systems are a sustainable resource. Histopathological evaluation confirmed that patient-derived orthotopic xenograft models closely resembled the patient tumor from which they were derived. In addition, the cohort of 130 patient-derived orthotopic xenografts, and if available the corresponding patient tumor, were subjected to extensive molecular characterization by methylation and gene expression profiling, as well as by whole exome and whole genome sequencing.

Molecular subtyping of patient-derived orthotopic xenografts showed that the cohort represents 22 distinct molecular subtypes of pediatric brain tumors, many of which could previously not be modeled. Within the cohort, there was a bias for more aggressive tumor subgroups, even within WHO stage IV tumors, and more benign entities were not represented. Comparing the landscape of genetic alterations per tumor subgroup within the cohort of patient-derived orthotopic xenograft models to primary patient cohorts identified an enrichment of genetic alterations linked to a poor prognosis in various tumor subgroups. In addition, enrichments of *KBTBD4* insertions in Group 3 and *GFI1B* activations in Group 4 medulloblastoma were detected, which could mean that these alterations are linked to a poor prognosis in patients as well.

Overall, patient-derived xenografts closely resembled the corresponding patient tumors on the levels of mutations, copy-number alterations, methylome, and transcriptome, and stayed relatively stable over multiple passages. Presumed driver alterations were almost exclusively maintained in PDOX. However, the models also continued to evolve. Changes in the methylome and the transcriptome between patient tumor and PDOX were confined mostly to the loss of the human stroma. Strong clonal outgrowth events were rare and limited to entity-specific lesions, such as *MYC* amplifications in Group 3 medulloblastoma, and occurred mostly in the first passage.

Preclinical evaluation of patient-derived orthotopic xenografts confirmed sensitivity to targeted inhibitors based on the presence of molecular targets. As observed in patients, long-term treatment of SHH medulloblastoma patient-derived orthotopic xenografts with the SMO inhibitor Erismodegib was able to induce resistant tumors.

In order to make the model systems and associated molecular data available to the scientific community, an online tool called "PDX Explorer" (https://hgserver1.amc.nl/cgi-bin/r2/main.cgi?&dscope=PDX_OLSON&option=about_dscope) was established, which makes it possible to browse through the collection of patient-derived orthotopic xenografts to find the suitable model systems for specific scientific questions.

In summary, this study comprises the largest collection of patient-derived orthotopic xenograft model systems for pediatric brain tumors to date and highlights that patient-derived orthotopic xenografts are effective model systems. This work represents a thus far unique resource for studying tumor biology and offers approaches for improving treatment strategies for children with malignant brain tumors.

List of abbreviations

450k arrays	Illumina Infinium 450k Methylation BeadChip Arrays
ALL	acute lymphoblastic leukemia
ATRT	atypical teratoid/rhabdoid tumor
bp	base pairs
CBTRUS	Central Brain Tumor Registry of the United States
CNS	central nervous system
CNS, NB FOXR2	CNS neuroblastoma with FOXR2 activation
CNV	copy number variation
COG	Children's Oncology Group
D/N	desmoplastic nodular
ddNTPs	dideoxynucleotides
DMSO	dimethyl sulfoxide
dNTPs	deoxyribonucleotides
EFS	event-free survival
EFT, CIC	Ewing family tumor with CIC fusion
EGFR	epidermal growth factor receptor
emPCR	water-in-oil emulsion PCR
epic arrays	Illumina Infinium EPIC Methylation BeadChip Arrays
EPN	ependymoma
ER^+	estrogen receptor positive
ETANTR	embryonal tumors with abundant neuropil and true rosettes
ETMR	embryonal tumor with multilayered rosettes
FACS	Fluorescence-activated Cell Sorting
FBS	fetal bovine serum
FDA	Food and Drug Administration
GEMM	genetically engineered mouse model
HGG	pediatric high-grade glioma
HGNET, BCOR	high grade neuroepithelial tumor with BCOR alteration
HGNET, MN1	high-grade neuroepithelial tumor with MN1 fusion
HL	Hodgkin's lymphoma
ICGC	International Cancer Genome Consortium
IHC	immunohistochemistry
indels	insertions/deletions
LCA	large cell and/or anaplastic
LGG	low-grade glioma

MB	medulloblastoma
MBEN	MB with extensive nodularity
MRI	magnetic resonance imaging
mRNA	messenger RNA
NHL	non-Hodgkin lymphoma
NIH	National Institutes of Health
NSCLC	non-small cell lung cancer
NSG	NOD-scid IL2Rgamma^{null}
OS	overall survival
PA	pilocytic astrocytoma
PBS	phosphate buffered saline
PCT	PDX Clinical Trial
PDGFRA	platelet-derived growth factor receptor A
PDOX	patient-derived orthotopic xenograft(s)
PDX	patient-derived tumor xenograft(s)
PF	posterior fossa
pGF1	pGreenFire1
PI	principal investigator
PNET	primitive neuroectodermal tumor
PXA	pleomorphic xanthoastrocytoma
RT-qPCR	reverse transcription quantitative PCR
SMRT	single molecule real time
SNP	single nucleotide polymorphism
SNV	single nucleotide variant
ST	supratentorial
TBE	TRIS-Borat-EDTA
TCGA	The Cancer Genome Atlas
WES	whole exome sequencing
WGS	whole genome sequencing
WGSlc	low-coverage whole genome sequencing
WHO	World Health Organization

Contents

List of figures

List of tables

1 Introduction

1.1 Cancer

1.1.1 Cancer – a global health challenge

Cancer is a tremendous challenge for global health. In 2012, 14.1 million new patients were diagnosed with cancer worldwide, while 8.2 million cancer-related deaths were registered, and 32.6 million people were living with cancer within 5 years of their diagnosis[1].

The median age at diagnosis is 65, but this varies dramatically among cancer types[2]. The age-standardized cancer incidence rate is almost 25% higher in men than in women (205 and 165 cases per 100,000 person-years, respectively)[1]. In addition, tumor sites differ between genders; incidence and mortality for men is highest for lung cancer, while in women breast cancer is the most common cancer site[1]. The lifelong probability of developing cancer in the U.S. is 42% for men and 38% for women, whereas the probability for individuals of developing cancer prior to the age of 50 is higher for women (5.4%) compared to men (3.4%), due to the high incidence of genital, breast, and thyroid cancer in young women[3]. Over the past few years, the number of cancer survivors has been continuously increasing despite declining incidence rates[3]. This reflects an increased survival rate as well as demographic changes toward a more elderly population[2]. Since 1991, the overall cancer death rate has dropped by 23%[3]. However, the 5-year survival rates differ dramatically between sites, ranging from 5% in patients with pancreas tumors to 98% in patients with tumors in the thyroid gland[2]. Despite all the progress that is being made, cancer is still the leading cause of death in the U.S. after heart disease[4].

1.1.2 The hallmarks of cancer

Cancer is not one disease. It stands for a multitude of different diseases, which all follow the same biological concept. Cancers are neoplastic lesions that originate from normal tissue. During the process of transforming normal cells into tumor cells, also called oncogenesis, defects are introduced into regulatory cellular circuits that control normal cell proliferation and homeostasis. In two central publications, Hanahan and Weinberg categorized the heterogeneity of cancer characteristics into eight so-called “hallmarks” and two “enabling characteristics” of cancer cells[5,6]. These are distinct, yet complementary, biological capabilities allowing for the malignant transformation of cells (Figure 1, page 2)[5,6]. During the process of oncogenesis, cells acquire a succession of these hallmarks.

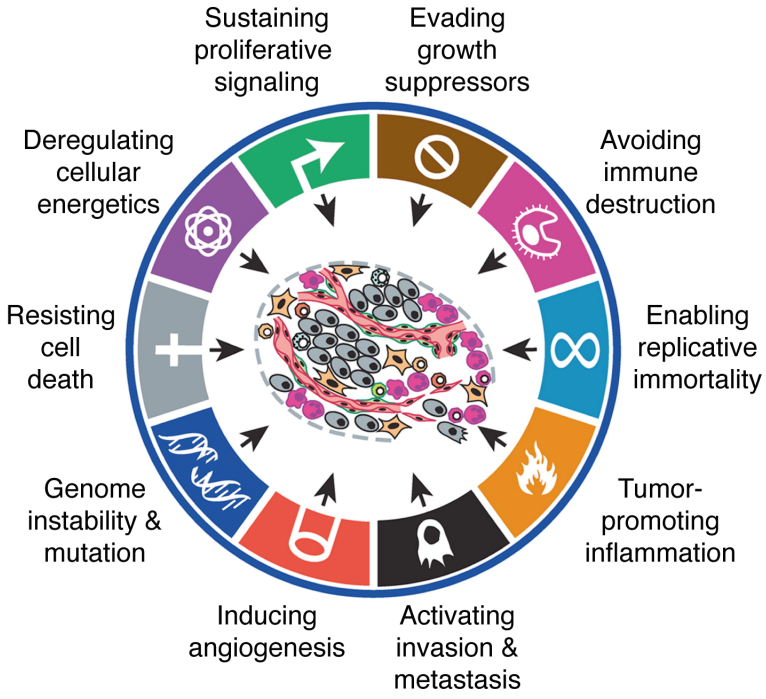

Figure 1: The hallmarks of cancer.
Overview representing the eight hallmarks and the two enabling characteristics of cancer cells as proposed by Hanahan and Weinberg (modified from Hanahan and Weinberg, 2011)[6].

One of the key characteristics of cancer cells is the maintenance of sustained proliferation[7-10]. In normal cells, proliferation is tightly regulated by the presence of growth factors that allow the cells to move forward through the cell cycle; deprivation of growth factors therefore halts proliferation[5]. Cancer cells can acquire independence from growth factors by 'sustaining proliferative signaling' through various methods[5,6]. They can start to produce the necessary growth factors in addition to the growth factor receptors, therefore stimulating themselves via autocrine signaling[5]. Alternatively, cancer cells can also stimulate surrounding normal cells (tumor microenvironment) to provide the necessary growth factors[11,12]. Another option is to up-regulate or modify growth factor receptors on the cell membrane to induce hypersensitivity to growth factors, effectively reducing the concentration required to induce proliferation[6]. This is, for example, typically seen for platelet-derived growth factor receptor A (PDGFRA) or epidermal growth factor receptor (EGFR) in gliomas[13]. Instead of activating the entire growth factor cascade via a ligand-receptor interaction, the downstream signaling can also be activated by modifying proteins within the cascade itself, e.g. activating mutations in serine/threonine-protein kinase B-Raf in melanoma[14] or in various types of glioma[15]. In many cases, multiple different downstream signaling cascades propagate from one ligand-receptor interaction into the cells, which, in turn, means that downstream activations are only partly mirroring the physiological growth factor receptor cascade[6]. Other important aspects in the homeostasis of growth signals are feedback loops, which dampen the effects of receptor activation in the

regulatory cellular circuits[16-19]. Typical examples of disruptions of feedback loops in cancer are mutations in the GTPase K-ras, which do not directly activate the protein, but instead affect the GTPase domain, thereby deactivating the intrinsic feedback-loop that normally guarantees transitory activation only[20]. Another similarly prominent example is the loss or deactivation of the phosphatase PTEN, which regulates PI3-kinase signaling by dephosphorylating its product phosphatidylinositol-(3,4,5)-trisphosphate[21]. In this context, *KRAS* acts as an oncogene, a gene that upon activation causes tumor growth, while *PTEN* acts as a tumor suppressor, a gene that promotes tumor growth after its deactivation[22]. However, unlimited activation of growth pathways can also induce cellular senescence, an irreversible arrest of cell growth and proliferation in response to physiological stimuli, which normally protects against neoplastic outgrowth[23]. Therefore, 'evading growth suppressors' is also an essential hallmark of cancer cells[5,6]. In healthy cells, there is a huge variety of regulatory circuits controlling cell proliferation and homeostasis[5,6]. Another prototypic tumor suppressor is TP53, titled "the guardian of the genome"[24]. The TP53 protein responds to cellular stress such as DNA damage, hyperproliferative signaling, hypoxia, oxidative stress, ribonucleotide depletion, and nutrient starvation, and can then trigger transient or permanent cell cycle arrest and apoptosis[24]. Due to the central gatekeeper function of *TP53*, it is the most commonly mutated gene in adult and pediatric cancers[25,26]. Its significance is further highlighted by the susceptibility of individuals with Li-Fraumeni syndrome, who inherit a mutant *TP53* allele and of whom 50% develop cancer prior to the age of 30 compared to 1% in the normal population[27-32]. The apoptosis-inducing function of TP53 also plays a role in the hallmark of 'resisting cell death'[5,6]. Apoptosis is the process of controlled cell death, which is a physiologic process acting as a protection against oncogenesis[33]. Apoptosis is tightly regulated by a machinery of pro- and anti-apoptotic proteins that are often altered in cancers[34]. One of the key aspects driving TP53-triggered apoptosis is 'genome instability and mutation', a cancer-enabling characteristic[6]. By altering their genome, cancer cells are able to acquire new characteristics that drive tumor growth as described above. Another central hallmark of cancer is to 'enable replicative immortality'[5,6]. While normal cells are able to undergo only about 52 mitoses, which is referred to as the "Hayflick limit", cancer cells do not underlie this limitation[35,36]. After reaching the Hayflick limit, normal cells go into senescence or even into apoptosis[23]. The mechanism behind the Hayflick limit is a shortening of telomeres, the ends of chromosomes consisting of tandem repeats of the nucleotides TTAGGG that are bound by specific proteins, with each cell cycle[37]. This makes these chromosomal regions vulnerable to degradation or recombination activities[37]. The conventional way for cancer cells to counteract the loss of these segments over time is the expression of the telomerase protein, a DNA polymerase that adds new telomeric sequences to the ends of chromosomes, protecting the cell against the induction of senescence and telomere crisis/apoptosis[37]. In current scientific thinking, this is central in preventing the outgrowth of

neoplastic clones – although pre-neoplastic cells can outgrow the surrounding normal tissue, without circumventing telomere loss their growth is somewhat limited[6]. Intriguingly, the absence of TP53 can allow cells to survive even though they have short telomeres and to exploit the additionally induced genome instability to accelerate oncogenesis[38,39].

All mammalian cells require oxygen and nutrients for survival and must therefore be located within 100-200 µm of blood vessels in a multicellular organism – the diffusion limit for oxygen[40]. Tumor cells are no exception here, and therefore, during tumor progression, an "angiogenic switch" is nearly always switched on and maintained in order to sprout new blood vessels[41]. In most cases, the tumor cells prompt angiogenesis through the secretion of pro-angiogenic factors, resulting in the recruitment of endothelial cells from the stroma, but tumor cells may also trans-differentiate into endothelial cells themselves[42-44]. The necessity of 'inducing angiogenesis' during tumor growth beyond a certain tumor size makes it an important hallmark of oncogenesis[6].

A tumor is more than just a homogenous mass of proliferating cells, but rather a complex "organ" consisting of fibroblasts, immune cells, endothelial cells, and specialized mesenchymal cells in addition to cancer cells[45]. The interaction between tumor cells and the associated stroma is thus highly complex and plays a major role during tumorigenesis. Already in the 1980s, pathologists recognized that tumor tissue is heavily infiltrated by immune cells of both the native and the adaptive immune systems, mirroring normal inflammatory conditions[46]. To survive within this high density of immune cells, cancer cells must acquire certain characteristics in order to 'avoid immune destruction'[6]. However, tumor-associated inflammation also has the paradoxical effect of boosting tumor growth via promoting various other hallmarks such as supplying growth factors or promoting angiogenesis – mostly through the innate immune system[47-50]. Due to these capacities, 'tumor-promoting inflammation' was proposed as an enabling characteristic[5,6]. Interestingly, certain oncogenes can remodel the tumor microenvironment through recruitment of leukocytes and lymphocytes[51,52]. Therefore, tumors require a tight balance between promoting tumor growth through inflammation while avoiding an immune reaction against the tumor itself – a process which is orchestrated by tumor cells through interactions with the immune cells of the tumor-associated stroma[49].

The continuous proliferation of tumor cells demands an adjustment of the cellular energetics to meet the new demands – the 'reprogramming of the energy metabolism'[6]. Otto Warburg described the first indications of atypical cell metabolism in cancer cells[53-55]: Under aerobic conditions normal cells produce energy by dismantling glucose, initially into pyruvate in the cytosol, and then to carbon dioxide in the mitochondria, while under anaerobic conditions, glucose is processed by glycolysis into pyruvate, which produces less energy than does the mitochondrial pathway[56]. Cancer cells can re-program their metabolic pathways to perform

glycolysis even under aerobic conditions[53-55] – probably due to the production of glycolytic intermediates that can be fed into different biosynthetic pathways[57]. Anaerobic glycolysis can also occur in genetically normal cells during proliferation and also in virus-infected cells, and therefore may be beneficial in phases of increased biosynthetic demand[58-61]. Since the description of this so-called "Warburg effect", the field has evolved dramatically, and now cancer-specific metabolic changes are classified into six hallmarks: (1) deregulated uptake of glucose and amino acids, (2) use of opportunistic modes of nutrient acquisition, (3) use of glycolysis/tricarboxylic acid cycle intermediates for biosynthesis and nicotinamide-adenine-dinucleotidephosphate (NADPH) production, (4) increased demand for nitrogen, (5) alterations in metabolite-driven gene regulation, and (6) metabolic interactions with the microenvironment[61].

The unique characteristic that distinguishes malignant tumors from benign tumors is their ability to invade the surrounding normal tissue. Along these lines, 'activating invasion and metastasis' is also a hallmark of cancer[5,6]. The invasion-metastasis cascade describes the metastatic process starting from a local invasion to the establishment of a distant metastasis after traveling through the blood stream[62-64]. In carcinomas, the developmental program of epithelial-mesenchymal transition can convey key characteristics within the invasion-metastasis cascade that allow cancer cells to invade the adjacent tissue, resist anoikis – apoptosis triggered by detachment from the original extracellular matrix[65] – and to disseminate[66-70]. The significance of metastasis in cancer is highlighted by the fact that 90% of cancer-associated deaths are caused by the metastasis of cancer cells to both nearby and distant, vital organs[71].

In order to understand how cancer cells acquire these varied hallmarks through changes in the (epi-)genome, large collaborative approaches, such the "International Cancer Genome Consortium" (ICGC) and "The Cancer Genome Atlas" (TCGA), have utilized high-throughput techniques to systematically map the genomic differences between cancer cells and normal cells in order to design therapeutic approaches specifically targeting cancer cell dependencies[72-74].

1.1.3 Cancer – a disease of the genome

Over a century ago, Theodor Boveri proposed for the first time that "malignant tumours might be the consequence of a certain abnormal chromosome constitution", which can be translated into contemporary language as "cancer is a disease of the genome"[75,76]. It took science until the 1970s to discover the first cancer-inducing nucleic acid, the *v-Src* gene of the Rous sarcoma virus[77], and to prove that cancers arise not only by introducing these external genes into normal cells, but also after they have edited the endogenous host's DNA sequence, turning a normal

gene into an oncogene[78,79]. This knowledge led to the establishment of the concept of oncogenes and tumor-suppressors, which need to be activated or de-activated, respectively, in order to promote tumorigenesis[80]. Even then, scientists began to appreciate the considerable complexity underlying oncogenesis, and that oncogenes and tumor suppressors differ among different tumor sites and subtypes[76].

In a visionary commentary in 1986, Renato Dulbecco proposed "to sequence the whole genome" of the human species instead of trying "to discover the genes important in malignancy by a piecemeal approach"[81]. Based on the data generated by this approach, probes could be designed for every gene to systematically analyze it in a healthy state as well as in a diseased state[81]. This and other calls were answered by the initiation of the Human Genome Project in 1990, which resulted in the first "draft" sequence of the human genome in 2000[82,83], and a final sequence in 2003[84].

This finalization of the sequence of the human genome marks the birth of "cancer genomics", a scientific field trying to understand the changes that distinguish tumors from normal tissue on the genomic level[76]. Initial approaches searching for mutations in cancer genes were successful and discovered, for example, mutations in the *BRAF* gene in melanoma, or mutations in the *PIK3CA* gene in colon cancer[85,86]. Strikingly, in lung cancer, the response to the EGFR inhibitors Erlotinib and Gefitinib could be associated with activating mutations in *EGFR,* giving first hints into the usefulness of sequencing technology for biomarker discovery[87-89]. Driven by the success of these first discoveries, the National Institutes of Health (NIH) launched the "Human Cancer Genome Project", first as a pilot project in 2006, and then the full project, now called TCGA, in 2009[74]. Also, in parallel, the ICGC, an international consortium consisting of researchers from 15 countries, was launched[73]. By defining the genomic landscape of cancer entities and identifying new cancer genes, biomarkers, and tumor subtypes within histological entities previously assumed to be homogenous, both projects revolutionized the way we think about cancer today and present a resource for cancer researchers worldwide[76,90].

1.2 Cancer genomics

Within the past 20 years, a new strategic cornerstone, in addition to the classical hypothesis testing, has emerged in oncology research: the unbiased genomic analysis of tumor tissue[76]. Initially, this new approach to cancer research was not generally endorsed and caused heated discussions within the scientific community[91,92]. Today, the value of cancer genomics has repeatedly been proven and now offers the option of personalized oncology through molecular characterization and stratification of individual tumors[76]. This rapid growth of the field would

not have been possible without tremendous technological and scientific advancement in the field of sequencing technologies[93].

1.2.1 First-generation sequencing

In 1953, Watson and Crick solved the three-dimensional structure of DNA based on crystallographic data from Franklin and Wilkins[94,95]. It took scientists until 1965 to be able to sequence the first nucleic acid, the alanine tRNA from *Saccharomyces cerevisiae*[96]. In 1972, using a modified sequencing technique by Fred Sanger[97], Walter Fiers and his team generated the first complete protein-coding sequence[98], and in 1976, the first complete genome of the bacteriophage MS2[99]. The purification of DNA genomes of bacteriophages allowed scientists to apply technologies from RNA studies to DNA research[100]. At first, only the ends of cohesive DNA overhangs were sequenced by measuring the incorporation of radio-labeled nucleotides through DNA polymerase one by one[101,102], but then this was extended to entire stretches of DNA by priming the DNA polymerase with specific oligonucleotides[103-105]. The separation by polynucleotide length via electrophoresis through polyacrylamide gels enabled two techniques to revolutionize the field, allowing now the sequencing of longer stretches of DNA[100]. First, the plus and minus system[106], and second, the chemical cleavage technique[107]. The plus and minus system uses a two-step polymerization. In the first step, a DNA strand with radiolabeled nucleotides is synthesized by extending a primer. In the second step, four paired plus and minus reactions are performed, whereby the plus reactions contain only one nucleotide and the minus reactions contain the three other nucleotides. By separating these fragments on polyacrylamide gels, the sequence can be inferred. Using this technique, the first DNA genome, that of the bacteriophage ϕX174, was sequenced[108]. The chemical cleavage technique uses a completely different approach in which radiolabeled cells are treated with specific chemical compounds that break the DNA at certain positions; the specific fragment sizes can then be detected by running them through polyacrylamide gels. Both techniques are now being described as first-generation DNA sequencing techniques[100]. However, shortly thereafter, with the development of the 'chain-termination' or dideoxy technique, Fred Sanger accomplished the largest breakthrough[109]. This technique is based on the use of dideoxynucleotides (ddNTPs), which, compared to deoxyribonucleotides (dNTPs), lack the 3′ hydroxyl group, and thus do not allow an extension of the DNA strand after incorporation of ddNTPs[109,110]. Here, the polymerase reaction is split into four reactions, each containing all four different dNTPs and a spike-in of only one type of ddNTP, which will randomly stop the polymerization reaction when being incorporated. Running all fragments on polyacrylamide gels allows for the reconstruction of the sequence. This technique was improved by replacing radiolabeled with fluorescence-labeled nucleotides, allowing the reaction to be performed in one tube, and by the use of improved

capillary electrophoresis[111-117]. This resulted in the development of the first commercial DNA sequencer[118]. These machines were able to sequence DNA fragments of almost 1kb[100]. Cloning, sequencing, and then overlapping the sequenced fragments, termed shotgun sequencing, was performed to analyze larger sequences[119,120]. The further improvement of the techniques, such as through better polymerases[121], enabled the development of a new generation of sequencers[122], which could sequence hundreds of fragments in parallel[123]. These machines were then deployed to generate the first draft of the human genome[82-84].

1.2.2 Second-generation sequencing

In addition to the classic Sanger sequencing, another sequencing technique called pyrosequencing emerged[100]. This technique measures pyrophosphate levels by transforming pyrophosphate, released upon the incorporation of a nucleotide into a DNA strand, into ATP, which is then used as a substrate for the luciferase enzyme, which produces light[124]. As each type of nucleotide is subsequently washed through the system in which the template DNA is fixed, a successful elongation of the DNA strand can be detected[125]. Advantages of this technology are the real-time measurement of nucleotide integration and the possibility of using natural nucleotides, while more than four to five repeats of the same nucleotide are problematic due to non-linearity of the light signal[126-128]. The first commercial machines produced by 454 Life Technologies greatly increased the throughput of DNA sequencing[129]. These machines used DNA libraries, generated by shearing the entire genome into small fragments, which were attached to DNA beads with adapters, and then subjected to a water-in-oil emulsion PCR (emPCR), where the PCR reaction takes place[130]. In an optimal scenario, only one DNA fragment would bind to a bead, and only one of these would be enclosed in one water droplet, in which only this one DNA fragment is amplified until it finally covers the entire bead[100]. Afterwards, each bead is placed in a single well of a picotiter reaction plate with approximately 1.6 million wells, while a charged couple device sensor beneath the wells monitors the pyrosequencing reaction[129]. However, the drastically higher throughput comes at a cost of shorter sequencing reads of about 400-500 base pairs (bp)[129]. This massively parallel sequencing technique allowed the sequencing of the entire human genome in a much faster time frame than that of Sanger sequencing[131,132].

Following the success of 454 Life Technologies, several new massively parallel sequencing technologies emerged[100]. The most successful technique is the Solexa method, later acquired by Illumina[133], now dominating the market in a near monopoly[134]. Instead of using the emPCR to amplify DNA fragments, the bridge amplification was introduced[133]: both ends of the DNA fragments are ligated to adapters, which are used to immobilize the fragments on a flow-cell with complementary sequences. The bridge amplification then relies on the fixated DNA

fragment "arching" between two anchors to amplify the fragments, generating clusters of over 1,000 clonal DNA fragments. The sequencing itself is also different: the DNA is denaturated, and primers complementary to the anchor, the polymerase enzyme, and four types of reversible dye terminator nucleotides are added. The introduction of the dye terminators in the strand produces a base-specific fluorescent signal, and only after an additional washing step is termination chemically reversed and then polymerization can continue. Due to the nature of the sequencing technique, it is possible to take into account either only the forward adapters, called single-end sequencing, or to take both into account, called paired-end sequencing. The latter is especially powerful with short sequencing reads because it gives an additional layer of information by stating how both reads relate to each other[100]. Initially, Illumina started with 50 bp sequencing reads, but now allows the sequencing of reads as long as 300 bp[93]. Due to the dominant position of this technology, concerns that systematic technological artifacts could be introduced have been voiced, and therefore, researchers are working on alternative techniques[93]. These technologies include SOLiD sequencing[135], Complete Genomics' 'DNA nanoballs' technique[136], and torrent sequencing[137]. In essence, the distinguishing feature of all second-generation sequencing technologies is that in all scenarios, DNA is sheared, amplified, and clustered, and then afterwards arrayed through alternating cycles of enzyme-driven biochemistry and imaging-based data acquisition[138].

1.2.3 Third-generation sequencing

There is an ongoing discussion about which characteristics define the third generation of sequencing, including single molecule sequencing, which therefore avoids PCR amplification steps of second-generation sequencing, or real-time sequencing, or just diverging from current technologies in any way[100,139-142]. The most widely-used third-generation sequencing technology is the single molecule real time (SMRT) platform from Pacific Biosciences[143-145], which has several advantages over current second-generation technologies, such as detection of modified bases[146] or the generation of extremely long reads, exceeding even 10 kb[142,143]. The technology is developing rapidly and will most likely continue to do so in the next few years, which will allow for less expensive and more accurate sequencing of normal as well as cancerous tissue.

1.2.4 Microarray technology

Since around 2000, the complete sequencing of the human genome has allowed for the design of genome-wide microarrays to detect changes in the landscape of nucleic acids of the entire genome[147]. High-density microarrays consist of oligonucleotides bound to a surface onto which

labeled complementary DNA or RNA fragments hybridize[147]. A prominent application is to detect abundances of messenger RNAs (mRNA) and to compare these between different tissues. In the context of cancer genomics, scientists have compared the transcriptomes of tumors of the same histological entities to define biologically and clinically distinct subtypes, for example for medulloblastoma (MB), a malignant childhood brain tumor[148]. However, the use of microarrays is not limited to detecting gene expression from RNA, but can also be used to analyze DNA[149], such as for the detection of single nucleotide polymorphisms (SNPs) in the human genome[150] (as in the completed Hap Map project[151]), or to measure alterations in methylation patterns[152], gene copy-number aberrations[153], RNA splicing[154], and for pathogen detection[155]. Although microarrays are more limited than unbiased next-generation sequencing, they offer distinct advantages in certain scenarios, because the data generated from microarrays are much smaller in data volume and also less complex and thus easier to handle compared to sequencing data, the generation of array data is faster, and arrays often have larger reference cohorts for comparative analyses[156].

1.3 Tumors in children and adolescents

A child born in the U.S. has a chance of 1 in 408 of developing cancer prior to the age of 15 years and a chance of 1 in 285 of being diagnosed with cancer prior to the age of 20 years[157]. Childhood (age 0-14) and adolescent (age 15-19) cancer diagnoses make up 1% of the overall cancer diagnoses[157], showing that childhood cancers are much more rare than adult cancers[2]. The most common cancer types in children are acute lymphoblastic leukemia (ALL) (26%), central nervous system (CNS) tumors (21%), neuroblastoma (7%), and non-Hodgkin lymphoma (NHL) (6%), while the four most common tumors diagnosed in adolescents are Hodgkin's lymphoma (HL) (15%), thyroid carcinoma (11%), brain and CNS tumors (10%), and testicular germ cell tumors (8%)[157]. These entities are not the ones typically seen in adults, but rather completely different diseases arising mostly in young patients[25].

Since the 1970s, the incidence rates for pediatric cancers have steadily increased with an annual rate of 0.6%[157] (Figure 2a, page 11) in the U.S. as well as in Europe[158]. Reasons for this remain unclear, but it could possibly be linked to better access to medical care as well as improved diagnosis and detection, without which children might have died from the complications of their cancer without an acknowledgement of the underlying cause[159]. The rise of the incidence of CNS tumors in the 1980s can for example be possibly explained by the introduction of magnetic resonance imaging (MRI) and stereotactic biopsies that have improved the diagnosis of the disease[160]. In contrast to the increased incidence rates, the mortality rates for childhood

and adolescent cancer patients have been steadily declining at an annual rate of 2.1% since 1975[157] (Figure 2b).

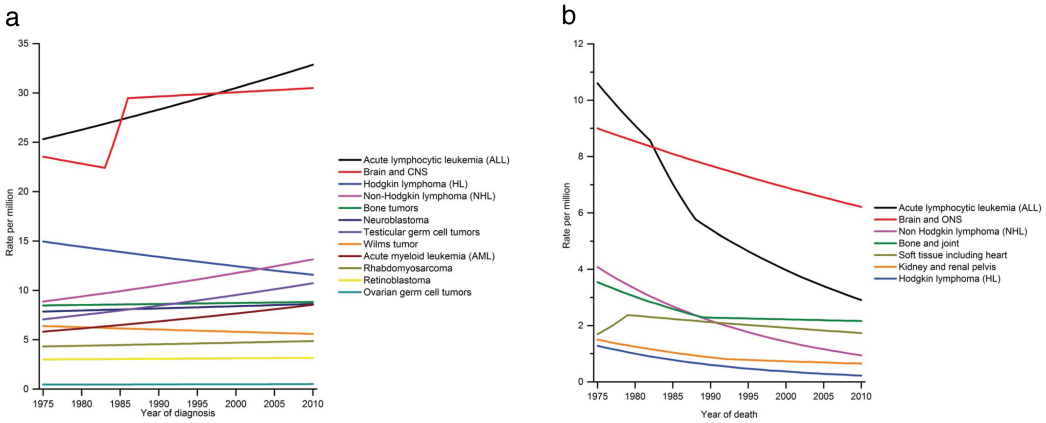

Figure 2: Incidence and mortality rates of pediatric cancers.
Trends in pediatric cancer (**a**) incidence and (**b**) mortality rates by site over time, birth to 19 years, 1975 to 2010 (modified from Ward *et al.*, 2014)[157].

Concordant with these findings, the 5-year survival rate of nearly all pediatric cancers has increased in this period[157]. Nevertheless, diagnosis and treatment have dramatic effects on the individual patient[161]. In 2009, 300,000 childhood cancer survivors lived in the U.S.[162]. To accommodate their specific needs, the Children's Oncology Group (COG) designed guidelines for the treating physicians that are based on the therapy the individual patient received[163]. Since 1994, the Childhood Cancer Survivor Study has systematically collected data on patients who survived five or more years after a diagnosis of cancer during childhood or adolescence[164], because in many cases clinical trials do not report on the long-term follow-up data of these patients[165]. The reported sequelae are widely spread[161]: Up to half of all patients may develop endocrinopathies, which can be defects of the hypothalamic-pituitary axis[166], thyroid[167,168] or gonades[166,169-172], or abnormalities of the glucose metabolism[173,174]. Cardiovascular disease-associated mortality is 7-fold higher in pediatric cancer survivors[175]; in particular survivors of leukemia, brain tumors, lymphoma, and rhabdomyosarcoma are at risk due to the type of treatment[175,176]. An increased pulmonary morbidity has also been reported due to treatment directly or indirectly targeting the lung, such as radiation or cyclophosphamide treatment[177]. Neurological sequelae, such as visual deficits, hearing loss, and motor, sensory, or coordination disorders, as well as seizures, are typically seen in survivors of CNS malignancies and can be induced by surgery, chemotherapy, and/or radiation[170,178]. The symptoms can occur during treatment or even years later[170,178]. Other long-term side effects include gastrointestinal toxicities[179], nephrotoxicity[180,181], bladder[182,183] or sexual dysfunction[182,184,185], osteopenia, and osteoporosis[186-189]. In addition, pediatric cancer survivors have a 15.2-fold higher risk of

developing a secondary malignancy compared to the normal population of developing a primary malignancy[190]. This can be ascribed to the intensive treatment regimens, such as chemotherapy and radiation, but also potentially due to the fact that a considerable proportion of young cancer patients may have cancer-predisposing genetic syndromes[161]. Thus, although around 80% of all childhood cancers can be cured[157], the drastic long-term side effects of current therapies highlight the necessity of developing alternative, less toxic therapies.

Compared to adult cancers, pediatric cancers do not have many preventable causes, such as smoking in lung cancer[157,191]. However, there are some established risk factors. In 1950, it was demonstrated that low doses of ionizing radiation on children *in utero* are associated with a higher risk of leukemias and other pediatric cancers[192]. Also, other kinds of radiation exposure early in life have been associated with a higher risk of developing cancer[193,194]. Furthermore, there are reports linking high or low birth weight[195-202] and also *in vitro* fertilization[203-205] to different types of cancers. The International Agency for Research on Cancer states that there is enough evidence to conclude that parental smoking increases the risk of hepatoblastoma for children, as well as some evidence that it is also associated with childhood leukemia[206]. In addition, there is minor evidence that maternal exposure to paint is linked to childhood leukemia[206]. In line with these few extrinsic factors is a recent pan-pediatric cancer study, which performed an analysis of mutational signatures on a cohort of 539 childhood tumors, and in which no signatures corresponding to typical cancerous substances were found[25]. This study, in concordance with previous observations, also determined a prevalence of probably cancer-predisposing germline variants in children with cancer to be about 6%[25,207], compared to a frequency of 3% in adults[208]. Overall, the lack of extrinsic risk factors as well as the similarity of some childhood cancer symptoms with some common childhood disease symptoms, makes an early detection very challenging[209]. It is also important to note that patients with hereditary cancer syndromes are a high-risk group for pediatric cancers and should be specifically monitored[210].

1.4 Pediatric brain tumors

Brain tumors are the leading cause of mortality in childhood after accidents, although they are only the second most common group of tumors in childhood after leukemias[157]. The definition of brain tumors includes only neoplasms that originate *de novo* from the CNS and not metastases deriving from other primary tumors, which, remarkably, are 5-10 times more common in adults than are primary brain tumors[211]. The clinical presentation of brain tumors varies based on tumor location, tumor growth rate, and patient age; while infants (0-3 years) often present with non-localizing symptoms, children older than three years may present

localizing findings more often, but many patients show only symptoms of intracranial pressure such as headache, ataxia, and morning vomiting[212]. Due to the non-specific symptoms of pediatric brain tumors, especially early on, the time between onsets of early symptoms to final diagnosis is even longer than in other childhood cancers[213]. MRI of the head as well as the spinal cord, with or without intravenous injection of a contrast agent, can then establish the diagnosis of a brain tumor[212]. In most cases, open resection is the first treatment choice, because it allows a reduction of the tumor size and, at the same time, gives access to tumor tissue in order to finalize the diagnosis[212]. The value of the open resection is illustrated by the dramatic impact of residual tumor volume after surgery on the prognosis of the patient[214-216]. The analysis of tumor tissue, acquired either through surgical resection or a biopsy, consists of a histopathological and if possible molecular evaluation and delivers the final diagnosis, which then guides the following therapy. The usual therapeutic concept after surgery consists of radiotherapy, followed by chemotherapy, whereby the intensity of the therapy can be adjusted based on the aggressiveness of the tumor[212].

For the past century, the classification of brain tumors has been largely based on the similarity of tumor cells to their presumed cell of origin, evaluated mostly by light microscopy, but also by immunohistochemical expression of lineage-associated proteins and ultrastructural characterization[217]. Using both conventional and molecular information, pathologists categorize tumors based on their aggressiveness into four grades, ranging from grade I (benign) to grade IV (very aggressive)[218]. Through the findings of cancer genomics in the field of brain tumors, it has become increasingly clear to the neuropathology and neurooncology community that genetic analysis can objectively refine diagnoses[219]. In 2016, this led to an update of the World Health Organization (WHO) classification of CNS tumors, which, for the first time, included genetic information such as mutation status or molecular subgroup information for some brain tumor types[218]. In the Central Brain Tumor Registry of the United States (CBTRUS) statistical report for infants and children, the most common brain tumors in children are gliomas (52.9%) and embryonal tumors (15.0%), which together account for 87.2% of the brain tumor-related deaths in this age group[220]. Remaining tumors include entities such as craniopharyngioma, tumors of the pineal region, germ cell tumors, tumors of the meninges, or unclassified tumors[220].

1.4.1 Pediatric glioma

Gliomas are a heterogeneous population of tumors that show morphological similarities to neuroglial cell types of the brain[221]. The glial compartments of the human brain consist of at least four distinct cellular populations: 1) microglia, simplified immunocompetent and phagocytic cells of the nervous system[222]; 2) astrocytes, the most abundant glial population[222],

whose main functions are to maintain the water and ion homeostasis and to contribute to the tripartite synapses and to blood brain barrier maintenance[223,224]; 3) oligodendrocytes, responsible for myelin production, insulation, and trophic support of axons[225]; and 4) the NG2 glial precursors of adult oligodendrocytes, which are considered to be an independent group due to additional characteristics, but which have an unknown function[222].

1.4.1.1 Pilocytic astrocytoma

Pilocytic astrocytomas (PA) are the most common gliomas in children (33.2% of all gliomas) and are classified as WHO grade I tumors with an overall 5-year survival rate of 97.1%[220,226]. PAs can occur anywhere in the brain, from the cerebellum (40%) to supratentorial locations (35%), the optic pathway and hypothalamus (11%), or the brain stem (9%)[227]. High-throughput sequencing analysis of large cohorts of PA has shown that these tumors are mostly a "single pathway" disease, as almost all tumors have mutations in the MAP kinase pathway[228,229], with the most prominent event being a fusion between *KIAA1549* and *BRAF*[230-235].

1.4.1.2 Pediatric high-grade glioma

Pediatric high-grade gliomas (HGGs), including tumors previously diagnosed as diffuse intrinsic pontine glioma, comprise WHO astrocytomas grades III and IV, and have a dismal overall 5-year survival rate of 28.4%[218,220,236]. It is important to acknowledge that HGGs also occur in adults, but molecularly, childhood and adult HGGs are very different[226,237,238]. One of the key discoveries highlighting the uniqueness of pediatric HGGs is the identification of specific histone mutations[239,240]. These mutually-exclusive mutations are found in the two histone genes H3.3 (*H3F3A*) and H3.1 (*HIST1H3B, HIST1H3C*), and result in an amino acid exchange from lysine-to-methionine in the functionally-important histone tail at position 27 (K27M; H3.3 and H3.1) and glycine-to-arginine or -valine at position 34 (G34R/V; only H3.3)[225,226]. As reviewed by Jones and Baker, K27M and G34R/V mutations were shown to define clinically and biologically distinct molecular subgroups of HGGs[238,241]. Intriguingly, both subgroups are specific to the anatomic location of tumors – K27M mutations now also define the group of diffuse midline gliomas and are observed mostly in tumors of the midline structures (78%) and the thalamus (40%)[238-245], while G34R/V mutations are restricted to tumors of the cerebral hemispheres (15%)[238-240,243,245-248]. In the updated WHO classification for CNS tumors, K27 histone mutations now also define the entity "diffuse midline glioma, H3 K27M-mutant", which includes tumors previously classified as diffuse intrinsic pontine glioma[218]. Histones, as part of the nucleosome, play a central role in controlling gene transcription via regulating the overall chromatin landscape[249]. In turn, histones can be

regulated by the cell through modifications of the histone tail[250], which has been shown to be especially important during normal development[251], stem cell maintenance[252], and differentiation[253]. The mutation of the K27 position in either H3.3 or H3.1 blocks the methylation of the histone at this position in a dominant negative manner by trapping the histone methyltransferase EZH2[254], which otherwise would induce compaction of the DNA, therefore reducing gene expression[255-257]. Overall, the lower levels of H3K27 trimethylation lead to a reprogramming of the epigenetic landscape of the cell[258-260]. Typical additional genetic events in H3.3 K27 HGGs include *TP53* mutations, *PDGFRA* amplifications, and *FGFR1* mutations in thalamic tumors, while H3.1 K27 gliomas often present with *ACVR1* rather than *TP53* mutations[242,244,245,247]. Clinically, patients with K27 mutant gliomas have an extremely poor prognosis, because the location of the tumor often makes them inoperable, and therefore two years after diagnosis nearly all patients will have succumbed to the disease, while in this context H3.1 patients tend to have a slightly better outcome compared to H3.3 patients[261]. G34R/V patients also have a poor prognosis with a median survival time of 24 months compared to 12 months for K27 patients, which reflects the difference between the prognosis of gliomas in the midline and gliomas in the cerebral hemispheres[241]. However, the effect of the G34R/V on histone function is less clear – G34R/V by itself is not a target of post-translational histone modification; it has been shown to diminish the trimethylation at the K36 position, but only on the mutant allele[254]. In contrast to H3K27 trimethylation, H3K36 trimethylation is associated with the activation of gene expression, alternative splicing, and DNA repair[262]. Further work showed the binding of the mutant histone to genes associated with cortical development and stem cell maintenance, and, interestingly, also to *MYCN*, which had already been shown to be able to induce glioblastoma in mice[246,263]. Secondary genetic hits in this subgroup of pediatric HGGs are often *ATRX* and *TP53* mutations[239,245].

It is important to note that 50% of pediatric HGGs do not harbor histone mutations and, therefore, do not fall into these well-established subgroups[236]. Fewer than 5% of childhood HGGs present with mutations in *IDH1/2*[238], which are probably the younger patients from a broad age distribution peaking around 40-45 years[264]. Methylation profiling on a cohort of the remaining population of H3 and IDH wild-type tumors showed that a considerable proportion of histologically classified glioblastoma cluster together with reference samples of low-grade gliomas (LGGs) or pleomorphic xanthoastrocytomas (PXAs)[265]. These samples shared clinical and molecular characteristics of their respective entities, pointing toward a misclassification through conventional histopathological evaluation. The LGG-like tumors showed a favorable 3-year overall survival rate of 91%, and a subset (4/13; 31%) of samples harbored the typical *BRAF* V600E mutation with an overall balanced genome[265]. The PXA-like tumors also harbored *BRAF* V600E mutations (13/27; 48%) and loss of the *CDKN2A/B* locus (8/27; 30%),

which is typical for PXA but not for LGGs, and had a still favorable 3-year overall survival rate of 70%[265]. Analysis of the now remaining *H3* and *IDH* wild-type HGGs resulted in three subgroups: MYCN (enriched for *MYCN* and *ID2* amplification), pedRTK1 (enriched for *PDGFRA* amplification), and pedRTK2 (enriched for *EGFR* amplification)[266]. Clinically, with regard to median survival rates, MYCN patients had the worst prognosis with 14 months, pedRTK2 patients the best prognosis with 44 months, and pedRTK1 patients an intermediate prognosis with 21 months[266].

To summarize, pediatric HGGs can now be grouped into the following biologically and clinically distinct subgroups: K27, G34, IDH, MYCN, pedRTK1, and pedRTK2 – excluding LGG-like and PXA-like HGG, which are, based on their clinical and molecular characteristics, probably actually lower grade lesions.

1.4.2 Ependymoma

Similarly to HGGs, ependymomas (EPNs) can occur in children as well as in adults[267]. EPNs make up 5.5% of all CNS malignancies in children (0-14 years)[220]. Ependymal tumors can occur both intracranially and in the spinal cord, whereby 90% of all tumors are located intracranially, with two thirds occurring in the posterior fossa (PF) and one third within the supratentorial part of the brain (ST)[268]. The overall 10-year survival rate for children is 63.8%[220]. Here, for many years, the only prognostic factor had been the extent of surgical resection[269], because even for very experienced neuropathologists histological grading of EPNs remains very challenging[218,270], especially regarding the distinction between WHO grade II and III anaplastic EPNs[271,272].

In 2015, Pajtler *et al.* classified 500 ependymal tumors across all age groups and locations using methylation profiling and identified nine distinct subgroups, three each per anatomical area, spine, PF, and ST, respectively[273]. Of the nine subgroups, only four were relevant for pediatric patients: YAP1 (ST), RELA (ST), PF A (PF), and PF B (PF)[273]. Interestingly, only two, the PFA and the RELA subgroups, showed a poor prognosis, with a 10-year overall survival rate of only 50% compared to 88%-100% for the remaining subgroups[273]. The first recurrent driver event found in EPNs was the *C11orf95-RELA* fusion[274], which was shown to match one of the methylation subgroups, termed ST-EPN-RELA[273]. RELA is the principal effector of NF-κB[275,276], inducing a pathway activation in these tumors[274]. Thus far, the RELA subgroup is the only molecular subgroup that has been included in the updated WHO classification[218], although the overall molecular classification outperformed conventional histopathological grading in prognostication[273]. The other pediatric supratentorial EPN subgroup is driven by *YAP1* fusions and therefore termed ST-EPN-YAP1[273]. YAP1 is the core

transcription factor of the Hippo signaling pathway[277]. The driver events for the two intracranial subgroups, PF A and PF B, are currently unknown. However, chromosomal gain of chromosome 1q, which has been associated with a poor prognosis in EPN[278], was shown to have an impact on overall survival in PF A EPN and on progression free survival in only the PF A and PF B subgroups, but not in the RELA subgroup[277].

1.4.3 Embryonal tumors

After gliomas, embryonal tumors are the most common tumors in childhood and are comprised of a variety of different tumor entities[220]. Embryonal tumors are described in the WHO classification scheme as "undifferentiated small round cell tumors with divergent patterns of differentiation"[217,218,279]. Overall, they become less frequent the older the patient population gets: 24.9% in patients younger than one year, 20.2% from 1-4 years, 14.8% from 5-9 years, and 8.3% from 10-14 years[220]. Due to their aggressiveness, all embryonal tumors are classified as WHO grade IV lesions[218,270]. In 2016, with the updated WHO classification of brain tumors, the subclassification of embryonal tumors underwent substantial changes, defining new entities and partly removing old classifications[218].

1.4.3.1 Medulloblastoma

61.9% of all childhood embryonal tumors are medulloblastomas (MBs), a highly malignant tumor that originates in the cerebellum and is responsible for 14.3% of brain-tumor related deaths in this age group[220]. Although all MBs are classified as highly aggressive WHO grade IV lesions with an overall 10-year survival of 63%[280], the prognosis varies significantly with regard to molecular subtype[148,281-285]. Historically, MBs have been divided into five different histological subtypes: classic, desmoplastic nodular (D/N), MB with extensive nodularity (MBEN), anaplastic, and large cell[217,286]. Molecularly, the consensus is that MBs can be classified into four molecular subgroups with distinct biological and clinical characteristics and which are termed WNT, SHH, Group 3, and Group 4[148,281-285] (Figure 3, page 18). The molecular subgrouping has been included into the recent updated WHO classification of brain tumors, and, if possible, pathologists now integrate standard histopathological and molecular analyses to determine diagnoses[218].

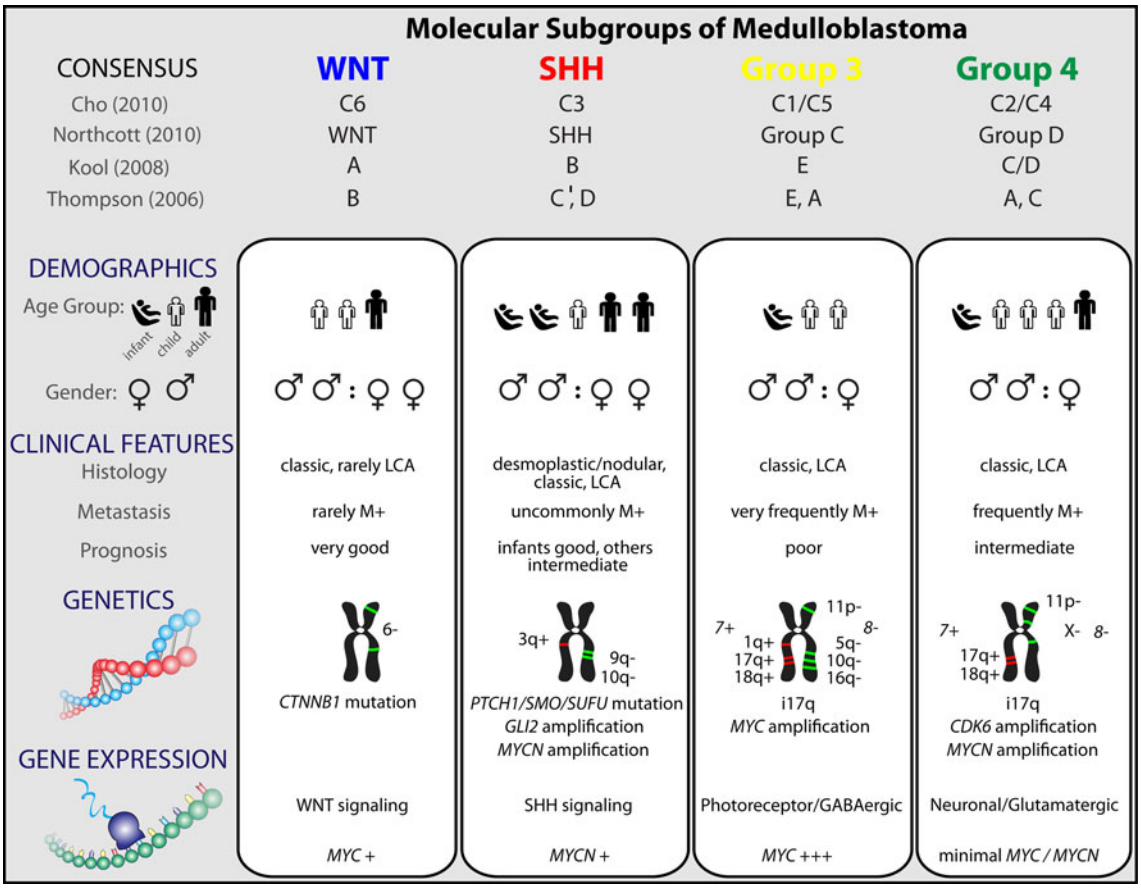

Figure 3: Molecular subgroups of medulloblastoma.
Overview of the demographics, clinical features, genetics, and gene expression of the molecular subgroups of medulloblastoma (from Taylor *et al.*, 2012)[148].

WNT medulloblastoma is the least common subtype of MB with an overall frequency of 10% of diagnoses[285,287] but with the best prognosis, with >95% of patients surviving the disease[288,289]. Typically, these tumors occur in children older than three years and are infrequently metastatic[285]. More than 90% of WNT MBs harbor mutations in the *CTNNB1* gene[290-294]. The mutation in the *CTNNB1* gene, which encodes for β-catenin, a central component of the WNT signaling pathway, makes the mutant protein resistant to degradation, which allows unlimited signaling[295]. Most of the remaining cases of WNT MBs without *CTNNB1* mutation can be explained by germline *APC* mutations[294]. Other recurrent somatic mutations in these tumors affect *TP53, DDX3X,* and genes associated with the SWI/SNF nucleosome remodeling complex[294]. With the exception of monosomy 6, which is found in nearly all WNT MBs, these tumors present with a mostly balanced genome[285].

SHH medulloblastoma account for 30% of all MB diagnoses[296]. The 5-year overall survival is about 75% for patients treated with the current standard therapy, but can vary dramatically between patient subpopulations within this molecular subgroup[148,286,297,298]. Nearly all tumors harbor mutations at various stages of the SHH signaling cascade[290,292-294,299]. *PTCH1*, *SMO*, and

SUFU alterations occur mutually exclusively, while *MYCN* and *GLI2* amplifications often co-occur, but also again mutually exclusive from *PTCH1*, *SMO* or *SUFU* mutations[289,291-293,298]. Remarkably, SHH tumors show a bimodal age distribution, being more common in infants (0-3 years) and adults (18+ years), and more rare in children (4-17 years)[299]. This age distribution also correlates with different SHH pathway mutations; while *PTCH1* events are common in all age groups (about 50%), *SMO* mutations are strongly enriched in adult patients, *SUFU* events in infants, and *MYCN*/*GLI2* amplifications always co-occur with *TP53* mutations in about 50% of the pediatric cases[299]. These children with *MYCN*/*GLI2*/*TP53* events have an overall 5-year survival rate of only 41% and the co-occurring *TP53* mutation is in 56% of the cases found in the germline (Li-Fraumeni Syndrome)[285,298-302]. Overall, tumors in these patients harbor an unbalanced genome, even showing chromothripsis, an event in which an entire chromosome is shattered[303]. The specific characteristics of these patients and the large differences in outcome led the WHO to introduce *TP53*-wild-type and *TP53*-mutant SHH MB as separate categories in order to clearly define these patients[218]. SHH MBs with pathway lesions in *SMO* and *PTCH1* are expected to respond to SMO inhibitors[299], and first clinical trial results are promising but highlight the risk of resistance development under monotherapy[304-307]. Secondary hits in SHH MBs, such as *TERT* promoter mutations that drive *TERT* promoter activation, also vary by age group and are seen nearly exclusively in adult patients[299,308]. Compared to other MB subgroups, there is an overrepresentation of somatic alterations targeting the histone acetyltransferase complexes, but the role of these mutations in the disease is still poorly defined[294].

Group 3 medulloblastoma, together with *TP53*-mutant SHH MB, is the subgroup with the worst prognosis of all four subgroups, and accounts for 25% of all MB diagnoses[148,285]. The poor prognosis is largely dependent on the enrichment of adverse prognostic factors in this subgroup. Patients are typically younger and tumors are often metastatic at diagnosis, present with a large cell and/or anaplastic (LCA) histology, and in 17% of the cases have a *MYC* amplification[148,285,286,291,294]. Intriguingly, in this subgroup there is a male predominance (male/female ratio 2:1) and patients are typically infants or children, rarely adolescents, and never adults[286,297]. Initial sequencing studies found recurrent events only in fewer than 50% of the cases[281,290,292,293], but a recent landmark paper including the analysis of 500 tumors was able to push the explainable cases to 76% through the discovery of less frequent, but still recurrent events[294]. High-level amplifications of *MYC* are strongly enriched in Group 3 MBs and nearly all cases present with at least elevated *MYC* expression[283,284,291]. Other recurrent events include mutations in *SMARCA4* (9%), *KBTBD4* (6%), *CTDNEP1* (5%), and *KMT2D* (5%) or focal amplifications of *OTX2* (3%)[281,290,292-294]. Recently, a novel mechanism of oncogene activation, termed enhancer hijacking, was discovered in MB: Through structural rearrangements, an enhancer is moved to the proximity of the proto-oncogene *GFI1/1B*, thereby activating it as an

oncogene[309]. Activation of both *GFI1* and *GFI1B* occurs in both Group 3 (*GFI1B*: 11%, *GFI1*: 4%) and Group 4 MBs (*GFI1B*: 9%, *GFI1*: 3%) and are mutually exclusive[294,309]. Furthermore, pathway enrichment analysis on the variety of recurrent genetic events in Group 3 identified an overrepresentation of genes involved in Notch and TGFβ signaling[294]. However, the involvement of these pathways in Group 3 MB oncogenesis has so far not been proven on a functional level.

The most prevalent MB subgroup, with 35% of diagnoses, is Group 4 MB[285]. Overall, patients with Group 4 MB are seen across all age groups, again with a higher male prevalence (male/female ratio 3:1), and show an intermediate outcome[148]. The underlying biology behind these tumors is still poorly understood[286,297]. Similar to Group 3 MBs, the collection of a 500 tumor landscape cohort could, through detection of recurrent events, greatly increase the number of explainable cases from 30% in 2012[281,290,292,293] to now 82%[294]. The most common alteration is another enhancer hijacking event, which activates *PRDM6* in 17% of Group 4 cases[294]. Interestingly, the tandem duplication in the *SNCAIP* gene leading to the activation of *PRDM6* was already discovered in 2012, but misinterpreted as being connected to *SNCAIP* itself rather than *PRDM6*[310]. Other events include activation of *GFI1B* (9%), mutations in *KDM6A* (7%), *ZMYM3* (6%), *KMT2SC* (6%), and *KBTBD4* (6%), as well as amplifications of *OTX2* (6%) and *MYCN* (6%)[267,276,278-280]. Genes associated with chromatin modifications are enriched among this multitude of recurrent events[294]. Cytogenetically, an isochromosome 17, a replacement of the short arm of the chromosome with another copy of the long arm, is very often found in Group 4 MBs, and female patients often lose one copy of the X chromosome[286,291].

Although additional heterogeneity within the MB subgroups was already appreciated in the 2012 MB consensus grouping[148], it was 2017 before this heterogeneity was further investigated. To this date, three different further subgroupings have been proposed: 1) Heidelberg subgrouping based on pairwise sample similarities using *t*-distributed stochastic neighbor embedding (t-SNE) of methylation array data[294], 2) Toronto subgrouping based on similarity network fusion of methylation profiling and expression data[311], and 3) Newcastle subgrouping based on non-negative matrix factorization (NMF) of methylation profiling data integrated with clinicopathological data[312]. The main discrepancy between these subgroupings is apparent in the distinction between Group 3 and Group 4 MBs. While the Heidelberg subgrouping sees overlaps between the classic Group 3 and Group 4 MB groups, defining subtypes between the traditional subgroups, Toronto and Newcastle strictly keep this separation and provide further subgrouping only within the former structure[294,311,312]. Between these three proposals, a consensus will shortly emerge, further improving the biological and clinical segregation of MBs.

1.4.3.2 Atypical teratoid/rhabdoid tumor

The second most prevalent embryonal tumors are atypical teratoid/rhabdoid tumors (ATRTs), which make up 15% of all embryonal tumors and about 2% of all brain tumors in children, but 10-20% of all brain tumors in children younger than three years[220,313-315]. ATRT are most common in infants and, therefore, 90% of them occur prior to the age of three[316]. After HGGs and MBs, ATRTs are responsible for most pediatric brain tumor-associated deaths (9.8%)[220]. The overall survival rate of patients diagnosed with an ATRT is very poor, with a median of only 17 months[317]. The molecular hallmark of ATRTs, present in >95% of the cases, is the inactivation/loss of the *SMARCB1* protein by mutation, chromosomal loss, or epigenetic deactivation[318,319]. This information is used in the clinical setting for routine diagnosis by performing immunohistochemistry (IHC) to confirm the loss of the SMARCB1 protein as a specific marker[317]. In the rare cases where *SMARCB1* has been maintained (<5%), loss of *SMARCA4* was detected[320]. Both *SMARCB1* and *SMARCA4* are core components of the SWI/SNF chromatin remodeling complex[321]. Germline defects in either of these two genes were estimated to affect about a third of all rhabdoid tumor patients; these result in a condition called rhabdoid tumor predisposition syndrome[322]. Recently, there were two reports about further subgrouping of ATRTs. First, Johann *et al*. described three different epigenetic subgroups, termed TYR, SHH, and MYC, each of which differs in gene expression, type of *SMARCB1* deactivation, tumor location, and epigenetic landscape[316]. Second, Torchia *et al.* also described three different subgroups, which they termed Group 1, Group 2A and Group 2B, driven by transcriptional networks around *NOTCH*, *BMP*, and *PDGFRB*, with distinct clinic-pathological features[323]. Due to the description of distinct core signal pathways in both publications, a meta-analysis will be necessary to work out the overlap between the two studies. Initial analyses of these meta-analyses indicate that both studies identified the same three subgroups, respectively, Group 1/SHH, Group 2A/TYR, and Group 2B/MYC (Johann *et al.*, unpublished).

1.4.3.3 Embryonal tumor with multilayered rosettes

The understanding of the remaining embryonal tumors was significantly revamped in the recent update to the WHO classification, in which the term “primitive neuroectodermal tumor” (PNET), covering a variety of histological appearances, was removed[218]. This was largely driven by the discovery that many of the rare PNETs harbor an amplification of the C19MC region on chromosome 19 (19q13.42)[324,325]. This molecular alteration is typically seen in lesions previously known as ETANTR (embryonal tumors with abundant neuropil and true rosettes), in ependymoblastomas, and in medulloepitheliomas, which therefore had already

been proposed to be one molecular entity (except for medulloepitheliomas that occur in the eye)[325]. Accordingly, the updated WHO classification now defines all tumors with the C19MC amplification as "embryonal tumor with multilayered rosettes (ETMR), C19MC-altered", and tumors with matching histology but without the amplification as "ETMR, NOS"[218]. ETMR patients are typically younger than four years old and the prognosis is very poor, with a 5-year overall survival rate of near 0%[326]. The amplification of the C19MC region leads to the overexpression of the 46 miRNAs encoded in this cluster[327-329], which up-regulate *DNMT3B*[330], a DNA methyltransferase playing a role in early development[331,332]. Interestingly, the amplification of the C19MC region generates a fusion of the miRNA cluster and *TTYH1*, which is usually expressed in later development; this allows the expression of early brain development miRNAs in later stages of development, keeping the cells trapped in the developmental stage, leading to the formation of a tumor[330].

1.4.3.4 Embryonal tumor, not otherwise specified (NOS)

Other remaining embryonal tumors that previously were characterized as primitive neuroectodermal tumors of the CNS (CNS-PNETs) are now placed in a catch-all category termed "CNS embryonal tumor, NOS"[218]. However, the diagnosis of a CNS-PNET is challenging due to lack of molecular markers and histological overlap with other entities[218,270,333]. In a landmark study, Sturm *et al.* used DNA methylation profiling to molecularly classify tumors that were previously histologically classified as CNS PNETs[333]. In this study it was shown that many of these tumors could be classified into known and distinct histopathological and molecular categories[333]. Within the tumors that did not fall into known histopathological and molecular entities, four new distinct molecular subgroups were identified and were termed "CNS neuroblastoma with FOXR2 activation" (CNS, NB FOXR2), "high-grade neuroepithelial tumor with MN1 fusion" (HGNET, MN1), "high-grade neuroepithelial tumor with BCOR alteration" (HGNET, BCOR), and "Ewing family tumor with CIC fusion" (EFT, CIC). These four new molecular entities were not easily recognizable by histopathological appearance and in fact comprised several different histological diagnoses including glioblastoma and ependymoma among others, but each of the groups harbored characteristic recurrent genetic events[333]. Still, a subset of these histologically diagnosed CNS-PNETs (~15%), which probably belong to very rare subgroups still underrepresented in the current cohort, remained unclassifiable.

1.4.4 Molecular Neuropathology 2.0

DNA methylation profiles have been widely used for the subclassification of brain tumors[238,273,316,325,333-341] and as presented in Sturm *et al.*, they can also be used to discriminate

between distinct entities[333]. A very recent publication by Capper *et al.* transferred these findings into the clinical setting by generating methylation profiles of almost all WHO brain tumor entities (2801 profiles, at least 8 per group), creating a methylation landscape across 82 methylation-based tumor classes, matching these to the reference diagnosis, and, with this reference cohort, also developing a classifier algorithm (available online at http://www.molecularneuropathology.org) to automatically classify new diagnostic samples[342]. In routine clinical practice, in 12% of the cases, the diagnosis based on standard methods was changed based upon the methylation classifier results, dramatically impacting clinical decision-making[342]. A clinical trial, called "Molecular Neuropathology 2.0", objectively determining the benefits and limitations of methylation profiling to refine diagnoses for all diagnosed pediatric brain tumors, is currently ongoing in Germany (http://www.kitz-heidelberg.de/molecular-diagnostics).

1.4.5 Precision medicine for pediatric brain tumors

Initially, the term precision medicine was limited to the identification of the optimal treatment regimen for a subgroup of patients, but now includes many more applications such as the de-escalation of treatment, preventive interventions, or targeted therapy, all guided by molecular data[343]. Particularly, novel targeted agents are of high interest, because they promise both an increase in treatment efficacy, especially for diseases with still-poor prognosis, and a decrease of the short- and long-term toxicities usually associated with conventional therapy[344]. These targeted agents inhibit only specific interactions in the cell and therefore are effective only in tumors that depend on these specific biochemical conditions[345]. In this context, a biomarker is "any substance or biological structure that can be measured in the human body and may influence, explain or predict the incidence or outcome of disease"[346], and is much more important, because only a subset of patients will benefit from the targeted agent[343,345]. This principle, which is both an opportunity and also a challenge, can be illustrated by the development of targeted therapy against EGFR for non-small cell lung cancer (NSCLC)[345]. Gefitinib, an EGFR inhibitor, showed promising initial clinical results and in some patients, even caused dramatic responses[347]. However, in a subsequent Phase III clinical trial, the substance failed to show the clinical benefit when added to standard chemotherapy for advanced NSCLC[348,349]. Only after it was ascertained that activating *EGFR* mutations are important in defining a patient subpopulation that will likely respond to the therapy, could it be shown that patients benefit from the treatment[87,350]. However, due to the evolutionary nature of tumors, there is always the chance of developing resistance to a particular targeted agent, e.g. in this case an *EGFR* T790M mutation[351].

In pediatric oncology, large-scale sequencing efforts have identified a multitude of potential new therapeutic options for targeted agents[352-354]. In order to translate these findings into the clinical setting, several clinical sequencing projects have been launched to molecularly profile patients, and in the end report on potential druggable alterations in the tumors, including INFORM[355], MATCH[356,357], and MAPPYACTS[358], which all focus on relapsed and metastatic tumors, but have started to include more and more primary diagnoses for which no curative therapy is available. In this context, there are two challenges: First, the turnaround time of the analysis may not be longer than four weeks so that it can still be able to influence clinical decision making, and second, genetic events detected in the patients must be druggable[355]. Furthermore, druggable events must be prioritized and evaluated in the context of other genetic events and of the disease[359]. For example, V600E *BRAF* mutations indicate a likely response to *BRAF* targeted therapies in melanoma[360], but in colorectal cancer, the same mutation is associated with only a limited response[361]. In this context, pediatric oncology faces on the one hand the challenge of low patient numbers, which makes it difficult to run conclusive clinical trials, which are necessary to understand in which context a druggable lesion is a good target and in which not, but on the other hand the opportunity of lower genetic complexity, which makes it easier to understand dependencies[353].

1.5 Preclinical modeling of cancer

Currently, especially in adult oncology, there are many therapeutic and diagnostic options under clinical investigation, such as the targeted agents described previously[362-364]. Therefore, the current limitation in improving patient care may not be due to limited options of potentially effective therapies, but rather a lack of preclinical models that can link and validate with precision the therapeutic response to diagnostic parameters in order to adequately guide clinical trials[365]. Preclinical models are of particular importance in rare diseases, including all pediatric brain tumors, where human trials that compare two treatment arms may take more than a decade to complete[366]. At this rate, it would take unacceptably long to evaluate novel therapeutics across multiple distinct molecular subgroups of a disease. In an era precision oncology, preclinical data are especially needed, not only to find new therapeutic targets, but also to validate already-known targets in a disease-specific context.

1.5.1 Conventional cancer cell lines

Since the 1970s, human cancer models have been used for screening approaches during drug development, following an initial period in which drugs were screened in rapidly-growing murine models[367]. Since then, the methodology and systematic approaches for preclinically

evaluating novel anti-cancer agents *in vitro* and *in vivo* have been established by several studies[368,369]. So far, the best-characterized collection of preclinical model systems is the NCI-60 cancer cell line panel, a collection of human cancer cell lines, which is utilized primarily for *in vitro* high-throughput screening of novel drug candidates[370]. These cancer cell lines were derived from human patient material and have been adapted to grow indefinitely in artificial *in vitro* cancer cell culture conditions, and are, as subcutaneous xenografts in immunodeficient mice, the most commonly used *in vivo* preclinical oncology platform[367]. While these conventional cell lines are convenient and easy to use, they also have three major drawbacks. First, it has been shown that they are not very predictive for certain entities, and are prone to reveal unspecific cytotoxic or cytostatic effects[371]. This is reflected in the low Food and Drug Administration (FDA) approval rate of 5-7% for targeted therapeutics[372]. Second, the process of generating cell lines artificially introduces major changes into the biological properties of the tumor material, including alterations in the genome or in the phenotypic behavior of cells, or even causing loss of cell populations[373-375]. This suggests that these induced biological alterations are responsible for this method's poor clinical predictive ability. Third, cell lines can usually be established only from very aggressive tumors, and therefore, are not representative of the full spectrum of intertumoral heterogeneity as seen in the clinical setting[367]. Still, cancer cell lines, and especially their subcutaneous xenografts, are valuable for identifying non-targeted cytotoxic therapeutics, for the initial assessment of drug toxicity[376], for analyzing drug resistance[377], and for screening for potential drug candidates prior to validation in more representative models[365]. Improved *in vitro* techniques are currently being developed, in particular the organoid technique, a three dimensional *in vitro* culture based on culture conditions of healthy cells, which has proven to be successful in several tumor entities while preserving molecular fidelity and being able to grow organoids with a very high success rate[378].

1.5.2 *In vivo* models of cancer

More advanced preclinical model systems in oncology essentially consist of genetically engineered mouse models (GEMMs) and of patient-derived tumor xenografts (PDX)[367].

1.5.2.1 Genetically engineered mouse models

GEMMs provide the best representation of tumor development, since tumors develop from an initial lesion and interact with stroma within an intact immune system, but have the drawback of modeling the diseases in a foreign species and in many models not reflecting intratumoral heterogeneity[365]. Within the field, there are several different techniques with varying advantages and disadvantages, ranging from the classical germline model with an introduced

oncogene, to germline variants with a modification only in certain cell populations and/or at a certain time point, or even to somatic models in which, for example, oncogenes are introduced into the somatic cells of adult mice in order to induce tumor formation[365].

1.5.2.2 Patient-derived xenografts

PDX are the only mouse models which directly mirror the constellation of drug targets found in patients[365]. As early as the 1980s, it was shown that the response of PDX models to chemotherapy highly correlated to the response of the individual patient in the clinic[379-381]. Due to the various advantages of this system when compared to other preclinical systems, PDX models have become a major research interest for various tumor types, even becoming one of the preferred preclinical model for oncology drug development in both industry and academics[367,382-384].

Generating PDX models from fresh specimens of solid human tumors from a biopsy or surgery is an established method, which, in its conventional application, involves the subcutaneous transplantation of intact tissue pieces into the dorsal region of immunodeficient mice[367,382,383,385,386]. When the tumor reaches a critical size, it is re-transplanted into the next generation of mice, a process called serial transplantation[365]. However, it is also possible to generate PDX from fluids containing tumor cells, such as circulating tumor cells from the blood, cerebrospinal fluid or pleural effusions[387-389]. In addition to the conventional subcutaneous transplantation, it is also possible to transplant the tumor material into the same mouse organ as the original human tumor, termed orthotopic transplantation, which is more challenging technically and in most cancer types requires expensive imaging techniques in order to monitor responses in preclinical experiments[365,367]. Based on the injection location, it may also be necessary to dissociate the tumor material into a single-cell suspension. However, so-called patient-derived orthotopic xenograft (PDOX) models also offer distinct advantages compared to the conventional PDX. First, it has been known since the 1990s that PDOX are a better model for tumor metastasis than conventional PDX, because these rarely metastasize[390,391]. Second, the tumor location and microenvironment can influence therapy response[392,393]. Third, orthotopic xenografting increases tumor take rates[367,394] and allows the exclusive growth of certain tumor types in mice, such as estrogen receptor positive (ER^+) breast cancer without the external supplementation of hormones[395]. While the supplementation of estradiol pellets increased the engraftment rates of ER^+ PDX from 2.6% to 21.4%[386], the engraftment in the orthotopic location of the milk ducts of the breast could induce tumors in eleven out of eleven cases[395].

In general, engraftment rate and tumor growth vary greatly between various tumor entities but are also dependent on other factors, such as the quality and amount of material used, the mouse strain, or the lag time from sampling to transplantation of the human material[365,367,382,386]. However, engraftment rates also seem to correlate with the clinical aggressiveness of the disease, which is highlighted by intra-entity comparisons in breast[396,397] and in lung cancer[398] or the higher engraftment of metastases compared to primary tumors[399,400]. Most research groups use the more severely immunodeficient mouse strains, such as NOD/SCID or NOD/SCID/IL2Rɣ (NSG), because they are assumed to have the best engraftment rates[367], and a systematic comparison of NOD/SCID and NSG yielded similar take rates[386]. The necessity of using immunocompromised host mice comes at the price of losing the interaction of tumor and immune system in the PDX, which may be detrimental in tumors that normally need to actively escape from the immune system[401]. Therefore, it is not possible with PDX to assess the effects of the immune system on treatment regimens[402], or to test novel therapies attempting to modulate the immune system, such as immune checkpoint inhibitors[365,403]. Currently, there are three technologies that introduce the human immune system into immunodeficient mice in order to overcome this limitation: 1) The Hu-PBL-SCID model, which is created by injecting human peripheral blood leukocytes; 2) the Hu-SRC-SCID model, generated by intravenous or intrafemoral injection of human SCID repopulating cells; and 3) the BLT model established by transplanting human fetal liver and thymus under the kidney capsule and the intravenous injection of autologous fetal liver HSCs[404-406]. As reviewed by Welsh *et al.*[406], each of these techniques have distinct advantages and disadvantages, but all share the challenges high costs, technical variability, limited availability of human material from transplantation, and the highly technical complexity that severely limits the use of these techniques in PDX establishment and preclinical testing[365].

The higher value of PDX compared the use of conventional cell lines is based on the hypothesis that PDX models are a better preclinical model by being reflective of both the biology of the human disease, including inter- and intratumoral heterogeneity, and the clinical outcome. Both aspects have been evaluated intensively in the past[367]. Whether the biology of the human tumor is still preserved is evaluated by the comparison of the initial human tumor to the PDX, using various techniques. From the histopathological perspective, PDX models retain the core features of the originating primary tumor, including tumor-specific subcellular features evaluated by electron microscopy[386,396,397,400,407-411]. However, it must be stated that the human stroma is quickly replaced by its mouse counterpart[367,396,397,412]. Also, on the genomic and gene expression level, PDX models were shown to faithfully reflect the human disease[396,397,400,407-411,413-417]. Differences on the expression level can be explained mostly by the lack of human stroma in the PDX[408,410,414]. Therefore, PDX models have been used recently for the purification

of human tumor cells in order to improve gene expression-based classification of colorectal cancers[418]. In next-generation sequencing experiments with patient-derived xenografts, the mouse contamination can cause false-positive events, which must be removed by, for example, either a black list (for mutations only)[417] or by aligning the sequencing reads to the mouse and the human genome[397,419,420]. Recently, several reports have confirmed that PDX maintain clonal heterogeneity while continuously evolving, but some cases show more drastic clonal outgrowth events, such as minor clones taking over in the PDX, or clonal populations getting lost in the PDX[397,411,417,421]. The question of whether this continuous evolution also occurs in human patients is still not completely understood. One study that dissected a trio of primary tumor, derived xenograft, and matching brain metastasis showed that additional mutations found in the metastasis were also detected in the xenograft, highlighting a similar path of the evolution in the patient as in the PDX[422]. Another study pointing in the direction of a similar evolution in PDX as in patients showed that in sarcoma PDX, newly acquired focal amplifications are also typically found in sarcomas in patients[423]. Still, overall, PDX models have been shown to be phenotypically stable on the histopathologic and genomic level over multiple passages, which is highlighted in several studies comparing various passages[386,396,397,400,407,409-411,414,416,419], and also on the level of drug response[410,413]. Recently, in contrast with these previous findings, Ben-David *et al.* analyzed the copy number dynamics of 1,110 PDX and stated that the evolution of the copy number alterations is significantly different in PDX compared to tumor evolution in humans – hinting toward mouse-specific evolutionary pressure[424].

Correlation of results of preclinical testing in PDX with the actual clinical outcome is another way of evaluating the fidelity of PDX[367]. On the one hand, PDX preclinical trials can be compared to actual clinical trials, and on the other hand, PDX established from an individual patient can be compared on a one-to-one basis with the clinical behavior of the patient by trying to mirror the treatment regimen. It should be noted that direct comparisons of preclinical data to clinical data are challenging due to the different response criteria used[367]. However, overall there is a remarkable similarity between the activity of substances used in the clinic and similar preclinical experiments in PDX[367]. For example, a high correlation could be found for both Cetuximab in colorectal cancer models and Gemcitabine in pancreatic ductal adenocarcinoma models in the respective clinical trials[409,414,425]. Recently, a systematic approach, called the PDX Clinical Trial (PCT), was established in order to mimic clinic trials in PDX even more closely[419,426]. In this approach, instead of testing multiple PDX, each with a vehicle group versus a treatment group, only one animal per PDX model is treated with the testing agent and evaluated based on a response to therapy prior to treatment start instead of comparing it to a vehicle control. The use of only one animal is sufficient because the classification of a model into a response group based on mice was in 95% of the cases similar to the response of the

majority of animals[419]. However, in order to be successful, 29-45 PDX models per tumor type needed to be tested with this new technique[419]. Using this method, clinical observations of responses to BRAF inhibitors in melanoma[427,428], as well as of overcoming insensitivity to BRAF inhibition by a combination of BRAF inhibitors and MEK inhibitors[429,430], could be repeated in PDX models[419]. Another example is the discovery of combination therapies of CDK4/6 inhibitors with other targeted therapies that were missed in an *in vitro* cell line screen[419]. This new approach may be able to completely replace *in vitro* approaches in certain aspects of research, because it makes it feasible to get meaningful populations based on PDX data with many fewer animals than the conventional approach.

Data comparing the individual PDX donor patient's response with the response to conventional anticancer agents in the matching PDX have so far been impressive[386,407,408,425]. Recent work by Izumchenko *et al.* showed a systematic comparison for the first time[431]. In 127 individual treatment comparisons in 92 patients with a variety of solid tumors, 87% of the drug responses were concordant between patient and the matching PDX[431]. In the next step, using a PDX model in a concept known as co-clinical trial to predict the sensitivity of agents in the patient by testing in the matching PDX, termed avatar in this context, shows a high predictive power[432], but is very challenging to perform due to high costs, logistic challenges, and the difficulty of performing the preclinical testing in time[433].

Overall, many prior data described thus far highlight the fidelity of PDX models on various levels and make them superb tools for performing biomarker testing, understanding resistance mechanisms, and even predicting therapy success in a co-clinical trial format. Nearly all applications are based on large cohorts of PDX models reflecting the heterogeneity seen in the clinic, as highlighted by studies characterizing PDX cohorts in various entities such as leukemia[434], breast cancer[397], colorectal cancer[435], or pediatric solid tumors by using extensive molecular profiling[411]. These studies can be used as a resource to perform population-based studies in these PDX, but also to specifically select models with certain genetic alterations for a particular scientific question of basic biology. To improve the annotation of PDX models and to make them usable for other researchers, a consortium of PDX experts have now published PDX Minimal Information, which gives researchers guidelines for minimum reporting requirements when publishing a new PDX[436]. This will allow the funneling of many PDX cohorts, which are now mostly divided among entities and laboratories, into one single database thus becoming a shared resource.

1.6 Aim of the study

Pediatric brain tumors are devastating diseases, as survivors often suffer from the long-term side effects of conventional therapies. In the past several years, genomic profiling of these tumors has established a new classification system of these tumors and has also identified novel genetic alterations that may be druggable using new targeted therapeutics. However, due to the rarity of pediatric brain tumors, clinical trials take a long time to complete, so that not many new therapeutic agents can be evaluated within a reasonable time frame. Unfortunately, well-characterized preclinical model systems, which could pre-select drug candidates, have been lacking for many tumor subtypes so far.

The main focus of this study of this study was to generate and collect a large repertoire of fully molecularly characterized orthotopic PDOX models of pediatric brain tumors. Molecular profiles of the PDOX models were compared with their matching patient tumors in order to demonstrate the molecular fidelity of the PDOX models, and to determine whether the PDOX models are representative of the disease. Furthermore, the aim was to create a systematic overview of the genomic landscape of all PDOX models that are currently available to the scientific community. In addition, pilot *in vivo* experiments aimed to confirm sensitivity to targeted therapeutics based on tumor classification and the presence of specific biomarkers. As PDOX models of pediatric brain tumors are very rare, another aim of the study was to make this data easily accessible to the scientific community through an online portal, which will allow scientists all over the world to find the appropriate model system for their scientific questions.

2 Materials and Methods

2.1 Materials

The following section contains all reagents that were used by myself or by technicians under my supervision to perform experiments. Reagents used for experiments performed by collaboration partners are not included in these lists. This information can be found within the methods section of each individual method.

2.1.1 Cell lines

Cell line	Origin	Supplier
HEK 293T	Human Embryonic Kidney	ATCC, Wesel, Germany

2.1.2 PDOX models

Models generated by the group of Stefan M. Pfister were generated by myself and by technicians under my supervision (n = 11). Models generated by the group of Till Milde were established in the first passage by the group of Till Milde and then continuously passaged by myself and by technicians under my supervision (n = 10). All other lines were established independently from myself in the indicated laboratory, whereas the molecular characterization and also the re-establishment of some lines after cryo preservation, for the use in Heidelberg, were performed by myself.

Model	Generated by	Subgroup
A5108	Xiao-Nan Li, Houston, USA	ATRT, MYC
ATRT-312FH	James M. Olson, Seattle, USA	ATRT, MYC
A10593	Xiao-Nan Li, Houston, USA	ATRT, SHH
A6753	Xiao-Nan Li, Houston, USA	ATRT, SHH
AL1115	Xiao-Nan Li, Houston, USA	ATRT, SHH
ATRT-310FH	James M. Olson, Seattle, USA	ATRT, SHH
ATRT-310FH	James M. Olson, Seattle, USA	ATRT, SHH
B062_012	Stefan M. Pfister, Heidelberg, Germany	ATRT, SHH
HT099	Robert J. Wechsler-Reya, San Diego, USA	ATRT, SHH
M2123	Xiao-Nan Li, Houston, USA	ATRT, SHH
A1218	Xiao-Nan Li, Houston, USA	ATRT, TYR
NCH2315	Till Milde, Heidelberg, Germany	CNS NB, FOXR2

Model	Generated by	Subgroup
B062_015	Stefan M. Pfister, Heidelberg, Germany	DMG, K27
BT078	Till Milde, Heidelberg, Germany	DMG, K27
D1215	Xiao-Nan Li, Houston, USA	DMG, K27
DW0128	Xiao-Nan Li, Houston, USA	DMG, K27
PBT-01FH	James M. Olson, Seattle, USA	DMG, K27
PBT-03FH	James M. Olson, Seattle, USA	DMG, K27
D22909	Xiao-Nan Li, Houston, USA	EFT, CIC
D9850	Xiao-Nan Li, Houston, USA	EFT, CIC
B062_011	Stefan M. Pfister, Heidelberg, Germany	EPN, PF A
BT116	Till Milde, Heidelberg, Germany	EPN, PF A
E0614	Xiao-Nan Li, Houston, USA	EPN, PF A
E1499	Xiao-Nan Li, Houston, USA	EPN, PF A
E2002	Xiao-Nan Li, Houston, USA	EPN, PF A
E5323	Xiao-Nan Li, Houston, USA	EPN, PF A
EPD-210FH	James M. Olson, Seattle, USA	EPN, PF A
EPD-710FH	James M. Olson, Seattle, USA	EPN, PF A
NCH2053	Till Milde, Heidelberg, Germany	EPN, PF A
RCEP36	Robert J. Wechsler-Reya, San Diego, USA	EPN, PF A
RCMB19	Robert J. Wechsler-Reya, San Diego, USA	EPN, PF A
B062_005	Stefan M. Pfister, Heidelberg, Germany	EPN, RELA
BT165	Till Milde, Heidelberg, Germany	EPN, RELA
E1425	Xiao-Nan Li, Houston, USA	EPN, RELA
E9635	Xiao-Nan Li, Houston, USA	EPN, RELA
E9811	Xiao-Nan Li, Houston, USA	EPN, RELA
EPD-613FH	James M. Olson, Seattle, USA	EPN, RELA
B062_016	Stefan M. Pfister, Heidelberg, Germany	ETMR
D2373	Xiao-Nan Li, Houston, USA	ETMR
E1343	Xiao-Nan Li, Houston, USA	ETMR
M1129	Xiao-Nan Li, Houston, USA	ETMR
NCH3602	Till Milde, Heidelberg, Germany	ETMR
GA0818	Xiao-Nan Li, Houston, USA	GBM, G34
B062_004	Stefan M. Pfister, Heidelberg, Germany	GBM, MID
G10993	Xiao-Nan Li, Houston, USA	GBM, MID
G1227	Xiao-Nan Li, Houston, USA	GBM, MID

Model	Generated by	Subgroup
G1406	Xiao-Nan Li, Houston, USA	GBM, MID
G1621	Xiao-Nan Li, Houston, USA	GBM, MID
GBM-311FH	James M. Olson, Seattle, USA	GBM, MID
GBM-611FH	James M. Olson, Seattle, USA	GBM, MID
PBT-02FH	James M. Olson, Seattle, USA	GBM, MID
PBT-06FH	James M. Olson, Seattle, USA	GBM, MID
RCMB33	Robert J. Wechsler-Reya, San Diego, USA	GBM, MID
RCMB47	Robert J. Wechsler-Reya, San Diego, USA	GBM, MID
D2264	Xiao-Nan Li, Houston, USA	GBM, MYCN
G1128	Xiao-Nan Li, Houston, USA	GBM, MYCN
PBT-04FH	James M. Olson, Seattle, USA	GBM, MYCN
PBT-05FH	James M. Olson, Seattle, USA	GBM, MYCN
B062_014	Stefan M. Pfister, Heidelberg, Germany	GBM, RTK III
G3704	Xiao-Nan Li, Houston, USA	GBM, RTK III
RCMB23	Robert J. Wechsler-Reya, San Diego, USA	HGNET, BCOR
G9320	Xiao-Nan Li, Houston, USA	LYMPHO
ICN_PDX4	Olivier Ayrault, Paris, France	MB, G3
ICN_PDX7	Olivier Ayrault, Paris, France	MB, G3
M1197	Xiao-Nan Li, Houston, USA	MB, G3
M1299	Xiao-Nan Li, Houston, USA	MB, G3
M1494	Xiao-Nan Li, Houston, USA	MB, G3
M1572	Xiao-Nan Li, Houston, USA	MB, G3
M1595	Xiao-Nan Li, Houston, USA	MB, G3
M1744	Xiao-Nan Li, Houston, USA	MB, G3
M2164	Xiao-Nan Li, Houston, USA	MB, G3
M2555	Xiao-Nan Li, Houston, USA	MB, G3
M3130	Xiao-Nan Li, Houston, USA	MB, G3
MB002	Yoon-Jae Cho, Portland, USA	MB, G3
MB009	Yoon-Jae Cho, Portland, USA	MB, G3
Med-114FH	James M. Olson, Seattle, USA	MB, G3
Med-1911FH	James M. Olson, Seattle, USA	MB, G3
Med-210FH	James M. Olson, Seattle, USA	MB, G3
Med-2112FH	James M. Olson, Seattle, USA	MB, G3
Med-211FH	James M. Olson, Seattle, USA	MB, G3

Model	Generated by	Subgroup
Med-411FH	James M. Olson, Seattle, USA	MB, G3
NCH2194	Till Milde, Heidelberg, Germany	MB, G3
PBT-07FH	James M. Olson, Seattle, USA	MB, G3
RCMB20	Robert J. Wechsler-Reya, San Diego, USA	MB, G3
RCMB28	Robert J. Wechsler-Reya, San Diego, USA	MB, G3
RCMB40	Robert J. Wechsler-Reya, San Diego, USA	MB, G3
DMB006	Robert J. Wechsler-Reya, San Diego, USA	MB, G4
M0174	Xiao-Nan Li, Houston, USA	MB, G4
M1017	Xiao-Nan Li, Houston, USA	MB, G4
M1078	Xiao-Nan Li, Houston, USA	MB, G4
M1387	Xiao-Nan Li, Houston, USA	MB, G4
M8008	Xiao-Nan Li, Houston, USA	MB, G4
Med-1512FH	James M. Olson, Seattle, USA	MB, G4
Med-1612FH	James M. Olson, Seattle, USA	MB, G4
Med-2312FH	James M. Olson, Seattle, USA	MB, G4
Med-610FH	James M. Olson, Seattle, USA	MB, G4
RCMB37	Robert J. Wechsler-Reya, San Diego, USA	MB, G4
RCMB38	Robert J. Wechsler-Reya, San Diego, USA	MB, G4
RCMB45	Robert J. Wechsler-Reya, San Diego, USA	MB, G4
B062_008	Stefan M. Pfister, Heidelberg, Germany	MB, SHH CHL AD
B062_13315	Stefan M. Pfister, Heidelberg, Germany	MB, SHH CHL AD
BT084	Till Milde, Heidelberg, Germany	MB, SHH CHL AD
BT126	Till Milde, Heidelberg, Germany	MB, SHH CHL AD
ICN_PDX12	Olivier Ayrault, Paris, France	MB, SHH CHL AD
M3400	Xiao-Nan Li, Houston, USA	MB, SHH CHL AD
M5610	Xiao-Nan Li, Houston, USA	MB, SHH CHL AD
M5958	Xiao-Nan Li, Houston, USA	MB, SHH CHL AD
M984	Xiao-Nan Li, Houston, USA	MB, SHH CHL AD
Med-113FH	James M. Olson, Seattle, USA	MB, SHH CHL AD
Med-314FH	James M. Olson, Seattle, USA	MB, SHH CHL AD
Med-813FH	James M. Olson, Seattle, USA	MB, SHH CHL AD
RCMB18	Robert J. Wechsler-Reya, San Diego, USA	MB, SHH CHL AD
RCMB24	Robert J. Wechsler-Reya, San Diego, USA	MB, SHH CHL AD
B062_013	Stefan M. Pfister, Heidelberg, Germany	MB, SHH INF

Model	Generated by	Subgroup
M02036	Xiao-Nan Li, Houston, USA	MB, SHH INF
M1338	Xiao-Nan Li, Houston, USA	MB, SHH INF
Med-1712FH	James M. Olson, Seattle, USA	MB, SHH INF
RCMB12	Robert J. Wechsler-Reya, San Diego, USA	MB, SHH INF
RCMB25	Robert J. Wechsler-Reya, San Diego, USA	MB, SHH INF
RCMB32	Robert J. Wechsler-Reya, San Diego, USA	MB, SHH INF
M1140	Xiao-Nan Li, Houston, USA	MB, WNT
M1192	Xiao-Nan Li, Houston, USA	MB, WNT
Med-913FH	James M. Olson, Seattle, USA	MB, WNT
RCMB31	Robert J. Wechsler-Reya, San Diego, USA	MB, WNT
G6999	Xiao-Nan Li, Houston, USA	not classifiable
B062_006	Stefan M. Pfister, Heidelberg, Germany	PIN T, PB B
PBT-08FH	James M. Olson, Seattle, USA	PIN T, PB B
Pineo-113FH	James M. Olson, Seattle, USA	PIN T, PB B
P3635	Xiao-Nan Li, Houston, USA	PXA
BT216	Till Milde, Heidelberg, Germany	SCHW, MEL

2.1.3 Primers

2.1.3.1 Primers for Sanger sequencing

Gene Name	Forward Primer Sequence (5' – 3')	Reverse Primer Sequence (5' – 3')
ANKRD44	TGACTGACAGCCAAATTCACA	CACTGCAGCCTCATGTTGAT
ARID1A	TGGAGAGCATTTGTTCGCAT	TGTTTTCTCCTCTCACCCGT
ARID1A	GCTCAATCTGCCTCTCCAAT	GCCTTGGGTGGAGAACTGAT
ATM	GGTTGTCCTCCTTAAATTGTCCT	TTAAGATGCAGCTACTACCCAG
ATM	CTCAATGAATGGTAGTTGCTGC	ACCTAATTGTCCCAACTTGCT
ATM	CGAGAGCTGGAGTTGGATGA	TTCCTGACATCAAGGGGCTT
ATRX	ACGCCGGGCCATATTAAGAT	AAGCCAATCTTTCCTCTGATGA
BCOR	TAGGGAAGCTTGGTCTCAGC	AAGCTACAGAGAGGTCCACC
BCOR	CCCTCACCGACTCTGTCTAC	CCTCGGACATGCCTCACA
BCOR	TGAATCGGTCACCCACGTAA	GGCAGGTACCAACAAAGAGA
CREBBP	CGCTCACATTTCCTATTCCTGG	CGTGGCAGTTGGAGAGCT
EGFR	GAGCTAGACGTCCGGGCA	AGGAAACAGGAAAGGACGGG
EGFR	CCCCTTCAGTGTTTGTTGAGT	GCAACTGAACCTGTGACTCA
FGFR1	CCCCTTCCCTAGCTGTGG	TCCCTTCCCAAGTAAATGAGTCT

Gene Name	Forward Primer Sequence (5' – 3')	Reverse Primer Sequence (5' – 3')
GNAS	TCTTACGGAGCCCCAAACTT	TGAATGCCGGGTTGAGGAC
KBTBD4	ACTGCGTTGGAGAGGGTATC	ACTCGTTGGCTGTGTCCTT
KBTBD4	ACACAGTTTCATGATGCCTTG	CCCACTTTGCTCTCACTTCT
MSH2	TACTGCCTTGGCCAATCAGA	CCCAGACTGTGAATTAAGGGG
MSH2	TGACTCCTCTTACTGATCTTCGT	ATCCTTTTCCCATCTGTCACTT
MSH2	ACTGTTATTTCGATTTGCAGCAA	GCCAGGTGACATTCAGAACA
NF1	ACATGGATAGAAACACTGGGAGT	GGGAGGAAGGAGAAGCTGAA
NF1	CCATACCGGGCCTAGCAAT	CCAGTTTCCCAGGACAGTCT
PIK3CA	GTGACTTTAGAATGCCTCCGT	AGAAAGGGACAACAGTTAAGCT
PIK3CA	GCCATCTTATTCCAGACGCA	AACAAAGGACTGTGAGCTGT
PIK3R1	GGAAAGTGCAAAAGCCCAGA	AGCCATGAAATAAGGGTAGAACA
PPM1D	GGACCATATACCTGCCCTGG	TGGCCAGGAGTTGACATCTT
PTCH1	GGGACTGAAATCTTTACTGGGTC	CTGGTGGCAGAGTCCTAAC
PTEN	AACCCACCACAGCTAGAACT	TCTTAAATGCTTTCACCCTGGG
SETD1B	CACCTAAGAAGCGCCATGAG	GTGCATGCTGTCACCTTCAT
SMARCB1	TGTGCAGAGAGAGAGGCTGA	CCGACTGCCTTGTACCATTC
SYNE1	GTAGTGCAGCAACTCAAGGA	TTCACTGCATTCTTCTCGCA
TP53	CTCCCAGAGACCCCAGTTG	ACAAGCAGTCACAGCACATG
TP53	CATGTGCTGTGACTGCTTGT	CTAGTGGGTTGCAGGAGGTG
TP53	GGTGATAAAAGTGAATCTGAGGC	TTGGGAGTAGATGGAGCCTG
TP53	GGAGGTCAAATAAGCAGCAGG	GGAGAGACGACAGGGCTG
VPS13C	TGTCATTCCCTGCAGTTTGA	TGTGATGTAAGTTTTCCAGCCA
ZNF462	GTTGTGAGTGGTGCAGCTAC	ATGGAGCCCCTGAAGTTGG

2.1.3.2 Primers for reverse transcription quantitative PCR (RT-qPCR)

Gene Name	Forward Primer Sequence (5' – 3')	Reverse Primer Sequence (5' – 3')
GLI1	CTGGATCGGATAGGTGGTCT	CAGAGGTTGGGAGGTAAGGA
GLI2	CCCCTACCGATTGACATGCG	GAAAGCCGGATCAAGGAGATG
MYCN	TGATCCTCAAACGATGCCTTC	GGACGCCTCGCTCTTTATCT
PTCH1	CCAGAAAGTATATGCACTGGCA	GTGCTCGTACATTTGCTTGGG
PTCH2	AGGAGCTGCATTACACCAAG	CCCAGGACTTCCCATAGAGT
TBP	GAACCACGGCACTGATTTTC	CCCCACCATGTTCTGAATCT

2.1.4 Plasmids

Plasmid	Supplier
pGreenFire1 (pGF1) Reporter Vector	System Biosciences, Palo Alto, USA
pMD2.G	Addgene, Cambridge, USA
psPAX2	Addgene, Cambridge, USA

2.1.5 Inhibitors

Article	Catalog No.	Supplier
Cisplatin	HY-17394	MedChemExpress, New Jersey, USA
Erismodegib Diphosphate	HY-16582	MedChemExpress, New Jersey, USA
Erlotinib	S7786	Selleckchem, Munich, Germany
Glasdegib	-	Pfizer, New York, USA
PF-05274857	-	Pfizer, New York, USA
Vismodegib	S1082	Selleckchem, Munich, Germany

2.1.6 Cell culture reagents and materials

Article	Catalog No.	Supplier
24-well plates, adherent cells	92424	TPP, Schaffhausen, Switzerland
Accumax™	00-4666-56	eBioscience, Inc., San Diego, USA
Corning® Costar® reagent reservoir (50 ml)	CLS4870	Sigma-Aldrich, Munich, Germany
Dimethyl sulfoxide (DMSO)	472301	Sigma-Aldrich, Munich, Germany
DMEM (Dulbecco's modified eagle medium)	D6046	Sigma-Aldrich, Munich, Germany
Dulbecco's PBS	21600010	Thermo Fisher Scientific, Waltham, USA
Fetal Bovine Serum (FBS), heat-inactivated, Gibco®	10082147	Thermo Fisher Scientific, Waltham, USA
L-Glutamine	25030081	Gibco®, Thermo Fisher Scientific, Waltham, USA
Neurobasal™-A Medium	10888022	Gibco®, Thermo Fisher Scientific, Waltham, USA
NeuroCult™ NS-A Basal Medium (Human)	05750	STEMCELL Technologies, Vancouver, Canada

Article	Catalog No.	Supplier
NeuroCult™ NS-A Proliferation Supplement (Human)	05751	STEMCELL Technologies, Vancouver, Canada
Nunc® CryoTubes® (1.8 ml)	V7884	Sigma-Aldrich, Munich, Germany
Opti-MEM I reduced serum medium	31985062	Thermo Fisher Scientific, Waltham, USA
Penicillin/Streptomycin (10,000 U/ml, 100 µg/ml) Gibco™	15140122	Thermo Fisher Scientific, Waltham, USA
T-75 adhesion flask	90076	TPP, Schaffhausen, Switzerland
TransIT®-LT1 transfection reagent	MIR2300	Mirus Bio, Madison, USA
Trypan Blue Dye (0.4 %)	1450021	Bio-Rad, Munich, Germany
Trypsin EDTA solution (0.5 %)	T3924	Sigma-Aldrich, Munich, Germany

2.1.7 Biochemicals and chemicals

Article	Catalog No.	Supplier
Agar	05039	Sigma-Aldrich, Munich, Germany
Agarose	A9539	Sigma-Aldrich, Munich, Germany
Ampicillin	10835242001	Roche, Diagnostics, Mannheim, Germany
DNA ladder, 100 bp, GeneRuler	SM0243	Thermo Fisher Scientific, Waltham, USA
DNA loading dye (6x)	R0611	Thermo Fisher Scientific, Waltham, USA
Ethanol	32205	Sigma-Aldrich, Munich, Germany
Ethidium bromide	E1510	Sigma-Aldrich, Munich, Germany
Glucose	G7021	Sigma-Aldrich, Munich, Germany
LB medium (Luria-Miller)	X968.1	Carl Roth, Karlsruhe, Germany
Magnesium chloride ($MgCl_2$)	208337	Sigma-Aldrich, Munich, Germany
NaCl 0.9 % solution (10 ml)	2350748	B. Braun, Melsungen, Germany
Nuclease-free water, Ambion®	AM9916	Thermo Fisher Scientific, Waltham, USA

Proteinase K, recombinant, PCR grade	EO0491	Thermo Fisher Scientific, Waltham, USA
Sodium chloride (NaCl)	S3014	Sigma-Aldrich, Munich, Germany

2.1.8 Buffers and solutions

Buffer/Solution	Composition
1x Phosphate buffered saline (PBS)	137 mM NaCl, 2.7 mM KCl, 9.2 mM Na_2HPO_4, 1.8 mM KH_2PO_4, pH 7.4
1x TRIS-Borat-EDTA (TBE)	0.445 M Tris-Borat, 10 mM EDTA, pH 8

2.1.9 Bacteria

Bacteria cells	Supplier
OneShot STABL3 chemically competent *E.coli*	Thermo Fisher Scientific, Waltham, USA

2.1.10 Mice

Mouse Strain	Source
NOD.Cg-Prkdc^{scid} Il2rg^{tm1Wjl}/SzJ (Nonobese diabetic/severe combined immunodeficiency gamma, NOD-SCID gamma®)	In-house breeding facility of the German Cancer Research Center (DKFZ), Heidelberg, Germany

2.1.11 *In vivo* reagents and materials

Article	Supplier
Bepanthen®	Bayer Vital, Leverkusen, Germany
Carprofen/Rimadyl	Pfizer, New York, USA
Fine-Ject® Needles for single use, 30Gx1/2”	Henke-Sass Wolf, Tuttlingen, Germany
Histacryl® tissue adhesive	Braun, Melsungen, Germany
Isoflurane	Abbott, Wiesbaden, Germany
Nanofil needle with syringe	World Precision Instruments, Sarasota, USA
Precision Scale (portable) PLS/PLJ	Kern®, Balingen, Germany
Reusable feeding needle, 50 mm length	Fine Science Tools®, Heidelberg, Germany

Soft-Ject® Syringes, 1 ml	Henke-Sass Wolf, Tuttlingen, Germany
VivoGlo™ luciferin	Promega, Madison, USA

2.1.12 Kits

Kit	Company
Agilent RNA 6000	Agilent Technologies, Santa Clara, USA
DNeasy® Blood & Tissue Kit	Qiagen, Hilden, Germany
EnVision Detection Systems Peroxidase/DAB, Rabbit/Mouse	Dako Agilent Pathology Solutions, Hamburg, Germany
HotStarTaq Plus Master Mix Kit	Qiagen, Hilden, Germany
Maxi preparation DNA Kit	Qiagen, Hilden, Germany
Maxwell® RSC Blood DNA Kit	Promega, Madison, USA
Maxwell® RSC simplyRNA Tissue Kit	Promega, Madison, USA
Maxwell® RSC Tissue DNA Kit	Promega, Madison, USA
Power SYBR® Green RNA-to-CT™ 1-Step Kit	Thermo Fisher Scientific, Waltham, USA
Qiagen Maxiprep Kit	Qiagen, Hilden, Germany
QIAquick PCR Purification Kit	Qiagen, Hilden, Germany
RNeasy® Mini Kit	Qiagen, Hilden, Germany

2.1.13 Databases

Databases	Source
Gene Cards (Human Genes Database)	http://www.genecards.org/
PubMed	http://www.ncbi.nim.nih.gov/PubMed/
R2: Microarray Analysis and Visualization Platform	http://hgserver1.amc.nl/cgi-bin/r2/main.cgi

2.1.14 Software

Software	Supplier
Bioanalyzer 2100 Expert	Agilent Technologies, Santa Clara, USA
EndNote X6	Thomson, ResearchSoft, Carlsbad, USA
FACS-Diva	BD Biosciences, Heidelberg, Germany
GraphPad Prism 7	GraphPad, San Diego, USA
Microsoft Office 2013	Microsoft, Redmond, USA

R Statistics Environment	https://www.r-project.org/

2.1.15 Equipment

Equipment	Company
7900HT Fast Real-Time PCR System	Thermo Fisher Scientific, Waltham, USA
Bioanalyzer Agilent 2100	Agilent Technologies, Santa Clara, USA
Biofuge Fresco table top centrifuge	Haraeus Instruments, Hanau, Germany
Bruker 1 Tesla MRI	Bruker, Billerica, USA
Cytostatics Hood Maxisafe 2020	Sigma-Aldrich, Munich, Germany
Electrophoresis chamber	NeoLab, Heidelberg, Germany
FACS Canto™II	BD Biosciences, Heidelberg, Germany
FACSAria III cell sorter	BD Biosciences, Heidelberg, Germany
Gel Doc UV gel documentation system	Bio-Rad, Munich, Germany
GeneAmp® PCR System 9700	Applied Biosystems, Foster City, USA
Heating Block QBT	Grant Instruments, Cambridge, UK
Incubator HERA cell 150	Thermo Fisher Scientific, Waltham, USA
IVIS Lumina Series III pre-clinical in vivo imaging platform	PerkinElmer, Waltham, USA
L8-M ultracentrifuge	Beckmann Coulter, Krefeld, Germany
Leica DMIRBE inverted microscope	Leica Biosystems, Wetzlar Germany
Maxwell® RSC Instrument	Promega, Madison, USA
NanoDrop® ND-1000 spectrometer	NanoDrop, Wilmington, USA
Sonicator water bath	Arrayit Microarray Technology, Sunnyvale, USA
T20 Automated Cell Counter	Bio-Rad Laboratories, Munich, Germany
Vortex Genie 2	Scientific Industries Inc., New York, USA
Water bath B-480	Büchi, Flawil, Switzerland

2.1.16 Other materials

Article	Supplier
Chromatography Paper, 3 mm, Whatman®	Sigma-Aldrich, Munich, Germany
Cover slips (26 x 76 mm)	Thermo Fisher Scientific Gerhard Menzel, Braunschweig, Germany
FACS tubes	BD Biosciences, Heidelberg, Germany

Article	Supplier
Falcon® tubes (15 ml and 50 ml)	BD Biosciences, Heidelberg, Germany
Filtered Pipette tips (10 µl, 20 µl, 100 µl, 200 µl, 1000 µl)	Biozym®, Hessisch Oldenburg, Germany
GeneChip® Human Genome U133 Plus 2.0 Array	Affymetrix, Thermo Fisher Scientific, Waltham, USA
Infinium Human-Methylation450 BeadChip Kit	Illumina®, San Diego, USA
Infinium MethylationEPIC Kit	Illumina®, San Diego, USA
PCR tubes (0.2 ml)	Molecular BioProducts, San Diego, USA
Rainin sterile filter tips (300 µl)	Mettler-Toledo, Giessen, Germany
Reaction tubes (1.5 ml and 2 ml)	Eppendorf, Hamburg, Germany
Stripetten, Corning® Costar® (5, 10, 25, 50 ml)	Sigma-Aldrich, Munich, Germany
Ultracentrifuge tubes, PPCO (PA), thinwall (14 ml)	Herolab, Heidelberg, Germany

2.2 Methods

Parts of the written contents and figures of the following chapter have been submitted in the research article "*A biobank of patient-derived molecularly characterized orthotopic pediatric brain tumor models*", Brabetz, Leary, Gröbner *et al.* (List of Publications, page 125) to *Nature Medicine* in July 2017. Contributions of authors other than myself are indicated.

2.2.1 Large scale plasmid preparation (Maxiprep)

300 ml of LB medium was inoculated with *E.coli* expressing the plasmid of interest and incubated overnight at 37°C on a bacterial shaker. Plasmid isolation was performed with the Qiagen Maxiprep Kit according to the manufacture's recommendations, and DNA concentration was measured with the NanoDrop® ND-1000 spectrometer.

2.2.2 HEK 239T cell culture

HEK 293T cells were cultured in 75 cm^2 adhesion cell culture flasks in DMEM media, supplemented with 10% FBS and 1% (v/v) penicillin/streptomycin under standard conditions (37°C, 95% humidity, 5% CO_2). Upon reaching 80% confluence the supernatant was decanted, cells were washed with PBS, and 3 ml 0.5% Trypsin-EDTA was added. After 5 min at 37°C,

media was added, and thus the reaction stopped. Afterwards cells were centrifuged at 1,200 rpm for 5 min and cells were split into new flasks at a ratio of 1:10 – 1:20.

2.2.3 Cell number and viability measurements

Cell numbers were measured prior to seeding HEK 239T cells and also for passaging and establishing of PDOX, via staining viable cells with a 1:2 Tryptan blue stain and counting viable cells per ml using the TC20 automated cell counter according to the manufacture's recommendations.

2.2.4 Viral production

Young HEK293T cells (< P10) were plated in 10cm dishes ($4x10^6$ cells in 6 ml fresh media). The next day, 600 µL Opti-MEM were mixed with 30 µL Mirus IT and incubated for 5 min at room temperature. Afterwards, 2 µg of packaging plasmid psPAX2, 2 µg of packaging plasmid pMD2.G, and 4 µg of lentivirus construct/plasmid, were mixed and added to the solution, and the final mixture was incubated for 20 min at room temperature. During this process, the media of the HEK 239T cells was exchanged with fresh media. After the incubation time, the transfection mixture was dropped onto the HEK 239T cells and the plate was moved carefully to evenly distribute the solution. After 72 h, the media was carefully collected, filtered through a 45 µm syringe filter into ultraclear SW41 centrifuge tubes, and spun down for 80 min at 4°C at 25,000 rpm using an L8-M ultracentrifuge. Afterwards, the supernatant was decanted and 100 µl PBS were added to the pellet, and it was left overnight at 4°C. The next day, the virus pellet was carefully re-suspended, aliquoted in 10 µl tubes, and stored at -80°C.

2.2.5 HEK titer test

HEK 293T cells were seeded into a 24-well plate at $5x10^4$ cells/well in 500 µl medium. The next day, cells from 2 wells were counted with the T20 Automated Cell Counter, while the remaining wells were transduced with various concentrations of a GFP-labeled virus. After 72 h, cells were trypsinized and washed with PBS, and then the transduction efficiency was evaluated with a FACS Canto™II. The virus titer was evaluated with the following formula: Percentage GFP-positive cells * cell number at time of transduction * virus dilution / (Volume of virus suspension). The virus titer allowed the comparison of different batches of virus productions.

2.2.6 Animal studies

All animal experiments were conducted in accordance with legal and ethical regulations and approved by the regional council (Germany, Regierungspräsidium Karlsruhe; G-64/14, G-259/14, and G-164/17). Mice were housed in IVC caging in the Center for Preclinical Research of the DKFZ (Heidelberg, Germany) and monitored daily for the presence of tumor-related symptoms. Sample sizes were chosen to minimize the number of animals required to get statistically significant results.

2.2.7 Patient samples

Pediatric brain tumor specimens were obtained through the "Pediatric Brain Tumor Preclinical Testing Program" (indicated as "generated by Till Milde/Stefan M. Pfister, Heidelberg, Germany"). Informed consent of the parent or legal guardian and the patient was obtained according to institutional regulatory standards prior to surgery. Samples from Heidelberg University Hospital were transferred from the operating room to the laboratory on wet ice. Other samples from across Germany and Europe were shipped overnight on wet ice and typically processed the next day.

The processing of patient material by collaborating centers each followed a local workflow, always including informed consent (James M. Olson, Seattle, USA; Olivier Ayrault, Paris, France; Robert J. Wechsler-Reya, San Diego, USA, Heidelberg, Germany; Yoon-Jae Cho, Portland, USA; Xiao-Nan Li, Houston, USA).

2.2.8 PDOX establishment and propagation

The fresh tumor tissue (whether PDOX or patient tumor) was placed in a small volume of NeuroCult media, including NeuroCult NSA-Proliferation agent, was dissociated into a single-cell suspension by careful pipetting. Patient tumors were also processed through dissociation via a scalpel. If the tumor was not dissociable by mechanical means, the cells were washed with PBS, and placed in 1 ml Accumax^{TM} solution. After an incubation time of 15 min at 37°C, the reaction was stopped by the addition of media. To remove the Accumax^{TM} solution, the suspension was centrifuged at 1,200 rpm, the supernatant carefully removed, and media added again. In order to remove non-dissociated cells, the cells were pushed through a 45 µm cell strainer. Afterward the cells were counted with the TC20 automated cell counter. In cases where the viability was below 40%, an additional centrifugation step was introduced. The material was split into 3 parts: At least 2 pellets ($1x10^6$ cells per pellet) for molecular characterization (centrifugation at 1,200 rpm for 5 min, remove supernatant, shock freeze in liquid nitrogen), a suspension for injection in mice (4 µl per mouse) (max. $1x10^6$ cells per

mouse) (centrifugation at 1,200 rpm for 5 min, remove supernatant, adjust volume with media to approximately 5 µl per mouse), and cryo preservation of remaining material (90% media, 10% DMSO, $1.5x10^6$ cells).

Collection of material during PDOX passaging:

Per mouse: 2x pellets (at least) for molecular characterization ($1x10^6$ cells per pellet), remaining material was split into cryo vials ($1.5x10^6$ cells per vial).

Per passage: 1x direct re-transplantation of fresh tumor material into the next generation of mice, 1x half of a brain fixed in formalin solution for subsequent histological evaluation.

2.2.9 Intracranial injection of tumor tissue

20 min after subcutaneous injection of carprofen (5 mg/kg) as perioperative analgesia, female NSG mice (6-8 weeks, DKFZ in-house breeding) were anaesthetized by isoflurane (1.5-2.5 Vol%). After negative reflex testing, animals were fixated in a stereotactical frame and a 5 mm incision in the scalp was introduced. For local anesthesia, 0.25 % bupivacaine was applied to the incision. A 18G cannula (diameter: 1.27 mm) was used to drill a small hole into the skull (location was based on patient tumor location, see Table 1). Then the Hamilton needle was introduced into the brain (depth varies by injection site) and the cell suspension (4 µl media, max. $1x10^6$ cells) was injected within a time frame of 1 min. The needle stayed in the tissue for another 2 min to avoid any reflux of the cell suspension. After the slow removal of the needle the incision was closed by tissue adhesive. Only after recovery of the animal in a separate clean cage, was it placed back into the original cage. Operated animals were treated with carprofen subcutaneously (5 mg/kg) every 12 h for 48 h (in the case of pain symptoms an additional 5 days).

Table 1. Coordinates for intracranial injection of PDOX cells.

Injection site (mouse)	Coordinate (mm; bregma)	Coordinate (mm; lateral left)	Coordinate (mm; depth)
Striatum	-3	2.5	3
Cerebellum	-7	1	2
Cortex	-1	1	2
Brain Stem	-5.5	0	4.5

Animals injected with patient-derived tumor cells were continually monitored for signs of tumor-related symptoms and any signs of pain. Upon observation of symptoms, animals were euthanized and tumor tissue was processed as mentioned in section 2.2.8, PDOX establishment and propagation (page 44). If material for histopathological analysis was to be collected (once per PDOX passage), half of the brain (cut frontal – caudal) was placed in a formalin solution (including tumor tissue), while the remaining tumor was processed as usual.

2.2.10 DNA and RNA isolation

Total RNA extraction was performed from snap-frozen tumor tissues using either TRIZOL in combination with the Qiagen miRNeasy Mini Kit (Qiagen, Hilden, Germany) or the Maxwell® RSC simplyRNA Tissue Kit and analyzed on an Agilent Bioanalyser for quality assessment. Only samples with an RNA integrity number (RIN) > 6.0 and no evidence of ribosomal degradation were analyzed for gene expression. Genomic DNA was isolated using either Qiagen DNeasy Blood & Tissue Kit or the Maxwell® RSC Blood/Tissue DNA Kit and used for methylation and sequencing analysis.

2.2.11 Gene expression array analysis

PDOX samples with sufficient quantity and quality of RNA were analyzed on the Affymetrix GeneChip Human Genome U133 Plus 2.0 Array in the Microarray Department at the University of Amsterdam in the Netherlands. Sample library preparation, hybridization, and quality control were performed according to protocols recommended by the manufacturer. The RMA algorithm of the Simpleaffy package in R was used for normalization of the expression data[437]. Differentially-expressed genes were estimated with linear models using the Limma package in R[438]. Only genes that were expressed in at least one sample were considered for the analysis (>100 intensity). Differential expression was calculated with a moderated paired t-test, and *P*-values were corrected for multiple testing with the Bonferroni method ($p < 0.05$). Significant genes that changed more than 2-fold between groups were used for the follow-up analysis. DAVID 6.7 was used for pathway enrichment analysis using the GOTERM_BP_DIRECT and GOTERM_CC_DIRECT gene ontology annotations[439,440].

2.2.12 DNA methylation array analysis

Whole genome DNA methylation data of 247 samples presented in this study were generated from fresh frozen and FFPE material, using the Illumina Infinium 450k Methylation BeadChip Arrays (450k arrays) or Illumina Infinium EPIC Methylation BeadChip Arrays (epic arrays).

Methylation profiling was performed according to the manufacturer's instructions at the DKFZ Genomics and Proteomics Core Facility (Heidelberg, Germany). All analyses were performed in R version 3.3.0 (Development Core Team, 2016). Downstream analyses as described in Hovestadt *et al.*[441] were performed in R using β-values. Reference cases of primary human tumors for subgrouping were taken from various previous publications as indicated in individual figure legends. Individual normalization of each sample and correction for the type of material was performed as in Capper *et al.*[342].

The following filters were applied in order to filter out probes from 450k arrays that yielded inaccurate methylation levels: Removal of probes targeting the X and Y chromosomes (*n* = 11,551), removal of probes containing a single-nucleotide polymorphism (dbSNP132 Common) or the following base for type I probes (*n* = 7,998), probes not mapping uniquely to the human reference genome (hg19) (*n* = 3,965), and probes not being present on the epic array (*n* = 32,260). In total, 428,676 probes were kept for analysis. The same probes were then also extracted from the epic arrays.

Pairwise Pearson correlations were calculated using the wtd.cors function of the weights package version 0.85. For the pan-brain tumor analysis (Figure 6, page 62), the standard deviation was used as weight, while in the analysis for the MBs and the HGGs, the standard deviation minus 0.25 was used as weight, giving more variable probes greater influence. The resulting matrix was used to perform the t-SNE analysis (t-Distributed Stochastic Neighbor Embedding, Rtsne package version 0.11)[442]. The following non-default parameters were used for the pan-brain tumor and HGG analyses: theta=0, is_distance=T, pca=F, max_iter=40,000. The MB analysis across all subgroups (Figure 8a, page 64) used the following non-default parameters: theta=0, is_distance=T, pca=F, max_iter=2,000. For the G3/G4-specific analysis (Figure 8b, page 64), an initial t-SNE analysis was performed using the entire MB cohort with the following non-default settings: theta=0, is_distance=T, pca=F, max_iter=150. The positions resulting from this analysis were used as a starting point for a t-SNE analysis using the weighted correlation of the G3-G4 exclusive cohort (again using as a weight the standard deviation minus 0.25, but this time calculated only for the G3/G4 exclusive cohort) and the following non-standard default parameters theta=0, is_distance=T, pca=F, max_iter=2,000-150.

Differentially-methylated probes between groups of patient tumors and early PDOX passages were performed as described in Mazor *et al.*[443]. In short, beta values for individual GpG sites were made more Gaussian using the logit transformation. The transformed beta values from the patient-matched patient tumor were subtracted from the early PDOX passage and compared using Limma[438]. Differentially methylated CpG were defined as those with a nominal *P*-value < 0.05 and an average methylation change between groups >= 0.2 or =< -0.2.

Copy number variation (CNV) analysis from methylation arrays data was performed using the Conumee Bioconductor package version 1.3.0. Two sets of 50 control samples each displaying a balanced copy-number profile from both male and female donors were used for normalization. Scoring of focal amplifications and deletions as well as chromosomal gains and losses was performed by manual inspection of each profile. In order to adjust for different methylation array types, the Conumee CNV calls were mapped back to a genome, which was binned in 50,000 windows. Afterwards, unsupervised hierarchical clustering of CNV profiles was performed by using the 1-Pearson correlation coefficient as the distance measure and average linkage for hierarchical clustering.

2.2.13 Whole exome and whole genome sequencing

The whole genome libraries as well as the exome libraries were prepared according to the Agilent SureSelectXT Target Enrichment System for Illumina Paired-End Sequencing Library kit, following the manufacturer's instructions, at the DKFZ Genomics and Proteomics Core Facility (Heidelberg, Germany). Briefly, genomic DNA was sheared by acoustic fragmentation (Covaris, MA, USA) to ~300 bp insert size, followed by size selection. Exome capturing was carried out with Agilent SureSelect Human All Exon V4 or V5 bait library in-solution capture reagents. The quality of the libraries was assessed with the Agilent 2100 Bioanalyzer. Sequencing was done on an Illumina HiSeq2000 instrument (Illumina, CA, USA) with paired-end 100-bp runs or 125-bp runs (v3 and v4) at the DKFZ Genomics and Proteomics Core Facility (Heidelberg, Germany).

Whole genome (WGS) and exome sequencing (WES) data were processed with a standardized workflow by Susanne N. Gröbner (DKFZ, Heidelberg, Germany), in close collaboration with myself, to define the correct criteria for the various filtering steps. Susanne N. Gröbner therefore wrote some parts of this methods section. The alignment and variant calling procedures were adapted from a pipeline developed in the context of the ICGC Pan-Cancer project (https://github.com/ICGC-TCGA-PanCancer). Essentially, reads were aligned to a reference genome using bwa-mem (v. 0.6.2). A merged human and murine reference genome (based on hs37d5 and GRChm38mm10) was used for capturing contaminating reads derived from mouse tissue. Aligned reads were sorted by coordinates, and duplicates were marked using biobambam bamSort and bammarkduplicates (v. 0.0.148).

Single nucleotide variant (SNVs) calls were based on SAMtools (v. 0.1.19) mpileup and short insertions/deletion (indels) calls on Platypus (v. 0.7.4), followed by specially tailored quality filters taking into account coverage, frequency, and surrounding sequence of variants. Additional filtering was performed by removing mutations in typical artifact genes and

positions, which were found mutated at non-hotspot locations in multiple samples, being therefore most likely SNPs or artifacts. Variants were annotated using ANNOVAR (http://annovar.openbioinformatics.org/en/latest/)[444].

If no germline was available, SNVs/indels that fulfilled the following criteria were excluded:

- >0.01% minor allele frequency in 1000g2015aug (in any population) (1000 Genomes Project)
- >0.01% minor allele frequency in exac03 (in any population) (latest Exome Aggregation Consortium datasets)
- >0.01% minor allele frequency esp6500siv2 (in any population) (latest NSHLBI-ESP project with 6500 exomes)

Subsequently, genes that were reported to be mutated in a reference cohort of primary tumors (only for MB[294] and HGG[445]) as well as in databases of known cancer genes (http://cancer.sanger.ac.uk/census/)[446], tumor suppressors (http://bioinfo.mc.vanderbilt.edu/TSGene)[447], and oncogenes (http://www.uniprot.org) were highlighted. For comparisons of the mutational landscape of individual patient tumors and matching PDOX, mutation calls of both samples were compared. If mutations only were found in one sample by the variant calling pipeline, an mpileup on that position was performed in the paired sample and, in addition, it was also verified whether this position was covered in this sample. Only mutations that were covered and were not found in the mpileup, were annotated as being lost in the sample. Based on this analysis, the following confidence classes emerged:

PASS:	Mutation called via pipeline.
LOW_SCORE:	Mutation did not pass the quality threshold in this sample, but passed it in the paired tissue.
MPILEUP_RESCUE:	Mutation found in paired tissue and not found in this sample via regular variant calling. However, mpileup confirmed the presence of this mutation.
MPILEUP_RESCUE_LOW:	MPILEUP_RESCUE, except that there were no 10 reads covering the position and/or 3 reads on the mutant base.
MANUAL_CURATION:	Mutation was manually curated (low pipeline score in both tissues).

NOT_FOUND:	Mutation found in paired tissue, but was not detected by either pipeline or mpileup in this tissue.
NOT_FOUND_NO_COVERAGE:	Mutation found in paired tissue, but was not detected by either pipeline or mpileup in this tissue. However, there were no 10 reads covering the position and/or 3 reads on the mutant base (excluded from some analyses).
NOT_FOUND_NO_MPILEUP:	Mutation found in paired tissue, but was not detected by the pipeline in this tissue. However, no mpileup was performed on this position (indel only) (excluded for some analyses).

Copy number plots from low-coverage whole genome sequencing data were generated by determining the read count within 10kb windows along the genome in a tumor and a pseudo-control sample without any copy number alterations in order to account for ambiguously covered regions. Coverage is displayed as $\log_2$-ratio of read counts in tumor versus the control sample, normalized for the total read count in each sample.

2.2.14 Preclinical experiments

Med-1712FH cells were labeled with luciferase using pGF1 lentivirus and subsequently after one passage, GFP-positive cells were sorted by Fluorescence-activated Cell Sorting (FACS). 100,000 cells were intracranially injected into the cerebellum of NSG mice. Two months afterward, weekly bioluminescence imaging was initiated. In detail, animals were injected with 150 mg/kg luciferin solution, and 10 minutes later imaged using an IVIS Lumina Series III pre-clinical *in vivo* imaging platform with an exposure time of 5 min. Upon reaching a signal intensity of $2x10^6$ p/s, animals were randomized into various treatment arms of the study and continuously treated until the signal intensity reached $1x10^6$ p/s, then the animals were put on treatment break until the signal recovered the signal intensity of $2x10^6$ p/s, and then the cycle was started again. Animals were euthanized as soon as they showed tumor-related symptoms or lost more than 20% of their initial weight prior to study entry. Kaplan–Meier analysis was done using GraphPad Prism, and statistical significance was calculated using a log–rank test. For target engagement, tumor-bearing animals were treated with Erismodegib (20 mg/kg, p.o.) for two days and then sacrificed 4 hours after the last dosage.

Table 2. Dosing schedules.

Drug	Vehicle	Dose	Dosing schedule	Application route
Erismodegib (-diphosphate)	0.5% Methyl Cellulose/ 0.5% Tween 80	20 mg/kg	5/7 days	Oral gavage
Glasdegib	0.5% Methyl Cellulose	100 mg/kg	5/7 days	Oral gavage
PF-05274857	0.5% Methyl Cellulose	30 mg/kg	5/7 days	Oral gavage
Cisplatin	0.9% NaCl solution	2 mg/kg	1/7 days	Intraperitoneal injection

2.2.15 RT-qPCR

RT-qPCR was performed from total RNA with the Power SYBR® Green RNA-to-CT™ 1-Step Kit according to the manufacturer's specifications on the 7900HT Fast Real-Time PCR System. Probes used for qRT-PCR are listed in section 2.1.3.2 Primers for reverse transcription quantitative PCR (RT-qPCR) (page 36). Transcript levels were determined by absolute quantification using a standard curve and then normalizing the expression level to the *TBP* housekeeping gene.

2.2.16 Validation of mutations in late PDOX passages

Driver/cancer mutations with an allele frequency of at least 20% found in patient tumors or early PDOX passages were validated in late PDOX passages by Sanger sequencing (only for lines from the laboratory of James M. Olson (Seattle, USA). Segments of DNA were amplified via PCR using the HotStarTaq Plus Master Mix Kit with the cycler Gene Amp® PCR System 9700. Primers used for these reactions are listed in 2.1.3.1 Primers for Sanger sequencing (page 35). The following PCR protocol was used:

95°C – 2 minutes

95°C – 30 seconds
59°C – 30 seconds
72°C – 1 seconds
} 40 cycles

72°C – 5 minutes

Afterward, the correct length of the PCR products was determined via agarose gel electrophoresis. Finally, PCR products were purified with the QIAquick PCR Purification Kit, and sent for Sanger sequencing to GATC Biotech (Konstanz, Germany).

2.2.17 Statistical analysis

Statistical analysis was performed using either GradPad Prism software or the R Statistics Environment. If not otherwise indicated, mean values were always given with a confidence interval of alpha = 0.05. Group comparisons were performed using Student's t-test or ANOVA, based on whether two or more groups were compared, respectively. Tests were always performed two-sided and, unless not otherwise specified, the variance was always assumed to be uneven. Within box plots, the box illustrates the borders of the lower and upper quartile, and the line within the box represents the median. The whiskers highlight the limits of the nominal range inferred from the upper and lower quartiles. To compare engraftment rates and mutation frequencies between populations MedCalc software (https://www.medcalc.org/calc/comparison_of_proportions.php) was used, specifically the „*N*-1" χ^2 test as recommended[448,449]. The statistical significance of Kaplan-Meier survival curves was assessed using the log-rank (Mantel-Cox) test using GraphPad Prism. For all experiments, *P* values of 0.05 or lower were considered statistically significant.

2.2.18 Information sharing

Molecular data from PDOX lines can be freely accessed through the "PDX Explorer" (https://hgserver1.amc.nl/cgi-bin/r2/main.cgi?&dscope=PDX_OLSON&option=about_dscope). The concept of the PDOX Explorer was designed and the data were pre-processed and collated by myself, while Jan Koster in Amsterdam (Netherlands) performed the implementation into the R2 platform. Within the "PDX Explorer" in R2, the one-page overviews for all PDOX lines generated in Seattle are also accessible. The one-page overviews were again designed by myself, and automated PDF generation was performed with LaTex (https://www.latex-project.org/) by Susanne N. Gröbner (DKFZ, Heidelberg, Germany).

2.2.19 Methods of collaboration partners*

Some experiments were performed at the Fred Hutch Cancer Center from the group of James M. Olson. The PDX models of the Olson lab are the subject of the previously mentioned manuscript "*A biobank of patient-derived molecularly characterized orthotopic pediatric brain tumor models*" and therefore were included in this the thesis, as they were performed in close

*This section of the thesis was taken in its entirety from the research article "*A biobank of patient-derived molecularly characterized orthotopic pediatric brain tumor models*". The described experiments were performed by the laboratory of James M. Olson in Seattle (USA), and therefore this part of text was written jointly with members of the Olson laboratory.

collaboration. Specific reagents used in these experiments are specified in this section and did not appear in section 2.1 Materials (page 31).

2.2.19.1 Patient samples

Brain tumor tissue was obtained through the Children's Oncology Group (COG) biology study ACNS02B3 and through Seattle Children's Hospital local banking and biology study. Informed consent of the parent or legal guardian, and patient assent when appropriate, was obtained according to institutional regulatory standards prior to surgery or autopsy. Fresh tumor tissue for research was selected by the pathologist or surgeon at each treating institution after clinical diagnostic tissue was obtained. For each sample approximately 100 mg of fresh tissue was placed in a 15 ml polypropylene tube with DMEM-F12. Samples from Seattle Children's Hospital were transferred on wet ice and processed withina few hours of patient surgery. Other samples from across the United States and Canada were shipped overnight on wet ice and typically processed within 24 hours of surgery. Patient age, gender, and preliminary diagnosis were provided at the time of tissue shipment. Final institutional pathologic diagnosis was provided once available. Patient tumor tissue was triturated with an 18G needle, to yield a single-cell suspension. The resulting suspension of cells was filtered through a nylon mesh 100 μm sterile cell strainer (cat.22363549, Fisher Scientific) and concentrated to 50,000 cells per microliter in serum-free DMEM in preparation for intracranial xenograft into five recipient mice. 2 to 3 million cells of remaining sample were plated for growth in tissue culture. Up to 1 million remaining cells were used for pathogen testing.

2.2.19.2 Xenograft development

Xenograft of tumor cell suspension was carried out in immune-compromised mice (Nod-scid IL2Rgamma^{null} (NSG) or athymic nude) immediately following processing. Female athymic Nu/Nu mice were purchased from Jackson Laboratories or Harlan Laboratories (now Envigo Laboratories). NSG mice were obtained from the laboratory breeding colony, established by breeding pairs purchased from Jackson Laboratories. All mice were maintained in accordance with the NIH Guide for the Care and Use of Experimental Animals with approval from the Fred Hutchinson Cancer Research Center Institutional Animal Care and Use Committee (IR#1457).

Analgesia was administered by subcutaneous buprenorphine injection approximately one hour before beginning the procedure. Mice were anesthetized using inhaled Isoflurane. Establishment of anesthesia was determined by monitoring respiratory rate and toe pinch reflex. The surgical site was prepared by shaving the fur between the ears and partially down the back of the neck. Puralube Vet Ointment sterile ocular lubricant (027505, MWI Veterinary Supply)

was applied to both eyes, and a 1 ml subcutaneous bolus of sterile saline (sys-5-5, Braintree Scientific Inc) was administered. Surgery was performed in a clean surgical field. The surgical site was cleaned by scrubbing the skin with a cotton swab impregnated with betadine (sc-359867, Santa Cruz Biotechnology) followed by a sterile 70% ethanol wipe (22-363-750, Fisher Scientific). An incision of ~1 cm was made along the mediolateral line starting between the ears and ending near the back of the skull using a disposable scalpel (29550, Exel Int). Using cotton tipped applicators (25-806 10WC, Puritan) the skull was exposed and cleaned of any minor connective tissues or blood. Once the area was clean, a handheld microdrill (Ideal Microdrill #67-1000, Cell Point Scientific) with a 0.9 mm burr (19007-09 Fine Scientific Tools) was used to create a burr hole into the cortex or cerebellum, corresponding to the in situ location of the source tissue. 2 µl of cell suspension (100,000 cells) was deposited into the intracranial space by inserting a 10 µl Rainin Pipette-lite fitted with a 2-10 µl ART tips barrier non-filtered pipette tip (2139, Thermo Scientific). A small piece of surgical foam (09-0396-05 Pfizer Injectables) was placed onto the burr hole before pulling the incision closed and bonding the skin together with veterinary-grade surgical glue (Vetbond, 3M). Following closure of the incision, mice were removed from Isofluorane and transferred to a clean recovery cage placed on a heat mat for duration of recovery. After recovery the mouse was returned to its home cage.

Mice implanted with patient-derived tumor cells were monitored regularly for signs of tumor formation, which can include distention of the calvarium, head tilt, reduced feeding, weight loss, dehydration, hunched posture, eye irritation, or poor grooming habits. Upon observation of symptoms, mice were euthanized and tumor presence was confirmed visually during tissue resection. Tumor tissue was formalin-fixed, cryopreserved, and processed for serial transplantation into a new cohort of mice.

2.2.19.3 Preclinical experiments

Orthotopic xenografts were surgically implanted as described above with tumor cells originating from symptomatic intracranial tumors in donor mice. Adult male and female NSG mice between 8 and 16 weeks of age were used in these experiments. The time between surgical implant of tumors and initiation of treatment was based on the typical latency between surgery and symptomatic tumor for each tumor model. When the first mouse in the cohort became symptomatic with a cranial bulge, the entire cohort was randomized into experimental groups of vehicle- or drug-treated. Experimental groups were normalized for age, gender, and severity of brain tumor symptoms. Vismodegib-treated mice received 1 mg/mouse of Vismodegib (S1082, Selleckchem) by oral gavage, five days on and then two days off, in a vehicle of 0.5% methylcellulose with 0.2% Tween-80 in water. Erlotinib-treated mice received 2 mg/mouse Erlotinib (S7786, Selleckchem) by oral gavage in a vehicle of 1% methylcellulose

with 0.1% tween-20 in water, every day for up to 30 days. Mice were monitored daily for symptoms of tumor progression until moribund. Tumors were harvested after euthanasia and frozen or fixed in 10% formalin. Differences in survival were evaluated using the log-rank (Mantel-Cox) test.

2.2.19.4 Tumor pathology

A pediatric pathologist evaluated PDOX tumors in comparison to the primary human tumor for all samples obtained from Seattle Children's and COG samples when available. Immunohistochemistry (IHC) analyses were performed on 4 μm paraffin sections of whole brain mounts stained using an automated Ventana Benchmark Stainer (Tucson, AZ). Sections were incubated with primary antibodies in the following concentrations: beta catenin, 1:200 (Dako, Carpinteria, CA); SFRP1, 1:50 (Thermo Scientific, Waltham, MA); NPRC 1:100 (Thermo Scientific, Waltham, MA); Kv1.1, 1:1000 (Novus Biologicals, Littleton, CO); CMYC, 1:200 (Thermo Scientific, Waltham, MA); NMYC 1:500 (Novus Biologicals, Littleton, CO); INI-1, 1:300 (BD Biosciences, San Jose, CA); EGFR 1:100 (Invitrogen, Carslbad, CA); ERBB2, 1:1000 (Dako, Carpinteria, CA); CD117, 1: 2000 (Dako, Carpinteria, CA); pERK, 1:50 (Cell Signaling Technology, Danvers, MA); PDGFR-alpha, 1:100 (Santa Cruz Biotechnology Inc., Dallas, TX); Synaptophysin, 1:800 (BioGenex, Fremont, CA); GFAP, 1:400 (Dako Carpinteria, CA); Ki67, 1:100 (Dako Carpinteria, CA); CD31, 1:100 (Dako, Carpinteria, CA); RB 1:200 (Thermo Scientific, Waltham, MA); PTEN, 1:50 (Thermo Scientific, Waltham, MA); p53, 1:50 (Proteintech, Chicago, IL); and GAB-1, 1:100 (Santa Cruz Biotechnology Inc., Dallas TX). Slides stained with PECAM, 1:50 (BD Biosciences) were blocked with mouse on mouse (M.O.M.) blocking reagent (Vector Laboratories, CA) prior to being run on the Ventana Benchmark Stainer. All antibodies were diluted in phosphate-buffered solution (PBS). Slides were incubated with biotinylated secondary antibodies, followed by incubation with the streptavidin and biotinylated peroxidase complex. Sections were counterstained with hematoxylin and mounted.

3 Results

Parts of the written contents and figures of the following chapter have been submitted in the research article "*A biobank of patient-derived molecularly characterized orthotopic pediatric brain tumor models*", Brabetz, Leary, Gröbner *et al.* (List of Publications, page 125) to *Nature Medicine* in July 2017. This research article included 30 PDOX lines generated in the laboratory of James M. Olson in Seattle (USA) and their molecular characterization. Some analyses were performed only for PDOX lines included in this manuscript and this group of PDOX lines will be referred to as "Seattle cohort" within this thesis. Contributions of authors other than myself are indicated.

3.1 Model generation and tumor engraftment

For this study, 130 PDOX models, which were created from freshly-obtained pediatric brain tumor specimens orthotopically transplanted into the corresponding brain region of NOD-scid IL2Rgamma^{null} (NSG) mice, were collected (Figure 4a, page 59). These 130 PDOX lines were created at six different centers around the world including DKFZ (Till Milde/Stefan M. Pfister, Heidelberg, Germany), Fred Hutchinson Cancer Research Center (James M. Olson, Seattle, USA), Institute Curie (Olivier Ayrault, Paris, France), Sanford Burnham Medical Discovery Institute (Robert J. Wechsler-Reya, San Diego, USA), Oregon Health and Science University (Yoon-Jae Cho, Portland, USA), and Baylor College of Medicine (Xiao-Nan Li, Houston, USA). All centers focused on the generation of PDOX lines from high-grade pediatric brain tumor entities, because low-grade pediatric brain tumors are known to not engraft in mice[450]. Only one low-grade tumor, P3635, a pleomorphic xanthoastrocytoma (PXA), was included in this cohort, which transformed during passaging from a grade II tumor to a grade III tumor[450]. In the Seattle cohort, an overall engraftment rate of 31.91% (30/94) was observed (Figure 4b). Engraftment rates varied between tumor entities (MB 40%, HGG 32%, EPN 19%, ATRT 25%), but did not differ significantly ($P > 0.05$) (Figure 4b). Interestingly, in the Seattle cohort, there was no difference of engraftment rates between tumor specimens that were transplanted on the same day of surgery and specimens that were shipped from various U.S. locations to Seattle overnight (Figure 4c). Indeed, seven of the 21 models generated in the center in Heidelberg had also been shipped overnight from sending centers, highlighting that it is possible to ship samples from collaborating centers to a central PDX generation center – the only possible way to reach reasonable numbers of PDX models for rare tumor entities. In order to test whether PDOX lines can easily be shared with other researchers using cryo preservation, twenty-two PDOX lines from the Seattle cohort were evaluated. All twenty-two PDOX lines could successfully be re-grown after cryo preservation (Figure 4d). Overall, 98% (52/53) of

thawing events were successful, with an average successful engraftment rate of 68% (213/311) in the entire test cohort (Figure 4d, page 59). Noteworthy, the percentage of mice where the tumor grew successfully per experiment varied between cryo vial batches from the same model (Figure 4d). This confirms that PDOX models can be used as a resource to be shared with other researchers, which makes it possible to generate reasonable cohorts, even of PDOX models of rare tumor entities, in order to conduct systematic preclinical screens.

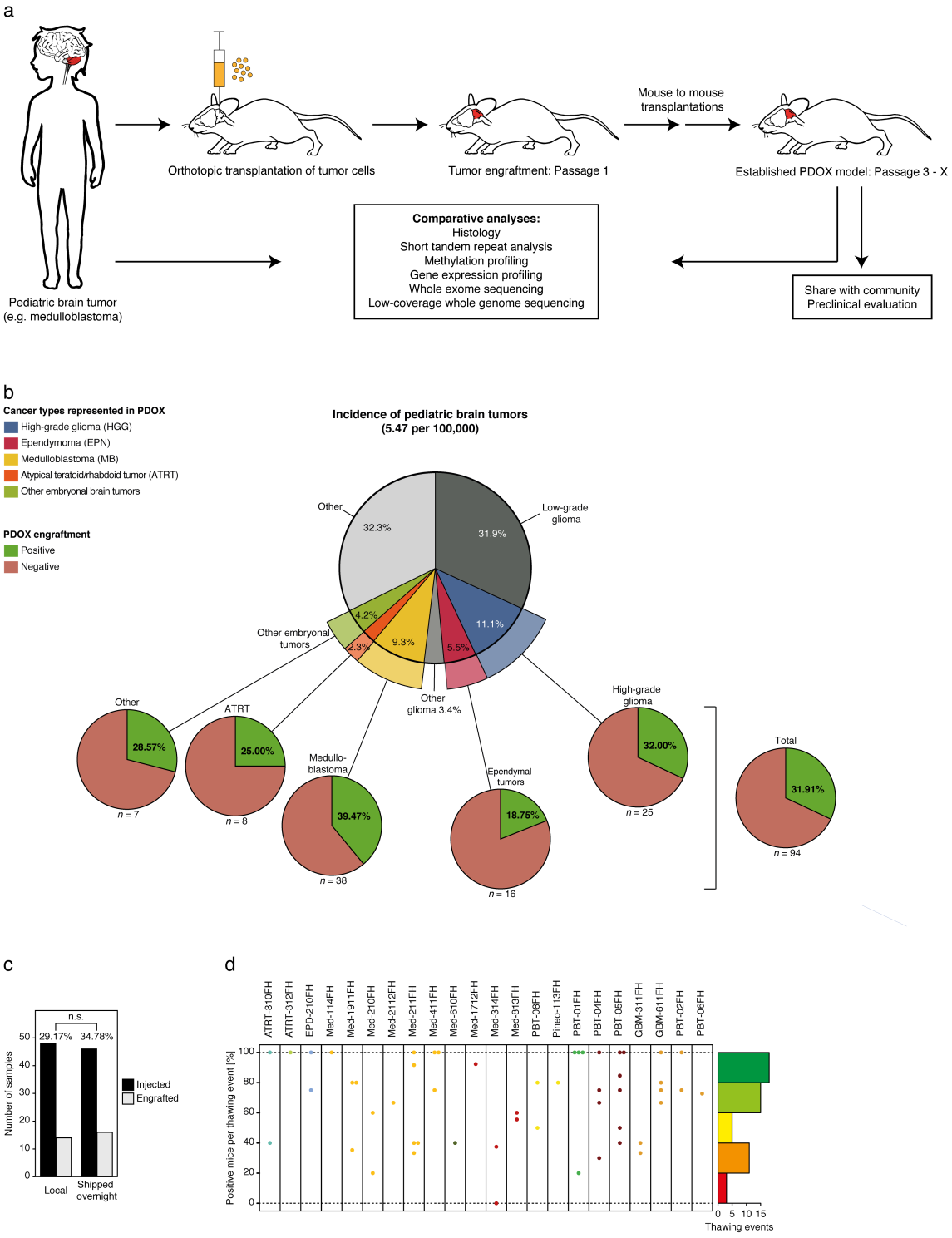

Figure 4: PDOX of pediatric brain tumors.
(**a**) Schematic illustration of the establishment and characterization pipeline of PDOX models of pediatric brain tumors. Example is for a tumor located in the posterior fossa (e.g. MB). Tumors were injected in the brain region in the mouse corresponding to the location of the tumor in the patient. Drawings of the child and the mouse were kindly provided by Susanne N. Gröbner (DKFZ, Heidelberg, Germany). (**b**) PDOX engraftment rates of pediatric brain tumors (Seattle cohort) in context of entities and incidences of pediatric brain tumors[220]. (**c**) Comparison of engraftment rates between patient samples transplanted the same day (local) and external samples shipped overnight and transplanted the next day (n = 96, P = n.s.) (Seattle cohort). (**d**) Engraftment rates per re-transplantation of a cryo-preserved PDOX line (Seattle cohort). Each dot represents one thawing event. Color of dots is based on the molecular subgroup of the individual line (Figure 6, page 62). Data for panels (**b**), (**c**), and (**d**) were generated in the

laboratory of James M. Olson (Fred Hutchinson Cancer Research Center, Seattle, USA) and were analyzed by myself.

3.2 Tumor histology*

Histologically, PDOX tumors of the Seattle cohort closely resembled the human tumors from which they were derived. Representative comparative histology and IHC stains from several patient tumors and PDOX models are shown in Figure 5.

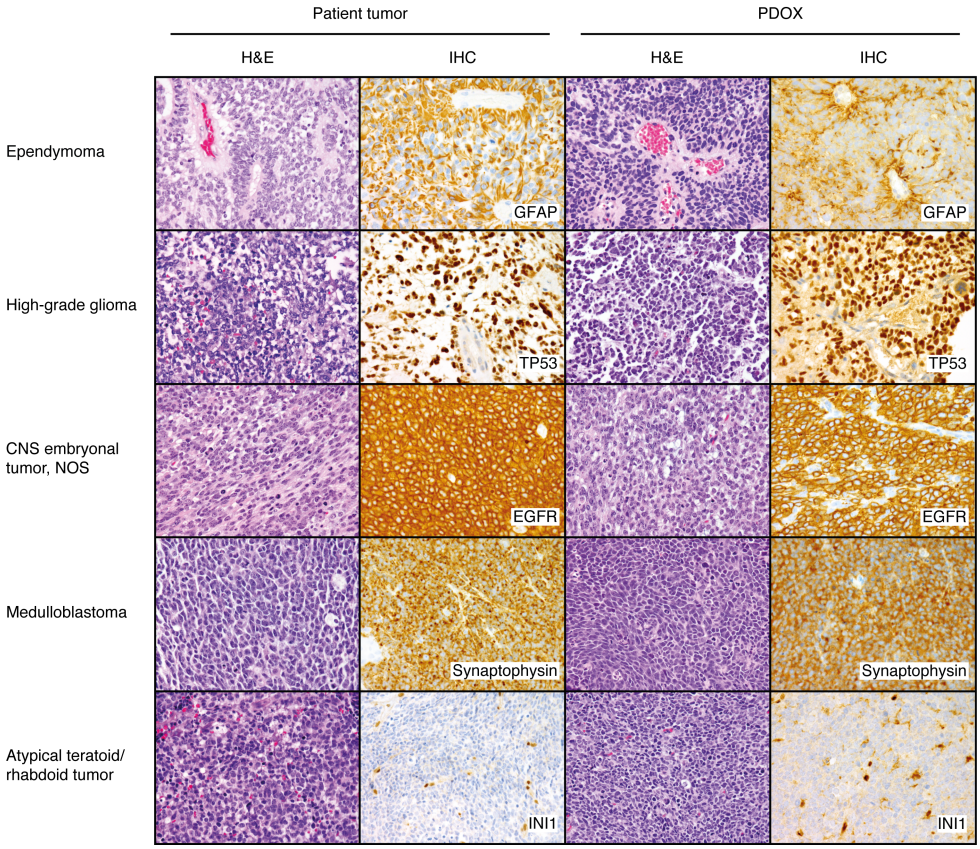

Figure 5: Histology and IHC are conserved in PDOX.
Representative comparative histology showing stable morphologic appearance of PDOX tumors in reference to patient tumor used to generate the PDOX. Histopathological analyses were performed by Bonnie Cole (Seattle Children's and the University of Washington, Seattle, USA).

For instance, characteristic pseudorosette formation present in primary EPN was maintained in the corresponding PDOX model. Synaptophysin staining, typically seen in MB tumors, was still present in the MB PDOX models. In addition, molecular alterations detected by IHC were maintained in the corresponding PDOX models, such as the absence of SMARCB1/INI1 in the

*This section of the thesis was taken in its entirety from the research article "*A biobank of patient-derived molecularly characterized orthotopic pediatric brain tumor models*". The described experiments were performed by the laboratory of James M. Olson in Seattle (USA), and therefore this part of text was written jointly with members of the Olson laboratory.

ATRT models or the nuclear accumulation of TP53 or EGFR overexpression in HGG or PNET models.

3.3 Molecular subgrouping of PDOX models

In the past few years, DNA methylation profiling using Illumina arrays has proven to be a powerful tool for tumor classification and identification of distinct molecular subtypes within histological entities[273,316,333,342,451]. Therefore, all PDOX models (early passage [XP1-XP3] n = 130, late passage [XP5-XP6] n = 26) and, if available, their matching patient tumors (n = 91) were molecularly characterized by DNA methylation profiling. t-Distributed Stochastic Neighbor Embedding (tSNE) analysis of pairwise sample similarities of the generated methylation profiles, supplemented by 2,796 reference profiles[342] representing nearly all WHO classified brain tumor types[218] (Figure 6a, page 62), robustly grouped 129 preclinical models into various subgroups of pediatric brain tumors (Figure 6b). Only one PDOX line (G6999) and its matching patient tumor were not classifiable (Figure 6b), because they clustered separately from all reference cases, and therefore likely represent a very rare brain tumor type that was not represented in the reference cohort at this stage. Collectively, methylation profiling grouped the PDOX models in the following tumor (sub)groups: 62 MBs, consisting of four MB WNT, 21 MB SHH (14 adult, 7 infant), 24 MB Group 3, and 13 MB Group 4; 24 HGG models, six of the K27 subgroup, one model of the G34 subgroup, and 17 non-IDH mutant and non histone-mutant pediatric glioma models; 17 EPN PDOX models, 11 of the PF A subgroup, and six of the RELA subgroup; 11 ATRT PDOX, eight of the SHH subgroup, two of the MYC subgroup, and one of the TYR subgroup; three pineoblastoma subgroup B PDOX models; five ETMR PDOX models; four former PNET PDOX lines, consisting of one CNS NB FOXR2 PDOX line, two EFT CIC lines, and one HGNET BCOR line; one PXA PDOX line; one CNS melanoma PDOX line; and one B-cell lymphoma PDOX (Figure 6b). Within the tSNE analysis, primary patient tumor and corresponding early and late PDOX tumors clustered closely together within their respective cluster, confirming that both early and later PDOX passages faithfully reflect the original disease (Figure 6b). As non-IDH-mutant and non-histone-mutant glioma models are a challenge for sub-classification within the pan-brain tumor reference set, the candidate PDOX lines were also clustered with reference samples from the three newly-detected IDH-/histone-wild-type pediatric glioma subgroups[266]. This reliably classified the 17 models into four models of the MYCN subgroup, 11 models of the midline/pedRTK1 subgroup, and two models of the RTKIII/pedRTKII subgroup[266] (Figure 7, page 63). In summary, 129 PDOX models, representing 22 distinct molecular subgroups of pediatric brain tumors, were successfully characterized and classified.

a

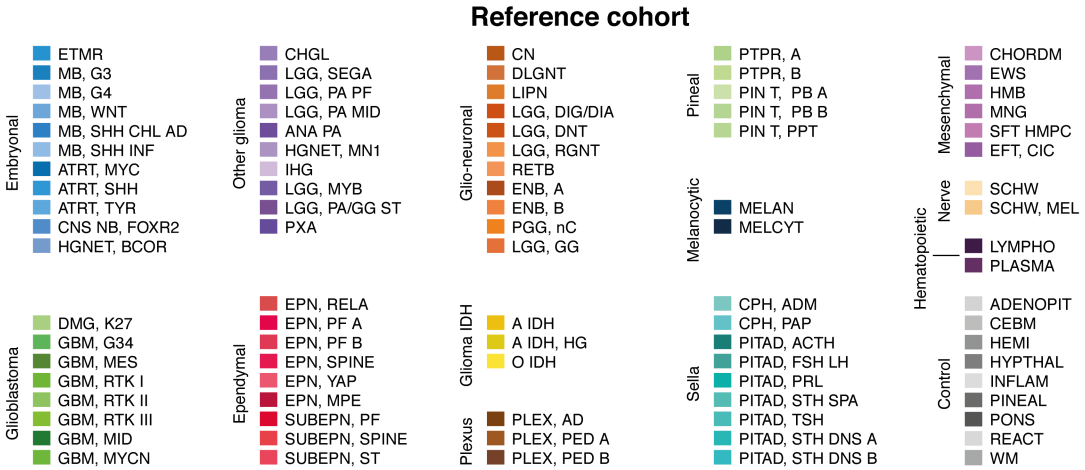

b

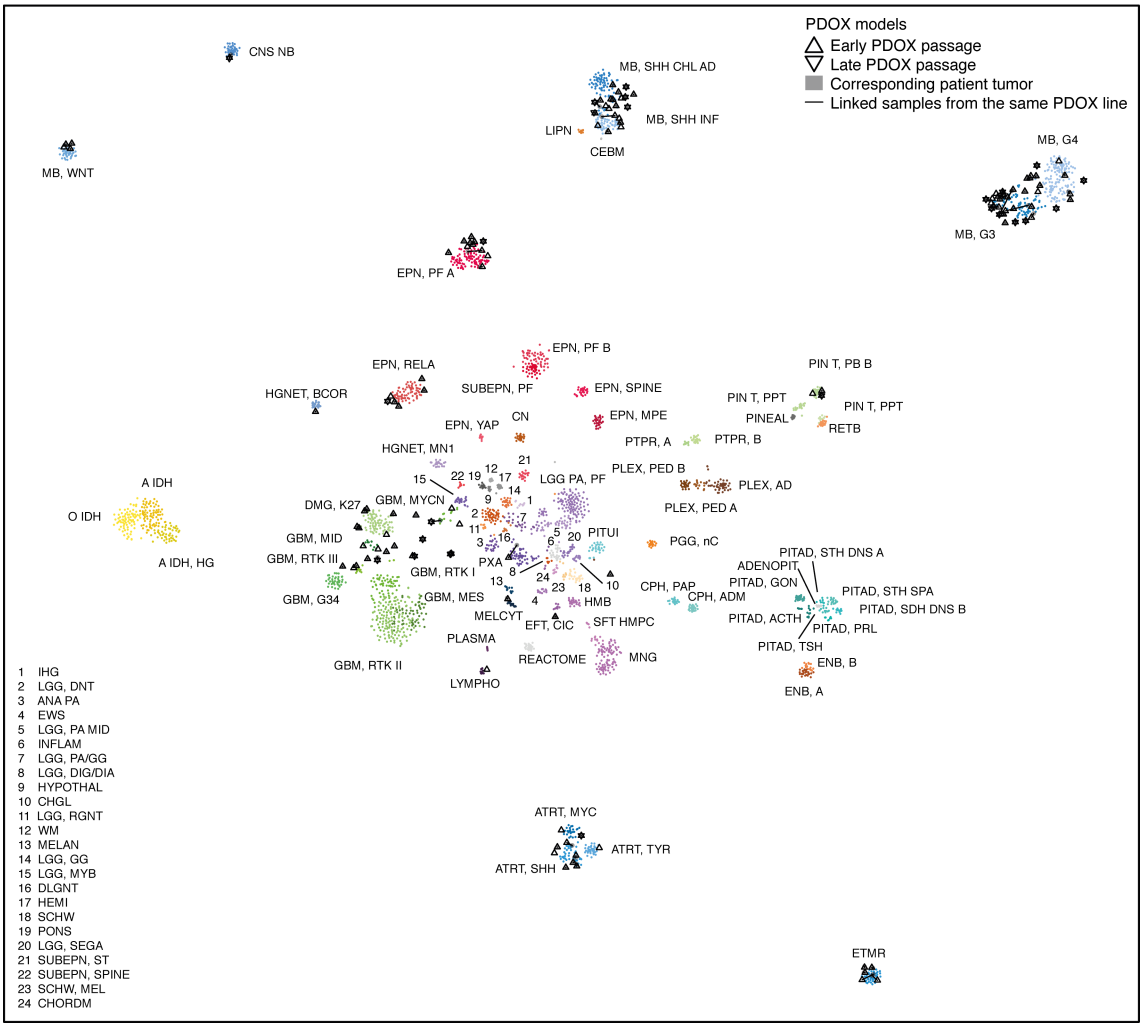

Figure 6: Molecular subgrouping of PDOX.
(**a**) Methylation subgroups of brain tumors as defined by Capper *et al.*[342]. A basic explanation of the subtypes can be found in Table 3 (page 103). An in-depth description can be found at http://www.molecularneuropathology.org or its associated research article[342]. (**b**) 2D representation of pairwise sample correlations of methylation probes by tSNE dimension reduction of 3,043 samples, consisting of 130 early PDOX passages, 26 late PDOX passages, 91 matching patient tumors and 2,796

reference cases[342]. Reference samples are colored according to their molecular reference entity. Early PDOX passages are shown as triangles pointed up, late PDOX passages as triangles pointed down. Samples belonging to the same model/tumor are linked with black lines.

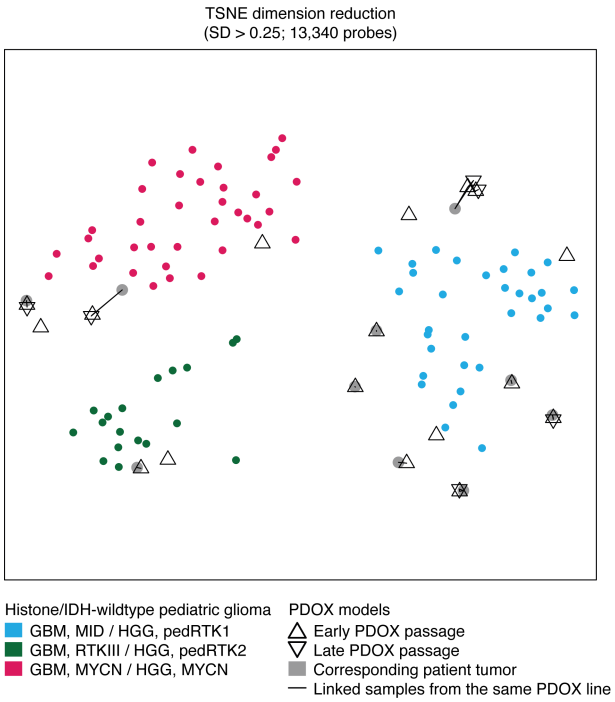

Figure 7: Molecular subgrouping of non IDH-mutant and non histone-mutant glioma models.
2D representation of pairwise sample correlations of methylation probes (SD > 0.25) by tSNE dimension reduction of 120 samples, comprising of 17 early PDOX passages, 6 late PDOX passages, 10 matching patient tumors, and 87 reference cases[266].

For MB, the tumor entity with the longest history of molecular subgrouping, additional heterogeneity beyond the classic four subgroups had been discovered in recent research[294,311,312]. tSNE analysis of all MB PDOX lines within the reference cohort of 1,251 samples from Northcott *et al.*[294] reliably disaggregated the PDOX lines into the four classic MB subgroups – WNT, SHH, Group 3, and Group 4 (Figure 8a, page 64), with a significant overlap between Group 3 and Group 4 tumors being observed. Repeating the analysis and restricting it to only Group 3 and Group 4 PDOX lines, the matching patient tumors, and reference samples, annotated with the new Group 3 and Group 4 subtypes determined in Northcott *et al.*[294], split the 37 Group 3 and Group 4 PDOX lines into each of the eight newly defined subtypes (I: 4, II: 19, III: 3, IV: 2, V: 2, VI: 2, VII: 2, VIII: 3) (Figure 8b). Thus, overall, this PDOX cohort represents the entire subgroup heterogeneity of Group 3 and Group 4 MB, although there is a strong over-representation of PDOX lines from the high-risk subtype II, which is enriched for tumors with *MYC* amplifications. Both PDOX line and matching patient tumor always clustered into the same subtype, except for one model (Med-2112FH), for which the human tumor clustered in subtype IV and the PDOX in subtype II.

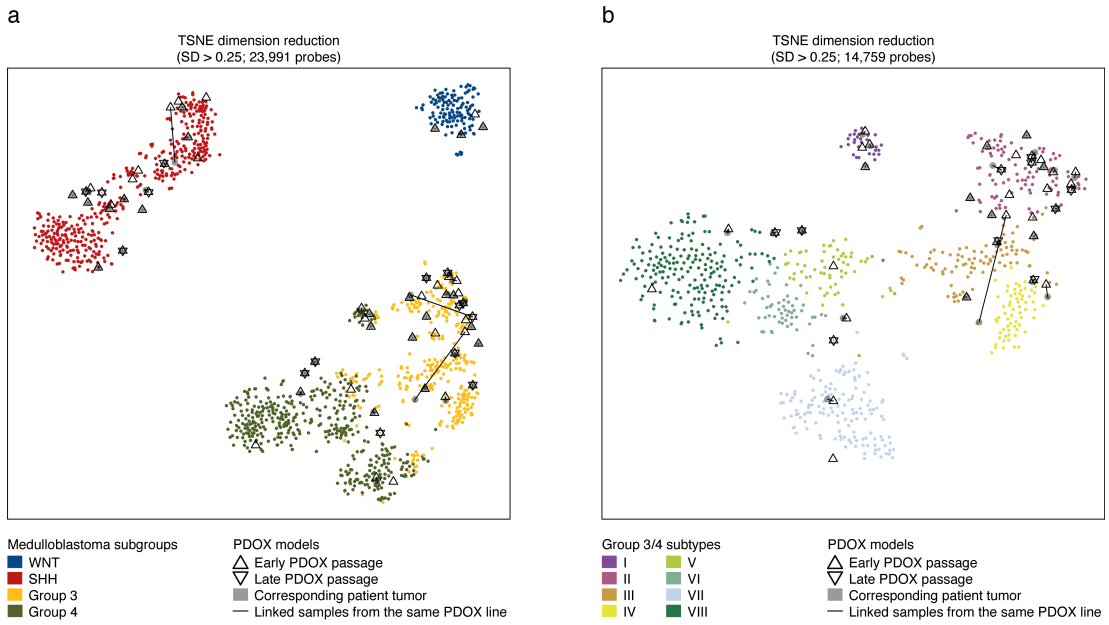

Figure 8: Molecular subgrouping of medulloblastoma PDOX.
2D representation of pairwise sample correlations of methylation probes (SD > 0.25) by tSNE dimension reduction. (**a**) 1,370 samples, consisting of 62 early PDOX passages, 15 late PDOX passages, 42 matching patient tumors, and 1,251 reference cases, representing medulloblastoma. (**b**) 849 samples, consisting of 37 early PDOX passages, 10 late PDOX passages, 26 matching patient tumors and 776 reference cases[294], representing Group 3 and Group 4 medulloblastoma. Reference samples are colored according to their molecular reference entity. Early PDOX passages are shown as triangles pointed up, late PDOX passages as triangles pointed down. Samples belonging to the same model/tumor are linked with black lines.

3.4 Genomic landscape of PDOX models

In order to select the most appropriate PDOX model for preclinical studies, it is essential to know the underlying mutation pattern of disease-relevant oncogenes and tumor suppressor genes, even after accounting for molecular subgroups. For instance, targeted therapy of SHH MB using SMO-inhibitors is expected to be effective only when the SHH pathway is activated by upstream mutations in either *PTCH1* or *SMO*, but not when it is activated by downstream mutations in *SUFU* or amplification of *MYCN* and/or *GLI2*[299]. Therefore, PDOX models were examined using whole exome (WES) (n = 62) and low-coverage whole genome sequencing (WGSlc) (n = 60), and, if available, also the matching patient tumors (WES n = 26, WGSlc n = 24, whole genome sequencing n = 5). In addition, for 48 potential driver mutations, the presence of the mutations detected in the early PDOX passage was validated in the late passage (when available) by Sanger sequencing (Seattle cohort). If sequencing data was not available, information on the copy number status was taken from copy number profiles based on methylation arrays. In addition, gene expression profiles were generated (PDOX n = 77, matching patient tumors n = 32) using Affymetrix U133 plus 2.0 arrays. As matching germline controls were unavailable for 51 of the 62 PDOX models available for sequencing, the comprehensive calling of somatic variants for these samples was not possible. Hence, variants

with a minor allele frequency of lower than 0.1% in the population were excluded and cancer genes, recurrently mutated in the specific tumor entities as identified in previous sequencing studies, were highlighted as potential driver genes[294,445].

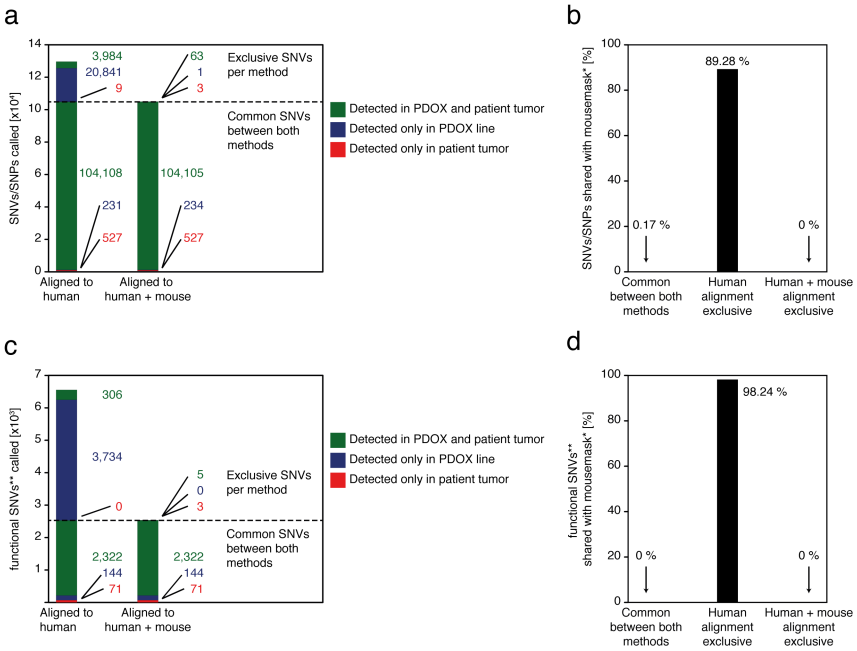

Figure 9: Aligning next-generation sequencing data to a combined human and murine genome filters out artifacts introduced by murine contamination.
Comparison of SNVs/SNPs (**a**) or functional SNVs** (**c**) called in a cohort of WES data of 19 paired human tumors and PDOX models (Seattle cohort) by aligning to only a human reference genome (hg19) or to a combined human and murine reference genome (hg19 + mm10). The mutations shown are split (dotted line) based on whether the mutations were detected by both methods or not, and colored based on whether they are present only in the patient tumor or the PDOX, or in both of them. Overlap of SNVs/SNPs (**b**) or functional SNVs** (**d**) with mousemask* to estimate the artifact burden introduced by mouse tissue. *The mousemask, which contains artifacts introduced by mouse tissue being present in human exome data, was generated by performing WES on murine brain tissue and aligning to the human genome. **The illustrated counts are predicted somatic mutations, as no germline control was available. Susanne N. Gröbner performed alignment and variant calling of sequencing data, whereas downstream analyses were performed by myself.

In order to avoid potential false positive mutation calls induced by contaminating mouse DNA, all sequencing reads were aligned to a combined human and mouse reference genome, and all reads mapped to the mouse genome were excluded[420]. The results from this method were benchmarked against alignment to the human reference genome only. Indeed, mutation calling after aligning only to the human genome resulted in far more mutation calls (6,605) than after alignment to a merged reference (2,549) on a dataset of 19 human tumor and PDOX WES pairs (Seattle cohort) (Figure 9c). This was also true without the filter for potentially somatic mutations (human: 129,902; merged: 105,038) (Figure 9a). Of the potentially somatic SNVs exclusively found after alignment to only the human genome, 92.47% were found only in the PDOX and not in the matching human tumor (Figure 9c), supporting the hypothesis that these

additional mutations are probably false positive calls. To prove that these additional mutations are artifacts induced by mouse reads, WES data from mouse tissue were aligned only to the human genome, and subjected to variant calling. Indeed, these artifact mutations overlapped with 98% of all human alignment-specific mutations, but not with mutation calls either shared between alignment methods or exclusive to alignment to the merged chromosomes (Figure 9d, page 65).

The sequencing analyses showed that all models harbored genetic alterations characteristic of the respective disease (Figure 10 - Figure 14). Within MB, the different subgroups are characterized by various driver mutations, which are preserved in the matching PDOX. For instance, the MB-WNT model Med-913FH contains a prototypic *CTNNB1* mutation (Figure 10a, page 67), and 94% (16/17) of SHH PDOX models were characterized by the presence of SHH pathway activations at distinct levels of the pathway[299]. The *PTCH1* locus was affected in 29% (5/17[*]) of the lines, and the *SUFU* locus in 18% (3/17[*]), while 29% (8/21) of the lines harbor an amplification of either *MYCN* and/or *GLI2* in combination with a *TP53* defect (Figure 10b). *SMO* alterations, typically found in adult MB patients, were found only once in combination with a *MYCN* amplification in the RCMB18 line (Figure 10b). This most likely reflects the strong bias for pediatric patients in this cohort. In one case with complete DNA sequencing data (WES + WGSlc), no lesion in the SHH pathway was found, which turned out to be a patient with a bi-allelic germline *BRCA2* deficiency (B062_13315) (Figure 10b). The remaining five cases presented in Figure 10b without lesions in the SHH pathway lacked WES data, so it was only possible to exclude copy number alterations as the driver, but other driving mutations could not yet be examined. In addition to the main drivers of SHH MB, other alterations that are typically found in this disease, such as *CREBBP*, *YAP1*, or *ARID1A*, were identified (Figure 10b). A comparison of the frequency of alterations in the PDOX cohort with a published cohort of primary MB[294] highlighted a significant overrepresentation of alterations targeting *MYCN* (29% in PDOX cohort vs. 8% in reference cohort; $P < 0.01$), *GLI2* (29% vs. 9%; $P < 0.05$), *TP53* (35% vs. 13%; $P < 0.05$), and *ARID1A* (18% vs. 2%; $P < 0.01$). Except for *ARID1A,* all genes characterize the high-risk group of *TP53*-mutant SHH MB, which is also highly enriched for Li-Fraumeni Syndrome patients harboring germline *TP53* variants[285,298-302] (Figure 10b).

[*]PDOX models negative for the target lesion and lacking WES data were excluded from the statistical analysis.

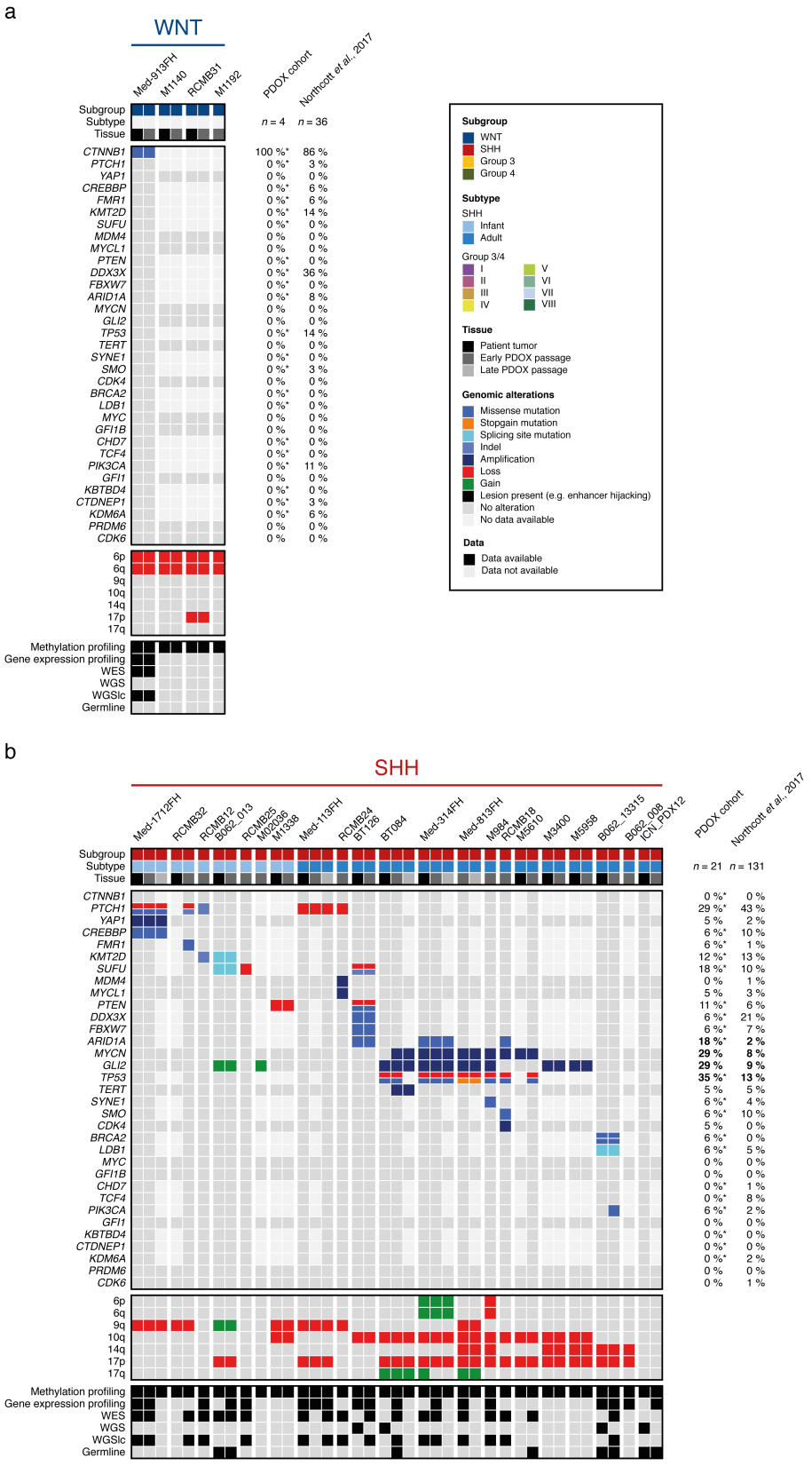

Figure 10: Molecular landscape of WNT and SHH medulloblastoma PDOX models.
Hallmark genomic alterations including amplifications, deletions, mutations, and chromosomal arm changes are consistent between patient tumor and PDOX models at early and late passages in (**a**) WNT MB and (**b**) SHH MB. Population frequencies are based on the reference cohort of Northcott *et al.*, 2017[294]. *PDOX models negative for the target lesion and lacking WES data were excluded from the statistical analysis.

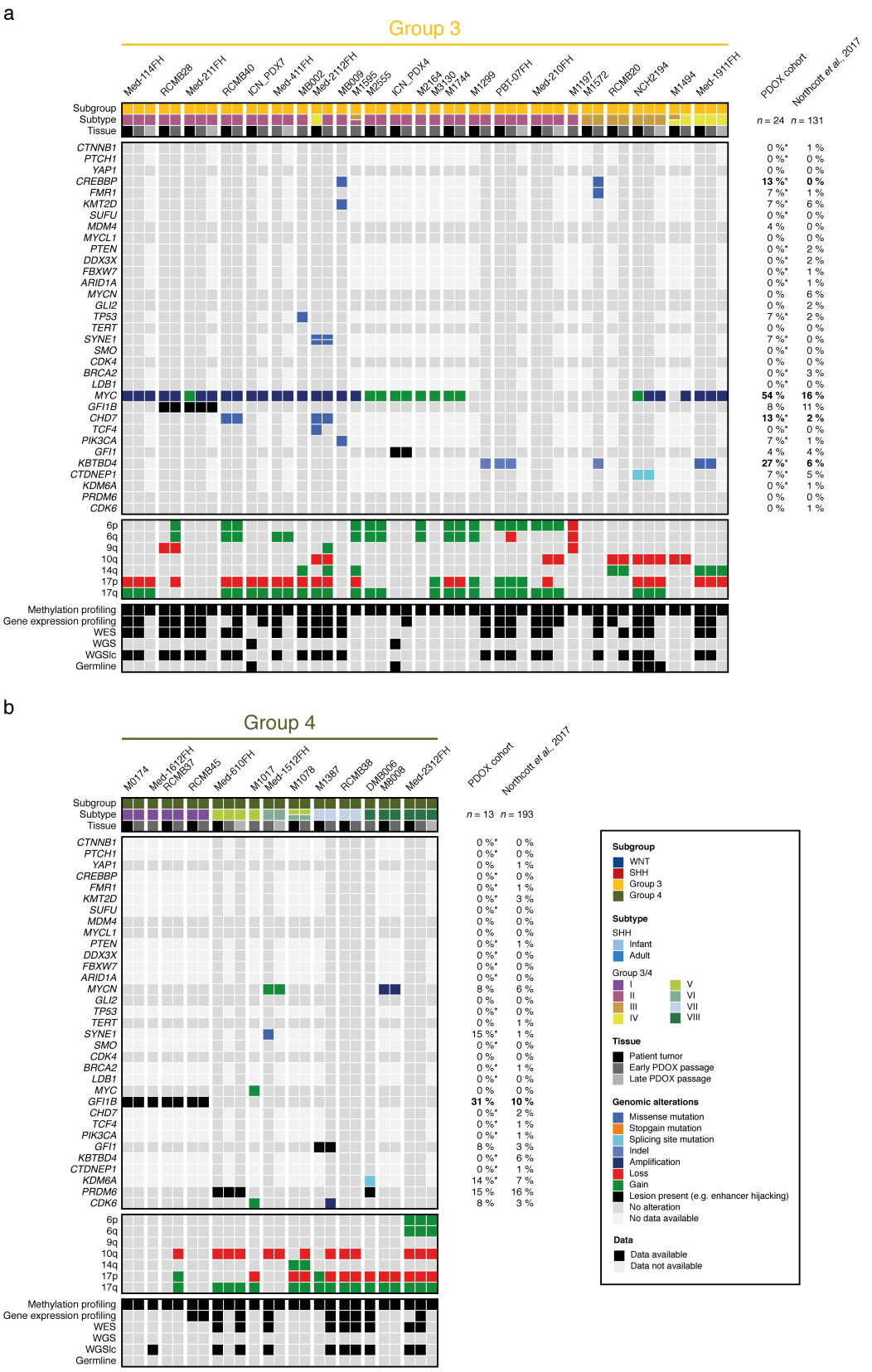

Figure 11: Molecular landscape of Group 3 and Group 4 medulloblastoma PDOX models. Hallmark genomic alterations including amplifications, deletions, mutations, and chromosomal arm changes are consistent between patient tumor and PDOX models at early and late passages in (**a**) Group 3 MB and (**b**) Group 4 MB. Population frequencies are based on the reference cohort of Northcott *et al.*, 2017[294]. *PDOX models negative for the target lesion and lacking WES data were excluded from the statistical analysis.

In concordance, Group 3 MB PDOX, typically characterized by a MYC gene signature, harbored an amplification of the *MYC* locus in 54% (13/24) of the cases, which is a significant overrepresentation compared to primary tumor cohorts (16%; $P < 0.0001$) (Figure 11a, page 68) and also defines a population of very high-risk tumors with a poor prognosis[298]. Of note, in 23% (3/13) of *MYC* amplified PDOX lines, the *MYC* amplification was not found in the patient tumor, highlighting the possibility of clonal outgrowth after transplantation (Figure 11a). Mutually exclusive to the *MYC* amplification, the recently described hotspot insertion in *KBTBD4*[294] was detected in three PDOX lines (Figure 11a). In addition, one potentially rare SNP or SNV in *KBTBD4* in a *MYC* amplified line (Med-1911FH) was identified (Figure 11a). Out of the four lines without *MYC* amplification with available WES data, only one line (Med-210FH) did not harbor the *KBTBD4* hotspot insertion, and overall, compared to the reference population, *KBTBD4* events were enriched in the PDOX cohort (27% vs. 6%; $P < 0.01$) (Figure 11a). In addition to these events, other typical alterations were detected, such as mutations in *KMT2D* or *CTDNEP1* (Figure 11a). Mutations in *CREBBP* were also detected in two lines without germline control (MB009, M1572) (Figure 11a), which usually occur only somatically in SHH MB, but have been reported to occur in the germline of Group 3 and 4 MB patients[452,453]. A novel finding in the biology of Group 3 and Group 4 MB in the past few years was the identification of enhancer hijacking events, where, through a structural alteration, an active enhancer is translocated into the proximity of an oncogene, thereby activating its expression[294,309]. Overall, eleven PDOX lines with a focal structural alteration and associated gene upregulation (when expression data was available) in the candidate genes *GFI1* (Figure 12a,b, page 70), *GFI1B* (Figure 12c,d), and *PRDM6* (Figure 12e,f) were detected in the entire PDOX cohort. Two *GFI1B* events and one *GFI1* event were detected in the cohort of Group 3 MB (Figure 11a). Unexpectedly, in the *MYC*-amplified PDOX line RCMB28, the structural alteration close to the *GFI1B* locus was preserved in the PDOX when compared to the patient tumor, but the expression of *GFI1B* in the PDOX was not elevated any further (Figure 12c,d). This observation might suggest that under certain circumstances, the expression of *GFI1B* may be important only for the initiation of the tumor, but not for tumor maintenance. Within Group 4 MB, all four lines of subtype I were found to have a *GFI1B* event; one additional line (M1387) showed *GFI1* activation, and two lines, both in the new subtype V, harbored a *PRDM6* enhancer hijacking event (Figure 11b). Other events detected in Group 4 MB PDOX were a *KDM6A* mutation, a *CDK6* amplification, or a *MYCN* amplification (Figure 12b). However, within the Group 4 MB PDOX, the *MYCN* amplified lines were not enriched as in SHH MB (Figure 10b, page 67; Figure 11b), corresponding to *MYCN* amplifications being associated only with a poor prognosis in the SHH subgroup and not in the Group 4 subgroup of MB[298]. In contrast, *GFI1B* activated lines were significantly enriched only in Group 4 MB

PDOX (31% vs. 10%; $P < 0.05$), but not in Group 3 MB PDOX (8% vs. 11%; P = n.s.) (Figure 11, page 68).

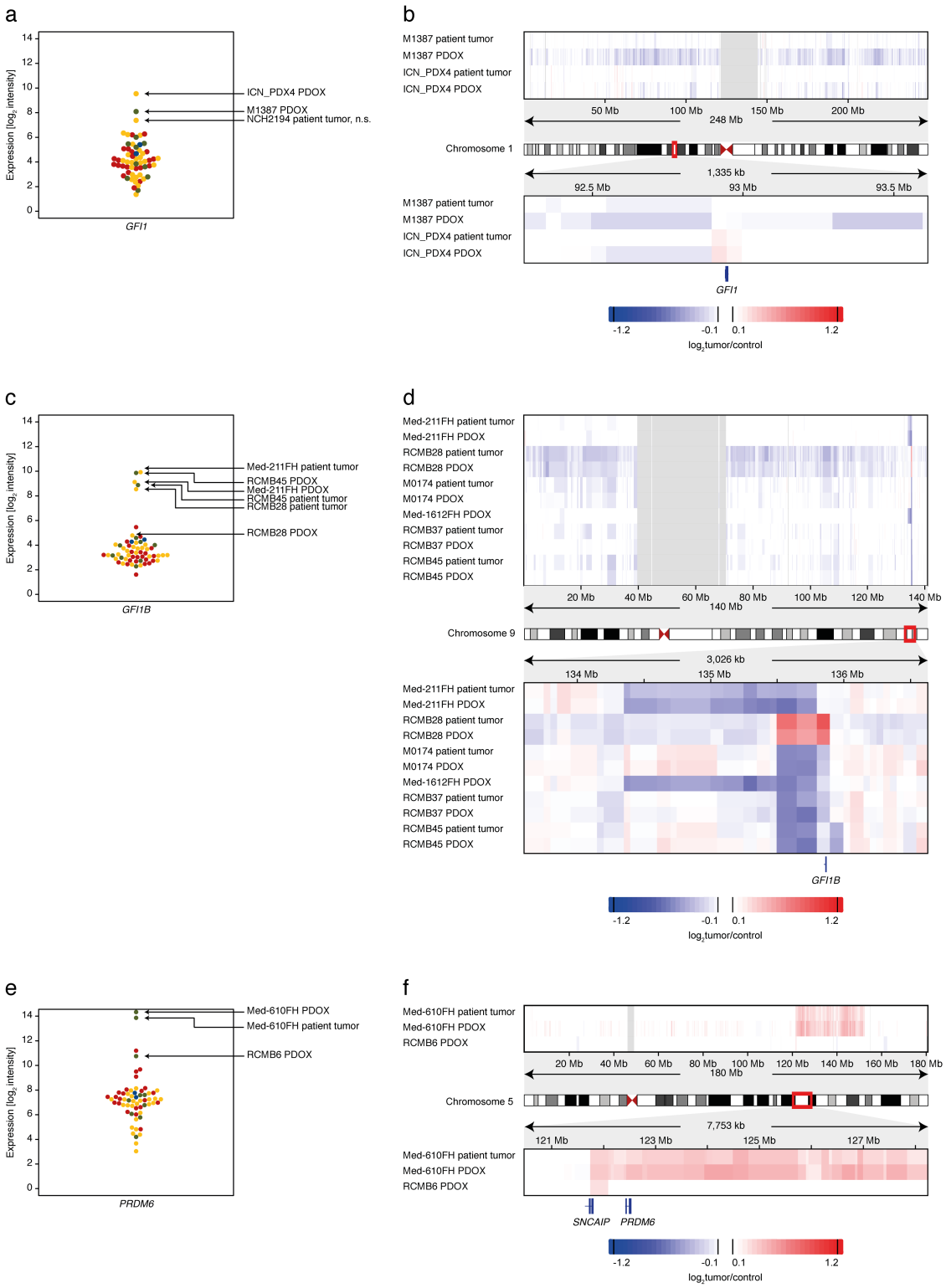

Figure 12: Enhancer hijacking events detected in medulloblastoma PDOX.
Expression values of (**a**) *GFI1*, (**c**) *GFI1B*, and (**e**) *PRDM6* across the cohort of patient tumors and PDOX (MB only). Outliers with gene activation are highlighted. The shown tumors are colored based on their molecular subgroup (WNT – blue, SHH – red, Group 3 – yellow, Group 4 – green). Copy number

states (based on methylation array data) of enhancer hijacking candidates in PDOX and patient tumors of the (**a**) *GFI1*, (**c**) *GFI1B*, and (**e**) *PRDM6* loci. Relative copy number is coded as indicated in the legend (high – red, low – blue). In (**d**), PDOX lines of methylation subtype I were also included.

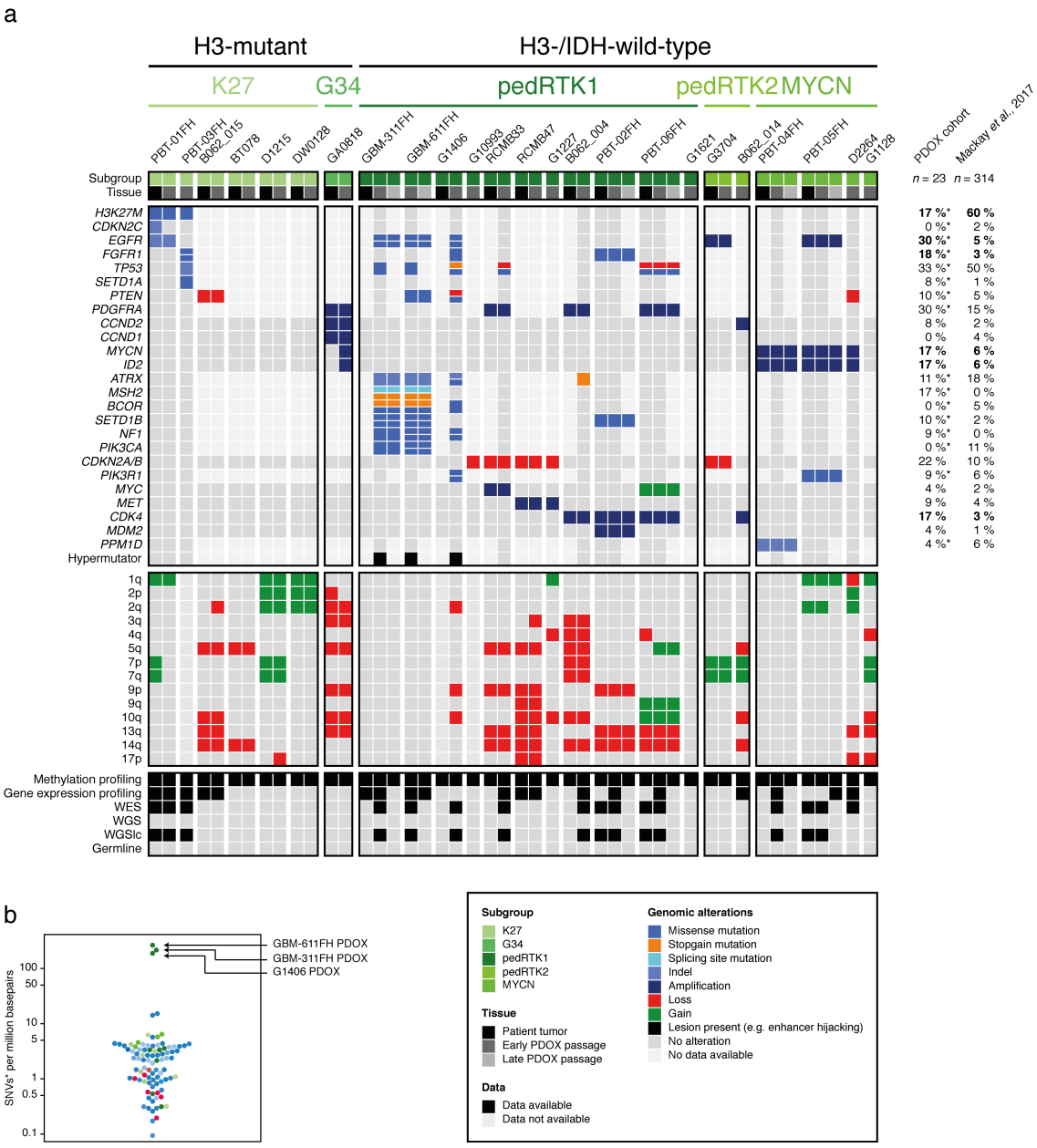

Figure 13: Molecular landscape of high-grade glioma PDOX models.
(**a**) Hallmark genomic alterations including amplifications, deletions, mutations, and chromosomal arm changes are consistent between patient tumor and PDOX models at early and late passages in high-grade glioma. Population frequencies are based on the reference cohort of Mackay *et al.*, 2017[445]. (**b**) Single nucleotide variant frequency per megabase across cohort of PDOX and patient tumors. Outliers (hypermutators) are highlighted. The tumors are colored based on their molecular subgroup (Figure 6, page 62). *PDOX models negative for the target lesion and lacking WES data were excluded from the statistical analysis. **The illustrated counts are predicted somatic mutations, because, except for in eight cases, no germline control was available.

PDOX models of pediatric HGG also showed subgroup-specific alterations. PDOX models of the K27 methylation subgroup harbored mutations in either *H3F3A* or *HIST1H3B,* and models

of the MYCN subgroup contained the prototypic *MYCN* and *ID2* co-amplification in 75% (3/4) of the cases (Figure 13a, page 71). Other typical alterations included *CDKN2A/B* loss or alterations in receptor tyrosine kinases such as *PDGFRA* or *EGFR*, which are characteristic for the pedRTK1 or pedRTK2 subgroup, respectively (Figure 13a). Comparing the landscape of PDOX models to a reference cohort of pediatric HGG[445], a strong under-representation of histone-mutant models (17% vs. 60%; $P < 0.01$) and an overrepresentation of lesions in *EGFR* (17 % vs. 5%; $P < 0.001$), *FGFR1* (18% vs. 3%; $P < 0.01$), *MYCN* (17% vs. 6%; $P < 0.05$), *ID2* (17% vs. 6%; $P < 0.05$), and *CDK4* (17% vs. 3%; $P < 0.001$) was observed (Figure 13a). Remarkably, three PDOX lines (GBM-311FH, GBM-611FH, G1406) of the pedRTK1 subgroup showed a hypermutator phenotype (Figure 13b). GBM-311FH and GBM-611FH were both generated from the same patient, at the point of primary tumor lesion and autopsy, respectively, and both harbored *MSH2* mutations, explaining the hypermutator phenotype (Figure 13a). The genetic cause for the hypermutator phenotype in G1406 is not yet known.

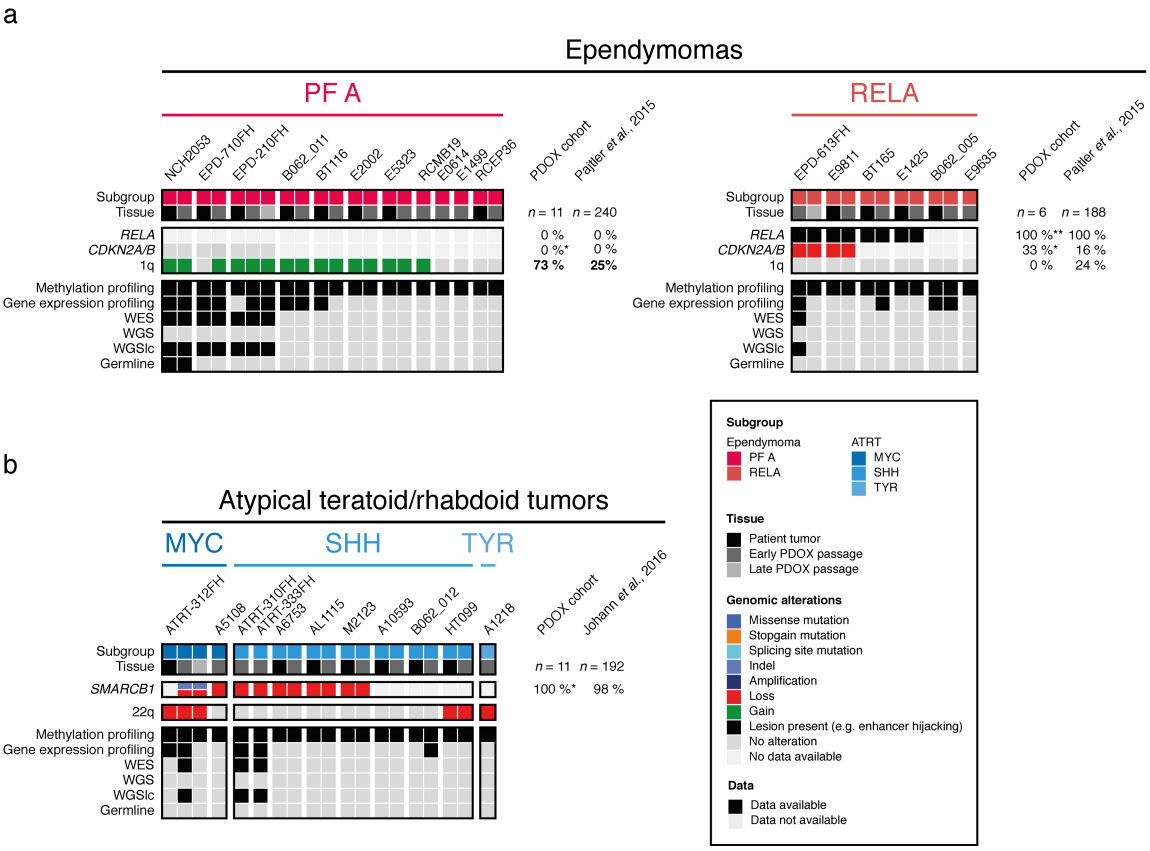

Figure 14: Molecular landscape of ependymoma and atypical teratoid/rhabdoid tumor PDOX models.
Hallmark genomic alterations including amplifications, deletions, and mutations are consistent between patient tumor and PDOX models at early and late passages in (**a**) EPN and (**b**) ATRT. Population frequencies are based on the reference cohort of Pajtler *et al.*, 2015[273] and Johann *et al.*, 2016[316]. *PDOX models negative for the target lesion and lacking WES data were excluded from the statistical analysis. **PDOX models negative for the target lesion and lacking RNAseq data were excluded from the statistical analysis.

PDOX models of EPNs and ATRTs also harbored the typical lesions such as *RELA* fusions or *CDKN2A/B* loss in RELA subgroup EPN or *SMARCB1* deactivation in ATRT (Figure 14, page 72). As in the primary tumors, no oncogenic drivers were found in the EPN PF A models. However, compared to a published reference cohort[273], a strong overrepresentation (73% (8/11) vs. 25%; $P < 0.001$) of PDOX with chromosome 1q gains, associated with a poor prognosis in this disease[454], was observed (Figure 14a).

Overall, this PDOX cohort represents a variety of patient populations even within tumor subgroups. However, the molecular landscape is biased toward very aggressive tumor subgroups, such as *TP53*-mutant SHH MB, *MYC* amplified Group 3 MB, *MYCN* and *ID2* amplified HGG, or 1q gained EPN PF A. The enrichment of genetic alterations not previously linked to a poor prognosis in our PDOX cohort, such as *GFI1B* only in Group 4 and not in Group 3 MB, may be the result of the cohort used for injection having a bias toward high-risk patients, but also may provide indications for the prognostic implications of certain genetic alterations, which have not yet been evaluated in a clinical setting.

3.5 Molecular fidelity of PDOX models

In addition to evaluating the genomic landscape of PDOX models of pediatric brain tumors on the demographic level and assessing which model could represent which group of patients, it was also systematically assessed how PDOX models may differ from their originating patient tumor at the mutational, copy number, methylome, and transcriptome levels.

In general, recurrently mutated events of reference cohorts found in the patient tumor were always maintained in the PDOX. However, two exceptions were observed: 1) Loss of a subclonal *TCF4* mutation in a Group 3 MB PDOX (Med-2112FH); and 2) loss of expression of the enhancer hijacking target *GFI1B* in a Group 3 MB PDOX (RCMB28). In contrast, the selection of entity-specific driver events in PDOX lines was observed more often: Gain of a *CDKN2C* indel in a K27 HGG PDOX (PBT-01FH), *MYCN* amplification in SHH MB (BT084), a subclonal *PIK3CA* mutation (B062_13315), *MYC* amplification in Group 3 MB (NCH2194, Med-211FH, M1494), and 1q gain in EPN PFA (EPD-710FH). Both kinds of events are most likely the result of a clonal outgrowth of a minor clone during PDOX engraftment. In the context of the *MYC* outgrowth of Med-211FH, intratumoral heterogeneity was evaluated via immunohistochemistry (IHC). Indeed, MYC protein expression was found in every cell in the PDOX, while the patient tumor contained tumor cells with both high and low MYC protein expression (Figure 15, page 74).

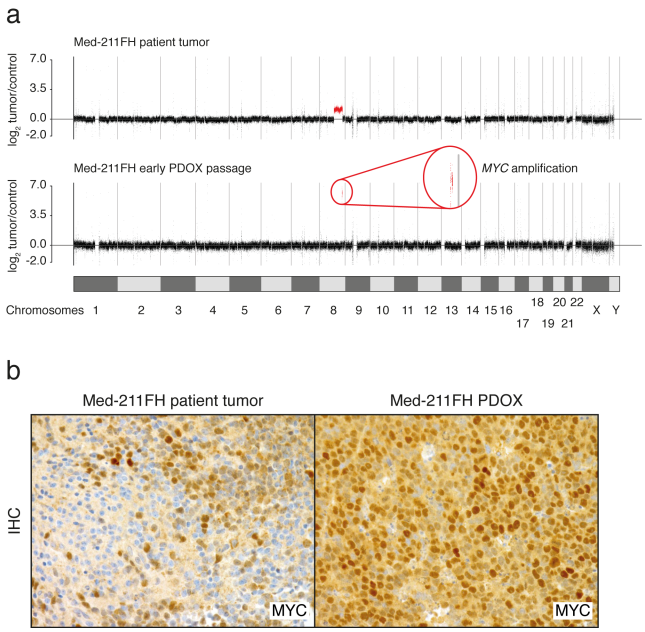

Figure 15: Outgrowth of a *MYC*-amplified clone in Med-211FH.
(**a**) Copy number profile of patient tumor and early PDOX passage of Med-211FH. Data was generated using binned whole genome sequencing reads normalized to the total number of reads and normalizing the result to control tissue (log_2 tumor/control). Regions of interest are highlighted in red. This figure was jointly created by Susanne N. Gröbner (DKFZ, Heidelberg, Germany) and myself. (**b**) MYC immunohistochemistry of patient tumor and PDOX Med-211FH. Histopathological analysis was performed by Bonnie Cole (Seattle Children's and the University of Washington, Seattle, USA).

While in this cohort driver events were almost always maintained, the overall mutational landscape and clonal composition of tumors can still change, which was seen in other studies of PDX[397,411,417], but also in cohorts of primary and relapse tumor pairs[455]. In our cohort of eight PDOX models with matching patient tumor and germline, 88% (7/8) of models did not maintain all mutations in the patient tumor (Figure 16a-h, page 75). Assessing the models based on the correlation coefficient of mutational allele frequencies of patient tumor and PDOX, two models (B062_13315, BT084) emerged as high fidelity models ($r > 0.8$), three models (BT126, NCH2194, NCH2053) had significant clonal changes ($0.8 > r > 0.4$), and the three remaining models (B062_013, NCH2315, NCH3602) did not share most of their mutations ($r < 0.4$) (Figure 16a-h). Of note, all three presumed low-fidelity models are driven by a single driver event that is preserved in all three lines (B062_013 – *SUFU* germline defect, NCH2315 – *FOXR2* activation, NCH3602 – *C19MC* miRNA cluster amplification), which makes it plausible that most mutations lost or gained in the PDOX might represent passenger events. Analyzing the cohort of patient tumor and PDOX pairs without germline, on average 98.40% ± 0.99% of predicted somatic SNVs were maintained in the PDOX, while on average 3.17% ± 2.22% of SNVs were newly acquired in the PDOX (Figure 16i,j). Because the true somatic mutation count may be over-estimated in samples without germline, and SNPs introduced as

false positive SNVs are maintained in PDOX, these numbers probably slightly underestimate the true clonal variation in these PDOX.

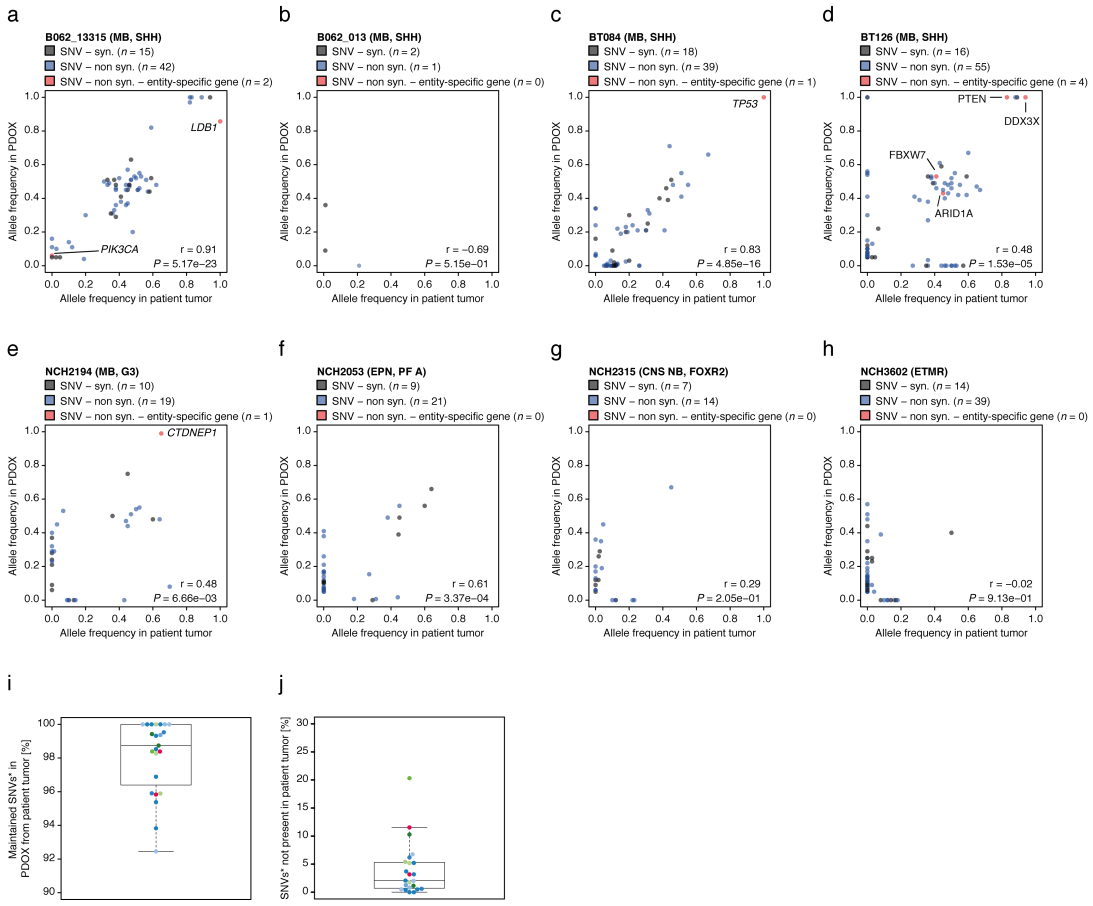

Figure 16: Clonal evolution from patient tumor to PDOX.
(**a-h**) Correlations of allele frequencies for patient tumors and matching PDOX based on SNVs called from WES or WGS data (only models with germline controls). Red-highlighted entity-specific genes are genes determined to be significantly recurrently mutated in the reference cohort Northcott *et al.*, 2017[294]. (**b,e,f**) WES pairs. (**a,c,d,g,h**) WES PDOX data and WGS patient tumor data. (**i**) Maintained SNVs* in PDOX from patient tumor. Each PDOX and patient tumor pair is represented as a dot, colored by the molecular subgroup of the PDOX line (Figure 6, page 62). (**j**) Newly acquired SNVs* present only in PDOX and not in the initial patient tumor. Each PDOX and patient tumor pair is represented as a dot, colored by the molecular subgroup of the PDOX line (Figure 6, page 62). *The illustrated counts are predicted somatic mutations, as no germline control was available.

To evaluate whether the global copy number landscape of PDOX models changed compared to their patient tumors, unsupervised clustering of copy number profiles with multiple methylation profiles per PDOX (patient tumor n = 88, early PDOX passage n = 93, late PDOX passage n = 26) was performed. Fourteen percent (12/88) of patient tumor PDOX pairs did not cluster next to each other in this analysis (Figure 17a, page 76). After manual inspection, pairs with either low tumor cell purity in the patient tumor or overall flat copy number plots without any distinct copy number alteration between both states were excluded (n = 5). Out of the remaining seven discordant pairs (8%), only two were linked to a clonal outgrowth, in which the PDOX clone

would be classified as being more aggressive than the patient tumor (Med-211FH – *MYC* amplification, EPD-710FH – 1q gain).

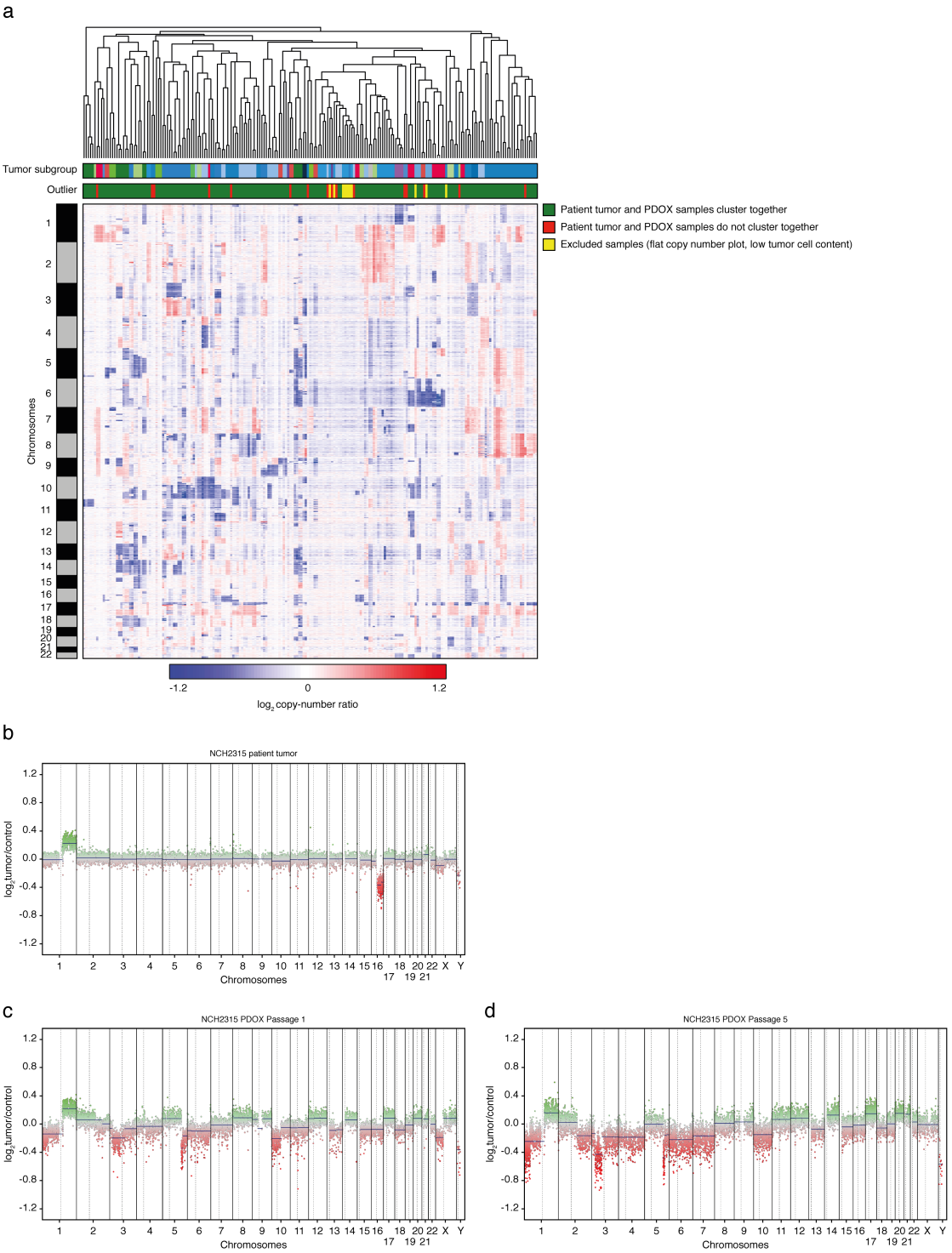

Figure 17: The copy-number landscape of patient tumors is maintained in PDOX models.
(**a**) Unsupervised hierarchical clustering of copy number variations derived from methylation data of all PDOX models with more than one methylation profile per model (patient tumor n = 88, early PDOX passage n = 93, late PDOX passage n = 26). The relative intensity is depicted in the heatmap along the chromosomes (y-axis) (red – high, blue - low). Samples are colored based on their molecular subgroup (Figure 6, page 62), and based on whether the samples of the individual PDOX lines cluster with the

matching patient tumor or not. Samples with a flat copy number plot or low tumor cell content were excluded from this analysis (yellow). (**b**,**c**,**d**) Copy number plots generated from methylation array data of the (**b**) patient tumor, (**c**) early PDOX passage, and (**d**) late PDOX passage of NCH2315.

The other five discordant pairs (6%) changed in the CNV landscape, but there was no obvious explanation as to why the new clone should be more aggressive than the dominant clone in the patient tumor. Only two out of five models that were found in the previous analysis of driver event maintenance and were driven by an alteration in the CNV landscape were picked up in this analysis, highlighting that in the overall context of the entire copy number landscape, focused alteration in a driver event is a minor event and cannot be picked up by this unbiased analysis. While some PDOX and patient tumor pairs clustered discordantly, all 26 early and late PDOX pairs clustered very close to each other, even in the two cases in which the patient tumor did not cluster with both PDOX passages (NCH2315, Med-211FH). Particularly in NCH2315, there were dramatic changes from the patient tumor to the early PDOX passage in the CNV landscape, while the CNV landscape after this rearrangement was mostly consistent (Figure 17b-d, page 76). In concordance with the change in CNV landscape, this line also showed clonal changes in the previous analysis of SNVs (Figure 16g, page 75).

DNA methylation as an epigenetic mark plays a major regulatory role in many biological processes and also in human cancer[456]. The methylome of pediatric brain tumors is of major interest in research, as it can be used not only for reliable tumor subgrouping[342], but also is a result of the cell of origin and of oncogenic-specific reshaping of the methylome, as for example in IDH-mutant glioma[238]. As DNA methylation is very important in defining the identity of tumor subgroups, an examination of whether PDOX maintain the methylation profiles from their matching patient tumor was carried out. In cluster analyses based on methylation array data, PDOX and matching human tumors nearly always clustered very closely to each other (Figure 6, page 62; Figure 7, page 63; Figure 8, page 64) and had an average pairwise Pearson correlation coefficient of $r = 0.9246 \pm 0.0063$ ($n = 91$) (Figure 18a, page 78). However, evaluating the average raw methylation in patient tumors and PDOX highlights a small consistent demethylation ($n = 91$, patient tumor: 0.4700 ± 0.0064, PDOX: 0.4602 ± 0.0080; $P < 0.001$) (Figure 18b,c). To check whether the same CpG-sites are consistently being demethylated, differential methylated CpG-sites were identified through pairwise comparisons. Only 59 differentially-methylated probes ($P < 0.05$, $-0.2 > \Delta\beta > 0.2$) (Figure 18d) were revealed, which means that not always the same CpG sites are the target of demethylation. It is possible that the various tumor subtypes show different grades of demethylation, which would be why not many differentially methylated probes were detected in the prior analysis.

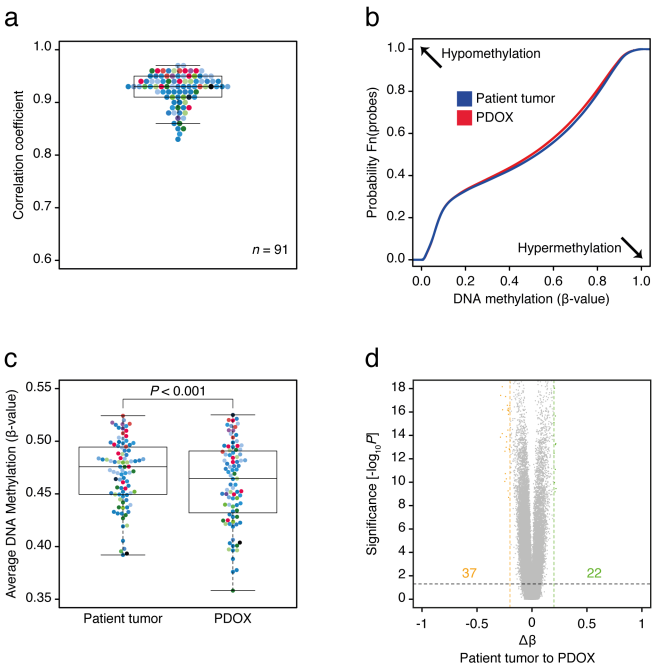

Figure 18: Molecular fidelity of the methylome in PDOX models.
(**a**) Pairwise Pearson correlation coefficient of DNA methylation profiles of patient tumor PDOX pairs (*n* = 91). (**b**) The empirical cumulative distribution function for DNA methylation levels (β-values) plotted individually for paired patient tumors and PDOX (*n* = 91). (**c**) Average DNA methylation status per individual sample, colored based on the tumor subgroup (Figure 6, page 62). Statistical significance was determined by a paired t-test. (**d**) Mean methylation change from patient tumors to PDOX at each CpG site. Colored dots represent CpG sites that show significant hypomethylation (orange dots, total count provided) or hypermethylation (green dots, total count provided) (*P*-value < 0.05 and |Δβ| > 0.2).

Indeed, if PDOX and patient tumor pairs were analyzed separately by tumor subgroup, differences in demethylation behavior were detected even within entities (Figure 19, page 79). EPN PF A (*n* = 8), ATRT SHH (*n* = 6), HGG pedRTK1 (*n* = 7), MB SHH (*n* = 13), MB WNT (*n* = 3), and MB Group 4 (*n* = 9) did not show a significant methylation change between patient tumor and PDOX, while EPN RELA (*n* = 4; *P* < 0.01), K27 mutant glioma (*n* = 5; *P* < 0.01), and MB Group 3 (*n* = 17; *P* < 0.01) showed significant demethylation in the PDOX (Figure 19). Of note, MB Group 3 PDOX were not further demethylated during passaging in mice (*n* = 7) (Figure 19t), while in GBM pedRTK1, late PDOX were significantly hypermethylated from early to late PDOX (*n* = 4; *P* < 0.05) (Figure 19l). Overall, in all tumor subgroups, methylation levels did not changing uniformly, as individual models developed against the general trend, pointing toward individual evolution. However, in K27 mutant glioma, MB Group 3, and EPN RELA, the overall trend favors hypomethylation significantly. It should be noted that the low number of comparisons limits the statistical power of analyses for some subtypes, e.g. for SHH ATRT.

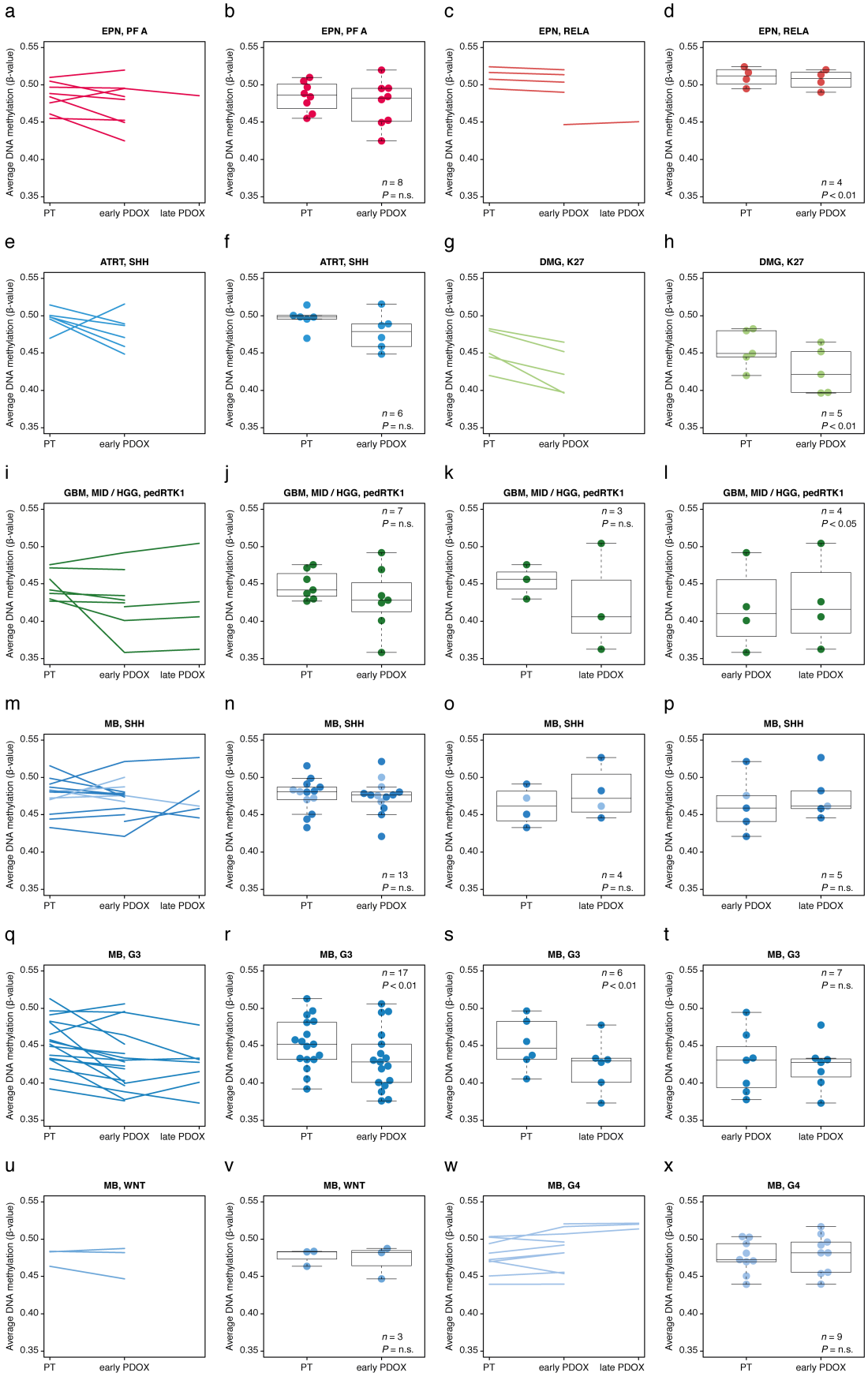

Figure 19: Tumor subtype-specific demethylation in PDOX models.
(**a,c,e,g,i,m,q,u,w**) Overall DNA methylation levels (mean β-value) of individual PDOX models over time, split per tumor subgroup. (**b,d,f,h,j,k,l,n,o,p,r,s,t,v,x**) Average DNA methylation status per

individual sample is plotted as a dot that is colored based on the tumor subgroup (Figure 6, page 62). Only paired samples for the individual comparison are included. Statistical significance was determined by a paired t-test comparing the difference in methylation between each pair. PT = patient tumor.

In concordance with other layers of molecular data, PDOX models also maintain the gene expression profile of their matching patient tumor, shown by a pairwise Pearson correlation coefficient of r = 0.9319 ± 0.010 (n = 32) (Figure 20a). A comparative analysis of differentially-expressed genes (P < 0.05, -1 > $\log_2$FC > 1) between PDOX and patient tumors identified many more down- (385) than upregulated (14) genes in PDOX (Figure 20b). DAVID pathway enrichment analysis identified that reduced expression genes were almost exclusively associated with human stroma (Figure 20c), that, during passaging in mice, is replaced by murine stroma, but in case of the immune system nearly completely lost due to the use of immunocompromised mice[396,397,412].

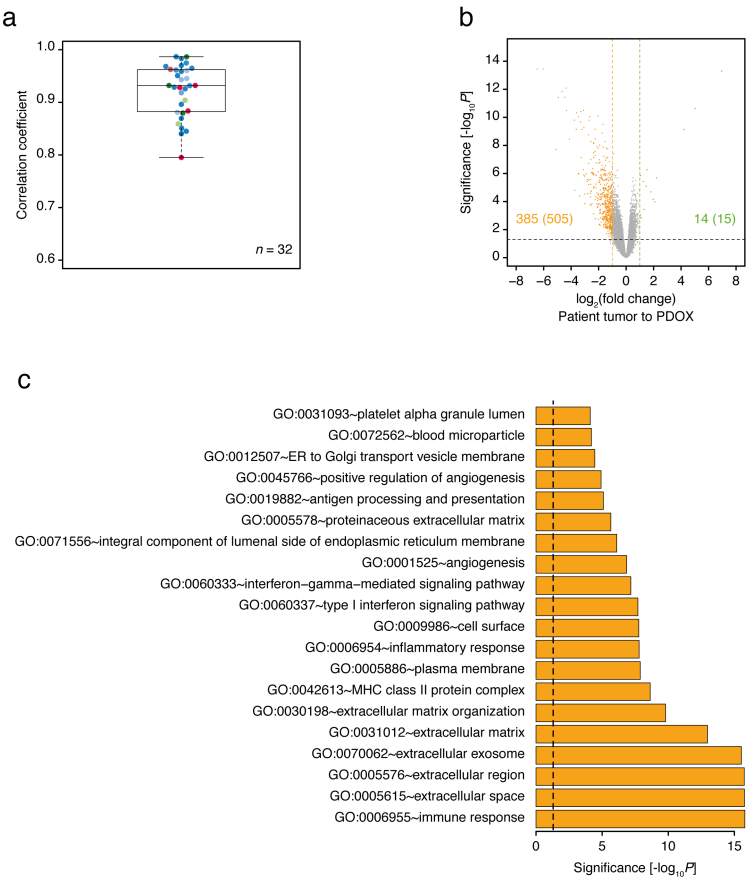

Figure 20: Molecular fidelity of the transcriptomes in PDOX models.
(**a**) Pairwise Pearson correlation coefficient of gene expression profiles of patient tumor PDOX pairs (n = 32), colored by tumor subgroup (Figure 6, page 62) (**b**) Mean expression level changes from human tumor to PDOX passage (n = 32 pairs). Significantly differentially-expressed probes are highlighted in orange (505 probes ~ 385 genes down-regulated in PDOX passage) and green (15 probes ~ 14 genes up-regulated in PDOX passage) (P-value < 0.05 and $\log_2$ (fold change) > 1). (**c**) DAVID Gene-Enrichment Analysis (GO term BP and CC) of significantly overexpressed genes in PDOX passages. The top 20 GO terms ranked by P-value are depicted. The dashed line illustrates the P-value cutoff of 0.05.

Based on the analyses of multiple layers of genomic data, it can be concluded that PDOX models faithfully reflect the patient tumors from which they were derived and that they remain relatively stable when being passaged in mice. However, PDOX models continuously evolve over time, which may lead to changes in the genomic landscape of these lines. In rare events, clonal outgrowth of drivers, not previously detected in the patient tumor, were found in the PDOX, which is most likely a result of a heterogeneous patient tumor.

3.6 A resource for the scientific community

Due to the rarity of pediatric brain tumors and the multitude of different entities, subgroups, and additional inter-tumoral heterogeneity within these groups, it is important that the scientific community is able to study this repertoire of preclinical models that represents the entire spectrum of pediatric brain tumors in comparison to conventional cancer cell lines. In order to make this PDOX resource accessible to the entire scientific community, the molecular and histopathological data were made publicly available and can now be explored through the R2 "PDX Explorer" (currently containing the Seattle cohort, https://hgserver1.amc.nl/cgi-bin/r2/main.cgi?&dscope=PDX_OLSON&option=about_dscope), allowing scientists from all over the world to find the most relevant PDOX lines for their scientific questions. A summary of the essential information for each PDOX is available online in the PDX explorer (see example, Figure 21, page 82).

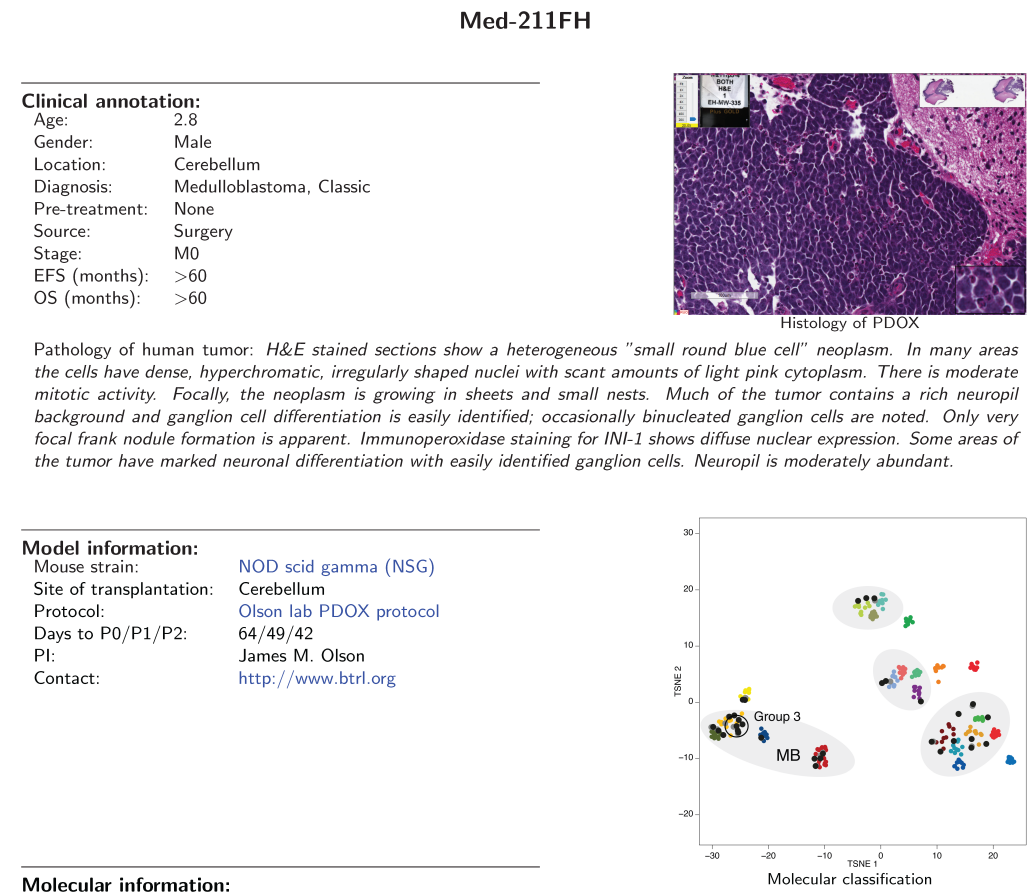

Figure 21: Example of PDOX fact sheet: Med-211FH.
PDOX fact sheet that summarizes the essential information about this particular PDOX line. All individual PDOX fact sheets are available at www.btrl.org and r2.amc.nl.

3.7 Therapeutic response confirms genetic vulnerability predicted by molecular analysis*

To assess whether genomic vulnerabilities identified by molecular analysis can be translated into potential therapeutic targets, two comparisons between predicted sensitive- and resistant tumor models were made. First, two PDOX models (PBT-04FH and PBT-05FH), both molecularly classified as HGG of the MYCN subgroup and both harboring a *MYCN* amplification, but differentiating by *EGFR* amplification, overexpression, and activation, were evaluated for sensitivity to *EGFR* kinase inhibition with Erlotinib. PBT-04FH (no *EGFR* amplification) and PBT-05FH (*EGFR* amplification) tumors were treated with Erlotinib at 2 mg/mouse daily by oral gavage. Mice transplanted with *EGFR*-amplified PBT-05FH tumors survived significantly longer on treatment compared to the vehicle-treated control group (26 versus 6 days; $P = 0.0001$) (Figure 22a, page 84). In stark contrast, mice transplanted with the low-*EGFR*-expressing tumor model PBT-04FH fared worse on Erlotinib treatment with a median survival of only eight days compared to 17 days for the vehicle group (Figure 22b). Animals treated with Erlotinib lost weight due to toxicity, which, in combination with weight loss due to tumor growth, lead to an earlier death if the drug could not stall tumor progression. In the second comparison, two MB-SHH models, each with different mutational status, were treated with the SMO-inhibitor Vismodegib. Med-1712FH, harboring a *PTCH1* mutation, had an improved median survival time of 16 days when treated with Vismodegib, versus 10 days for the vehicle-treated cohort ($P = 0.05$) (Figure 22c). In contrast, Med-813FH, driven by *MYCN* and *GLI2* amplifications, showed no improvement in median survival (6 days with Vismodegib treatment versus 8.5 days with vehicle treatment) (Figure 22d).

*This section of the thesis describing Figure 22 was taken in its entirety from the research article "*A biobank of patient-derived molecularly characterized orthotopic pediatric brain tumor models*". The described experiments were performed by the laboratory of James M. Olson in Seattle (USA), and therefore this part of text was written jointly with members of the Olson laboratory.

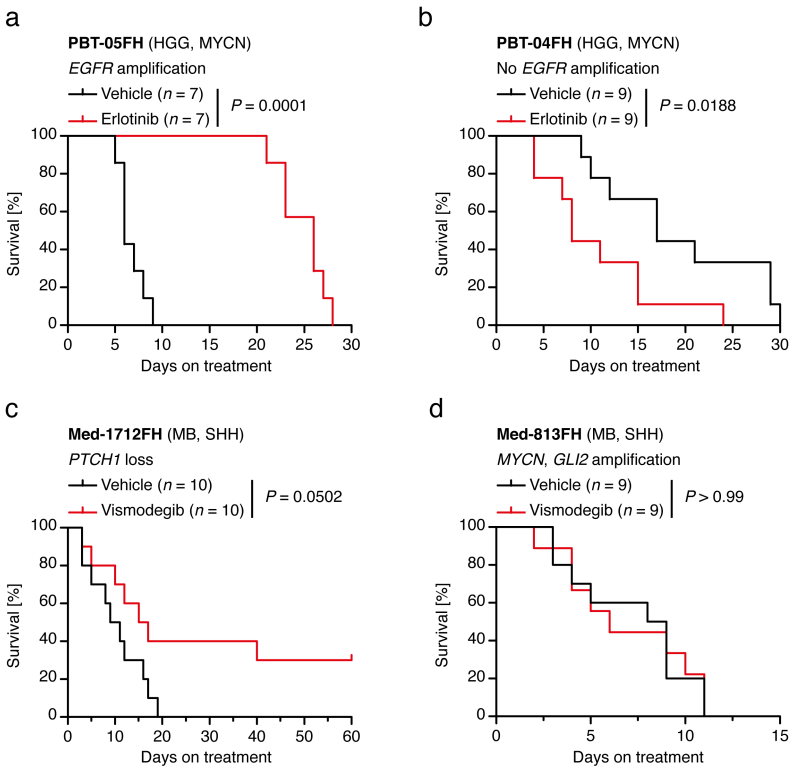

Figure 22: Preclinical evaluation of targeted therapeutics shows differential response to therapy based on molecular drivers.
Kaplan-Meier analyses of (**a**) PBT-05FH treated with and without Erlotinib 2 mg/mouse p.o. daily; $n = 7$ per group ($P = 0.0001$), (**b**) PBT-04FH treated with and without Erlotinib 2 mg/mouse p.o. daily; $n = 9$ per group ($P = 0.0188$), (**c**) Med-1712FH treated with and without Vismodegib 1 mg/mouse p.o. daily; $n = 10$ per group ($P = 0.0502$), and (**d**) Med-813FH treated with and without Vismodegib 1 mg/mouse p.o. daily; $n = 9$ per group ($P > 0.99$). These experiments were performed by Emily J. Girard (Fred Hutchinson Cancer Research Center, Seattle, USA).

Although orthotopic PDX models offer unique advantages when compared to conventional subcutaneous PDX, measurement of tumor growth is much more challenging in orthotopic PDX, as subcutaneous tumor growth can be monitored more easily through caliper measurement, while in PDOX it must be measured indirectly through the use of imaging modalities. Because of this, in many scenarios preclinical experiments in PDOX are evaluated based on survival differences only and not on assessment of objective response (i.e., volumetric measurement). However, comparing the tumor size at the start of therapy to the tumor size at the end of a treatment period is the typical clinical outcome parameter used to evaluate therapy success. In order to evaluate therapy response during orthotopic tumor growth in the brain, the PDOX line Med-1712FH was labeled with a lentiviral construct containing GFP and Luciferase, which allows for continuous intravital imaging of tumor growth. Using this technique, the protocol for the preclinical experiments was adjusted. Instead of an enrollment of all animals at a pre-defined time after injection of the tumor cells, animals were individually enrolled upon reaching a pre-defined bioluminescence signal threshold ($2x10^6$ p/s). Evaluation of the SMO-inhibitors Glasdegib and PF-05274857 in the *PTCH1*-driven SHH MB line Med-

1712FH showed a significant delay in tumor growth as measured by bioluminescence (Figure 23a, page 86), which translates into an improvement of the median survival rate of 18.5 days ($P < 0.01$) for Glasdegib and of 32.5 days ($P < 0.0001$) compared to vehicle-treated animals (Figure 23b). While considered successful scientifically, in a clinical setting, this response would still classify as progressive disease. In an additional experiment, the SMO-inhibitor Erismodegib (a.k.a. Sonidegib or LDE225) and the standard-of-care chemotherapeutic Cisplatin were evaluated in the same setting, observing an average reduction of tumor size of 57.87% ± 14.44% of the initial signal intensity after 28 days of treatment with Erismodegib, while Cisplatin treatment did not alter tumor growth (Figure 22c). Evaluating tumor response based on the RECIST clinical characteristics, 78% (7/9) of responses classified as tumor regression (< 70% of initial lesion) (Figure 23e). In order to confirm that Erismodegib actually inhibited the SMO pathway, tumor-bearing Med-1712FH mice were treated with Erismodegib for two days, and then the potent downregulation of SHH pathway target genes *PTCH1*, *PTCH2*, *GLI1*, and *MYCN* was confirmed (Figure 22f). To allow the animals to recover from long-term treatments with Erismodegib, treatment was halted after reaching a threshold of $1x10^6$ p/s and re-initiated at $2x10^6$ p/s signal intensity. This protocol led to a longer median survival rate of 192 days compared to vehicle controls ($P < 0.0001$) (Figure 23d).

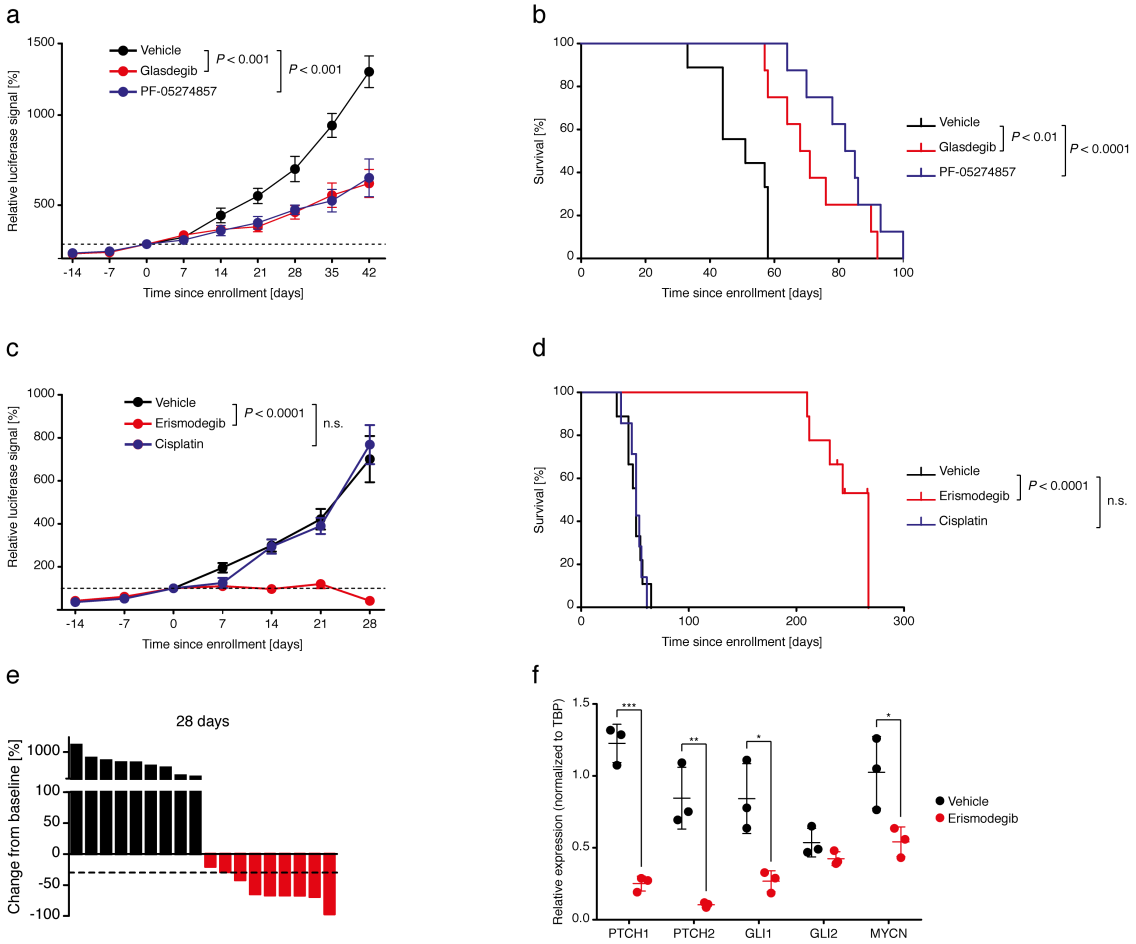

Figure 23: Preclinical evaluation of SMO inhibitors.
Animals injected with luciferase-labeled Med-1712FH cells were enrolled weekly into the study upon reaching a signal threshold of $2x10^6$ p/s. (**a**,**c**) Average relative luciferase signal normalized to luciferase signal at treatment start over the period of the study. Error bars represent the standard error of the mean (**a**) Glasdegib (n = 8) vs. Vehicle (n = 9) (P < 0.001, 42 days after enrollment); PF-05274857 (n = 8) vs. Vehicle (n = 9) (P < 0.001, 42 days after enrollment); (**c**) Erismodegib (n = 9) vs. Vehicle (n = 9) (P < 0.0001, 28 days after enrollment); Cisplatin (n = 7) vs. Vehicle (n = 9) (P = n.s., 28 days after enrollment). (**b**,**d**) Kaplain-Meier curves of associated experiments: (**b**) Glasdegib (n = 8) vs. Vehicle (n = 9) (P < 0.01); PF-05274857 (n = 8) vs. Vehicle (n = 9) (P < 0.0001); (**d**) Erismodegib (n = 9) vs. Vehicle (n = 9) (P < 0.0001); Cisplatin (n = 7) vs. Vehicle (n = 9) (n.s.). (**e**) Relative luciferase signal change per individual animal after four weeks of treatment w/o Erismodegib. Each bar, colored based on the treatment group (Vehicle – black, Erismodegib – red), represents one mouse. (**f**) qPCR analysis of Med-1712FH tumor-bearing animals treated with and without Erismodegib, 20 mg/kg, p.o., for two days.

Animals responded continuously to treatment for about four cycles until the tumors started to become resistant and to grow under therapy (Figure 24, page 87). Unexpectedly, treatment response in the first cycle was always slower than the treatment responses in the following cycles. Resistant tumors were collected and are currently being molecularly analyzed in order to find the genetic lesion leading to the resistance to SMO inhibition. In addition, the resistant tumors were used to generate new resistant PDOX sublines to be able to test new therapy concepts after identification of the resistance mechanism.

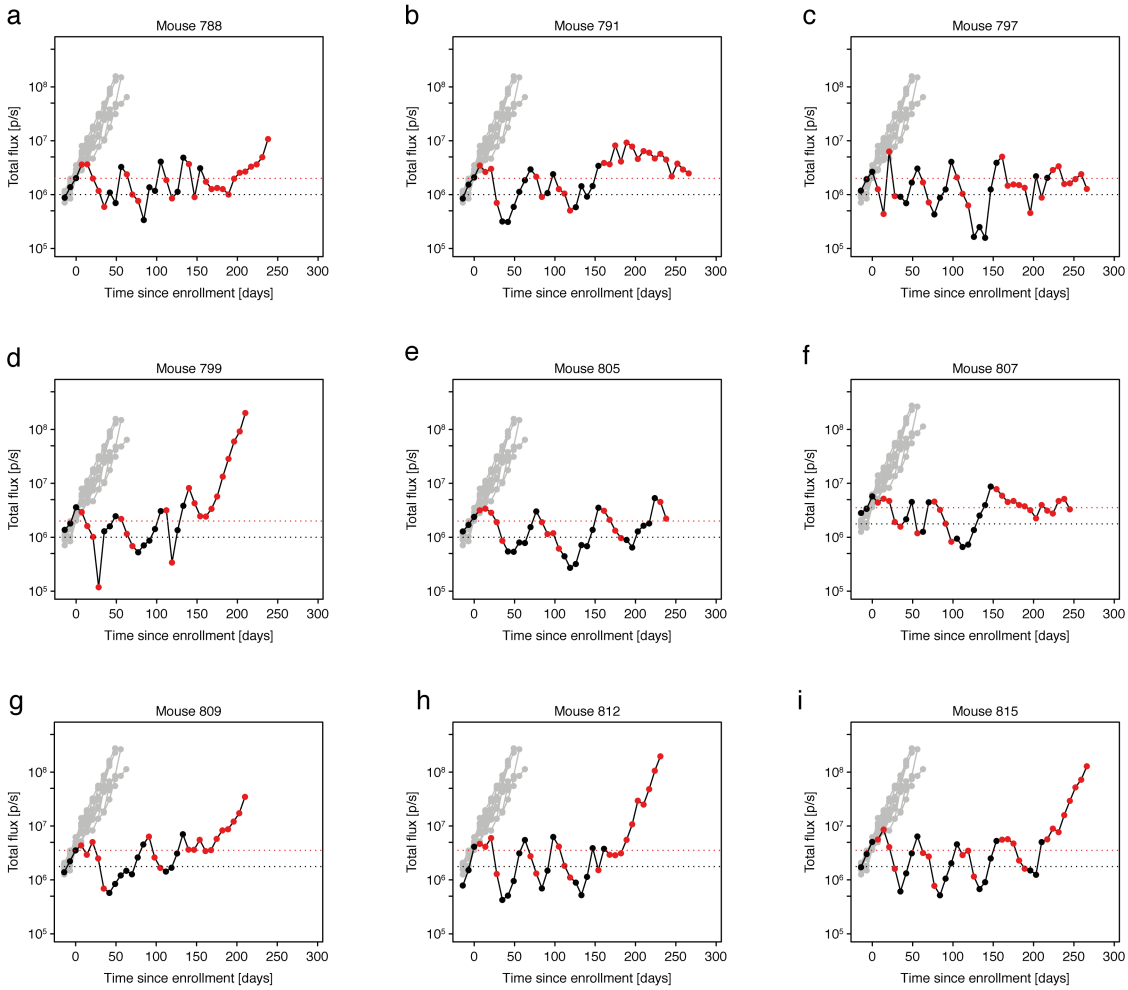

Figure 24: Treatment cycles of Erismodegib can induce treatment resistance in the PDOX model Med-1712FH.
Individual luciferase signal of animals, injected with Luciferase-labeled Med-1712FH, which were individually enrolled into the study upon reaching a signal threshold of $2x10^6$ p/s (red dotted line) and treated w/o Erismodegib 20 mg/kg, p.o., 5/7 days. Upon tumor regression below $1x10^6$ p/s (black dotted line), animals were taken off treatment until they reached $2x10^6$ p/s again. Red dots indicate weeks during which animals were treated with Erismodegib and black dots indicate weeks during which animals were not treated with Erismodegib. Grey curves indicate the luciferase signal of individual animals treated with a vehicle control ($n = 9$).

4 Discussion

4.1 PDOX models in pediatric neurooncology

Until recently, relatively few PDX models of pediatric brain tumors were described, and these do not represent the multitude of brain tumor subtypes[299,416,450,457-467]. Moreover, existing models have often been established as *in vitro* cultures, grown only subcutaneously, and have not been extensively molecularly characterized[299,416,450,457-467]. In this study, the cohort of 130 molecularly characterized PDOX lines, representing 22 distinct subtypes of pediatric brain tumors, is until now the largest collection of PDX models in pediatric neurooncology and highlights the power of the PDOX methodology. One the one hand, it was possible to identify model systems for tumor subtypes that so have far not been modeled, including, but not limited to, non-*MYC* amplified Group 3 MB, *KBTBD4*-mutant MB, *PRDM6*-driven Group 4 MB, hypermutant HGG, MYCN HGG, different subgroups of ATRT, CNS NB FOXR2, pineoblastoma, and PF A EPN. On the other hand, for the first time, it was also possible to assemble a reasonable-sized cohort of preclinical models representing defined patient populations of pediatric brain tumors, such as six RELA EPN models from various patients. In contrast, until 2015, only 60 conventional cell lines had been described in the field of pediatric neurooncology, many of which have been in culture for decades[468]. The characterization of these conventional cell lines is mostly very basic and often includes only the histopathological diagnosis and the age of the patient[468]. As exemplified by medulloblastoma, the molecular heterogeneity of these cell lines is very uniform, because eleven out of eighteen cell lines were classified as Group 3 MBs and all eleven harbored *MYC* amplifications[469]. Furthermore, the evidence that the remaining cell lines are truly WNT, SHH, and Group 4 is questionable[469]. For example, in typical SHH pathway experiments, the DAOY cell line, supposedly representing SHH MBs, must be stimulated with an external SHH ligand. However, SHH MBs should have an intrinsic activation of the pathway, which should render them independent of external SHH stimulation[299]. In contrast, the Med-1712FH PDOX line that harbors the typical loss of *PTCH1* and was here shown to be dependent upon this associated intrinsic SHH activation, is a much more appropriate model system than the previously used DAOY cell line. The difficulty in modeling the heterogeneity of pediatric brain tumors with *in vitro* cultures may be explained by the fact that although cell lines are much easier to handle than PDOX, they in theory require a better biological understanding of the tumor, because in tissue culture, all external stimuli need to be provided by the investigators, while in PDOX, the murine tissue supplies a microenvironment. This concept is illustrated by the development of colorectal cancer organoids in the past few years. First, growth conditions for healthy tissue were defined[470], then, organoids could be grown from tumor biopsies[471], and finally, it could be understood,

based on the oncogenic lesion present, which external growth factors are dispensable for cancer cells[472]. Thus, the lack of *in vitro* model systems is probably a lack of optimized culture conditions, and, therefore, a lack of understanding of the tumor-stroma interaction. However, even when *in vitro* cultures are established, the culture conditions may be over-optimized, for example by adding EGFR to an *in vitro* culture although in the patient tumor no EGFR is present. This aspect may also be a reason for the poor prognostic power of conventional cell lines[371,372], in addition to the generally rather artificial growth conditions *in vitro* and associated molecular reshaping[373-375].

4.2 A bias for more aggressive tumor subtypes

Although model systems for 22 different molecular subtypes of high-grade pediatric brain tumors were cataloged, a bias for more aggressive tumor subtypes was observed, and, consequently, PDOX were not identified for all tumor subgroups, such as EPNs of the YAP or PF B subgroups. Due to the lack of molecular data from the patient tumors that did not engraft, it cannot be excluded that this trend is due to a bias in the injection cohort. However, due to similar observations in other entities, it is very likely that more aggressive tumors engraft much more easily than more benign tumors[396,397,419]. This hypothesis is further strengthened by the fact that low-grade pediatric brain tumors do not engraft at all[450], and therefore, many research groups have stopped transplanting these tumors into mice. Even within tumor subgroups, there was an enrichment of genetic alterations linked to poor prognosis, such as *TP53*-mutant SHH MB[285,298-302] or PF A EPN with 1q gain[278]. This finding is in line with early observations in breast cancer showing that patients with successful PDX engraftment had a worse prognosis than patients with failed PDX engraftment[396]. An interesting example highlighting that PDX engraftment is not linked to a specific genetic alteration in pediatric brain tumors, but instead more to the prognosis of the patient, is the enrichment of *MYCN*-amplified PDOX models in SHH MB, in which this lesion is correlated with a poor prognosis[473], but no enrichment in Group 4 MB, where *MYCN* amplification is not associated with a poor prognosis[473]. While the presence of *MYCN* amplifications in SHH MB or Group 4 MB patient samples is roughly similar (6-8%), 6/21 (29%) SHH MB PDOX models but only 1/13 (8%) Group 4 MB PDOX models harbored a *MYCN* amplification. The same holds true for 1q gain in ependymoma PDOX. It was found only to be enriched in the PF A subtype, in which 1q gain was associated with a poor prognosis, and not in the RELA subtype, where this chromosomal gain could not be linked to a poor clinical outcome[273]. Assuming that events linked to a poor outcome are enriched in PDOX cohorts, the enrichment of *KBTBD4* insertions poses the possibility that these are also linked to a poor outcome, which has not yet been validated in clinical cohorts. Interestingly, up until now, only one Group 3 MB PDOX without *MYC* amplification or

KBTBD4 insertion was identified, highlighting that the Group 3 MB PDOX in this cohort represent only about 22% (16% *MYC* amplification, 6% *KBTBD4* insertions)[294] of all Group 3 MB tumors. This underscores the necessity for generating and characterizing even more Group 3 MB PDOX models in order to have a good representation of Group 3 MB patients in preclinical studies. Another interesting finding is that *GFI1B* activation was enriched only in Group 4 MB PDOX and not in Group 3 MB PDOX, implying that the oncogene possibly has a different role in each of the two subtypes, as does *MYCN* in SHH and Group 4 MB. Indeed, *GFI1B* expression was not correlated with a poor prognosis in Group 3 MB; similar analyses in Group 4 MB have not yet been performed[309]. This hypothesis is further strengthened by the fact that the RCMB28 Group 3 MB PDOX line lost expression of *GFI1B*, while the matching patient tumor still expressed the oncogene. In Group 3 MB, *GFI1B* may play an essential role in initiating the disease, because only the cooperation of *GFI1B* and *MYC* was able to drive MB growth in murine stem cells, but whether *GFI1B* is also important for tumor maintenance has not yet been evaluated[309]. Based on these findings, it is essential to not simply extrapolate findings from PDOX cohorts to clinical cohorts, because PDOX cohorts represent a biased patient population, but rather to match individual PDOX or PDOX cohorts to specifically-defined patient subpopulations, as even tumor subgrouping is not sufficient to define these populations.

4.3 PDX models in relation to their patient tumors

The analyses presented here show in multiple layers of data that pediatric brain tumor PDOX closely resemble the patient tumors from which they were derived, and are relatively stable over time. However, several examples of strong clonal outgrowths in the PDOX from its corresponding patient tumor were observed, with the most common event being the outgrowth of a *MYC*-amplified clone in Group 3 MB. In concordance, MBs that relapse also tend to develop more *MYC* amplifications[455], which implies that the clonal outgrowth event observed could be an event that would have occured in the patient eventually. Although *TP53* mutations are also enriched in Group 3 MB upon relapse, an enrichment of *TP53* mutations was not found in this PDOX cohort. Potentially, acquired *TP53* mutations could be associated with resistance to conventional therapy, which PDOX do not undergo. These facts lead to the conclusion that PDOX may either model the patient tumor in a later disease stage or possibly even an alternate evolutionary path. This may result in a situation where a PDOX of another patient may be the better molecular model for a patient than his or her "own" PDOX. Interestingly, it has been shown in breast cancer PDX that these outgrowth events usually occur very early during PDX development, mostly in the first passage[417]. Indeed, in the 26 PDOX lines, which were characterized at an early and at a late passage, this could be confirmed in pediatric brain

tumors, because no drastic clonal outgrowth events were detected between early and late PDOX passages. Still, limited continuous evolution of these PDOX during passaging was observed, which probably also occurs in the patient. It should be noted that the relative stability of these PDOX was evaluated only over five to six passages, which however should be a long enough time frame to perform any preclinical experiment.

In the presented cohort, the copy number landscape and mutations of unknown significance sometimes varied between patient tumor and PDOX, but, in the vast majority of cases, were still very close to the patient tumor. Presumed "driver" events were always maintained except in two cases (Med-2112FH, MB Group 3, *TCF4* mutation; RCMB28, MB Group 3, *GFI1B* activation). This observation holds true also for breast cancer, in which clonal populations, which mostly do not contain a breast cancer "driver", can change upon engraftment of PDX[397,474]. The distinction between true evolutionary pressure and background evolution of passenger events is difficult, and additional time and data will be needed to understand why certain clones expand and others do not. In fact, the evolution of patient tumors over time may be more drastic due to very aggressive treatment regimens. This is illustrated by the analysis of primary relapse pairs of pediatric tumors showing that only 37% of druggable lesions were maintained in the relapse from the primary tumor[25], while in PDOX, such drastic changes of the "driver" landscape were not observed.

One essential question in the preclinical field is whether PDX models still represent patient populations and do not acquire out-of-context oncogenic drivers, e.g. *MYC* amplifications in all brain tumors. Based on studies so far, no obvious artificial evolutionary drifts of PDX could be identified. However, a recent publication by Ben-David *et al.* has challenged this view[424]. Based on copy number information derived from gene expression data from multiple time points during PDX evolution, and on comparisons of primary tumors and relapses, it was observed that different chromosomal arm changes were selected for in the murine environment as compared to the human environment[424]. It should be noted that this analysis did not take into account some essential aspects, such as a differentiation between tumor subgroups, or the fact that relapsed tumors were treated with aggressive therapy whereas the PDX were not. Another confounding aspect in this analysis is that conventional PDX models are passaged via splitting tumors into tissue pieces, which can lead to the outgrowth of an individual clone based merely on anatomical heterogeneity. The role of anatomical or spatial tumor heterogeneity has been recognized in multiple different entities, most prominently shown in renal[475] and lung cancer[476], but also in MB[477], which could impose a bias on the analyses. While PDOX models are typically passaged as a dissociated single-cell suspension, material for molecular characterization is also often taken prior to preparing a single-cell suspension – for both the injection of the patient tumor and for later passages. Considering these limitations, a similar

analysis on this PDOX cohort of pediatric brain tumors would most likely not be able to address the question of a potential mouse-specific evolution in a meaningful manner. Currently, we lack the understanding of how and why tumors evolve in the human environment, and, considering that they undergo evolutionary pressure from other factors, including chemotherapy, radiation, and surgery, it is thus difficult to compare the tumor evolution of a patient to the evolution of a xenograft tumor in an immunodeficient environment.

In addition to analyzing the copy number and mutation landscape, differences in the methylation and gene expression from patient tumor to PDOX were also systematically investigated. A central aspect for comparing patient tumors and PDOX on the molecular level is that in PDOX, murine stroma replaces the human stroma over multiple passages, which in the end results in a PDOX which consists of both human tumor cells and murine stroma that lacks most immune cells[396,397,412]. The murine component of the PDOX tumor is either not detected by certain techniques, such as microarrays, or can be easily differentiated from the human component by *in silico* algorithms as shown in Figure 9 (page 65)[420]. Comparisons of patient tumors and PDOX are therefore challenging, because a mixture of human tumor cells and human stroma from the patient tumor is being compared only to the human tumor cells from the PDOX. For mutations and also copy number alterations, events in the patient tumor can easily be distinguished from the surrounding stroma, because all non-neoplastic cells have the same non-altered genome, and thereby the non-tumorigenic compartment of a neoplasia in patient samples can easily be eliminated by an *in silico* analysis step[478]. For the copy number and mutation landscape, it is now possible to simply compare the tumor cell content of the patient tumor with the tumor cell content of the PDOX. However, gene expression and methylation data from patient tumors cannot be easily split into tumor cell and stromal component, because for each type of data, the various normal cell populations differ, and, therefore, a universal normal state cannot be clearly defined. This fact led to the finding that when differential gene expression between patient tumor and PDOX was systematically assessed in this cohort, genes associated almost exclusively with the human stroma were identified. Remarkably, this purification of tumor cells in PDX was exploited by Isella *et al.* to define stromal expression profiles in patient tumors and to classify tumors only by the expression of tumor cells without contamination of stromal tissue[418]. Based on the data presented in this thesis, it can be concluded that the major driver of change in gene expression in PDOX from pediatric brain tumors is the loss of human stroma, but it cannot be excluded that there are also additional tumor-specific changes. Future analyses in larger cohorts should address subtype-specific comparisons in order to identify subtype-specific changes that may have been diluted out of this pooled analysis, and also determine which compartments of the human stroma, in addition to most immune cells, are not replaced by the murine stroma. In

contrast, there is already evidence that the cultivation of cells *in vitro* irreversibly changes their gene expression profile, even when being re-injected into mice[375], hinting toward the superior modeling capacity of PDOX as compared to cell lines.

The analysis of the methylome landscape showed a very high fidelity between PDOX models and their matching patient tumors. In clustering analyses, PDOX models clustered right next to the matching patient tumor in nearly all lines. However, in rare instances, there was some distance between patient tumor and PDOX, representing a clonal shift. In these examples, the PDOX still retained the same subgroup, but, based on the methylation profiles, they were more similar to other reference samples of the same subgroup than to the patient tumor, which is in line with the observations from the analysis of the copy number and mutational landscape. Of note, one PDOX line was identified as having a different Group 3 / Group 4 MB subtype than the matching patient tumor within the classic Group 3 MB. Because the novel Group 3 and Group 4 MB subtypes are not yet very clearly defined, it remains to be seen whether this holds true. Still, this finding may suggest that these novel subtypes could also represent stages during tumor evolution, as they represent a continuum rather than a strict separation. Although clustering and correlation analyses confirmed a high fidelity of PDOX lines, an overall systematic demethylation of PDOX compared to the corresponding patient tumor was detected. Because a relatively small number of significantly demethylated probes was identified across the entire cohort, demethylation was not specific to CpG sites. It was hypothesized that the effect could potentially be diluted by subgroup specificities, and indeed, after performing the analysis per tumor subgroup, it could be shown that only a few tumor subgroups showed demethylation in PDOX. Due to low sample sizes, some trends may not yet be statistically significant, such as in SHH ATRT. The most striking finding was that Group 3 MB demethylate from patient tumor to PDOX, while SHH MB do not show a similar behavior. Similar to the gene expression analyses, the comparison here is biased by the presence of human stroma. Indeed, Hovestadt *et al.* showed that the average methylation at CpG sites, which was determined by bisulfite sequencing, is higher in normal cerebellar tissue, both in embryonal and in adult tissue, than in MB, while methylation in Group 3 MB is much lower than in SHH MB[451]. Assuming that both subgroups have a similar quantity and composition of stromal content, it is conceivable that the loss of the hypermethylated stroma is easier to detect in Group 3 MB, in which the difference in methylation between tumor and normal cells is also larger. This hypothesis is further strengthened by the fact that K27 HGGs, a tumor subgroup known for its high stromal content and for hypomethylation, also showed this trend despite low sample numbers[238,260]. Furthermore, in these tumor subgroups, the trend toward demethylation did not continue from the early PDOX passage to the late PDOX passage. Although the sample numbers for this comparison are not high enough, the current data point toward a direct effect

of changing the microenvironment instead of a continuous demethylation. However, in addition to the loss of human stroma, the DNA methylome was also continuously evolving, as also shown in the copy number or mutation data. Individual PDOX evolved against the trend and were hypermethylated compared to their matching patient tumor, highlighting the individual evolution of each PDOX.

4.4 The PDOX model as a tool for preclinical research

In order to evaluate whether the molecular characterization of PDOX might be able to guide treatment decisions, the response of PDOX models to targeted therapeutics was evaluated *in vivo*, in the context of possibly predictive biomarkers. Patients with tumors of the HGG MYCN subgroup have a detrimental prognosis with a median survival rate of only 14 months[266]. In addition to the hallmark *MYCN* and *ID2* co-amplification, 25% of these tumors harbor an additional *EGFR* amplification[266]. In this study, it could be shown that *EGFR* amplifications may be predictive for a response to EGFR inhibition. This is interesting for two reasons. First, it was surprising that inhibition of EGFR signaling using Erlotinib could influence tumor growth in a tumor entity defined by *MYCN* amplifications. This means that EGFR activation cooperates with MYCN in HGG MYCN glioma and that EGFR could be a valid target even without targeting in parallel the subgroup-defining *MYCN* amplification. Second, Erlotinib failed in clinical trials for adult gliomas, even in tumors with *EGFR* amplification and/or *EGFR* mutation[479-481]. This could be explained by, on the one hand, the fact that adult glioma and pediatric glioma are different diseases, and on the other hand, that although there is a survival advantage, the animals still succumb to the disease relatively quickly. Without imaging modalities, it can only be speculated whether Erlotinib simply slowed down tumor growth or whether there was an initial response and the tumors quickly developed resistance. At any rate, this finding merely represents a starting point for identifying a combination therapy using Erlotinib that is able to induce a durable response in the PDOX, prior to moving this therapy concept forward into the clinical setting.

In contrast, the SMO inhibitor Erismodegib (a.k.a. Sonidegib/LDE225) can be used as a benchmark for a working preclinical therapy, which would be worthwhile to pursue through clinical investigation. In addition to finding the correct drug class for a specific indication, PDOX models also helped to identify the most potent compound within the drug class of SMO inhibitors. For Erismodegib, bioluminescence imaging showed durable regression after four weeks of treatment. Resistance to therapy emerged only after at least three successful treatment cycles with Erismodegib. While targeting SMO functioned without a doubt in the *PTCH1*-driven PDOX line Med-1712FH with Erismodegib, the SMO inhibitors Glasdegib and PF-

05274857 were able to only slow down tumor growth; however, they still produced a significant survival advantage. The potency of Erismodegib compared to Glasdegib and PF-05274857 was also accompanied by much stronger side effects, hinting toward a more potent and more durable inhibition of the SHH pathway. Vismodegib, tested in a non-image guided study by collaborators in Seattle, gave mixed results with only three out of ten animals surviving until the end of the observation period, possibly due to late onset of therapy. In a clinical setting, Vismodegib was able to induce responses in patients with loss of *PTCH1*, but was not effective in non-SHH MB patients or in patients with lesions in the SHH pathway downstream of SMO[482], as already shown preclinically[299]. The example of SMO inhibition highlights that in addition to knowledge about the matching biological target, the intrinsic characteristics of the small molecule, and also the timing of treatment onset, have a huge impact on the outcome of a preclinical experiment. For brain tumors, one of the most important questions is whether the drug can reach reasonable concentrations in the tumor behind the blood-brain barrier. Glasdegib was not expected to cross the blood-brain barrier (data not shown; personal communication D. Shields, Pfizer), while PF-05274857 was shown to do so[483], however the effect on the Med-1712FH PDOX line did not significantly differ between these two inhibitors. Assuming that PF-05274857 reaches the brain at higher concentrations, this would mean that Glasdegib is probably the more potent inhibitor. Another interesting observation in this context was that the time until the tumor started shrinking on treatment with Erismodegib was longer in the first cycle than in the later cycles. Thus, either the concentration of drug reaching the tumor was increased in later cycles, perhaps due to increased angiogenesis or even leakiness of the blood-brain barrier, or the tumor cells were sensitized to the inhibitor in later treatment cycles. Interestingly, in allografts of $PTCH^{+/-}$ GEMM tumors, responses to SMO inhibition are seen immediately and not with a delay, as it was in the first cycle of treatment in this experiment, which points toward the first option: Increased drug exposure after the first cycle[280]. Resistance to therapy through SMO inhibition, defined as growth under treatment, was observed after roughly three successful cycles of treatment. In 2010, experiments to induce resistance to Erismodegib were performed in subcutaneous mouse allografts from $PTCH^{+/-}$ GEMMs, partly in a $TP53^{-/-}$ background, and found, to varying degrees, either *SMO* mutations or *GLI2* amplifications, and in general PI3K activation as resistance mechanisms[280]. A year earlier, a point mutation in SMO was also identified in a relapsed medulloblastoma patient after treatment with Vismodegib[305]. Since then, several other studies have shown potential resistance pathways to SHH inhibition, but in those studies, subcutaneous GEMM allograft MB models were always used to induce resistance[484,485], and the genetic event causing resistance could often not be pinpointed. In the current study, however, for the first time, resistance to SMO inhibition was induced both in the orthotopic location of the tumor and in a human setting. Interestingly, the time until resistance was much longer in the PDOX than in the previously

published GEMM allograft, which can most likely be attributed to the smaller tumor size at treatment start in the mouse brain as compared to the subcutaneous situation[486]. Therefore, it is expected that monotherapy of SMO inhibitors will induce an early development of resistance, which was also observed in the previously mentioned clinical trial of Vismodegib in relapsed medulloblastoma[482]. To determine the genetic lesion driving the resistance to Erismodegib, a complete molecular characterization of the resistant tumors will be performed in the future. The major question to be answered here is whether in a human system, resistance to SMO inhibition is always acquired by re-activating the SHH pathway, or perhaps through the activation of an alternative pathway. Follow-up analyses will try to pinpoint the exact lesion responsible for tumor resistance. In addition to analyzing the resistant tumors on a molecular level, resistant tumors were also cryo-preserved so that they can be re-challenged with Erismodegib, and can also be used to test new therapy concepts after the resistance-driving lesions have been identified.

4.5 Future and Outlook

4.5.1 Improving PDX techniques

PDX models have evolved into the preferred preclinical model for drug development in academia and the pharmaceutical industry[367,382-384]. This study has shown that in pediatric neurooncology PDOX models allow, for the first time, the modeling of many tumor subtypes that until now were only able to be descriptively characterized from patient samples. Continuous establishment of PDOX will allow the increase in numbers of PDOX for even very rare tumor subgroups, so that in a few years it should be possible to run systematic preclinical experiments in multiple different PDOX models for even the rarest diseases. However, the bias for very highly aggressive tumors in PDOX cohorts, even within WHO stage IV-classified entities, is currently a strong hindrance to the modeling of even more tumor subgroups. Even on the rare occasion when an underrepresented tumor subtype engrafts as a PDOX, considerable caution is necessary, because this tumor is also highly likely to be a more aggressive exception to the otherwise less aggressive tumor subtype. For example, a patient with a WNT MB, from which a PDOX was generated, relapsed twice, which is highly unusual for this subtype[288], and highlights the atypical behavior of this particular patient tumor and the associated model.

Therefore, considerable efforts still need to be made to develop improved techniques for systematically generating PDOX from currently-underrepresented disease subtypes, as illustrated by the recent publication of Sflomos *et al.*, in which it was shown that the injection of ductal breast cancer into the milk ductus dramatically increased engraftment rates, which now allows the modeling of the disease[395]. Although in pediatric neurooncology the scientific

community already prefers orthotopic PDX, there are several additional technical points which could further increase engraftment rates, in addition to the optimization of the current setup (for example, reducing the time between surgery and transplantation into the mouse). It is conceivable that the choice of mouse strain has a large impact on PDX engraftment, although the only study comparing engraftment rates between two different mouse strains did not find a difference in engraftment rates[386]. Depending on the tumor entity, it may be beneficial to use an even more immunodeficient mouse strain than NSG mice, while other entities could be dependent upon the interaction with the immune system and need a humanized mouse strain to grow as a PDOX. However, based on the current status of humanized mouse strains, it seems unlikely that PDX passaging will be feasible in these mice in the near future[474]. In addition to changing the mouse microenvironment, it may also be possible to maintain the human stroma during the first passages by preserving the architecture of the tumor through the transplantation of only very small tumor pieces into the brain instead of dissociating the tumor into a single-cell suspension – an approach combining the advantages of the subcutaneous and the orthotopic xenograft. Overall, improving the techniques for generating and maintaining PDOX should allow the modeling of new tumor subtypes, and would also make the existing models better preclinical systems, more closely resembling the situation in the patient.

4.5.2 Additional and extended uses of PDX in pediatric neurooncology

Currently, the main use of PDX models is for the evaluation of new treatment concepts mainly for targeted compounds. However, this study and previously published preclinical work in pediatric neurooncology represent, in most scenarios, only an anecdotal testing of a therapeutic concept, e.g. here the preclinical evaluation of Erlotinib in MYCN HGG was tested only in one PDOX line with, and in one line without, *EGFR* amplification. This is primarily due to the lack of additional PDOX lines with the fitting molecular setup, but also due to limited resources. Examples of exhaustive testing in PDX using large cohorts are seen in the studies of Bertotti *et al.*[435], in which the authors evaluated the response to Cetuximab in 129 PDX models, or the study by Gao *et al.*[419], in which Novartis evaluated various therapeutic strategies in large numbers of PDX using the "*n* = 1" concept. However, the cohort of 130 pediatric brain tumor PDX models is not exhaustive enough for similar approaches, because numbers for most tumor subtypes are still too low or certain patient populations are underrepresented. For example, although 37 MB Group 3 PDOX models were collected, the overrepresentation of *MYC* amplification and *KBTBD4* insertion would severely bias the analysis, making it impossible to draw conclusion about the remaining patient populations. In order to increase sample sizes for future studies, an IMI2-funded preclinical proof-of-concept platform for pediatric cancer (ITCC-P4, https://www.itccp4.eu/) is being developed, which aims to contain up to 400 PDOX

lines split across 10 malignant pediatric solid tumors having the highest clinical need, including both brain and non-brain tumors. The consortium, co-sponsored by the European Union and the pharmaceutical industry, aims to molecularly classify all PDOX lines, and to perform *in vivo* testing of both standard-of-care and experimental drugs in order to systematically assess new therapeutic options for children. In addition to testing in reasonable cohort sizes, preclinical research in general, and in pediatric neurooncology specifically, must attempt to better mimic the real-life situation in clinical trials. In most clinical trial settings, patients are treated with a new targeted inhibitor after or in combination with a standard-of-care therapeutic. However, in pediatric neurooncology patients often receive even complex multimodal treatment regimens – very often neurosurgical resection, followed by radiotherapy and chemotherapy. In an enormous effort, Nimmervoll *et al.* showed that tumor resection in combination with radiotherapy and then followed by the test compound can be modeled in mice[487]. This approach is very resource-intensive, but can find potential interactions between different treatment regimens, such as which new targeted inhibitors synergize well with surgical resection. Furthermore, this extensive technique may also be needed if PDOX co-clinical trials are to be conducted in pediatric neurooncology.

However, even in the biggest consortia, not all potential drugs can be tested *in vivo*, and therefore, drug candidates need to be selected based on either biological hypotheses, such as whether BRAF inhibitors work in *BRAF* mutant tumors, or based on unbiased screening efforts *in vitro*. To make screening efforts more feasible, a high-throughput drug screening on short-term cultures of PDOX lines was conducted, together with the laboratory of Robert J. Wechsler-Reya in San Diego (USA), and is currently being evaluated in the context of genomic molecular data. A success story resulting from this concept is the discovery that HDAC and PI3K antagonists can inhibit tumor growth of MYC-driven MB via high-throughput drug screening of the MYC/DNp53 model (overexpression of MYC and dominant-negative TP53 in cerebellar stem cells) and subsequent validation *in vivo* in multiple PDOX[462]. Of note, in breast cancer 33/40 *in vitro* predictions of short-time cultures could be validated *in vivo*[397], showing the potential of this methodology. Still, in addition to false positive results, false negative results might also be a central problem of *in vitro* screening, such as SMO inhibitors in SHH MBs, which did not show any response *in vitro* (data not shown), but showed exceptional responses *in vivo*.

In addition to classic therapeutic questions, PDOX should also be expanded into a tool for functional genomics, because until now they have been the only available model systems for many pediatric brain tumor subgroups. Initial data from melanoma and pancreatic cancer highlight that it is possible to perform *in vivo* pooled shRNA screens in PDX with a maximum *in vitro* time of about five days to transduce and select the cells[488,489]. Systematic evaluation of

multiple PDOX with this method and then integration of molecular data with the newly generated functional data will allow the generation of a map of genetic dependencies based on the mutational status of the tumor. This method might also be a superior method to screen for good drug candidates *in vivo* than the previously presented short-time *in vitro* culture.

Further to perturbation experiments, PDOX can be used to track tumor evolution. It is still an open question as to why and when certain genomic alterations occur during evolution. The data presented here highlights that although the "driver" events are maintained, in some models the clonal composition changes over time. More in-depth analysis will require WGS data instead of WES data in order to increase the number of mutations, which can be used to define clonal populations and, furthermore, the analysis of multiple time points during PDX development. Current literature, mostly on subcutaneous xenografts, which, as mentioned previously, are prone to the propagation of anatomical heterogeneity, performed WGS only on the patient tumors and usually one PDX tumor, and then validated the identified mutations via targeted-amplicon sequencing in multiple passages[411,417]. This method obviously cannot identify *de novo* mutations in PDX passages other than the initial one. However, the study by Bruna *et al.* included some data on WES of multiple different time points of breast cancer PDX in comparison to relapsed patient samples and could show that although the overall heterogeneity is preserved, some additional clones emerge in later PDOX passages[397]. Further analyses need to address which mutational processes are still active in PDX, in order to understand what is driving the accumulation of additional mutations[490,491]. Comparisons to relapsed samples of the same patients are very interesting, but highly delicate, because the patient samples have undergone intensive treatment, which must be mirrored in PDX to be able to draw any conclusions.

In addition to extending the use of PDOX lines, the self-renewing features of PDOX also make them a great tool for establishing other model systems without using actual precious patient tissue. Together with the research group of Hans Clevers in Utrecht, the Netherlands, efforts are ongoing to generate organoids of pediatric brain tumors by establishing the conditions for organoid culture from fresh PDOX tumors. Organoid cultures have so far shown a great promise in other tumor entities, and would be a strong addition to the portfolio of preclinical model systems in pediatric neurooncology[378].

4.5.3 Toward a shared resource of cancer models

As pediatric brain tumors and their associated PDOX are rare, it is essential that the model systems are shared within the scientific community. This is possible because they can be easily re-grown after cryo preservation. The finding that the transportation of tumor samples

overnight did not significantly alter the engraftment rate in the Seattle cohort, highlights than even centers without the capacity to generate PDOX can contribute to the generation of new model systems by supplying fresh tumor material to centralized institutions for PDOX generation. In addition to openly sharing PDOX models generated in Heidelberg, the molecular data have been made available in a user-friendly manner through the "PDX Explorer" (https://hgserver1.amc.nl/cgi-bin/r2/main.cgi?&dscope=PDX_OLSON&option=about_dscope). The "PDX Explorer" also includes the "PDX Minimal Information" standards and consequently it therefore reports about clinical characteristics of the patients as well as extensive information about the techniques used to generate the model system[436]. This will make it possible to integrate these data into pan-cancer PDX repositories such as the "PDX Finder" (www.pdxfinder.org). With this open resource, many new therapeutic concepts that previously lacked suitable model systems or were tested in an inappropriate model system can be tested.

In the future, the aim is to develop the "PDX Explorer" into a central platform that contains most of the PDOX lines in the field, and then re-direct people to the individual laboratory that generated the line, for requests for cryo-preserved material. Due to this de-centralized structure and limited resources "academic centers are ill suited to bear the burden of housing, expanding, archiving, characterizing, and disseminating PDX to investigators (academic and industrial) across the world" as mentioned by the PRoXe and the EurOPDX consortia[434,474], but with the current structure of cancer research, it is the only possible way to share model systems with the scientific community. A step toward automating the sharing process could be the establishment of a central facility that collects cryo vials of established PDOX from scientific groups, archives them, and then shares these models with other interested parties upon signing of a standardized material transfer agreement. While the groups would still be responsible for establishing, expanding, and characterizing the models, they would not be involved any longer in sharing these models with each individual party. The group around James M. Olson in Seattle (USA) has already employed this system (www.btrl.org), and it would be the first step toward a shared resource if other groups were to join in, sharing their models in an automated manner. Because the lack of model systems is currently one of the major factors holding back cancer research, increasing the availability of, and knowledge about, model systems will have a tremendous positive effect on the quality of future research.

Supplementary tables

Table 3. Methylation classes of brain tumors.
This table was extracted from the publication Capper *et al.*, 2018.

Methylation Class Name Abbreviated	Methylation Class Name
ETMR	methylation class embryonal tumor with multilayered rosettes
MB, WNT	methylation class medulloblastoma, WNT
DMG, K27	methylation class diffuse midline glioma H3 K27M mutant
CN	methylation class central neurocytoma
DLGNT	methylation class diffuse leptomeningeal glioneuronal tumor
LIPN	methylation class cerebellar liponeurocytoma
LGG, DIG/DIA	methylation class low grade glioma, desmoplastic infantile astrocytoma / ganglioglioma
LGG, DNT	methylation class low grade glioma, dysembryoplastic neuroepithelial tumor
LGG, RGNT	methylation class low grade glioma, rosette forming glioneuronal tumor
RETB	methylation class retinoblastoma
SCHW	methylation class schwannoma
SCHW, MEL	methylation class melanotic schwannoma
CPH, ADM	methylation class craniopharyngioma, adamantinomatous
CPH, PAP	methylation class craniopharyngioma, papillary
PITAD, ACTH	methylation class pituitary adenoma, ACTH
PITAD, FSH LH	methylation class pituitary adenoma, FSH/LH
PITAD, PRL	methylation class pituitary adenoma, prolactin
PITAD, STH SPA	methylation class pituitary adenoma, STH sparsely granulated
PITAD, TSH	methylation class pituitary adenoma, TSH
EPN, RELA	methylation class ependymoma, RELA fusion
CHGL	methylation class chordoid glioma of the third ventricle
LGG, SEGA	methylation class low grade glioma, subependymal giant cell astrocytoma
CHORDM	methylation class chordoma
EWS	methylation class Ewing sarcoma
HMB	methylation class hemangioblastoma
MELAN	methylation class melanoma

Methylation Class Name Abbreviated	Methylation Class Name
MELCYT	methylation class melanocytoma
LYMPHO	methylation class lymphoma
PLASMA	methylation class plasmacytoma
MB, G3	methylation class medulloblastoma, subclass group 3
MB, G4	methylation class medulloblastoma, subclass group 4
MB, SHH CHL AD	methylation class medulloblastoma, subclass SHH A (children and adult)
MB, SHH INF	methylation class medulloblastoma, subclass SHH B (infant)
ATRT, MYC	methylation class atypical teratoid/rhabdoid tumor, subclass MYC
ATRT, SHH	methylation class atypical teratoid/rhabdoid tumor, subclass SHH
ATRT, TYR	methylation class atypical teratoid/rhabdoid tumor, subclass TYR
GBM, G34	methylation class glioblastoma, IDH wild-type, H3.3 G34 mutant
GBM, MES	methylation class glioblastoma, IDH wild-type, subclass mesenchymal
GBM, MID	methylation class glioblastoma, IDH wild-type, subclass midline
GBM, MYCN	methylation class glioblastoma, IDH wild-type, subclass MYCN
GBM, RTK I	methylation class glioblastoma, IDH wild-type, subclass RTK I
GBM, RTK II	methylation class glioblastoma, IDH wild-type, subclass RTK II
GBM, RTK III	methylation class glioblastoma, IDH wild-type, subclass RTK III
ENB, A	methylation class esthesioneuroblastoma, subclass A
ENB, B	methylation class esthesioneuroblastoma, subclass B
PGG, nC	methylation class paraganglioma, spinal non-CIMP
PITAD, STH DNS A	methylation class pituitary adenoma, STH densely granulated, group A
PITAD, STH DNS B	methylation class pituitary adenoma, STH densely granulated, group B
LGG, PA PF	methylation class low grade glioma, subclass posterior fossa pilocytic astrocytoma
LGG, PA MID	methylation class low grade glioma, subclass midline pilocytic astrocytoma
PTPR, A	methylation class papillary tumor of the pineal region group A
PTPR, B	methylation class papillary tumor of the pineal region group B
PIN T, PB B	methylation class pineoblastoma group B
EPN, PF A	methylation class ependymoma, posterior fossa group A
EPN, PF B	methylation class ependymoma, posterior fossa group B
EPN, SPINE	methylation class ependymoma, spinal

Methylation Class Name Abbreviated	Methylation Class Name
EPN, YAP	methylation class ependymoma, YAP fusion
CNS NB, FOXR2	methylation class CNS neuroblastoma with FOXR2 activation
SFT HMPC	methylation class solitary fibrous tumor / hemangiopericytoma
PLEX, AD	methylation class plexus tumor, subclass adult
PLEX, PED A	methylation class plexus tumor, subclass paediatric A
PLEX, PED B	methylation class plexus tumor, subclass paediatric B
A IDH	methylation class IDH glioma, subclass astrocytoma
A IDH, HG	methylation class IDH glioma, subclass high grade astrocytoma
O IDH	methylation class IDH glioma, subclass 1p/19q codeleted oligodendroglioma
PIN T, PPT	methylation class pineal parenchymal tumor
LGG, GG	methylation class low grade glioma, ganglioglioma
PITUI, SCO, GCT	methylation class pituicytoma / granular cell tumor / spindle cell oncocytoma
LGG, PA/GG ST	methylation class low grade glioma, subclass hemispheric pilocytic astrocytoma and ganglioglioma
PXA	methylation class (anaplastic) pleomorphic xanthoastrocytoma
MNG	methylation class meningioma
EPN, MPE	methylation class ependymoma, myxopapillary
SUBEPN, PF	methylation class subependymoma, posterior fossa
SUBEPN, SPINE	methylation class subependymoma, spinal
SUBEPN, ST	methylation class subependymoma, supratentorial
PIN T, PB A	methylation class pineoblastoma group A / intracranial retinoblastoma
LGG, MYB	methylation class low grade glioma, MYB/MYBL1
HGNET, BCOR	methylation class CNS high grade neuroepithelial tumor with BCOR alteration
ANA PA	methylation class anaplastic pilocytic astrocytoma
HGNET, MN1	methylation class CNS high grade neuroepithelial tumor with MN1 alteration
IHG	methylation class infantile hemispheric glioma
EFT, CIC	methylation class CNS Ewing sarcoma family tumor with CIC alteration
CONTR, ADENOPIT	methylation class control tissue, pituitary gland anterior lobe
CONTR, CEBM	methylation class control tissue, cerebellar hemisphere

Methylation Class Name Abbreviated	Methylation Class Name
CONTR, HEMI	methylation class control tissue, hemispheric cortex
CONTR, HYPTHAL	methylation class control tissue, hypothalamus
CONTR, INFLAM	methylation class control tissue, inflammatory tumor microenvironment
CONTR, PINEAL	methylation class control tissue, pineal gland
CONTR, PONS	methylation class control tissue, pons
CONTR, REACT	methylation class control tissue, reactive tumor microenvironment
CONTR, WM	methylation class control tissue, white matter

Bibliography

1 Ervik M., L. F., Ferlay J., Mery L., Soerjomataram I., Bray F. Lyon, France: International Agency for Research on Cancer. Cancer Today. *Available from:* http://gco.iarc.fr/today, *accessed [8/8/2017]* (2016).

2 Miller, K. D. *et al.* Cancer treatment and survivorship statistics, 2016. *CA Cancer J. Clin.* **66**, 271-289, doi:10.3322/caac.21349 (2016).

3 Siegel, R. L., Miller, K. D. & Jemal, A. Cancer statistics, 2016. *CA Cancer J. Clin.* **66**, 7-30, doi:10.3322/caac.21332 (2016).

4 Murphy, S. L., Kochanek, K. D., Xu, J. & Arias, E. Mortality in the United States, 2014. *NCHS Data Brief*, 1-8 (2015).

5 Hanahan, D. & Weinberg, R. A. The hallmarks of cancer. *Cell* **100**, 57-70 (2000).

6 Hanahan, D. & Weinberg, R. A. Hallmarks of cancer: the next generation. *Cell* **144**, 646-674, doi:10.1016/j.cell.2011.02.013 (2011).

7 Hynes, N. E. & MacDonald, G. ErbB receptors and signaling pathways in cancer. *Curr. Opin. Cell Biol.* **21**, 177-184, doi:10.1016/j.ceb.2008.12.010 (2009).

8 Lemmon, M. A. & Schlessinger, J. Cell signaling by receptor tyrosine kinases. *Cell* **141**, 1117-1134, doi:10.1016/j.cell.2010.06.011 (2010).

9 Perona, R. Cell signalling: growth factors and tyrosine kinase receptors. *Clin. Transl. Oncol.* **8**, 77-82 (2006).

10 Witsch, E., Sela, M. & Yarden, Y. Roles for growth factors in cancer progression. *Physiology (Bethesda)* **25**, 85-101, doi:10.1152/physiol.00045.2009 (2010).

11 Cheng, N., Chytil, A., Shyr, Y., Joly, A. & Moses, H. L. Transforming growth factor-beta signaling-deficient fibroblasts enhance hepatocyte growth factor signaling in mammary carcinoma cells to promote scattering and invasion. *Mol. Cancer Res.* **6**, 1521-1533, doi:10.1158/1541-7786.MCR-07-2203 (2008).

12 Bhowmick, N. A., Neilson, E. G. & Moses, H. L. Stromal fibroblasts in cancer initiation and progression. *Nature* **432**, 332-337, doi:10.1038/nature03096 (2004).

13 Verhaak, R. G. *et al.* Integrated genomic analysis identifies clinically relevant subtypes of glioblastoma characterized by abnormalities in PDGFRA, IDH1, EGFR, and NF1. *Cancer Cell* **17**, 98-110, doi:10.1016/j.ccr.2009.12.020 (2010).

14 Holderfield, M., Deuker, M. M., McCormick, F. & McMahon, M. Targeting RAF kinases for cancer therapy: BRAF-mutated melanoma and beyond. *Nat. Rev. Cancer* **14**, 455-467, doi:10.1038/nrc3760 (2014).

15 Lassaletta, A. *et al.* Therapeutic and Prognostic Implications of BRAF V600E in Pediatric Low-Grade Gliomas. *J. Clin. Oncol.* **35**, 2934-2941, doi:10.1200/JCO.2016.71.8726 (2017).

16 Wertz, I. E. & Dixit, V. M. Regulation of death receptor signaling by the ubiquitin system. *Cell Death Differ.* **17**, 14-24, doi:10.1038/cdd.2009.168 (2010).

17 Cabrita, M. A. & Christofori, G. Sprouty proteins, masterminds of receptor tyrosine kinase signaling. *Angiogenesis* **11**, 53-62, doi:10.1007/s10456-008-9089-1 (2008).

18 Amit, I. *et al.* A module of negative feedback regulators defines growth factor signaling. *Nat. Genet.* **39**, 503-512, doi:10.1038/ng1987 (2007).

19 Mosesson, Y., Mills, G. B. & Yarden, Y. Derailed endocytosis: an emerging feature of cancer. *Nat. Rev. Cancer* **8**, 835-850, doi:10.1038/nrc2521 (2008).

20 Pylayeva-Gupta, Y., Grabocka, E. & Bar-Sagi, D. RAS oncogenes: weaving a tumorigenic web. *Nat. Rev. Cancer* **11**, 761-774, doi:10.1038/nrc3106 (2011).

21 Jiang, B. H. & Liu, L. Z. PI3K/PTEN signaling in angiogenesis and tumorigenesis. *Adv. Cancer Res.* **102**, 19-65, doi:10.1016/S0065-230X(09)02002-8 (2009).

22 Weinberg, R. A. Oncogenes and tumor suppressor genes. *CA Cancer J. Clin.* **44**, 160-170 (1994).

23 Campisi, J. Aging, cellular senescence, and cancer. *Annu. Rev. Physiol.* **75**, 685-705, doi:10.1146/annurev-physiol-030212-183653 (2013).

24 Bieging, K. T., Mello, S. S. & Attardi, L. D. Unravelling mechanisms of p53-mediated tumour suppression. *Nat. Rev. Cancer* **14**, 359-370, doi:10.1038/nrc3711 (2014).

25 Grobner, S. N. *et al.* The landscape of genomic alterations across childhood cancers. *Nature* **555**, 321-327, doi:10.1038/nature25480 (2018).

26 Kandoth, C. *et al.* Mutational landscape and significance across 12 major cancer types. *Nature* **502**, 333-339, doi:10.1038/nature12634 (2013).

27 Lustbader, E. D., Williams, W. R., Bondy, M. L., Strom, S. & Strong, L. C. Segregation analysis of cancer in families of childhood soft-tissue-sarcoma patients. *Am. J. Hum. Genet.* **51**, 344-356 (1992).

28 Varley, J. M., Evans, D. G. & Birch, J. M. Li-Fraumeni syndrome--a molecular and clinical review. *Br. J. Cancer* **76**, 1-14 (1997).

29 Gonzalez, K. D. *et al.* Beyond Li Fraumeni Syndrome: clinical characteristics of families with p53 germline mutations. *J. Clin. Oncol.* **27**, 1250-1256, doi:10.1200/JCO.2008.16.6959 (2009).

30 Upton, B., Chu, Q. & Li, B. D. Li-Fraumeni syndrome: the genetics and treatment considerations for the sarcoma and associated neoplasms. *Surg. Oncol. Clin. N. Am.* **18**, 145-156, ix, doi:10.1016/j.soc.2008.08.006 (2009).

31 Siegel, R., Naishadham, D. & Jemal, A. Cancer statistics, 2012. *CA Cancer J. Clin.* **62**, 10-29, doi:10.3322/caac.20138 (2012).

32 Sorrell, A. D., Espenschied, C. R., Culver, J. O. & Weitzel, J. N. Tumor protein p53 (TP53) testing and Li-Fraumeni syndrome : current status of clinical applications and future directions. *Mol. Diagn. Ther.* **17**, 31-47, doi:10.1007/s40291-013-0020-0 (2013).

33 Elmore, S. Apoptosis: a review of programmed cell death. *Toxicol. Pathol.* **35**, 495-516, doi:10.1080/01926230701320337 (2007).

34 Wong, R. S. Apoptosis in cancer: from pathogenesis to treatment. *J. Exp. Clin. Cancer Res.* **30**, 87, doi:10.1186/1756-9966-30-87 (2011).

35 Hayflick, L. & Moorhead, P. S. The serial cultivation of human diploid cell strains. *Exp. Cell Res.* **25**, 585-621 (1961).

36 Hayflick, L. The Limited in Vitro Lifetime of Human Diploid Cell Strains. *Exp. Cell Res.* **37**, 614-636 (1965).

37 Blasco, M. A. Telomeres and human disease: ageing, cancer and beyond. *Nat Rev Genet* **6**, 611-622, doi:10.1038/nrg1656 (2005).

38 Artandi, S. E. & DePinho, R. A. Mice without telomerase: what can they teach us about human cancer? *Nat. Med.* **6**, 852-855, doi:10.1038/78595 (2000).

39 Artandi, S. E. & DePinho, R. A. Telomeres and telomerase in cancer. *Carcinogenesis* **31**, 9-18, doi:10.1093/carcin/bgp268 (2010).

40 Carmeliet, P. & Jain, R. K. Angiogenesis in cancer and other diseases. *Nature* **407**, 249-257, doi:10.1038/35025220 (2000).

41 Hanahan, D. & Folkman, J. Patterns and emerging mechanisms of the angiogenic switch during tumorigenesis. *Cell* **86**, 353-364 (1996).

42 Folkman, J. Tumor angiogenesis: therapeutic implications. *N. Engl. J. Med.* **285**, 1182-1186, doi:10.1056/NEJM197111182852108 (1971).

43 Ricci-Vitiani, L. *et al.* Tumour vascularization via endothelial differentiation of glioblastoma stem-like cells. *Nature* **468**, 824-828, doi:10.1038/nature09557 (2010).

44 Wang, R. *et al.* Glioblastoma stem-like cells give rise to tumour endothelium. *Nature* **468**, 829-833, doi:10.1038/nature09624 (2010).

45 Bremnes, R. M. *et al.* The role of tumor stroma in cancer progression and prognosis: emphasis on carcinoma-associated fibroblasts and non-small cell lung cancer. *J. Thorac. Oncol.* **6**, 209-217, doi:10.1097/JTO.0b013e3181f8a1bd (2011).

46 Dvorak, H. F. Tumors: wounds that do not heal. Similarities between tumor stroma generation and wound healing. *N. Engl. J. Med.* **315**, 1650-1659, doi:10.1056/NEJM198612253152606 (1986).

47 Colotta, F., Allavena, P., Sica, A., Garlanda, C. & Mantovani, A. Cancer-related inflammation, the seventh hallmark of cancer: links to genetic instability. *Carcinogenesis* **30**, 1073-1081, doi:10.1093/carcin/bgp127 (2009).

48 DeNardo, D. G., Andreu, P. & Coussens, L. M. Interactions between lymphocytes and myeloid cells regulate pro- versus anti-tumor immunity. *Cancer Metastasis Rev.* **29**, 309-316, doi:10.1007/s10555-010-9223-6 (2010).

49 Grivennikov, S. I., Greten, F. R. & Karin, M. Immunity, inflammation, and cancer. *Cell* **140**, 883-899, doi:10.1016/j.cell.2010.01.025 (2010).

50 Qian, B. Z. & Pollard, J. W. Macrophage diversity enhances tumor progression and metastasis. *Cell* **141**, 39-51, doi:10.1016/j.cell.2010.03.014 (2010).

51 Sparmann, A. & Bar-Sagi, D. Ras-induced interleukin-8 expression plays a critical role in tumor growth and angiogenesis. *Cancer Cell* **6**, 447-458, doi:10.1016/j.ccr.2004.09.028 (2004).

52 Soucek, L. *et al.* Mast cells are required for angiogenesis and macroscopic expansion of Myc-induced pancreatic islet tumors. *Nat. Med.* **13**, 1211-1218, doi:10.1038/nm1649 (2007).

53 Warburg, O. The Metabolism of Tumours: Investigations from the Kaiser Wilhelm Institute for Biology, Berlin-Dahlem (London, UK: Arnold Constable). (1930).

54 Warburg, O. On the origin of cancer cells. *Science* **123**, 309-314 (1956).

55 Warburg, O. On respiratory impairment in cancer cells. *Science* **124**, 269-270 (1956).

56 Vander Heiden, M. G. & DeBerardinis, R. J. Understanding the Intersections between Metabolism and Cancer Biology. *Cell* **168**, 657-669, doi:10.1016/j.cell.2016.12.039 (2017).

57 Vander Heiden, M. G., Cantley, L. C. & Thompson, C. B. Understanding the Warburg effect: the metabolic requirements of cell proliferation. *Science* **324**, 1029-1033, doi:10.1126/science.1160809 (2009).

58 Brand, K., Leibold, W., Luppa, P., Schoerner, C. & Schulz, A. Metabolic alterations associated with proliferation of mitogen-activated lymphocytes and of lymphoblastoid cell lines: evaluation of glucose and glutamine metabolism. *Immunobiology* **173**, 23-34, doi:10.1016/S0171-2985(86)80086-9 (1986).

59 Chambers, J. W., Maguire, T. G. & Alwine, J. C. Glutamine metabolism is essential for human cytomegalovirus infection. *J. Virol.* **84**, 1867-1873, doi:10.1128/JVI.02123-09 (2010).

60 Noch, E. & Khalili, K. Oncogenic viruses and tumor glucose metabolism: like kids in a candy store. *Mol. Cancer Ther.* **11**, 14-23, doi:10.1158/1535-7163.MCT-11-0517 (2012).

61 Pavlova, N. N. & Thompson, C. B. The Emerging Hallmarks of Cancer Metabolism. *Cell Metab* **23**, 27-47, doi:10.1016/j.cmet.2015.12.006 (2016).

62 Fidler, I. J. The pathogenesis of cancer metastasis: the 'seed and soil' hypothesis revisited. *Nat. Rev. Cancer* **3**, 453-458, doi:10.1038/nrc1098 (2003).

63 Talmadge, J. E. & Fidler, I. J. AACR centennial series: the biology of cancer metastasis: historical perspective. *Cancer Res.* **70**, 5649-5669, doi:10.1158/0008-5472.CAN-10-1040 (2010).

64 Valastyan, S. & Weinberg, R. A. Tumor metastasis: molecular insights and evolving paradigms. *Cell* **147**, 275-292, doi:10.1016/j.cell.2011.09.024 (2011).

65 Frisch, S. M. & Francis, H. Disruption of epithelial cell-matrix interactions induces apoptosis. *J. Cell Biol.* **124**, 619-626 (1994).

66 Barrallo-Gimeno, A. & Nieto, M. A. The Snail genes as inducers of cell movement and survival: implications in development and cancer. *Development* **132**, 3151-3161, doi:10.1242/dev.01907 (2005).

67 Klymkowsky, M. W. & Savagner, P. Epithelial-mesenchymal transition: a cancer researcher's conceptual friend and foe. *Am. J. Pathol.* **174**, 1588-1593, doi:10.2353/ajpath.2009.080545 (2009).

68 Polyak, K. & Weinberg, R. A. Transitions between epithelial and mesenchymal states: acquisition of malignant and stem cell traits. *Nat. Rev. Cancer* **9**, 265-273, doi:10.1038/nrc2620 (2009).

69 Thiery, J. P. & Sleeman, J. P. Complex networks orchestrate epithelial-mesenchymal transitions. *Nat. Rev. Mol. Cell Biol.* **7**, 131-142, doi:10.1038/nrm1835 (2006).

70 Yilmaz, M. & Christofori, G. EMT, the cytoskeleton, and cancer cell invasion. *Cancer Metastasis Rev.* **28**, 15-33, doi:10.1007/s10555-008-9169-0 (2009).

71 Nguyen, D. X. & Massague, J. Genetic determinants of cancer metastasis. *Nat Rev Genet* **8**, 341-352, doi:10.1038/nrg2101 (2007).

72 Collins, F. S. & Barker, A. D. Mapping the cancer genome. Pinpointing the genes involved in cancer will help chart a new course across the complex landscape of human malignancies. *Sci. Am.* **296**, 50-57 (2007).

73 Hudson, T. J. *et al.* International network of cancer genome projects. *Nature* **464**, 993-998, doi:10.1038/nature08987 (2010).

74 Weinstein, J. N. *et al.* The Cancer Genome Atlas Pan-Cancer analysis project. *Nat. Genet.* **45**, 1113-1120, doi:10.1038/ng.2764 (2013).

75 Boveri, T. Concerning the origin of malignant tumours by Theodor Boveri. Translated and annotated by Henry Harris. *J. Cell Sci.* **121 Suppl 1**, 1-84, doi:10.1242/jcs.025742 (2008).

76 Garraway, L. A. & Lander, E. S. Lessons from the cancer genome. *Cell* **153**, 17-37, doi:10.1016/j.cell.2013.03.002 (2013).

77 Martin, G. S. The road to Src. *Oncogene* **23**, 7910-7917, doi:10.1038/sj.onc.1208077 (2004).

78 Stehelin, D., Varmus, H. E., Bishop, J. M. & Vogt, P. K. DNA related to the transforming gene(s) of avian sarcoma viruses is present in normal avian DNA. *Nature* **260**, 170-173 (1976).

79 Tabin, C. J. *et al.* Mechanism of activation of a human oncogene. *Nature* **300**, 143-149 (1982).

80 Macconaill, L. E. & Garraway, L. A. Clinical implications of the cancer genome. *J. Clin. Oncol.* **28**, 5219-5228, doi:10.1200/JCO.2009.27.4944 (2010).

81 Dulbecco, R. A turning point in cancer research: sequencing the human genome. *Science* **231**, 1055-1056 (1986).

82 Lander, E. S. *et al.* Initial sequencing and analysis of the human genome. *Nature* **409**, 860-921, doi:10.1038/35057062 (2001).

83 Venter, J. C. *et al.* The sequence of the human genome. *Science* **291**, 1304-1351, doi:10.1126/science.1058040 (2001).

84 International Human Genome Sequencing, C. Finishing the euchromatic sequence of the human genome. *Nature* **431**, 931-945, doi:10.1038/nature03001 (2004).

85 Davies, H. *et al.* Mutations of the BRAF gene in human cancer. *Nature* **417**, 949-954, doi:10.1038/nature00766 (2002).

86 Samuels, Y. *et al.* High frequency of mutations of the PIK3CA gene in human cancers. *Science* **304**, 554, doi:10.1126/science.1096502 (2004).

87 Lynch, T. J. *et al.* Activating mutations in the epidermal growth factor receptor underlying responsiveness of non-small-cell lung cancer to gefitinib. *N. Engl. J. Med.* **350**, 2129-2139, doi:10.1056/NEJMoa040938 (2004).

88 Paez, J. G. *et al.* EGFR mutations in lung cancer: correlation with clinical response to gefitinib therapy. *Science* **304**, 1497-1500, doi:10.1126/science.1099314 (2004).

89 Pao, W. *et al.* EGF receptor gene mutations are common in lung cancers from "never smokers" and are associated with sensitivity of tumors to gefitinib and erlotinib. *Proc. Natl. Acad. Sci. U. S. A.* **101**, 13306-13311, doi:10.1073/pnas.0405220101 (2004).

90 Stratton, M. R., Campbell, P. J. & Futreal, P. A. The cancer genome. *Nature* **458**, 719-724, doi:10.1038/nature07943 (2009).

91 Gabor Miklos, G. L. The human cancer genome project--one more misstep in the war on cancer. *Nat. Biotechnol.* **23**, 535-537, doi:10.1038/nbt0505-535 (2005).

92 Weinberg, R. Point: Hypotheses first. *Nature* **464**, 678, doi:10.1038/464678a (2010).

93 Goodwin, S., McPherson, J. D. & McCombie, W. R. Coming of age: ten years of next-generation sequencing technologies. *Nat Rev Genet* **17**, 333-351, doi:10.1038/nrg.2016.49 (2016).

94 Watson, J. D. & Crick, F. H. Molecular structure of nucleic acids; a structure for deoxyribose nucleic acid. *Nature* **171**, 737-738 (1953).

95 Zallen, D. T. Despite Franklin's work, Wilkins earned his Nobel. *Nature* **425**, 15, doi:10.1038/425015b (2003).

96 Holley, R. W. *et al.* Structure of a Ribonucleic Acid. *Science* **147**, 1462-1465 (1965).

97 Sanger, F., Brownlee, G. G. & Barrell, B. G. A two-dimensional fractionation procedure for radioactive nucleotides. *J. Mol. Biol.* **13**, 373-398 (1965).

98 Min Jou, W., Haegeman, G., Ysebaert, M. & Fiers, W. Nucleotide sequence of the gene coding for the bacteriophage MS2 coat protein. *Nature* **237**, 82-88 (1972).

99 Fiers, W. *et al.* Complete nucleotide sequence of bacteriophage MS2 RNA: primary and secondary structure of the replicase gene. *Nature* **260**, 500-507 (1976).

100 Heather, J. M. & Chain, B. The sequence of sequencers: The history of sequencing DNA. *Genomics* **107**, 1-8, doi:10.1016/j.ygeno.2015.11.003 (2016).

101 Wu, R. & Kaiser, A. D. Structure and base sequence in the cohesive ends of bacteriophage lambda DNA. *J. Mol. Biol.* **35**, 523-537 (1968).

102 Wu, R. Nucleotide sequence analysis of DNA. *Nat. New Biol.* **236**, 198-200 (1972).

103 Sanger, F., Donelson, J. E., Coulson, A. R., Kossel, H. & Fischer, D. Use of DNA polymerase I primed by a synthetic oligonucleotide to determine a nucleotide sequence in phage fl DNA. *Proc. Natl. Acad. Sci. U. S. A.* **70**, 1209-1213 (1973).

104 Padmanabhan, R. & Wu, R. Nucleotide sequence analysis of DNA. IX. Use of oligonucleotides of defined sequence as primers in DNA sequence analysis. *Biochem. Biophys. Res. Commun.* **48**, 1295-1302 (1972).

105 Padmanabhan, R., Jay, E. & Wu, R. Chemical synthesis of a primer and its use in the sequence analysis of the lysozyme gene of bacteriophage T4. *Proc. Natl. Acad. Sci. U. S. A.* **71**, 2510-2514 (1974).

106 Sanger, F. & Coulson, A. R. A rapid method for determining sequences in DNA by primed synthesis with DNA polymerase. *J. Mol. Biol.* **94**, 441-448 (1975).

107 Maxam, A. M. & Gilbert, W. A new method for sequencing DNA. *Proc. Natl. Acad. Sci. U. S. A.* **74**, 560-564 (1977).

108 Sanger, F. *et al.* Nucleotide sequence of bacteriophage phi X174 DNA. *Nature* **265**, 687-695 (1977).

109 Sanger, F., Nicklen, S. & Coulson, A. R. DNA sequencing with chain-terminating inhibitors. *Proc. Natl. Acad. Sci. U. S. A.* **74**, 5463-5467 (1977).

110 Chidgeavadze, Z. G. *et al.* 2',3'-Dideoxy-3' aminonucleoside 5'-triphosphates are the terminators of DNA synthesis catalyzed by DNA polymerases. *Nucleic Acids Res.* **12**, 1671-1686 (1984).

111 Ansorge, W., Sproat, B., Stegemann, J., Schwager, C. & Zenke, M. Automated DNA sequencing: ultrasensitive detection of fluorescent bands during electrophoresis. *Nucleic Acids Res.* **15**, 4593-4602 (1987).

112 Ansorge, W., Sproat, B. S., Stegemann, J. & Schwager, C. A non-radioactive automated method for DNA sequence determination. *J. Biochem. Biophys. Methods* **13**, 315-323 (1986).

113 Luckey, J. A. *et al.* High speed DNA sequencing by capillary electrophoresis. *Nucleic Acids Res.* **18**, 4417-4421 (1990).

114 Prober, J. M. *et al.* A system for rapid DNA sequencing with fluorescent chain-terminating dideoxynucleotides. *Science* **238**, 336-341 (1987).

115 Smith, L. M., Fung, S., Hunkapiller, M. W., Hunkapiller, T. J. & Hood, L. E. The synthesis of oligonucleotides containing an aliphatic amino group at the 5' terminus: synthesis of fluorescent DNA primers for use in DNA sequence analysis. *Nucleic Acids Res.* **13**, 2399-2412 (1985).

116 Swerdlow, H. & Gesteland, R. Capillary gel electrophoresis for rapid, high resolution DNA sequencing. *Nucleic Acids Res.* **18**, 1415-1419 (1990).

117 Kambara, H., Nishikawa, T., Katayama, Y. & Yamaguchi, T. Optimization of Parameters in a DNA Sequenator Using Fluorescence Detection. *Bio-Technology* **6**, 816-821, doi:Doi 10.1038/Nbt0788-816 (1988).

118 Hunkapiller, T., Kaiser, R. J., Koop, B. F. & Hood, L. Large-scale and automated DNA sequence determination. *Science* **254**, 59-67 (1991).

119 Anderson, S. Shotgun DNA sequencing using cloned DNase I-generated fragments. *Nucleic Acids Res.* **9**, 3015-3027 (1981).

120 Staden, R. A strategy of DNA sequencing employing computer programs. *Nucleic Acids Res.* **6**, 2601-2610 (1979).

121 Chen, C. Y. DNA polymerases drive DNA sequencing-by-synthesis technologies: both past and present. *Front Microbiol* **5**, 305, doi:10.3389/fmicb.2014.00305 (2014).

122 Smith, L. M. *et al.* Fluorescence detection in automated DNA sequence analysis. *Nature* **321**, 674-679, doi:10.1038/321674a0 (1986).

123 Ansorge, W. J. Next-generation DNA sequencing techniques. *N Biotechnol* **25**, 195-203, doi:10.1016/j.nbt.2008.12.009 (2009).

124 Nyren, P. & Lundin, A. Enzymatic method for continuous monitoring of inorganic pyrophosphate synthesis. *Anal. Biochem.* **151**, 504-509 (1985).

125 Hyman, E. D. A new method of sequencing DNA. *Anal. Biochem.* **174**, 423-436 (1988).

126 Nyren, P. Enzymatic method for continuous monitoring of DNA polymerase activity. *Anal. Biochem.* **167**, 235-238 (1987).

127 Ronaghi, M., Karamohamed, S., Pettersson, B., Uhlen, M. & Nyren, P. Real-time DNA sequencing using detection of pyrophosphate release. *Anal. Biochem.* **242**, 84-89, doi:10.1006/abio.1996.0432 (1996).

128 Ronaghi, M., Uhlen, M. & Nyren, P. A sequencing method based on real-time pyrophosphate. *Science* **281**, 363, 365 (1998).

129 Margulies, M. *et al.* Genome sequencing in microfabricated high-density picolitre reactors. *Nature* **437**, 376-380, doi:10.1038/nature03959 (2005).

130 Tawfik, D. S. & Griffiths, A. D. Man-made cell-like compartments for molecular evolution. *Nat. Biotechnol.* **16**, 652-656, doi:10.1038/nbt0798-652 (1998).

131 Levy, S. *et al.* The diploid genome sequence of an individual human. *PLoS Biol.* **5**, e254, doi:10.1371/journal.pbio.0050254 (2007).

132 Wheeler, D. A. *et al.* The complete genome of an individual by massively parallel DNA sequencing. *Nature* **452**, 872-876, doi:10.1038/nature06884 (2008).

133 Voelkerding, K. V., Dames, S. A. & Durtschi, J. D. Next-generation sequencing: from basic research to diagnostics. *Clin. Chem.* **55**, 641-658, doi:10.1373/clinchem.2008.112789 (2009).

134 Greenleaf, W. J. & Sidow, A. The future of sequencing: convergence of intelligent design and market Darwinism. *Genome Biol.* **15**, 303, doi:10.1186/gb4168 (2014).

135 Valouev, A. *et al.* A high-resolution, nucleosome position map of C. elegans reveals a lack of universal sequence-dictated positioning. *Genome Res.* **18**, 1051-1063, doi:10.1101/gr.076463.108 (2008).

136 Drmanac, R. *et al.* Human genome sequencing using unchained base reads on self-assembling DNA nanoarrays. *Science* **327**, 78-81, doi:10.1126/science.1181498 (2010).

137 Rothberg, J. M. *et al.* An integrated semiconductor device enabling non-optical genome sequencing. *Nature* **475**, 348-352, doi:10.1038/nature10242 (2011).

138 Shendure, J. & Ji, H. Next-generation DNA sequencing. *Nat. Biotechnol.* **26**, 1135-1145, doi:10.1038/nbt1486 (2008).

139 Gut, I. G. New sequencing technologies. *Clin. Transl. Oncol.* **15**, 879-881, doi:10.1007/s12094-013-1073-6 (2013).

140 Niedringhaus, T. P., Milanova, D., Kerby, M. B., Snyder, M. P. & Barron, A. E. Landscape of Next-Generation Sequencing Technologies. *Anal. Chem.* **83**, 4327-4341, doi:10.1021/ac2010857 (2011).

141 Pareek, C. S., Smoczynski, R. & Tretyn, A. Sequencing technologies and genome sequencing. *Journal of Applied Genetics* **52**, 413-435, doi:10.1007/s13353-011-0057-x (2011).

142 Schadt, E. E., Turner, S. & Kasarskis, A. A window into third-generation sequencing. *Hum. Mol. Genet.* **19**, R227-R240, doi:10.1093/hmg/ddq416 (2010).

143 van Dijk, E. L., Auger, H., Jaszczyszyn, Y. & Thermes, C. Ten years of next-generation sequencing technology. *Trends Genet.* **30**, 418-426, doi:10.1016/j.tig.2014.07.001 (2014).

144 Levene, M. J. *et al.* Zero-mode waveguides for single-molecule analysis at high concentrations. *Science* **299**, 682-686, doi:Doi 10.1126/Science.1079700 (2003).

145 Eid, J. *et al.* Real-time DNA sequencing from single polymerase molecules. *Science* **323**, 133-138, doi:10.1126/science.1162986 (2009).

146 Flusberg, B. A. *et al.* Direct detection of DNA methylation during single-molecule, real-time sequencing. *Nat Methods* **7**, 461-465, doi:10.1038/nmeth.1459 (2010).

147 Lockhart, D. J. & Winzeler, E. A. Genomics, gene expression and DNA arrays. *Nature* **405**, 827-836, doi:10.1038/35015701 (2000).

148 Taylor, M. D. *et al.* Molecular subgroups of medulloblastoma: the current consensus. *Acta Neuropathol.* **123**, 465-472, doi:10.1007/s00401-011-0922-z (2012).

149 Trevino, V., Falciani, F. & Barrera-Saldana, H. A. DNA microarrays: a powerful genomic tool for biomedical and clinical research. *Mol. Med.* **13**, 527-541, doi:10.2119/2006-00107.Trevino (2007).

150 Cutler, D. J. *et al.* High-throughput variation detection and genotyping using microarrays. *Genome Res.* **11**, 1913-1925 (2001).

151 Frazer, K. A. *et al.* A second generation human haplotype map of over 3.1 million SNPs. *Nature* **449**, 851-U853, doi:10.1038/nature06258 (2007).

152 Yan, P. S. *et al.* Dissecting complex epigenetic alterations in breast cancer using CpG island microarrays. *Cancer Res.* **61**, 8375-8380 (2001).

153 Pollack, J. R. *et al.* Genome-wide analysis of DNA copy-number changes using cDNA microarrays. *Nat. Genet.* **23**, 41-46 (1999).

154 Relogio, A. *et al.* Alternative splicing microarrays reveal functional expression of neuron-specific regulators in Hodgkin lymphoma cells. *J. Biol. Chem.* **280**, 4779-4784, doi:10.1074/jbc.M411976200 (2005).

155 Wang, D. *et al.* Microarray-based detection and genotyping of viral pathogens. *Proc. Natl. Acad. Sci. U. S. A.* **99**, 15687-15692, doi:10.1073/pnas.242579699 (2002).

156 Zhao, S., Fung-Leung, W. P., Bittner, A., Ngo, K. & Liu, X. Comparison of RNA-Seq and microarray in transcriptome profiling of activated T cells. *PLoS One* **9**, e78644, doi:10.1371/journal.pone.0078644 (2014).

157 Ward, E., DeSantis, C., Robbins, A., Kohler, B. & Jemal, A. Childhood and adolescent cancer statistics, 2014. *Ca-a Cancer Journal for Clinicians* **64**, 83-103, doi:10.3322/caac.21219 (2014).

158 Steliarova-Foucher, E. *et al.* Geographical patterns and time trends of cancer incidence and survival among children and adolescents in Europe since the 1970s (the ACCIS project): an epidemiological study. *Lancet* **364**, 2097-2105, doi:Doi 10.1016/S0140-6736(04)17550-8 (2004).

159 Kroll, M. E., Stiller, C. A., Richards, S., Mitchell, C. & Carpenter, L. M. Evidence for under-diagnosis of childhood acute lymphoblastic leukaemia in poorer communities within Great Britain. *Br. J. Cancer* **106**, 1556-1559, doi:10.1038/bjc.2012.102 (2012).

160 Smith, M. A., Freidlin, B., Ries, L. A. G. & Simon, R. Trends in reported incidence of primary malignant brain tumors in children in the United States. *J. Natl. Cancer Inst.* **90**, 1269-1277, doi:Doi 10.1093/Jnci/90.17.1269 (1998).

161 Kopp, L. M., Gupta, P., Pelayo-Katsanis, L., Wittman, B. & Katsanis, E. Late effects in adult survivors of pediatric cancer: a guide for the primary care physician. *Am. J. Med.* **125**, 636-641, doi:10.1016/j.amjmed.2012.01.013 (2012).

162 American Academy of Pediatrics Section on Hematology/Oncology Children's Oncology, G. Long-term follow-up care for pediatric cancer survivors. *Pediatrics* **123**, 906-915, doi:10.1542/peds.2008-3688 (2009).

163 Landier, W. *et al.* Development of risk-based guidelines for pediatric cancer survivors: the Children's Oncology Group Long-Term Follow-Up Guidelines from the Children's Oncology Group Late Effects Committee and Nursing Discipline. *J. Clin. Oncol.* **22**, 4979-4990, doi:10.1200/JCO.2004.11.032 (2004).

164 Robison, L. L. *et al.* The Childhood Cancer Survivor Study: a National Cancer Institute-supported resource for outcome and intervention research. *J. Clin. Oncol.* **27**, 2308-2318, doi:10.1200/JCO.2009.22.3339 (2009).

165 Robison, L. L. Research involving long-term survivors of childhood and adolescent cancer: methodologic considerations. *Curr. Probl. Cancer* **27**, 212-224 (2003).

166 Chemaitilly, W. & Sklar, C. A. Endocrine complications in long-term survivors of childhood cancers. *Endocr. Relat. Cancer* **17**, R141-159, doi:10.1677/ERC-10-0002 (2010).

167 Katsanis, E. *et al.* Thyroid dysfunction following bone marrow transplantation: long-term follow-up of 80 pediatric patients. *Bone Marrow Transplant.* **5**, 335-340 (1990).

168 Sklar, C. *et al.* Abnormalities of the thyroid in survivors of Hodgkin's disease: data from the Childhood Cancer Survivor Study. *J. Clin. Endocrinol. Metab.* **85**, 3227-3232, doi:10.1210/jcem.85.9.6808 (2000).

169 Green, D. M. *et al.* Ovarian failure and reproductive outcomes after childhood cancer treatment: results from the Childhood Cancer Survivor Study. *J. Clin. Oncol.* **27**, 2374-2381, doi:10.1200/JCO.2008.21.1839 (2009).

170 Hudson, M. M. *et al.* High-risk populations identified in Childhood Cancer Survivor Study investigations: implications for risk-based surveillance. *J. Clin. Oncol.* **27**, 2405-2414, doi:10.1200/JCO.2008.21.1516 (2009).

171 Ginsberg, J. P. Educational paper: the effect of cancer therapy on fertility, the assessment of fertility and fertility preservation options for pediatric patients. *Eur. J. Pediatr.* **170**, 703-708, doi:10.1007/s00431-010-1359-4 (2011).

172 Green, D. M. *et al.* Pregnancy outcome of female survivors of childhood cancer: a report from the Childhood Cancer Survivor Study. *Am. J. Obstet. Gynecol.* **187**, 1070-1080 (2002).

173 Meacham, L. R. *et al.* Diabetes Mellitus in Long-term Survivors of Childhood Cancer Increased Risk Associated With Radiation Therapy: A Report for the Childhood Cancer Survivor Study. *Arch. Intern. Med.* **169**, 1381-1388 (2009).

174 Nathan, P. C. & Urbach, S. L. The metabolic cost of childhood ALL. *Blood* **117**, 4404-4405, doi:10.1182/blood-2011-02-334532 (2011).

175 Diller, L. *et al.* Chronic Disease in the Childhood Cancer Survivor Study Cohort: A Review of Published Findings. *J. Clin. Oncol.* **27**, 2339-2355, doi:10.1200/JCO.2008.21.1953 (2009).

176 Tukenova, M. *et al.* Role of Cancer Treatment in Long-Term Overall and Cardiovascular Mortality After Childhood Cancer. *J. Clin. Oncol.* **28**, 1308-1315, doi:10.1200/JCO.2008.20.2267 (2010).

177 Huang, T. T. *et al.* Pulmonary Outcomes in Survivors of Childhood Cancer A Systematic Review. *Chest* **140**, 881-901, doi:10.1378/chest.10-2133 (2011).

178 Packer, R. J. *et al.* Long-term neurologic and neurosensory sequelae in adult survivors of a childhood brain tumor: Childhood cancer survivor study. *J. Clin. Oncol.* **21**, 3255-3261, doi:10.1200/JCO.2003.01.202 (2003).

179 Goldsby, R. *et al.* Survivors of Childhood Cancer Have Increased Risk of Gastrointestinal Complications Later in Life. *Gastroenterology* **140**, 1464-U1142, doi:10.1053/j.gastro.2011.01.049 (2011).

180 Jones, D. P., Spunt, S. L., Green, D. & Springate, J. E. Renal Late Effects in Patients Treated for Cancer in Childhood: A Report From the Children's Oncology Group. *Pediatr. Blood Cancer* **51**, 724-731, doi:10.1002/pbc.21695 (2008).

181 Paulino, A. C. *et al.* Late effects in children treated with radiation therapy for Wilms' tumor. *International Journal of Radiation Oncology Biology Physics* **46**, 1239-1246, doi:Doi 10.1016/S0360-3016(99)00534-9 (2000).

182 Raney, B. *et al.* Late effects in 164 patients with rhabdomyosarcoma of the bladder/prostate region: A report from the international workshop. *J. Urol.* **176**, 2190-2194, doi:10.1016/j.juro.2006.07.064 (2006).

183 Ritchey, M., Ferrer, F., Shearer, P. & Spunt, S. L. Late Effects on the Urinary Bladder in Patients Treated for Cancer in Childhood: A Report From the Children's Oncology Group. *Pediatr. Blood Cancer* **52**, 439-446, doi:10.1002/pbc.21826 (2009).

184 Spunt, S. L. *et al.* Late effects of pelvic rhabdomyosarcoma and its treatment in female survivors. *J. Clin. Oncol.* **23**, 7143-7151, doi:10.1200/JCO.2005.12.096 (2005).

185 Beck, S. D., Bey, A. L., Bihrle, R. & Foster, R. S. Ejaculatory status and fertility rates after primary retroperitoneal lymph node dissection. *J. Urol.* **184**, 2078-2080, doi:10.1016/j.juro.2010.06.146 (2010).

186 Wasilewski-Masker, K. *et al.* Bone mineral density deficits in survivors of childhood cancer: Long-term follow-up guidelines and review of the literature. *Pediatrics* **121**, E705-E713, doi:10.1542/peds.2007-1396 (2008).

187 Tylavsky, F. A. *et al.* Nutritional Intake of Long-Term Survivors of Childhood Acute Lymphoblastic Leukemia. Evidence for Bone Health Interventional Opportunities. *Pediatr. Blood Cancer* **55**, 1362-1369, doi:10.1002/pbc.22737 (2010).

188 Sinha, A., Avery, P., Turner, S., Bailey, S. & Cheetham, T. Vitamin D Status in Paediatric Patients With Cancer. *Pediatr. Blood Cancer* **57**, 594-598, doi:10.1002/pbc.22963 (2011).

189 Odame, I. *et al.* Osteopenia, physical activity and health-related quality of life in survivors of brain tumors treated in childhood. *Pediatr. Blood Cancer* **46**, 357-362, doi:10.1002/pbc.20512 (2006).

190 Mertens, A. C. *et al.* Late mortality experience in five-year survivors of childhood and adolescent cancer: The childhood cancer survivor study. *J. Clin. Oncol.* **19**, 3163-3172 (2001).

191 Proctor, R. N. The history of the discovery of the cigarette-lung cancer link: evidentiary traditions, corporate denial, global toll. *Tob. Control* **21**, 87-91, doi:10.1136/tobaccocontrol-2011-050338 (2012).

192 Doll, R. & Wakeford, R. Risk of childhood cancer from fetal irradiation. *Br. J. Radiol.* **70**, 130-139 (1997).

193 Mathews, J. D. *et al.* Cancer risk in 680 000 people exposed to computed tomography scans in childhood or adolescence: data linkage study of 11 million Australians. *Bmj-British Medical Journal* **346**, doi:10.1136/bmj.f2360 (2013).

194 Pearce, M. S. *et al.* Radiation exposure from CT scans in childhood and subsequent risk of leukaemia and brain tumours: a retrospective cohort study. *Lancet* **380**, 499-505, doi:10.1016/S0140-6736(12)60815-0 (2012).

195 Bjorge, T. *et al.* Fetal Growth and Childhood Cancer: A Population-Based Study. *Pediatrics* **132**, E1265-E1275, doi:10.1542/peds.2013-1317 (2013).

196 Chokkalingam, A. P. *et al.* Fetal growth and body size genes and risk of childhood acute lymphoblastic leukemia. *Cancer Causes Control* **23**, 1577-1585, doi:10.1007/s10552-012-0035-6 (2012).

197 MacLean, J., Partap, S., Reynolds, P., Von Behren, J. & Fisher, P. G. Birth Weight and Order as Risk Factors for Childhood Central Nervous System Tumors. *J. Pediatr.* **157**, 450-455, doi:10.1016/j.jpeds.2010.04.006 (2010).

198 Milne, E. *et al.* Fetal growth and childhood acute lymphoblastic leukemia: Findings from the childhood leukemia international consortium. *Int. J. Cancer* **133**, 2968-2979, doi:10.1002/ijc.28314 (2013).

199 O'Neill, K. A., Bunch, K. J. & Murphy, M. F. G. Intrauterine growth and childhood leukemia and lymphoma risk. *Expert Rev. Hematol.* **5**, 559-576, doi:10.1586/EHM.12.39 (2012).

200 Ognjanovic, S. *et al.* Birth characteristics and the risk of childhood rhabdomyosarcoma based on histological subtype. *Br. J. Cancer* **102**, 227-231, doi:10.1038/sj.bjc.6605484 (2010).

201 Rangel, M. *et al.* Leukemia, non-Hodgkin's lymphoma, and Wilms tumor in childhood: the role of birth weight. *Eur. J. Pediatr.* **169**, 875-881, doi:10.1007/s00431-010-1139-1 (2010).

202 Roman, E. *et al.* Childhood acute lymphoblastic leukaemia and birthweight: Insights from a pooled analysis of case-control data from Germany, the United Kingdom and the United States. *Eur. J. Cancer* **49**, 1437-1447, doi:10.1016/j.ejca.2012.11.017 (2013).

203 Chronopoulou, E. & Harper, J. C. IVF culture media: past, present and future. *Hum. Reprod. Update* **21**, 39-55, doi:10.1093/humupd/dmu040 (2015).

204 Kallen, B. *et al.* Cancer risk in children and young adults conceived by in vitro fertilization. *Pediatrics* **126**, 270-276, doi:10.1542/peds.2009-3225 (2010).

205 Williams, C. L. *et al.* Cancer risk among children born after assisted conception. *N. Engl. J. Med.* **369**, 1819-1827, doi:10.1056/NEJMoa1301675 (2013).

206 Cogliano, V. J. *et al.* Preventable Exposures Associated With Human Cancers. *J. Natl. Cancer Inst.* **103**, 1827-1839, doi:10.1093/jnci/djr483 (2011).

207 Zhang, J. *et al.* Germline Mutations in Predisposition Genes in Pediatric Cancer. *N. Engl. J. Med.* **373**, 2336-2346, doi:10.1056/NEJMoa1508054 (2015).

208 Rahman, N. Realizing the promise of cancer predisposition genes. *Nature* **505**, 302-308, doi:10.1038/nature12981 (2014).

209 Dang-Tan, T. & Franco, E. L. Diagnosis delays in childhood cancer - A review. *Cancer* **110**, 703-713, doi:10.1002/cncr.22849 (2007).

210 Strahm, B. & Malkin, D. Hereditary cancer predisposition in children: Genetic basis and clinical implications. *Int. J. Cancer* **119**, 2001-2006, doi:10.1002/ijc.21962 (2006).

211 Gavrilovic, I. T. & Posner, J. B. Brain metastases: epidemiology and pathophysiology. *J. Neurooncol.* **75**, 5-14, doi:10.1007/s11060-004-8093-6 (2005).

212 Pollack, I. F. & Jakacki, R. I. Childhood brain tumors: epidemiology, current management and future directions. *Nature Reviews Neurology* **7**, 495-506, doi:10.1038/nrneurol.2011.110 (2011).

213 Haimi, M., Nahum, M. P. & Ben Arush, M. W. Delay in diagnosis of children with cancer: A retrospective study of 315 children. *Pediatr. Hematol. Oncol.* **21**, 37-48, doi:10.1080/08880010490263579 (2004).

214 Finlay, J. L. *et al.* Randomized phase III trial in childhood high-grade astrocytoma comparing vincristine, lomustine, and prednisone with the eight-drugs-in-1-day regimen. Childrens Cancer Group. *J. Clin. Oncol.* **13**, 112-123, doi:10.1200/JCO.1995.13.1.112 (1995).

215 Wisoff, J. H. *et al.* Primary neurosurgery for pediatric low-grade gliomas: a prospective multi-institutional study from the Children's Oncology Group. *Neurosurgery* **68**, 1548-1554; discussion 1554-1545, doi:10.1227/NEU.0b013e318214a66e (2011).

216 Zeltzer, P. M. *et al.* Metastasis stage, adjuvant treatment, and residual tumor are prognostic factors for medulloblastoma in children: conclusions from the Children's Cancer Group 921 randomized phase III study. *J. Clin. Oncol.* **17**, 832-845, doi:10.1200/JCO.1999.17.3.832 (1999).

217 Louis, D. N. *et al.* The 2007 WHO classification of tumours of the central nervous system (vol 114, pg 97, 2007). *Acta Neuropathol.* **114**, 547-547, doi:10.1007/s00401-007-0278-6 (2007).

218 Louis, D. N. *et al.* The 2016 World Health Organization Classification of Tumors of the Central Nervous System: a summary. *Acta Neuropathol.* **131**, 803-820, doi:10.1007/s00401-016-1545-1 (2016).

219 Louis, D. N. The next step in brain tumor classification: "Let us now praise famous men"... or molecules? *Acta Neuropathol.* **124**, 761-762, doi:10.1007/s00401-012-1067-4 (2012).

220 Ostrom, Q. T. *et al.* Alex's Lemonade Stand Foundation Infant and Childhood Primary Brain and Central Nervous System Tumors Diagnosed in the United States in 2007-2011. *Neuro Oncol.* **16 Suppl 10**, x1-x36, doi:10.1093/neuonc/nou327 (2015).

221 Weller, M. *et al.* Glioma. *Nat Rev Dis Primers* **1**, 15017, doi:10.1038/nrdp.2015.17 (2015).

222 Jakel, S. & Dimou, L. Glial Cells and Their Function in the Adult Brain: A Journey through the History of Their Ablation. *Front. Cell. Neurosci.* **11**, doi:10.3389/Fncel.2017.00024 (2017).

223 Kimelberg, H. K. Functions of Mature Mammalian Astrocytes: A Current View. *Neuroscientist* **16**, 79-106, doi:10.1177/1073858409342593 (2010).

224 Kimelberg, H. K. & Nedergaard, M. Functions of Astrocytes and their Potential As Therapeutic Targets. *Neurotherapeutics* **7**, 338-353 (2010).

225 Nave, K. A. Myelination and support of axonal integrity by glia. *Nature* **468**, 244-252, doi:10.1038/nature09614 (2010).

226 Collins, V. P., Jones, D. T. W. & Giannini, C. Pilocytic astrocytoma: pathology, molecular mechanisms and markers. *Acta Neuropathol.* **129**, 775-788, doi:10.1007/s00401-015-1410-7 (2015).

227 Burkhard, C. *et al.* A population-based study of the incidence and survival rates in patients with pilocytic astrocytoma. *J. Neurosurg.* **98**, 1170-1174, doi:Doi 10.3171/Jns.2003.98.6.1170 (2003).

228 Jones, D. T. W. *et al.* Recurrent somatic alterations of FGFR1 and NTRK2 in pilocytic astrocytoma. *Nat. Genet.* **45**, 927-U295, doi:10.1038/ng.2682 (2013).

229 Zhang, J. H. *et al.* Whole-genome sequencing identifies genetic alterations in pediatric low-grade gliomas. *Nat. Genet.* **45**, 602-+, doi:10.1038/ng.2611 (2013).

230 Bar, E. E., Lin, A., Tihan, T., Burger, P. C. & Eberhart, C. G. Frequent gains at chromosome 7q34 involving BRAF in pilocytic astrocytoma. *J. Neuropathol. Exp. Neurol.* **67**, 878-887, doi:Doi 10.1097/Nen.0b013e3181845622 (2008).

231 Deshmukh, H. *et al.* Identification of transcriptional regulatory networks specific to pilocytic astrocytoma. *BMC Med. Genomics* **4**, doi:10.1186/1755-8794-4-57 (2011).

232 Forshew, T. *et al.* Activation of the ERK/MAPK pathway: a signature genetic defect in posterior fossa pilocytic astrocytomas. *J. Pathol.* **218**, 172-181, doi:10.1002/path.2558 (2009).

233 Jones, D. T. W. *et al.* Tandem Duplication Producing a Novel Oncogenic BRAF Fusion Gene Defines the Majority of Pilocytic Astrocytomas. *Cancer Res.* **68**, 8673-8677, doi:10.1158/0008-5472.CAN-08-2097 (2008).

234 Pfister, S. *et al.* BRAF gene duplication constitutes a mechanism of MAPK pathway activation in low-grade astrocytomas. *J. Clin. Invest.* **118**, 1739-1749, doi:10.1172/JCI33656 (2008).

235 Sievert, A. J. *et al.* Duplication of 7q34 in Pediatric Low-Grade Astrocytomas Detected by High-Density Single-Nucleotide Polymorphism-Based Genotype Arrays Results in a Novel BRAF Fusion Gene. *Brain Pathol.* **19**, 449-458, doi:10.1111/j.1750-3639.2008.00225.x (2009).

236 Jones, C. *et al.* Pediatric high-grade glioma: biologically and clinically in need of new thinking. *Neuro Oncol.* **19**, 153-161, doi:10.1093/neuonc/now101 (2017).

237 Fangusaro, J. Pediatric high grade glioma: a review and update on tumor clinical characteristics and biology. *Front. Oncol.* **2**, 105, doi:10.3389/fonc.2012.00105 (2012).

238 Sturm, D. *et al.* Hotspot mutations in H3F3A and IDH1 define distinct epigenetic and biological subgroups of glioblastoma. *Cancer Cell* **22**, 425-437, doi:10.1016/j.ccr.2012.08.024 (2012).

239 Schwartzentruber, J. *et al.* Driver mutations in histone H3.3 and chromatin remodelling genes in paediatric glioblastoma. *Nature* **482**, 226-231, doi:10.1038/nature10833 (2012).

240 Wu, G. *et al.* Somatic histone H3 alterations in pediatric diffuse intrinsic pontine gliomas and non-brainstem glioblastomas. *Nat. Genet.* **44**, 251-253, doi:10.1038/ng.1102 (2012).

241 Jones, C. & Baker, S. J. Unique genetic and epigenetic mechanisms driving paediatric diffuse high-grade glioma. *Nature Reviews Cancer* **14**, 651-661, doi:10.1038/nrc3811 (2014).

242 Buczkowicz, P. *et al.* Genomic analysis of diffuse intrinsic pontine gliomas identifies three molecular subgroups and recurrent activating ACVR1 mutations. *Nat. Genet.* **46**, 451-456, doi:10.1038/ng.2936 (2014).

243 Khuong-Quang, D. A. *et al.* K27M mutation in histone H3.3 defines clinically and biologically distinct subgroups of pediatric diffuse intrinsic pontine gliomas. *Acta Neuropathol.* **124**, 439-447, doi:10.1007/s00401-012-0998-0 (2012).

244 Taylor, K. R. *et al.* Recurrent activating ACVR1 mutations in diffuse intrinsic pontine glioma. *Nat. Genet.* **46**, 457-461, doi:10.1038/ng.2925 (2014).

245 Wu, G. *et al.* The genomic landscape of diffuse intrinsic pontine glioma and pediatric non-brainstem high-grade glioma. *Nat. Genet.* **46**, 444-450, doi:10.1038/ng.2938 (2014).

246 Bjerke, L. *et al.* Histone H3.3 Mutations Drive Pediatric Glioblastoma through Upregulation of MYCN. *Cancer Discov.* **3**, 512-519, doi:10.1158/2159-8290.CD-12-0426 (2013).

247 Fontebasso, A. M. *et al.* Recurrent somatic mutations in ACVR1 in pediatric midline high-grade astrocytoma. *Nat. Genet.* **46**, 462-466, doi:10.1038/ng.2950 (2014).

248 Fontebasso, A. M. *et al.* Mutations in SETD2 and genes affecting histone H3K36 methylation target hemispheric high-grade gliomas. *Acta Neuropathol.* **125**, 659-669, doi:10.1007/s00401-013-1095-8 (2013).

249 Talbert, P. B. & Henikoff, S. Histone variants - ancient wrap artists of the epigenome. *Nature Reviews Molecular Cell Biology* **11**, 264-275, doi:10.1038/nrm2861 (2010).

250 Bannister, A. J. & Kouzarides, T. Regulation of chromatin by histone modifications. *Cell Res.* **21**, 381-395, doi:10.1038/cr.2011.22 (2011).

251 Cantone, I. & Fisher, A. G. Epigenetic programming and reprogramming during development. *Nat. Struct. Mol. Biol.* **20**, 282-289, doi:10.1038/nsmb.2489 (2013).

252 Li, M., Liu, G. H. & Belmonte, J. C. I. Navigating the epigenetic landscape of pluripotent stem cells. *Nature Reviews Molecular Cell Biology* **13**, 524-535, doi:10.1038/nrm3393 (2012).

253 Hirabayashi, Y. & Gotoh, Y. Epigenetic control of neural precursor cell fate during development. *Nature Reviews Neuroscience* **11**, 377-388, doi:10.1038/nrn2810 (2010).

254 Lewis, P. W. *et al.* Inhibition of PRC2 Activity by a Gain-of-Function H3 Mutation Found in Pediatric Glioblastoma. *Science* **340**, 857-861, doi:10.1126/science.1232245 (2013).

255 Bracken, A. P., Dietrich, N., Pasini, D., Hansen, K. H. & Helin, K. Genome-wide mapping of Polycomb target genes unravels their roles in cell fate transitions. *Genes Dev.* **20**, 1123-1136, doi:10.1101/gad.381706 (2006).

256 Francis, N. J., Kingston, R. E. & Woodcock, C. L. Chromatin compaction by a polycomb group protein complex. *Science* **306**, 1574-1577, doi:Doi 10.1126/Science.1100576 (2004).

257 Rougeulle, C. *et al.* Differential histone H3 Lys-9 and Lys-27 methylation profiles on the X chromosome. *Mol. Cell. Biol.* **24**, 5475-5484, doi:10.1128/MCB.24.12.5475-5484.2004 (2004).

258 Chan, K. M. *et al.* The histone H3.3K27M mutation in pediatric glioma reprograms H3K27 methylation and gene expression. *Genes Dev.* **27**, 985-990, doi:10.1101/gad.217778.113 (2013).

259 Plass, C. *et al.* Mutations in regulators of the epigenome and their connections to global chromatin patterns in cancer. *Nature Reviews Genetics* **14**, 765-780, doi:10.1038/nrg3554 (2013).

260 Bender, S. *et al.* Reduced H3K27me3 and DNA Hypomethylation Are Major Drivers of Gene Expression in K27M Mutant Pediatric High-Grade Gliomas. *Cancer Cell* **24**, 660-672, doi:10.1016/j.ccr.2013.10.006 (2013).

261 Castel, D. *et al.* Histone H3F3A and HIST1H3B K27M mutations define two subgroups of diffuse intrinsic pontine gliomas with different prognosis and phenotypes. *Acta Neuropathol.* **130**, 815-827, doi:10.1007/s00401-015-1478-0 (2015).

262 Wagner, E. J. & Carpenter, P. B. Understanding the language of Lys36 methylation at histone H3. *Nature Reviews Molecular Cell Biology* **13**, 115-126, doi:10.1038/nrm3274 (2012).

263 Swartling, F. J. *et al.* Distinct Neural Stem Cell Populations Give Rise to Disparate Brain Tumors in Response to N-MYC. *Cancer Cell* **21**, 601-613, doi:10.1016/j.ccr.2012.04.012 (2012).

264 Sturm, D. *et al.* Paediatric and adult glioblastoma: multiform (epi)genomic culprits emerge. *Nature Reviews Cancer* **14**, 92-107, doi:10.1038/nrc3655 (2014).

265 Korshunov, A. *et al.* Integrated analysis of pediatric glioblastoma reveals a subset of biologically favorable tumors with associated molecular prognostic markers. *Acta Neuropathol.* **129**, 669-678, doi:10.1007/s00401-015-1405-4 (2015).

266 Korshunov, A. *et al.* H3-/IDH-wild type pediatric glioblastoma is comprised of molecularly and prognostically distinct subtypes with associated oncogenic drivers. *Acta Neuropathol.*, doi:10.1007/s00401-017-1710-1 (2017).

267 Korshunov, A. *et al.* Molecular Staging of Intracranial Ependymoma in Children and Adults. *J. Clin. Oncol.* **28**, 3182-3190, doi:10.1200/JCO.2009.27.3359 (2010).

268 Kilday, J. P. *et al.* Pediatric Ependymoma: Biological Perspectives. *Mol. Cancer Res.* **7**, 765-786, doi:10.1158/1541-7786.MCR-08-0584 (2009).

269 Merchant, T. E. *et al.* Conformal radiotherapy after surgery for paediatric ependymoma: a prospective study. *Lancet Oncol.* **10**, 258-266, doi:10.1016/S1470-2045(08)70342-5 (2009).

270 Louis, D. N. *et al.* The 2007 WHO classification of tumours of the central nervous system. *Acta Neuropathol.* **114**, 97-109, doi:10.1007/s00401-007-0243-4 (2007).

271 Tihan, T. *et al.* The prognostic value of histological grading of posterior fossa ependymomas in children: a Children's Oncology Group study and a review of prognostic factors. *Mod. Pathol.* **21**, 165-177, doi:10.1038/modpathol.3800999 (2008).

272 Ellison, D. W. *et al.* Histopathological grading of pediatric ependymoma: reproducibility and clinical relevance in European trial cohorts. *J Negat Results Biomed* **10**, 7, doi:10.1186/1477-5751-10-7 (2011).

273 Pajtler, K. W. *et al.* Molecular Classification of Ependymal Tumors across All CNS Compartments, Histopathological Grades, and Age Groups. *Cancer Cell* **27**, 728-743, doi:10.1016/j.ccell.2015.04.002 (2015).

274 Parker, M. *et al.* C11orf95-RELA fusions drive oncogenic NF-kappaB signalling in ependymoma. *Nature* **506**, 451-455, doi:10.1038/nature13109 (2014).

275 Hansen, S. K., Baeuerle, P. A. & Blasi, F. Purification, reconstitution, and I kappa B association of the c-Rel-p65 (RelA) complex, a strong activator of transcription. *Mol. Cell. Biol.* **14**, 2593-2603 (1994).

276 Nolan, G. P., Ghosh, S., Liou, H. C., Tempst, P. & Baltimore, D. DNA binding and I kappa B inhibition of the cloned p65 subunit of NF-kappa B, a rel-related polypeptide. *Cell* **64**, 961-969 (1991).

277 Piccolo, S., Dupont, S. & Cordenonsi, M. The biology of YAP/TAZ: hippo signaling and beyond. *Physiol. Rev.* **94**, 1287-1312, doi:10.1152/physrev.00005.2014 (2014).

278 Kilday, J. P. *et al.* Copy Number Gain of 1q25 Predicts Poor Progression-Free Survival for Pediatric Intracranial Ependymomas and Enables Patient Risk Stratification: A Prospective European Clinical Trial Cohort Analysis on Behalf of the Children's Cancer Leukaemia Group (CCLG), Societe Francaise d'Oncologie Pediatrique (SFOP), and International Society for Pediatric Oncology (SIOP). *Clin. Cancer Res.* **18**, 2001-2011, doi:10.1158/1078-0432.CCR-11-2489 (2012).

279 MacDonald, T. J. Aggressive Infantile Embryonal Tumors. *J. Child Neurol.* **23**, 1195-1204, doi:10.1177/0883073808321069 (2008).

280 Buonamici, S. *et al.* Interfering with resistance to smoothened antagonists by inhibition of the PI3K pathway in medulloblastoma. *Sci. Transl. Med.* **2**, 51ra70, doi:10.1126/scitranslmed.3001599 (2010).

281 Thompson, M. C. *et al.* Genomics identifies medulloblastoma subgroups that are enriched for specific genetic alterations. *J. Clin. Oncol.* **24**, 1924-1931, doi:10.1200/jco.2005.04.4974 (2006).

282 Kool, M. *et al.* Integrated Genomics Identifies Five Medulloblastoma Subtypes with Distinct Genetic Profiles, Pathway Signatures and Clinicopathological Features. *PLoS One* **3**, doi:10.1371/journal.pone.0003088 (2008).

283 Cho, Y. J. *et al.* Integrative Genomic Analysis of Medulloblastoma Identifies a Molecular Subgroup That Drives Poor Clinical Outcome. *J. Clin. Oncol.* **29**, 1424-1430, doi:10.1200/JCO.2010.28.5148 (2011).

284 Northcott, P. A. *et al.* Medulloblastoma Comprises Four Distinct Molecular Variants. *J. Clin. Oncol.* **29**, 1408-1414, doi:10.1200/JCO.2009.27.4324 (2011).

285 Kool, M. *et al.* Molecular subgroups of medulloblastoma: an international meta-analysis of transcriptome, genetic aberrations, and clinical data of WNT, SHH, Group 3, and Group 4 medulloblastomas. *Acta Neuropathol.* **123**, 473-484, doi:10.1007/s00401-012-0958-8 (2012).

286 Gajjar, A. J. & Robinson, G. W. Medulloblastoma-translating discoveries from the bench to the bedside. *Nature Reviews Clinical Oncology* **11**, 714-722, doi:10.1038/nrclinonc.2014.181 (2014).

287 Ellison, D. W. *et al.* Medulloblastoma: clinicopathological correlates of SHH, WNT, and non-SHH/WNT molecular subgroups. *Acta Neuropathol.* **121**, 381-396, doi:10.1007/s00401-011-0800-8 (2011).

288 Ellison, D. W. *et al.* beta-Catenin status predicts a favorable outcome in childhood medulloblastoma: the United Kingdom Children's Cancer Study Group Brain Tumour Committee. *J. Clin. Oncol.* **23**, 7951-7957, doi:10.1200/JCO.2005.01.5479 (2005).

289 Gajjar, A. *et al.* Risk-adapted craniospinal radiotherapy followed by high-dose chemotherapy and stem-cell rescue in children with newly diagnosed medulloblastoma (St Jude Medulloblastoma-96): long-term results from a prospective, multicentre trial. *Lancet Oncol.* **7**, 813-820, doi:10.1016/S1470-2045(06)70867-1 (2006).

290 Jones, D. T. W. *et al.* Dissecting the genomic complexity underlying medulloblastoma. *Nature* **488**, 100-105, doi:10.1038/nature11284 (2012).

291 Northcott, P. A. *et al.* Medulloblastomics: the end of the beginning. *Nat. Rev. Cancer* **12**, 818-834, doi:10.1038/nrc3410 (2012).

292 Pugh, T. J. *et al.* Medulloblastoma exome sequencing uncovers subtype-specific somatic mutations. *Nature* **488**, 106-110, doi:10.1038/nature11329 (2012).

293 Robinson, G. *et al.* Novel mutations target distinct subgroups of medulloblastoma. *Nature* **488**, 43-48, doi:10.1038/nature11213 (2012).

294 Northcott, P. A. *et al.* The whole-genome landscape of medulloblastoma subtypes. *Nature* **547**, 311-+, doi:10.1038/nature22973 (2017).

295 Gilbertson, R. J. Medulloblastoma: signalling a change in treatment. *Lancet Oncol.* **5**, 209-218, doi:Doi 10.1016/S1470-2045(04)01424-X (2004).

296 Kool, M. *et al.* Molecular subgroups of medulloblastoma: an international meta-analysis of transcriptome, genetic aberrations, and clinical data of WNT, SHH, Group 3, and Group 4 medulloblastomas. *Acta Neuropathol.* **123**, 473-484, doi:10.1007/s00401-012-0958-8 (2012).

297 Northcott, P. A., Korshunov, A., Pfister, S. M. & Taylor, M. D. The clinical implications of medulloblastoma subgroups. *Nature Reviews Neurology* **8**, 340-351, doi:10.1038/nrneurol.2012.78 (2012).

298 Shih, D. J. H. *et al.* Cytogenetic Prognostication Within Medulloblastoma Subgroups. *J. Clin. Oncol.* **32**, 886-+, doi:10.1200/JCO.2013.50.9539 (2014).

299 Kool, M. *et al.* Genome sequencing of SHH medulloblastoma predicts genotype-related response to smoothened inhibition. *Cancer Cell* **25**, 393-405, doi:10.1016/j.ccr.2014.02.004 (2014).

300 Korshunov, A. *et al.* Biological and clinical heterogeneity of MYCN-amplified medulloblastoma. *Acta Neuropathol.* **123**, 515-527, doi:10.1007/s00401-011-0918-8 (2012).

301 Ryan, S. L. *et al.* MYC family amplification and clinical risk-factors interact to predict an extremely poor prognosis in childhood medulloblastoma. *Acta Neuropathol.* **123**, 501-513, doi:10.1007/s00401-011-0923-y (2012).

302 Zhukova, N. *et al.* Subgroup-Specific Prognostic Implications of TP53 Mutation in Medulloblastoma. *J. Clin. Oncol.* **31**, 2927-+, doi:10.1200/JCO.2012.48.5052 (2013).

303 Rausch, T. *et al.* Genome Sequencing of Pediatric Medulloblastoma Links Catastrophic DNA Rearrangements with TP53 Mutations. *Cell* **148**, 59-71, doi:10.1016/j.cell.2011.12.013 (2012).

304 Rudin, C. M. *et al.* Treatment of medulloblastoma with hedgehog pathway inhibitor GDC-0449. *N. Engl. J. Med.* **361**, 1173-1178, doi:10.1056/NEJMoa0902903 (2009).

305 Yauch, R. L. *et al.* Smoothened mutation confers resistance to a Hedgehog pathway inhibitor in medulloblastoma. *Science* **326**, 572-574, doi:10.1126/science.1179386 (2009).

306 Metcalfe, C. & de Sauvage, F. J. Hedgehog Fights Back: Mechanisms of Acquired Resistance against Smoothened Antagonists. *Cancer Res.* **71**, 5057-5061, doi:10.1158/0008-5472.CAN-11-0923 (2011).

307 Robinson, G. W. *et al.* Vismodegib Exerts Targeted Efficacy Against Recurrent Sonic Hedgehog-Subgroup Medulloblastoma: Results From Phase II Pediatric Brain Tumor Consortium Studies PBTC-025B and PBTC-032. *J. Clin. Oncol.* **33**, 2646-U2106, doi:10.1200/JCO.2014.60.1591 (2015).

308 Remke, M. *et al.* TERT promoter mutations are highly recurrent in SHH subgroup medulloblastoma. *Acta Neuropathol.* **126**, 917-929, doi:10.1007/s00401-013-1198-2 (2013).

309 Northcott, P. A. *et al.* Enhancer hijacking activates GFI1 family oncogenes in medulloblastoma. *Nature* **511**, 428-434, doi:10.1038/nature13379 (2014).

310 Northcott, P. A. *et al.* Subgroup-specific structural variation across 1,000 medulloblastoma genomes. *Nature* **488**, 49-56, doi:10.1038/nature11327 (2012).

311 Cavalli, F. M. G. *et al.* Intertumoral Heterogeneity within Medulloblastoma Subgroups. *Cancer Cell* **31**, 737-+, doi:10.1016/j.ccell.2017.05.005 (2017).

312 Schwalbe, E. C. *et al.* Novel molecular subgroups for clinical classification and outcome prediction in childhood medulloblastoma: a cohort study. *Lancet Oncol.* **18**, 958-971, doi:10.1016/S1470-2045(17)30243-7 (2017).

313 Hilden, J. M. *et al.* Central nervous system atypical teratoid/rhabdoid tumor: results of therapy in children enrolled in a registry. *J. Clin. Oncol.* **22**, 2877-2884, doi:10.1200/JCO.2004.07.073 (2004).

314 Tekautz, T. M. *et al.* Atypical teratoid/rhabdoid tumors (ATRT): improved survival in children 3 years of age and older with radiation therapy and high-dose alkylator-based chemotherapy. *J. Clin. Oncol.* **23**, 1491-1499, doi:10.1200/JCO.2005.05.187 (2005).

315 Biegel, J. A. Molecular genetics of atypical teratoid/rhabdoid tumor. *Neurosurg. Focus* **20**, E11 (2006).

316 Johann, P. D. *et al.* Atypical Teratoid/Rhabdoid Tumors Are Comprised of Three Epigenetic Subgroups with Distinct Enhancer Landscapes. *Cancer Cell* **29**, 379-393, doi:10.1016/j.ccell.2016.02.001 (2016).

317 Ginn, K. F. & Gajjar, A. Atypical teratoid rhabdoid tumor: current therapy and future directions. *Front. Oncol.* **2**, 114, doi:10.3389/fonc.2012.00114 (2012).

318 Versteege, I. *et al.* Truncating mutations of hSNF5/INI1 in aggressive paediatric cancer. *Nature* **394**, 203-206, doi:10.1038/28212 (1998).

319 Biegel, J. A. *et al.* Germ-line and acquired mutations of INI1 in atypical teratoid and rhabdoid tumors. *Cancer Res.* **59**, 74-79 (1999).

320 Hasselblatt, M. *et al.* SMARCA4-mutated atypical teratoid/rhabdoid tumors are associated with inherited germline alterations and poor prognosis. *Acta Neuropathol.* **128**, 453-456, doi:10.1007/s00401-014-1323-x (2014).

321 Wilson, B. G. & Roberts, C. W. SWI/SNF nucleosome remodellers and cancer. *Nat. Rev. Cancer* **11**, 481-492, doi:10.1038/nrc3068 (2011).

322 Sredni, S. T. & Tomita, T. Rhabdoid tumor predisposition syndrome. *Pediatr. Dev. Pathol.* **18**, 49-58, doi:10.2350/14-07-1531-MISC.1 (2015).

323 Torchia, J. *et al.* Integrated (epi)-Genomic Analyses Identify Subgroup-Specific Therapeutic Targets in CNS Rhabdoid Tumors. *Cancer Cell* **30**, 891-908, doi:10.1016/j.ccell.2016.11.003 (2016).

324 Korshunov, A. *et al.* Focal genomic amplification at 19q13.42 comprises a powerful diagnostic marker for embryonal tumors with ependymoblastic rosettes. *Acta Neuropathol.* **120**, 253-260, doi:10.1007/s00401-010-0688-8 (2010).

325 Korshunov, A. *et al.* Embryonal tumor with abundant neuropil and true rosettes (ETANTR), ependymoblastoma, and medulloepithelioma share molecular similarity and comprise a single clinicopathological entity. *Acta Neuropathol.* **128**, 279-289, doi:10.1007/s00401-013-1228-0 (2014).

326 Korshunov, A. *et al.* LIN28A immunoreactivity is a potent diagnostic marker of embryonal tumor with multilayered rosettes (ETMR). *Acta Neuropathol.* **124**, 875-881, doi:10.1007/s00401-012-1068-3 (2012).

327 Pfister, S. *et al.* Novel genomic amplification targeting the microRNA cluster at 19q13.42 in a pediatric embryonal tumor with abundant neuropil and true rosettes. *Acta Neuropathol.* **117**, 457-464, doi:10.1007/s00401-008-0467-y (2009).

328 Li, M. *et al.* Frequent amplification of a chr19q13.41 microRNA polycistron in aggressive primitive neuroectodermal brain tumors. *Cancer Cell* **16**, 533-546, doi:10.1016/j.ccr.2009.10.025 (2009).

329 Bentwich, I. *et al.* Identification of hundreds of conserved and nonconserved human microRNAs. *Nat. Genet.* **37**, 766-770, doi:10.1038/ng1590 (2005).

330 Kleinman, C. L. *et al.* Fusion of TTYH1 with the C19MC microRNA cluster drives expression of a brain-specific DNMT3B isoform in the embryonal brain tumor ETMR. *Nat. Genet.* **46**, 39-44, doi:10.1038/ng.2849 (2014).

331 Jin, B. *et al.* DNA methyltransferase 3B (DNMT3B) mutations in ICF syndrome lead to altered epigenetic modifications and aberrant expression of genes regulating development, neurogenesis and immune function. *Hum. Mol. Genet.* **17**, 690-709, doi:10.1093/hmg/ddm341 (2008).

332 Watanabe, D., Uchiyama, K. & Hanaoka, K. Transition of mouse de novo methyltransferases expression from Dnmt3b to Dnmt3a during neural progenitor cell development. *Neuroscience* **142**, 727-737, doi:10.1016/j.neuroscience.2006.07.053 (2006).

333 Sturm, D. *et al.* New Brain Tumor Entities Emerge from Molecular Classification of CNS-PNETs. *Cell* **164**, 1060-1072, doi:10.1016/j.cell.2016.01.015 (2016).

334 Thomas, C. *et al.* Methylation profiling of choroid plexus tumors reveals 3 clinically distinct subgroups. *Neuro Oncol.* **18**, 790-796, doi:10.1093/neuonc/nov322 (2016).

335 Korshunov, A. *et al.* Histologically distinct neuroepithelial tumors with histone 3 G34 mutation are molecularly similar and comprise a single nosologic entity. *Acta Neuropathol.* **131**, 137-146, doi:10.1007/s00401-015-1493-1 (2016).

336 Holsken, A. *et al.* Adamantinomatous and papillary craniopharyngiomas are characterized by distinct epigenomic as well as mutational and transcriptomic profiles. *Acta Neuropathologica Communications* **4**, doi:10.1186/S40478-016-0287-6 (2016).

337 Heim, S. *et al.* Papillary Tumor of the Pineal Region: A Distinct Molecular Entity. *Brain Pathol.* **26**, 199-205, doi:10.1111/bpa.12282 (2016).

338 Reuss, D. E. *et al.* Adult IDH wild type astrocytomas biologically and clinically resolve into other tumor entities. *Acta Neuropathol.* **130**, 407-417, doi:10.1007/s00401-015-1454-8 (2015).

339 Koelsche, C. *et al.* Melanotic Tumors of the Nervous System are Characterized by Distinct Mutational, Chromosomal and Epigenomic Profiles. *Brain Pathol.* **25**, 202-208, doi:10.1111/bpa.12228 (2015).

340 Mack, S. C. *et al.* Epigenomic alterations define lethal CIMP-positive ependymomas of infancy. *Nature* **506**, 445-+, doi:10.1038/nature13108 (2014).

341 Lambert, S. R. *et al.* Differential expression and methylation of brain developmental genes define location-specific subsets of pilocytic astrocytoma. *Acta Neuropathol.* **126**, 291-301, doi:10.1007/s00401-013-1124-7 (2013).

342 Capper, D. *et al.* DNA methylation-based classification of central nervous system tumours. *Nature*, doi:10.1038/nature26000 (2018).

343 Ziegler, A., Koch, A., Krockenberger, K. & Grosshennig, A. Personalized medicine using DNA biomarkers: a review. *Hum. Genet.* **131**, 1627-1638, doi:10.1007/s00439-012-1188-9 (2012).

344 Bernstein, M. L. Targeted Therapy in Pediatric and Adolescent Oncology. *Cancer* **117**, 2268-2274, doi:10.1002/cncr.26050 (2011).

345 Schilsky, R. L. Personalized medicine in oncology: the future is now. *Nature Reviews Drug Discovery* **9**, 363-366, doi:10.1038/nrd3181 (2010).

346 Gallo, V. *et al.* STrengthening the Reporting of OBservational studies in Epidemiology-Molecular Epidemiology (STROBE-ME): An Extension of the STROBE Statement. *PLoS Med.* **8**, doi:10.1371/journal.pmed.1001117 (2011).

347 Kris, M. G. *et al.* Efficacy of gefitinib, an inhibitor of the epidermal growth factor receptor tyrosine kinase, in symptomatic patients with non-small cell lung cancer - A randomized trial. *Jama-Journal of the American Medical Association* **290**, 2149-2158, doi:Doi 10.1001/Jama.290.16.2149 (2003).

348 Giaccone, G. *et al.* Gefitinib in combination with gemcitabine and cisplatin in advanced non-small-cell lung cancer: a phase III trial--INTACT 1. *J. Clin. Oncol.* **22**, 777-784, doi:10.1200/JCO.2004.08.001 (2004).

349 Herbst, R. S. *et al.* Gefitinib in combination with paclitaxel and carboplatin in advanced non-small-cell lung cancer: a phase III trial--INTACT 2. *J. Clin. Oncol.* **22**, 785-794, doi:10.1200/JCO.2004.07.215 (2004).

350 Mok, T. S. *et al.* Gefitinib or carboplatin-paclitaxel in pulmonary adenocarcinoma. *N. Engl. J. Med.* **361**, 947-957, doi:10.1056/NEJMoa0810699 (2009).

351 Kobayashi, S. *et al.* EGFR mutation and resistance of non-small-cell lung cancer to gefitinib. *N. Engl. J. Med.* **352**, 786-792, doi:Doi 10.1056/Nejmoa044238 (2005).

352 Glade Bender, J., Verma, A. & Schiffman, J. D. Translating genomic discoveries to the clinic in pediatric oncology. *Curr. Opin. Pediatr.* **27**, 34-43, doi:10.1097/MOP.0000000000000172 (2015).

353 Janeway, K. A., Place, A. E., Kieran, M. W. & Harris, M. H. Future of Clinical Genomics in Pediatric Oncology. *J. Clin. Oncol.* **31**, 1893-+, doi:10.1200/JCO.2012.46.8470 (2013).

354 Saletta, F. *et al.* Molecular profiling of childhood cancer: Biomarkers and novel therapies. *BBA Clin* **1**, 59-77, doi:10.1016/j.bbacli.2014.06.003 (2014).

355 Worst, B. C. *et al.* Next-generation personalised medicine for high-risk paediatric cancer patients - The INFORM pilot study. *Eur. J. Cancer* **65**, 91-101, doi:10.1016/j.ejca.2016.06.009 (2016).

356 Conley, B. A. & Doroshow, J. H. Molecular analysis for therapy choice: NCI MATCH. *Semin. Oncol.* **41**, 297-299, doi:10.1053/j.seminoncol.2014.05.002 (2014).

357 Do, K., O'Sullivan Coyne, G. & Chen, A. P. An overview of the NCI precision medicine trials-NCI MATCH and MPACT. *Chin Clin Oncol* **4**, 31, doi:10.3978/j.issn.2304-3865.2015.08.01 (2015).

358 Birgit Geoerger, G. S., Gaelle Pierron, Ludovic Lacroix, Marc Deloger, Nadia Bessoltane, Anne Catherine Harttrampf, Stefan Michiels, Jean Yves Scoazec, Paul Freneaux, Xavier Paoletti, Olivier Delattre, Natalie Hoog-Labouret and Gilles Vassal. Abstract CT004: European pediatric precision medicine program in recurrent tumors: first results from MAPPYACTS molecular profiling trial towards AcSe-ESMART proof-of-concept study. *Proceedings: AACR Annual Meeting 2017; April 1-5, 2017; Washington, DC* (2017).

359 Meric-Bernstam, F. & Mills, G. B. Overcoming implementation challenges of personalized cancer therapy. *Nat. Rev. Clin. Oncol.* **9**, 542-548, doi:10.1038/nrclinonc.2012.127 (2012).

360 Chapman, P. B. *et al.* Improved survival with vemurafenib in melanoma with BRAF V600E mutation. *N. Engl. J. Med.* **364**, 2507-2516, doi:10.1056/NEJMoa1103782 (2011).

361 Barras, D. BRAF Mutation in Colorectal Cancer: An Update. *Biomark. Cancer* **7**, 9-12, doi:10.4137/BIC.S25248 (2015).

362 Chin, L., Andersen, J. N. & Futreal, P. A. Cancer genomics: from discovery science to personalized medicine. *Nat. Med.* **17**, 297-303, doi:10.1038/nm.2323 (2011).

363 Hood, L. & Friend, S. H. Predictive, personalized, preventive, participatory (P4) cancer medicine. *Nat. Rev. Clin. Oncol.* **8**, 184-187, doi:10.1038/nrclinonc.2010.227 (2011).

364 Yap, T. A., Omlin, A. & de Bono, J. S. Development of therapeutic combinations targeting major cancer signaling pathways. *J. Clin. Oncol.* **31**, 1592-1605, doi:10.1200/JCO.2011.37.6418 (2013).

365 Day, C. P., Merlino, G. & Van Dyke, T. Preclinical mouse cancer models: a maze of opportunities and challenges. *Cell* **163**, 39-53, doi:10.1016/j.cell.2015.08.068 (2015).

366 Packer, R. J. *et al.* Phase III study of craniospinal radiation therapy followed by adjuvant chemotherapy for newly diagnosed average-risk medulloblastoma. *J. Clin. Oncol.* **24**, 4202-4208, doi:10.1200/JCO.2006.06.4980 (2006).

367 Hidalgo, M. *et al.* Patient-derived xenograft models: an emerging platform for translational cancer research. *Cancer Discov.* **4**, 998-1013, doi:10.1158/2159-8290.CD-14-0001 (2014).

368 Venditti, J. M., Wesley, R. A. & Plowman, J. Current NCI preclinical antitumor screening in vivo: results of tumor panel screening, 1976-1982, and future directions. *Adv. Pharmacol. Chemother.* **20**, 1-20 (1984).

369 Boyd, M. R. in Anticancer Drug Development Guide: Preclinical Screening, Clinical Trials, and Approval (ed Beverly A. Teicher) 23-42 (Humana Press, 1997).

370 Abaan, O. D. *et al.* The exomes of the NCI-60 panel: a genomic resource for cancer biology and systems pharmacology. *Cancer Res.* **73**, 4372-4382, doi:10.1158/0008-5472.CAN-12-3342 (2013).

371 Johnson, J. I. *et al.* Relationships between drug activity in NCI preclinical in vitro and in vivo models and early clinical trials. *Br. J. Cancer* **84**, 1424-1431, doi:Doi 10.1054/Bjoc.2001.1796 (2001).

372 Sharpless, N. E. & Depinho, R. A. The mighty mouse: genetically engineered mouse models in cancer drug development. *Nat Rev Drug Discov* **5**, 741-754, doi:10.1038/nrd2110 (2006).

373 Hausser, H. J. & Brenner, R. E. Phenotypic instability of Saos-2 cells in long-term culture. *Biochem. Biophys. Res. Commun.* **333**, 216-222, doi:10.1016/j.bbrc.2005.05.097 (2005).

374 Gillet, J. P. *et al.* Redefining the relevance of established cancer cell lines to the study of mechanisms of clinical anti-cancer drug resistance. *Proc. Natl. Acad. Sci. U. S. A.* **108**, 18708-18713, doi:10.1073/pnas.1111840108 (2011).

375 Daniel, V. C. *et al.* A primary xenograft model of small-cell lung cancer reveals irreversible changes in gene expression imposed by culture in vitro. *Cancer Res.* **69**, 3364-3373, doi:10.1158/0008-5472.CAN-08-4210 (2009).

376 Teicher, B. A. Tumor models for efficacy determination. *Mol. Cancer Ther.* **5**, 2435-2443, doi:10.1158/1535-7163.MCT-06-0391 (2006).

377 Garraway, L. A. & Janne, P. A. Circumventing cancer drug resistance in the era of personalized medicine. *Cancer Discov.* **2**, 214-226, doi:10.1158/2159-8290.CD-12-0012 (2012).

378 Weeber, F., Ooft, S. N., Dijkstra, K. K. & Voest, E. E. Tumor Organoids as a Pre-clinical Cancer Model for Drug Discovery. *Cell Chem Biol* **24**, 1092-1100, doi:10.1016/j.chembiol.2017.06.012 (2017).

379 Houghton, J. A., Houghton, P. J. & Green, A. A. Chemotherapy of childhood rhabdomyosarcomas growing as xenografts in immune-deprived mice. *Cancer Res.* **42**, 535-539 (1982).

380 Fiebig, H. H., Schuchhardt, C., Henss, H., Fiedler, L. & Lohr, G. W. Comparison of tumor response in nude mice and in the patients. *Behring Inst. Mitt.*, 343-352 (1984).

381 Mattern, J., Bak, M., Hahn, E. W. & Volm, M. Human-Tumor Xenografts as Model for Drug-Testing. *Cancer Metastasis Rev.* **7**, 263-284, doi:Doi 10.1007/Bf00047755 (1988).

382 Tentler, J. J. *et al.* Patient-derived tumour xenografts as models for oncology drug development. *Nature Reviews Clinical Oncology* **9**, 338-350, doi:10.1038/nrclinonc.2012.61 (2012).

383 Calles, A., Rubio-Viqueira, B. & Hidalgo, M. Primary human non-small cell lung and pancreatic tumorgraft models--utility and applications in drug discovery and tumor biology. *Curr. Protoc. Pharmacol.* **Chapter 14**, Unit 14 26, doi:10.1002/0471141755.ph1426s61 (2013).

384 Siolas, D. & Hannon, G. J. Patient-Derived Tumor Xenografts: Transforming Clinical Samples into Mouse Models. *Cancer Res.* **73**, 5315-5319, doi:10.1158/0008-5472.CAN-13-1069 (2013).

385 Kim, M. P. *et al.* Generation of orthotopic and heterotopic human pancreatic cancer xenografts in immunodeficient mice. *Nat. Protoc.* **4**, 1670-1680, doi:10.1038/nprot.2009.171 (2009).

386 Zhang, X. *et al.* A renewable tissue resource of phenotypically stable, biologically and ethnically diverse, patient-derived human breast cancer xenograft models. *Cancer Res.* **73**, 4885-4897, doi:10.1158/0008-5472.CAN-12-4081 (2013).

387 Hodgkinson, C. L. *et al.* Tumorigenicity and genetic profiling of circulating tumor cells in small-cell lung cancer. *Nat. Med.* **20**, 897-903, doi:10.1038/nm.3600 (2014).

388 Yu, M. *et al.* Cancer therapy. Ex vivo culture of circulating breast tumor cells for individualized testing of drug susceptibility. *Science* **345**, 216-220, doi:10.1126/science.1253533 (2014).

389 Vidal, S. J. *et al.* A targetable GATA2-IGF2 axis confers aggressiveness in lethal prostate cancer. *Cancer Cell* **27**, 223-239, doi:10.1016/j.ccell.2014.11.013 (2015).

390 Fu, X., Guadagni, F. & Hoffman, R. M. A metastatic nude-mouse model of human pancreatic cancer constructed orthotopically with histologically intact patient specimens. *Proc. Natl. Acad. Sci. U. S. A.* **89**, 5645-5649 (1992).

391 Hoffman, R. M. Patient-derived orthotopic xenografts: better mimic of metastasis than subcutaneous xenografts. *Nat. Rev. Cancer* **15**, 451-452, doi:10.1038/nrc3972 (2015).

392 Talmadge, J. E., Singh, R. K., Fidler, I. J. & Raz, A. Murine models to evaluate novel and conventional therapeutic strategies for cancer. *Am. J. Pathol.* **170**, 793-804, doi:10.2353/ajpath.2007.060929 (2007).

393 Wilmanns, C. *et al.* Modulation of Doxorubicin sensitivity and level of p-glycoprotein expression in human colon-carcinoma cells by ectopic and orthotopic environments in nude-mice. *Int. J. Oncol.* **3**, 413-422 (1993).

394 Wang, X., Fu, X. & Hoffman, R. M. A new patient-like metastatic model of human lung cancer constructed orthotopically with intact tissue via thoracotomy in immunodeficient mice. *Int. J. Cancer* **51**, 992-995 (1992).

395 Sflomos, G. *et al.* A Preclinical Model for ERalpha-Positive Breast Cancer Points to the Epithelial Microenvironment as Determinant of Luminal Phenotype and Hormone Response. *Cancer Cell* **29**, 407-422, doi:10.1016/j.ccell.2016.02.002 (2016).

396 DeRose, Y. S. *et al.* Tumor grafts derived from women with breast cancer authentically reflect tumor pathology, growth, metastasis and disease outcomes. *Nat. Med.* **17**, 1514-1520, doi:10.1038/nm.2454 (2011).

397 Bruna, A. *et al.* A Biobank of Breast Cancer Explants with Preserved Intra-tumor Heterogeneity to Screen Anticancer Compounds. *Cell* **167**, 260-274 e222, doi:10.1016/j.cell.2016.08.041 (2016).

398 Ilie, M. *et al.* Setting up a wide panel of patient-derived tumor xenografts of non-small cell lung cancer by improving the preanalytical steps. *Cancer Med* **4**, 201-211, doi:10.1002/cam4.357 (2015).

399 Nemati, F. *et al.* Establishment and characterization of a panel of human uveal melanoma xenografts derived from primary and/or metastatic tumors. *Clin. Cancer Res.* **16**, 2352-2362, doi:10.1158/1078-0432.CCR-09-3066 (2010).

400 Sivanand, S. *et al.* A validated tumorgraft model reveals activity of dovitinib against renal cell carcinoma. *Sci. Transl. Med.* **4**, 137ra175, doi:10.1126/scitranslmed.3003643 (2012).

401 Vinay, D. S. *et al.* Immune evasion in cancer: Mechanistic basis and therapeutic strategies. *Semin. Cancer Biol.* **35 Suppl**, S185-S198, doi:10.1016/j.semcancer.2015.03.004 (2015).

402 Zitvogel, L., Apetoh, L., Ghiringhelli, F. & Kroemer, G. Immunological aspects of cancer chemotherapy. *Nat. Rev. Immunol.* **8**, 59-73, doi:10.1038/nri2216 (2008).

403 Postow, M. A., Callahan, M. K. & Wolchok, J. D. Immune Checkpoint Blockade in Cancer Therapy. *J. Clin. Oncol.* **33**, 1974-1982, doi:10.1200/JCO.2014.59.4358 (2015).

404 Lan, P., Tonomura, N., Shimizu, A., Wang, S. & Yang, Y. G. Reconstitution of a functional human immune system in immunodeficient mice through combined human fetal thymus/liver and CD34+ cell transplantation. *Blood* **108**, 487-492, doi:10.1182/blood-2005-11-4388 (2006).

405 Melkus, M. W. *et al.* Humanized mice mount specific adaptive and innate immune responses to EBV and TSST-1. *Nat. Med.* **12**, 1316-1322, doi:10.1038/nm1431 (2006).

406 Walsh, N. C. *et al.* Humanized Mouse Models of Clinical Disease. *Annu. Rev. Pathol.* **12**, 187-215, doi:10.1146/annurev-pathol-052016-100332 (2017).

407 Marangoni, E. *et al.* A new model of patient tumor-derived breast cancer xenografts for preclinical assays. *Clin. Cancer Res.* **13**, 3989-3998, doi:10.1158/1078-0432.CCR-07-0078 (2007).

408 Fichtner, I. *et al.* Establishment of patient-derived non-small cell lung cancer xenografts as models for the identification of predictive biomarkers. *Clin. Cancer Res.* **14**, 6456-6468, doi:10.1158/1078-0432.CCR-08-0138 (2008).

409 Bertotti, A. *et al.* A molecularly annotated platform of patient-derived xenografts ("xenopatients") identifies HER2 as an effective therapeutic target in cetuximab-resistant colorectal cancer. *Cancer Discov.* **1**, 508-523, doi:10.1158/2159-8290.CD-11-0109 (2011).

410 Keysar, S. B. *et al.* A patient tumor transplant model of squamous cell cancer identifies PI3K inhibitors as candidate therapeutics in defined molecular bins. *Mol. Oncol.* **7**, 776-790, doi:10.1016/j.molonc.2013.03.004 (2013).

411 Stewart, E. *et al.* Orthotopic patient-derived xenografts of paediatric solid tumours. *Nature* **549**, 96-100, doi:10.1038/nature23647 (2017).

412 Delitto, D. *et al.* Patient-derived xenograft models for pancreatic adenocarcinoma demonstrate retention of tumor morphology through incorporation of murine stromal elements. *Am. J. Pathol.* **185**, 1297-1303, doi:10.1016/j.ajpath.2015.01.016 (2015).

413 Rubio-Viqueira, B. *et al.* An in vivo platform for translational drug development in pancreatic cancer. *Clin. Cancer Res.* **12**, 4652-4661, doi:10.1158/1078-0432.CCR-06-0113 (2006).

414 Julien, S. *et al.* Characterization of a large panel of patient-derived tumor xenografts representing the clinical heterogeneity of human colorectal cancer. *Clin. Cancer Res.* **18**, 5314-5328, doi:10.1158/1078-0432.CCR-12-0372 (2012).

415 Reyal, F. *et al.* Molecular profiling of patient-derived breast cancer xenografts. *Breast Cancer Res.* **14**, R11, doi:10.1186/bcr3095 (2012).

416 Zhao, X. *et al.* Global gene expression profiling confirms the molecular fidelity of primary tumor-based orthotopic xenograft mouse models of medulloblastoma. *Neuro Oncol.* **14**, 574-583, doi:10.1093/neuonc/nos061 (2012).

417 Eirew, P. *et al.* Dynamics of genomic clones in breast cancer patient xenografts at single-cell resolution. *Nature* **518**, 422-426, doi:10.1038/nature13952 (2015).

418 Isella, C. *et al.* Stromal contribution to the colorectal cancer transcriptome. *Nat. Genet.* **47**, 312-319, doi:10.1038/ng.3224 (2015).

419 Gao, H. *et al.* High-throughput screening using patient-derived tumor xenografts to predict clinical trial drug response. *Nat. Med.* **21**, 1318-1325, doi:10.1038/nm.3954 (2015).

420 Callari, M. *et al.* Computational approach to discriminate human and mouse sequences in patient-derived tumour xenografts. *BMC Genomics* **19**, 19, doi:10.1186/s12864-017-4414-y (2018).

421 Li, S. *et al.* Endocrine-therapy-resistant ESR1 variants revealed by genomic characterization of breast-cancer-derived xenografts. *Cell Rep* **4**, 1116-1130, doi:10.1016/j.celrep.2013.08.022 (2013).

422 Ding, L. *et al.* Genome remodelling in a basal-like breast cancer metastasis and xenograft. *Nature* **464**, 999-1005, doi:10.1038/nature08989 (2010).

423 Kresse, S. H., Meza-Zepeda, L. A., Machado, I., Llombart-Bosch, A. & Myklebost, O. Preclinical xenograft models of human sarcoma show nonrandom loss of aberrations. *Cancer* **118**, 558-570, doi:10.1002/cncr.26276 (2012).

424 Ben-David, U. *et al.* Patient-derived xenografts undergo mouse-specific tumor evolution. *Nat. Genet.* **49**, 1567-1575, doi:10.1038/ng.3967 (2017).

425 Garrido-Laguna, I. *et al.* Tumor engraftment in nude mice and enrichment in stroma- related gene pathways predict poor survival and resistance to gemcitabine in patients with pancreatic cancer. *Clin. Cancer Res.* **17**, 5793-5800, doi:10.1158/1078-0432.CCR-11-0341 (2011).

426 Migliardi, G. *et al.* Inhibition of MEK and PI3K/mTOR suppresses tumor growth but does not cause tumor regression in patient-derived xenografts of RAS-mutant colorectal carcinomas. *Clin. Cancer Res.* **18**, 2515-2525, doi:10.1158/1078-0432.CCR-11-2683 (2012).

427 Ascierto, P. A. *et al.* Phase II trial (BREAK-2) of the BRAF inhibitor dabrafenib (GSK2118436) in patients with metastatic melanoma. *J. Clin. Oncol.* **31**, 3205-3211, doi:10.1200/JCO.2013.49.8691 (2013).

428 Sosman, J. A. *et al.* Survival in BRAF V600-mutant advanced melanoma treated with vemurafenib. *N. Engl. J. Med.* **366**, 707-714, doi:10.1056/NEJMoa1112302 (2012).

429 Flaherty, K. T. *et al.* Combined BRAF and MEK inhibition in melanoma with BRAF V600 mutations. *N. Engl. J. Med.* **367**, 1694-1703, doi:10.1056/NEJMoa1210093 (2012).

430 Robert, C. *et al.* Improved overall survival in melanoma with combined dabrafenib and trametinib. *N. Engl. J. Med.* **372**, 30-39, doi:10.1056/NEJMoa1412690 (2015).

431 Izumchenko, E. *et al.* Patient-derived xenografts effectively capture responses to oncology therapy in a heterogeneous cohort of patients with solid tumors. *Ann. Oncol.* **28**, 2595-2605, doi:10.1093/annonc/mdx416 (2017).

432 Hidalgo, M. *et al.* A pilot clinical study of treatment guided by personalized tumorgrafts in patients with advanced cancer. *Mol. Cancer Ther.* **10**, 1311-1316, doi:10.1158/1535-7163.MCT-11-0233 (2011).

433 Clohessy, J. G. & Pandolfi, P. P. Mouse hospital and co-clinical trial project--from bench to bedside. *Nat. Rev. Clin. Oncol.* **12**, 491-498, doi:10.1038/nrclinonc.2015.62 (2015).

434 Townsend, E. C. *et al.* The Public Repository of Xenografts Enables Discovery and Randomized Phase II-like Trials in Mice. *Cancer Cell* **30**, 183, doi:10.1016/j.ccell.2016.06.008 (2016).

435 Bertotti, A. *et al.* The genomic landscape of response to EGFR blockade in colorectal cancer. *Nature* **526**, 263-267, doi:10.1038/nature14969 (2015).

436 Meehan, T. F. *et al.* PDX-MI: Minimal Information for Patient-Derived Tumor Xenograft Models. *Cancer Res.* **77**, e62-e66, doi:10.1158/0008-5472.CAN-17-0582 (2017).

437 Wilson, C. L. & Miller, C. J. Simpleaffy: a BioConductor package for Affymetrix Quality Control and data analysis. *Bioinformatics* **21**, 3683-3685, doi:10.1093/bioinformatics/bti605 (2005).

438 Smyth, G. K. Linear models and empirical bayes methods for assessing differential expression in microarray experiments. *Stat. Appl. Genet. Mol. Biol.* **3**, Article3, doi:10.2202/1544-6115.1027 (2004).

439 Huang da, W., Sherman, B. T. & Lempicki, R. A. Systematic and integrative analysis of large gene lists using DAVID bioinformatics resources. *Nat. Protoc.* **4**, 44-57, doi:10.1038/nprot.2008.211 (2009).

440 Huang da, W., Sherman, B. T. & Lempicki, R. A. Bioinformatics enrichment tools: paths toward the comprehensive functional analysis of large gene lists. *Nucleic Acids Res.* **37**, 1-13, doi:10.1093/nar/gkn923 (2009).

441 Hovestadt, V. *et al.* Robust molecular subgrouping and copy-number profiling of medulloblastoma from small amounts of archival tumour material using high-density DNA methylation arrays. *Acta Neuropathol.* **125**, 913-916, doi:10.1007/s00401-013-1126-5 (2013).

442 van der Maaten, L. & Hinton, G. Visualizing Data using t-SNE. *Journal of Machine Learning Research* **9**, 2579-2605 (2008).

443 Mazor, T. *et al.* DNA Methylation and Somatic Mutations Converge on the Cell Cycle and Define Similar Evolutionary Histories in Brain Tumors. *Cancer Cell* **28**, 307-317, doi:10.1016/j.ccell.2015.07.012 (2015).

444 Wang, K., Li, M. & Hakonarson, H. ANNOVAR: functional annotation of genetic variants from high-throughput sequencing data. *Nucleic Acids Res.* **38**, e164, doi:10.1093/nar/gkq603 (2010).

445 Mackay, A. *et al.* Integrated Molecular Meta-Analysis of 1,000 Pediatric High-Grade and Diffuse Intrinsic Pontine Glioma. *Cancer Cell* **32**, 520-537 e525, doi:10.1016/j.ccell.2017.08.017 (2017).

446 Futreal, P. A. *et al.* A census of human cancer genes. *Nat. Rev. Cancer* **4**, 177-183, doi:10.1038/nrc1299 (2004).

447 Zhao, M., Sun, J. & Zhao, Z. TSGene: a web resource for tumor suppressor genes. *Nucleic Acids Res.* **41**, D970-976, doi:10.1093/nar/gks937 (2013).

448 Campbell, I. Chi-squared and Fisher-Irwin tests of two-by-two tables with small sample recommendations. *Stat. Med.* **26**, 3661-3675, doi:10.1002/sim.2832 (2007).

449 Richardson, J. T. The analysis of 2 x 2 contingency tables--yet again. *Stat. Med.* **30**, 890; author reply 891-892, doi:10.1002/sim.4116 (2011).

450 Kogiso, M. *et al.* Xenotransplantation of pediatric low grade gliomas confirms the enrichment of BRAF V600E mutation and preservation of CDKN2A deletion in a novel orthotopic xenograft mouse model of progressive pleomorphic xanthoastrocytoma. *Oncotarget* **8**, 87455-87471, doi:10.18632/oncotarget.20713 (2017).

451 Hovestadt, V. *et al.* Decoding the regulatory landscape of medulloblastoma using DNA methylation sequencing. *Nature* **510**, 537-541, doi:10.1038/nature13268 (2014).

452 Bourdeaut, F. *et al.* Rubinstein-Taybi syndrome predisposing to non-WNT, non-SHH, group 3 medulloblastoma. *Pediatr. Blood Cancer* **61**, 383-386, doi:10.1002/pbc.24765 (2014).

453 Merk, D. J. *et al.* Opposing Effects of CREBBP Mutations Govern the Phenotype of Rubinstein-Taybi Syndrome and Adult SHH Medulloblastoma. *Dev. Cell* **44**, 709-724 e706, doi:10.1016/j.devcel.2018.02.012 (2018).

454 Kilday, J. P. *et al.* Copy number gain of 1q25 predicts poor progression-free survival for pediatric intracranial ependymomas and enables patient risk stratification: a prospective European clinical trial cohort analysis on behalf of the Children's Cancer Leukaemia Group (CCLG), Societe Francaise d'Oncologie Pediatrique (SFOP), and International Society for Pediatric Oncology (SIOP). *Clin Cancer Res* **18**, 2001-2011, doi:10.1158/1078-0432.CCR-11-2489 (2012).

455 Hill, R. M. *et al.* Combined MYC and P53 Defects Emerge at Medulloblastoma Relapse and Define Rapidly Progressive, Therapeutically Targetable Disease. *Cancer Cell*, doi:10.1016/j.ccell.2014.11.002 (2014).

456 Kulis, M. & Esteller, M. DNA methylation and cancer. *Adv. Genet.* **70**, 27-56, doi:10.1016/B978-0-12-380866-0.60002-2 (2010).

457 Brun, S. N. *et al.* Survivin as a therapeutic target in Sonic hedgehog-driven medulloblastoma. *Oncogene* **34**, 3770-3779, doi:10.1038/onc.2014.304 (2015).

458 Houghton, P. J. *et al.* The pediatric preclinical testing program: description of models and early testing results. *Pediatr. Blood Cancer* **49**, 928-940, doi:10.1002/pbc.21078 (2007).

459 Lindsay, H. *et al.* Preservation of KIT genotype in a novel pair of patient-derived orthotopic xenograft mouse models of metastatic pediatric CNS germinoma. *J. Neurooncol.* **128**, 47-56, doi:10.1007/s11060-016-2098-9 (2016).

460 Liu, Z. *et al.* Intravenous injection of oncolytic picornavirus SVV-001 prolongs animal survival in a panel of primary tumor-based orthotopic xenograft mouse models of pediatric glioma. *Neuro Oncol.* **15**, 1173-1185, doi:10.1093/neuonc/not065 (2013).

461 Liu, Z. G. *et al.* A patient tumor-derived orthotopic xenograft mouse model replicating the group 3 supratentorial primitive neuroectodermal tumor in children. *Neuro Oncol.* **16**, 787-799, doi:10.1093/neuonc/not244 (2014).

462 Pei, Y. *et al.* HDAC and PI3K Antagonists Cooperate to Inhibit Growth of MYC-Driven Medulloblastoma. *Cancer Cell* **29**, 311-323, doi:10.1016/j.ccell.2016.02.011 (2016).

463 Shu, Q. *et al.* Direct orthotopic transplantation of fresh surgical specimen preserves CD133+ tumor cells in clinically relevant mouse models of medulloblastoma and glioma. *Stem Cells* **26**, 1414-1424, doi:10.1634/stemcells.2007-1009 (2008).

464 Yu, L. *et al.* A clinically relevant orthotopic xenograft model of ependymoma that maintains the genomic signature of the primary tumor and preserves cancer stem cells in vivo. *Neuro Oncol.* **12**, 580-594, doi:10.1093/neuonc/nop056 (2010).

465 Yu, L. T. *et al.* A single intravenous injection of oncolytic picornavirus SVV-001 eliminates medulloblastomas in primary tumor-based orthotopic xenograft mouse models. *Neuro Oncol.* **13**, 14-27, doi:10.1093/neuonc/noq148 (2011).

466 Zhao, X. *et al.* Cytogenetic landscape of paired neurospheres and traditional monolayer cultures in pediatric malignant brain tumors. *Neuro Oncol.* **17**, 965-977, doi:10.1093/neuonc/nou337 (2015).

467 Grasso, C. S. *et al.* Functionally defined therapeutic targets in diffuse intrinsic pontine glioma. *Nat. Med.* **21**, 827, doi:10.1038/nm0715-827a (2015).

468 Xu, J., Margol, A., Asgharzadeh, S. & Erdreich-Epstein, A. Pediatric brain tumor cell lines. *J. Cell. Biochem.* **116**, 218-224, doi:10.1002/jcb.24976 (2015).

469 Ivanov, D. P., Coyle, B., Walker, D. A. & Grabowska, A. M. In vitro models of medulloblastoma: Choosing the right tool for the job. *J. Biotechnol.* **236**, 10-25, doi:10.1016/j.jbiotec.2016.07.028 (2016).

470 Sato, T. *et al.* Single Lgr5 stem cells build crypt-villus structures in vitro without a mesenchymal niche. *Nature* **459**, 262-265, doi:10.1038/nature07935 (2009).

471 van de Wetering, M. *et al.* Prospective derivation of a living organoid biobank of colorectal cancer patients. *Cell* **161**, 933-945, doi:10.1016/j.cell.2015.03.053 (2015).

472 Drost, J. *et al.* Sequential cancer mutations in cultured human intestinal stem cells. *Nature* **521**, 43-47, doi:10.1038/nature14415 (2015).

473 Shih, D. J. *et al.* Cytogenetic prognostication within medulloblastoma subgroups. *J. Clin. Oncol.* **32**, 886-896, doi:10.1200/JCO.2013.50.9539 (2014).

474 Byrne, A. T. *et al.* Interrogating open issues in cancer precision medicine with patient-derived xenografts. *Nat. Rev. Cancer* **17**, 254-268, doi:10.1038/nrc.2016.140 (2017).

475 Gerlinger, M. *et al.* Intratumor heterogeneity and branched evolution revealed by multiregion sequencing. *N. Engl. J. Med.* **366**, 883-892, doi:10.1056/NEJMoa1113205 (2012).

476 de Bruin, E. C. *et al.* Spatial and temporal diversity in genomic instability processes defines lung cancer evolution. *Science* **346**, 251-256, doi:10.1126/science.1253462 (2014).

477 Morrissy, A. S. *et al.* Spatial heterogeneity in medulloblastoma. *Nat. Genet.* **49**, 780-788, doi:10.1038/ng.3838 (2017).

478 Ha, G. *et al.* TITAN: inference of copy number architectures in clonal cell populations from tumor whole-genome sequence data. *Genome Res.* **24**, 1881-1893, doi:10.1101/gr.180281.114 (2014).

479 Peereboom, D. M. *et al.* Phase II trial of erlotinib with temozolomide and radiation in patients with newly diagnosed glioblastoma multiforme. *J. Neurooncol.* **98**, 93-99, doi:10.1007/s11060-009-0067-2 (2010).

480 Wen, P. Y. *et al.* Phase I/II study of erlotinib and temsirolimus for patients with recurrent malignant gliomas: North American Brain Tumor Consortium trial 04-02. *Neuro Oncol.* **16**, 567-578, doi:10.1093/neuonc/not247 (2014).

481 Raizer, J. J. *et al.* A phase II study of bevacizumab and erlotinib after radiation and temozolomide in MGMT unmethylated GBM patients. *J. Neurooncol.* **126**, 185-192, doi:10.1007/s11060-015-1958-z (2016).

482 Robinson, G. W. *et al.* Vismodegib Exerts Targeted Efficacy Against Recurrent Sonic Hedgehog-Subgroup Medulloblastoma: Results From Phase II Pediatric Brain Tumor Consortium Studies PBTC-025B and PBTC-032. *J. Clin. Oncol.*, doi:10.1200/JCO.2014.60.1591 (2015).

483 Rohner, A. *et al.* Effective targeting of Hedgehog signaling in a medulloblastoma model with PF-5274857, a potent and selective Smoothened antagonist that penetrates the blood-brain barrier. *Mol. Cancer Ther.* **11**, 57-65, doi:10.1158/1535-7163.MCT-11-0691 (2012).

484 Dijkgraaf, G. J. *et al.* Small molecule inhibition of GDC-0449 refractory smoothened mutants and downstream mechanisms of drug resistance. *Cancer Res.* **71**, 435-444, doi:10.1158/0008-5472.CAN-10-2876 (2011).

485 Zhao, X. *et al.* RAS/MAPK Activation Drives Resistance to Smo Inhibition, Metastasis, and Tumor Evolution in Shh Pathway-Dependent Tumors. *Cancer Res.* **75**, 3623-3635, doi:10.1158/0008-5472.CAN-14-2999-T (2015).

486 Bozic, I. *et al.* Evolutionary dynamics of cancer in response to targeted combination therapy. *Elife* **2**, e00747, doi:10.7554/eLife.00747 (2013).

487 Nimmervoll, B. V. *et al.* Establishing a Preclinical Multidisciplinary Board for Brain Tumors. *Clin. Cancer Res.* **24**, 1654-1666, doi:10.1158/1078-0432.CCR-17-2168 (2018).

488 Bossi, D. *et al.* In Vivo Genetic Screens of Patient-Derived Tumors Revealed Unexpected Frailty of the Transformed Phenotype. *Cancer Discov.* **6**, 650-663, doi:10.1158/2159-8290.CD-15-1200 (2016).

489 Carugo, A. *et al.* In Vivo Functional Platform Targeting Patient-Derived Xenografts Identifies WDR5-Myc Association as a Critical Determinant of Pancreatic Cancer. *Cell Rep* **16**, 133-147, doi:10.1016/j.celrep.2016.05.063 (2016).

490 Alexandrov, L. B. *et al.* Signatures of mutational processes in human cancer. *Nature* **500**, 415-+, doi:10.1038/nature12477 (2013).

491 Alexandrov, L. B. Signatures of mutational processes in human cancer. *Mol. Cancer Res.* **15**, doi:10.1158/1557-3125.DNAREPAIR16-IA11 (2017).

Publications

Ongoing work:

Brabetz, S.*, Leary, S. E. S*., Grobner, S. N.*, Nakamato, M. W., Şeker-Cin, H., Girard, E. S., Cole, B., Strand, A. D., Bloom, K. L., Hovestadt, V., Mack, N. L., Schwalm, B., Korshunov, A., Balasubramanian, G., Northcott, P. A., Pedro, K., Dey, J., Hansen, S., Ditzler, S., Lichter, P., Chavez, L., Jones, D. T. W., Koster, J., Pfister, S. M., Kool, M. and Olson, J. M. "**A biobank of patient-derived molecularly characterized orthotopic pediatric brain tumor models.**" (in revision at Nature Medicine).

Forget, A., Matrtignetti, L., Puget, S., Calzone, L., **Brabetz, S.**, Picard, D., Montagud, A., Liva, S., Sta, A., Dingli, F., Arras, G., Loew, D., Besnard, A., Lacoombe, J., Pagès, M., Varlet, P., Dufour, C., Yu, H., Mercier, A. L., Leboucher, S., Sieber, L., Beccaria, K., Gombert, M., Meyer, F., Qin, N., Bartl, J., Chavez, L., Okonechnikov, K., Sharma, T., Thatikonda, V., Bordeaut, F., Ramaswamy, V., Korshunov, A., Borkhard, A., Reifenberger, G., Poullet, P., Taylor, M. D., Kool, M., Pfister, S. M., Kawauchi, D., Barillot, E., Remke, M. and Ayrault, O. "**Proteogenomic landscape of medulloblastoma subgroups.**" (in revision at Cancer Cell).

Hwang, E. I., Kool, M., Burger, P., Capper, D., Chavez, L., **Brabetz, S.**, Williams-Hughes, C., Billups, C., Heier, L., Jaju, A., Michalski, J., Li, J., Zhao, T., Leary, S. E. S., Heideman, N., von Deimling, A., Jones, D. T. W., Gajjar, A., Packer, R. J., Pfister, S. M. and Olson, J. M. "**Extensive Molecular and Clinical Heterogeneity in Histologically Diagnosed CNS-PNET Patients Treated as a Single Entity: A Report From the Children's Oncology Group Randomized ACNS0332 Trial.**" (accepted at Journal of Clinical Oncology).

Authorships in peer-reviewed journals:

Waszak, S. M., Northcott, P. A., Buchhalter, I., Robinson, G. W., Sutter, C., Groebner, S., Grund, K. B., Brugieres, L., Jones, D. T. W., Pajtler, K. W., Morrissy, A. S., Kool, M., Sturm, D., Chavez, L., Ernst, A., **Brabetz, S.**, Hain, M., Zichner, T., Segura-Wang, M., Weischenfeldt, J., Rausch, T., Mardin, B. R., Zhou, X., Baciu, C., Lawerenz, C., Chan, J. A., Varlet, P., Guerrini-Rousseau, L., Fults, D. W., Grajkowska, W., Hauser, P., Jabado, N., Ra, Y. S., Zitterbart, K., Shringarpure, S. S., De La Vega, F. M., Bustamante, C. D., Ng, H. K., Perry, A., MacDonald, T. J., Hernaiz Driever, P., Bendel, A. E., Bowers, D. C., McCowage, G., Chintagumpala, M. M., Cohn, R., Hassall, T., Fleischhack, G., Eggen, T., Wesenberg, F., Feychting, M., Lannering, B., Schuz, J., Johansen, C., Andersen, T. V., Roosli, M., Kuehni, C. E., Grotzer, M., Kjaerheim, K., Monoranu, C. M., Archer, T. C., Duke, E., Pomeroy, S. L., Shelagh, R., Frank, S., Sumerauer, D., Scheurlen, W., Ryzhova, M. V., Milde, T., Kratz, C. P., Samuel, D., Zhang, J., Solomon, D. A., Marra, M., Eils, R., Bartram, C. R., von Hoff, K., Rutkowski, S., Ramaswamy, V., Gilbertson, R. J., Korshunov, A., Taylor, M. D., Lichter, P., Malkin, D., Gajjar, A., Korbel, J. O. and Pfister, S. M. (2018). "**Spectrum and prevalence of genetic predisposition in medulloblastoma: a retrospective genetic study and prospective validation in a clinical trial cohort.**" Lancet Oncol. (in press)

Grobner, S. N., Worst, B. C., Weischenfeldt, J., Buchhalter, I., Kleinheinz, K., Rudneva, V. A., Johann, P. D., Balasubramanian, G. P., Segura-Wang, M., **Brabetz, S.**, Bender, S., Hutter, B., Sturm, D., Pfaff, E., Hubschmann, D., Zipprich, G., Heinold, M., Eils, J., Lawerenz, C., Erkek, S., Lambo, S., Waszak, S., Blattmann, C., Borkhardt, A., Kuhlen, M., Eggert, A., Fulda, S., Gessler, M., Wegert, J., Kappler, R., Baumhoer, D., Burdach, S., Kirschner-Schwabe, R., Kontny, U., Kulozik, A. E., Lohmann, D., Hettmer, S., Eckert, C., Bielack, S., Nathrath, M., Niemeyer, C., Richter, G. H., Schulte, J., Siebert, R., Westermann, F., Molenaar, J. J., Vassal, G., Witt, H., Project, I. P.-S., Project, I. M.-S., Burkhardt, B., Kratz, C. P., Witt, O., van Tilburg, C. M., Kramm, C. M., Fleischhack, G., Dirksen, U., Rutkowski, S., Fruhwald, M., von Hoff, K., Wolf, S., Klingebiel, T., Koscielniak, E., Landgraf, P., Koster, J., Resnick, A. C., Zhang, J., Liu, Y., Zhou, X., Waanders, A. J., Zwijnenburg, D. A., Raman, P., Brors, B., Weber, U. D., Northcott, P. A., Pajtler, K. W., Kool, M., Piro, R. M., Korbel, J. O., Schlesner, M., Eils, R., Jones, D. T. W., Lichter, P., Chavez, L., Zapatka, M. and Pfister, S. M. (2018). "**The landscape of genomic alterations across childhood cancers.**" Nature **555**(7696): 321-327.

Selt, F., Hohloch, J., Hielscher, T., Sahm, F., Capper, D., Korshunov, A., Usta, D., **Brabetz, S.**, Ridinger, J., Ecker, J., Oehme, I., Gronych, J., Marquardt, V., Pauck, D., Bachli, H., Stiles, C. D., von Deimling, A., Remke, M., Schuhmann, M. U., Pfister, S. M., Brummer, T., Jones, D. T., Witt, O. and Milde, T. (2017). "**Establishment and application of a novel patient-derived KIAA1549:BRAF-driven pediatric pilocytic astrocytoma model for preclinical drug testing.**" Oncotarget **8**(7): 11460-11479.

Schmidt, C., Schubert, N. A., **Brabetz, S.**, Mack, N., Schwalm, B., Chan, J. A., Selt, F., Herold-Mende, C., Witt, O., Milde, T., Pfister, S. M., Korshunov, A. and Kool, M. (2017). "**Preclinical drug screen reveals topotecan, actinomycin D, and volasertib as potential new therapeutic candidates for ETMR brain tumor patients.**" Neuro Oncol **19**(12): 1607-1617.

Meehan, T. F., Conte, N., Goldstein, T., Inghirami, G., Murakami, M. A., **Brabetz, S.**, Gu, Z., Wiser, J. A., Dunn, P., Begley, D. A., Krupke, D. M., Bertotti, A., Bruna, A., Brush, M. H., Byrne, A. T., Caldas, C., Christie, A. L., Clark, D. A., Dowst, H., Dry, J. R., Doroshow, J. H., Duchamp, O., Evrard, Y. A., Ferretti, S., Frese, K. K., Goodwin, N. C., Greenawalt, D., Haendel, M. A., Hermans, E., Houghton, P. J., Jonkers, J., Kemper, K., Khor, T. O., Lewis, M. T., Lloyd, K. C. K., Mason, J., Medico, E., Neuhauser, S. B., Olson, J. M., Peeper, D. S., Rueda, O. M., Seong, J. K., Trusolino, L., Vinolo, E., Wechsler-Reya, R. J., Weinstock, D. M., Welm, A., Weroha, S. J., Amant, F., Pfister, S. M., Kool, M., Parkinson, H., Butte, A. J. and Bult, C. J. (2017). "**PDX-MI: Minimal Information for Patient-Derived Tumor Xenograft Models.**" Cancer Res **77**(21): e62-e66.

Sturm, D., Orr, B. A., Toprak, U. H., Hovestadt, V., Jones, D. T., Capper, D., Sill, M., Buchhalter, I., Northcott, P. A., Leis, I., Ryzhova, M., Koelsche, C., Pfaff, E., Allen, S. J., Balasubramanian, G., Worst, B. C., Pajtler, K. W., **Brabetz, S.**, Johann, P. D., Sahm, F., Reimand, J., Mackay, A., Carvalho, D. M., Remke, M., Phillips, J. J., Perry, A., Cowdrey, C., Drissi, R., Fouladi, M., Giangaspero, F., Lastowska, M., Grajkowska, W., Scheurlen, W., Pietsch, T., Hagel, C., Gojo, J., Lotsch, D., Berger, W., Slavc, I., Haberler, C., Jouvet, A., Holm, S., Hofer, S., Prinz, M., Keohane, C., Fried, I., Mawrin, C., Scheie, D., Mobley, B. C., Schniederjan, M. J., Santi, M., Buccoliero, A. M., Dahiya, S., Kramm, C. M., von Bueren, A. O., von Hoff, K., Rutkowski, S., Herold-Mende, C., Fruhwald, M. C., Milde, T., Hasselblatt, M., Wesseling, P., Rossler, J., Schuller, U., Ebinger, M., Schittenhelm, J., Frank, S., Grobholz, R., Vajtai, I., Hans, V., Schneppenheim, R., Zitterbart, K., Collins, V. P., Aronica, E., Varlet, P., Puget, S., Dufour, C., Grill, J., Figarella-Branger, D., Wolter, M., Schuhmann, M. U., Shalaby, T., Grotzer, M., van Meter, T., Monoranu, C. M., Felsberg, J., Reifenberger, G., Snuderl, M., Forrester, L. A., Koster, J., Versteeg, R., Volckmann, R., van Sluis, P., Wolf, S., Mikkelsen, T., Gajjar, A., Aldape, K., Moore, A. S., Taylor, M. D., Jones, C., Jabado, N., Karajannis, M. A., Eils, R., Schlesner, M., Lichter, P., von Deimling, A., Pfister, S. M., Ellison, D. W., Korshunov, A. and Kool, M. (2016). "**New Brain Tumor Entities Emerge from Molecular Classification of CNS-PNETs.**" Cell **164**(5): 1060-1072.

Pei, Y., Liu, K. W., Wang, J., Garancher, A., Tao, R., Esparza, L. A., Maier, D. L., Udaka, Y. T., Murad, N., Morrissy, S., Seker-Cin, H., **Brabetz, S.**, Qi, L., Kogiso, M., Schubert, S., Olson, J. M., Cho, Y. J., Li, X. N., Crawford, J. R., Levy, M. L., Kool, M., Pfister, S. M., Taylor, M. D. and Wechsler-Reya, R. J. (2016). "**HDAC and PI3K Antagonists Cooperate to Inhibit Growth of MYC-Driven Medulloblastoma.**" Cancer Cell **29**(3): 311-323.

Johann, P. D., Erkek, S., Zapatka, M., Kerl, K., Buchhalter, I., Hovestadt, V., Jones, D. T., Sturm, D., Hermann, C., Segura Wang, M., Korshunov, A., Rhyzova, M., Grobner, S., **Brabetz, S.**, Chavez, L., Bens, S., Groschel, S., Kratochwil, F., Wittmann, A., Sieber, L., Georg, C., Wolf, S., Beck, K., Oyen, F., Capper, D., van Sluis, P., Volckmann, R., Koster, J., Versteeg, R., von Deimling, A., Milde, T., Witt, O., Kulozik, A. E., Ebinger, M., Shalaby, T., Grotzer, M., Sumerauer, D., Zamecnik, J., Mora, J., Jabado, N., Taylor, M. D., Huang, A., Aronica, E., Bertoni, A., Radlwimmer, B., Pietsch, T., Schuller, U., Schneppenheim, R., Northcott, P. A., Korbel, J. O., Siebert, R., Fruhwald, M. C., Lichter, P., Eils, R., Gajjar, A., Hasselblatt, M., Pfister, S. M. and Kool, M. (2016). "**Atypical Teratoid/Rhabdoid Tumors Are Comprised of Three Epigenetic Subgroups with Distinct Enhancer Landscapes.**" Cancer Cell **29**(3): 379-393.

Godin-Heymann, N., **Brabetz, S.**, Murillo, M. M., Saponaro, M., Santos, C. R., Lobley, A., East, P., Chakravarty, P., Matthews, N., Kelly, G., Jordan, S., Castellano, E. and Downward, J. (2016). "**Tumour-suppression function of KLF12 through regulation of anoikis.**" Oncogene **35**(25): 3324-3334.

Ernst, A., Jones, D. T., Maass, K. K., Rode, A., Deeg, K. I., Jebaraj, B. M., Korshunov, A., Hovestadt, V., Tainsky, M. A., Pajtler, K. W., Bender, S., **Brabetz, S.**, Grobner, S., Kool, M., Devens, F., Edelmann, J., Zhang, C., Castelo-Branco, P., Tabori, U., Malkin, D., Rippe, K., Stilgenbauer, S., Pfister, S. M., Zapatka, M. and Lichter, P. (2016). "**Telomere dysfunction and chromothripsis.**" Int J Cancer **138**(12): 2905-2914.

Acknowledgements

First, I would like to thank my thesis advisor and referee Stefan Pfister and my direct supervisor Marcel Kool for giving me the opportunity to do my Ph.D. in the department of "Pediatric Neurooncology" at the German Cancer Research Center. Both of you created a very simulating research atmosphere and gave me nearly limitless possibilities to pursue any scientific question that came into my mind. In parallel, you guided me into the right direction and taught me how to properly design and conduct projects, and to think "big"; of particular value was your pragmatic thinking on getting things done, looking at the bigger picture, and not getting lost in the last potentially interesting detail. Although both of you are always very busy, you always gave me very fast and insightful feedback, ranging from regular meetings to preparing my manuscript and now this Ph.D. thesis. I also valued the non-hierarchical environment, which allowed everybody to contribute to discussions. In addition, I would also like to thank you for your trust in me by providing me with additional the support of research technicians and sufficient financial resources.

I also want to thank David Jones, Daisuke Kawauchi, Till Milde, Martin Sill, and Jan Gronych for being very helpful and supporting me during the various stages of my Ph.D. – ranging from many technical questions concerning animal work to understanding the molecular heterogeneity of glioma. I am thankful to Michael Boutros for being my first examiner and for all of his insightful comments and helpful advice as a member of my TAC meetings. Furthermore, I would also like to thank the other members of my TAC, Christel Herold-Mende, Olaf Witt, and Peter Lichter for their guiding comments, and my other Ph.D. examiners, Karin Müller-Decker and Benedikt Brors, for participating in and reviewing my work.

Furthermore, I would like to thank my collaboration partners Sarah E. S. Leary, Emily Girard, Bonnie Cole, Madison Nakamoto, Andy Strand, James M. Olson, Jessica Rusert, James Jensen, Robert J. Wechsler Reya, Frank Braun, Xiao-Nan Li, Antoine Forget, Olivier Ayrault, and Jan Koster for contributing to my work, providing me with samples, sharing their experiences, and for the many discussions. It was and is a pleasure working with all of you. In particular, I want to thank the team of the Olson laboratory for the great collaboration leading into our current manuscript, and Jan Koster for building the "PDX Explorer" together with me – it is incredible how you turned a vision into a working website.

I want to thank Norman Mack and Benjamin Schwalm for their excellent work and the great atmosphere in our small team. Without both of you, I would not have been able to establish the PDX system in the way we have now (if at all). Both of you are very passionate about our PDX project, quickly understand the critical aspects of experiments, and are just very nice persons to work with. We started from basically nothing, trying to establish the intracranial injections, and

are now juggling thousands of samples and setting up automated systems to grow even more. Thank you so much.

In addition, I would like to thank all of my office colleagues, who welcomed me into the department and provided me with a great everyday working atmosphere; the “PhD pool”, Barbara, Kristian, Elke, Sander, Sjoerd, Jens, Sonja, and Marcel made sure that I always came into the office with a smile. I also want to thank the B06x and B062 departments for the great working atmosphere, which makes it very enjoyable to be part of it. In particular, I want to thank our great technician team, Andrea, Laura, and Monika, for helping me so many times and keeping the lab running, and our administrative staff, Ines, Iris, and Anna-Lisa, who helped me out on many occasions. In addition, I would like to thank Christina, who taught me how to transplant tumor cells into the murine brain. Within the DKFZ I am also very grateful to the data management group, in particular Ingrid, who re-organized my sequencing data multiple times and was always very helpful, and also all animal caretakers, who keep the animal facility running and take over so much of our work. I also want to thank my friends back at home and all over Germany, who were always supportive although I could not visit them as often as I used to. In particular, I would like to thank Sören and Ronny, who took my mind off of work through many fun evenings, but also regular workout sessions.

Finally, I owe eternal gratitude to my family, who always supported me and was always the anchor for me, even in the hardest times. Lisa, Reinhard, Ludwig, and Kathy were there when needed the most, and helped me to cope with the gravest loss. In particular, I would like to thank Kathy, who also helped tremendously in shaping this thesis by refining the language and finding mistakes. I am very grateful to my mother and father, who guided and supported me through the entirety of my life and without whom I would never have achieved this. I also want to thank my brother, Oliver, who is the best brother one could possibly think of. I am deeply thankful to Susanne, partly for contributing to this work, but overwhelmingly for always being there for me, diverting my focus away from work and showing me what is really important in life.